U.PORTO

DOUTORAMENTO

BIOLOGIA BASICA E APLICADA

Psychostimulants and neuroinflammation: finding critical players in the crosstalk between glial cells and neurons

Joana da Silva Bravo

D 2023

Psychostimulants and neuroniflammation: finding critical players in the crosstalk between glial cells and neurons

Joana Catarina da Silva Bravo

Instituto de Ciências Biomédicas Abel Salazar

Faculdade de Ciências

Faculdade de Medicina

JOANA CATARINA DA SILVA BRAVO

PSYCHOSTIMULANTS AND NEUROINFLAMMATION: FINDING CRITICAL PLAYERS IN THE CROSSTALK BETWEEN GLIAL CELLS AND NEURONS

Tese de Candidatura ao grau de Doutor em Biologia Básica e Aplicada;
Programa Doutoral da Universidade do Porto (Instituto de Ciências Biomédicas Abel Salazar)

Orientador - Doutora Maria Teresa Burnay Summavielle
Categoria – Investigadora Principal
Afiliação – Instituto de Investigação e Inovação em Saúde

Co-orientador – Doutor João Carlos Medeiros Bettencourt Relvas
Categoria – Investigador Principal
Afiliação - Instituto de Investigação e Inovação em Saúde

A tese de doutoramento aqui apresentada foi desenvolvida no âmbito de uma bolsa (PD/BD/135450/2017) individual de doutoramento financiada através FCT e União Europeia, pelo programa FCT PhD Programmes. Adicionalmente, este trabalho foi também apoiado através de uma bolsa excecional para mitigar os efeitos da COVID-19 (COVID/BD/152602/2022), financiada pela FCT e foi parte integrante dos projetos de investigação POCI-01-0145-FEDER-030647 financiado pelo COMPETE 2020 e FCT (PTDC/SAU-TOX/30647/2017) e PTDC/SAU-TOX/0067/2021 financiado pela FCT.

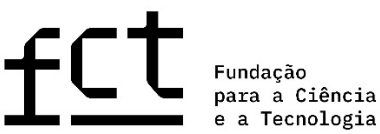

“If you want to really be innovative, you're almost working at the edge of science fiction because at that point people are willing to have flights of imagination. One of the aphorisms that I was raised on, "The difficult we do right away, the impossible takes a little longer." It takes the same amount of effort to work on big questions as little questions. So why not work on big questions?”

Mario Capecchi - Flights of Imagination

Agradecimentos

Embora todas as palavras de agradecimento sejam poucas, não posso deixar de agradecer a todas a pessoas que de alguma forma fizeram parte deste meu percurso.

Agradeço à minha orientadora, Teresa, por todo o apoio ao longo destes anos de doutoramento, foi uma jornada por vezes difícil, mas sem o seu apoio o grau de dificuldade teria sido com certeza ainda maior. Obrigada por toda a disponibilidade e por me tentar ajudar sempre. Obrigada por toda a partilha de conhecimentos, por me permitir explorar as minhas ideias científicas e por estabelecer limites sempre que necessário. Deixo ainda um enorme agradecimento por todos estes anos de partilha pessoal e profissional e por toda a sua dedicação. Um enorme obrigada será sempre pouco. Muito, muito obrigada!

Um enorme agradecimento ao meu co-orientador, João Relvas, pelo incentivo em concorrer a este Programa Doutoral e por toda a sua disponibilidade durante estes anos. Muito obrigada pelo seu entusiasmo científico, que nos faz querer ser sempre melhores.

Quero agradecer à Ana Magalhães por todo o seu contributo cientifico no trabalho desenvolvido, mas não menos importante, agradeço por toda a disponibilidade em me ouvires e me ajudares a gerir todas as emoções. Muito obrigada pelo teu companheirismo e amizade.

Agradeço ainda aos restantes membros do laboratório Addiction Biology pela sua ajuda durante este trabalho, principalmente à Teresa Canedo, à Ana Filipa e ao João Rodrigues por toda a sua ajuda direta ou indireta no trabalho desenvolvido. E ainda um agradecimento à Inês Ribeiro, ao Guilherme, ao Igor e à Andrea, que apesar de já não se encontrarem a trabalhar connosco, participaram também no desenvolvimento deste trabalho. Agradeço ainda à Sílvia, que embora já não faça parte do laboratório há algum tempo, se mostrou sempre disponível para me ajudar e tanto me ensinou no inicio do meu percurso em investigação.

Agradeço à Elva por toda a partilha de conhecimento e pela sua enorme disponibilidade para me ajudar e para me ouvir. Um enorme obrigada mesmo; tornaste-te crucial para o desenvolvimento deste trabalho e espero que possamos continuar a colaborar nas nossas vidas científicas e que a amizade que se iniciou neste percurso continue a florescer.

Um enorme agradecimento ao meu amigo Ricardo Vieira. Muito obrigada por tudo, pela leveza com que encaras todos os problemas e por teres sempre uma solução para todas as questões. Obrigada por toda tua enorme disponibilidade. E parabéns pelo teu percurso científico (está quase)!

Um agradecimento muito especial à Camila por toda ajuda que me deu e por toda a sua alegria contagiante. Muito obrigada, Camila!
Quero ainda agradecer à Maria Azevedo por toda a ajuda e pela disponibilidade constante. Muito obrigada, Maria!
Agradeço à minha amiga Cátia pela por toda a ajuda e obrigada por toda a tua disponibilidade mesmo agora mais longe.
Agradeço ainda à Inês Lorga, à Eva Carvalho, ao Miguel Morais e ao Hugo Osório por toda a ajuda que prestaram ao desenvolvimento deste trabalho.
À Andreia Costa um obrigada pela boa disposição constante e por se mostrar sempre disponível em ajudar.
Um agradecimento muito especial aos meus queridos amigos, a Filipa, a Inês, a Catarina, a Marta, a Sílvia, a Anaísa, a Ana Maria e o Manuel, que iniciaram esta jornada de doutoramento comigo. O inicio deste percurso foi muito bonito e muito enriquecedor a nível pessoal e profissional. Agradeço-vos por toda a partilha de conhecimentos, por todo o companheirismo e toda a amizade ao longo destes anos. Sou muito feliz em vos ter conhecido e tenho a certeza que a nossa amizade permanecerá mesmo que a distância nos continue a separar. Que as vossas imaginações continuem a voar…
Quero ainda agradecer à minha família que me deu todo o apoio necessário para que eu pudesse chegar até aqui. Um obrigado especial ao meu pai, ao meu irmão e à família Bravo Barbosa, em especial à tia Leninha e à Carla, por me terem dado toda a estrutura necessária para eu crescer e por me terem permitido estudar. Muito, muito obrigada!
Por fim, mas não menos importante, agradeço ao José e dedico este trabalho ao meu Afonso. Ao José, agradeço todo o apoio, compreensão, dedicação e por me ajudares sempre a acreditar que é possível. Muito obrigada por toda caminhada ao longo de todos estes anos! O Afonso chegou no meio deste percurso e se por um lado veio trazer algumas dificuldades ao trabalho, por outro veio tornar tudo muito mais bonito e pôr as prioridades no seu devido lugar, e por isso, sou muito feliz. Muito obrigada aos dois por todo o vosso amor. E como diz o Afonso tantas vezes e por outras razões “Tu consegues, mãe”. Parece que consegui….
Muito, muito obrigada a todos!

Resumo

A exposição à metanfetamina (Meth), um psicostimulante potente, tem sido classicamente associada ao dano neuronal. No entanto, evidência recente mostra que a adição a drogas de abuso pode resultar da interação entre células neuronais e células da glia. Tendo em conta esta evidência, colocámos a hipótese de que o controlo da resposta inflamatória pudesse ser importante para controlar o comportamento aditivo e reduzir os níveis de recaídas. Assim, neste projeto propusemos abordagens complementares para obter uma melhor compreensão do processo neuroinflamatório que ocorre durante a adição a drogas de abuso. Estas abordagens focaram-se na interação entre as células da glia e os neurónios, de forma a identificar mecanismos regulatórios deste processo.

Recentemente, demonstramos que a administração aguda de Meth promove microgliose e ativação da microglia através da libertação de glutamato pelos astrócitos, de modo dependente de TNF/IP_3R2-Ca^2. Neste trabalho, investigamos principalmente a contribuição das células neuronais para este processo.

Para validar a nossa hipótese, primeiramente estudamos a nível molecular a modulação neuronal da ativação da microglia pela Meth, usando culturas celulares primárias em câmara microfluidicas. Verificamos que o contacto entre os neurónios e a microglia, seja direto ou indireto, não é suficiente para promover uma resposta inflamatória quando apenas os neurónios são expostos à Meth. Pelo contrário, verificamos que a interação entre os neurónios e a microglia através de mecanismos dependentes de contato, em específico através da sinalização CD200/CD200r, reduz a reatividade da microglia causada pelos astrócitos expostos a Meth e aumenta a plasticidade neuronal. No global, estes dados indicam que as células neuronais poderão ter um papel importante na redução da reatividade da microglia aquando a exposição a Meth.

Tendo em conta estes resultados e visando entender melhor o processo inflamatório e de interação entre as células da glia e os neurónios quando expostos de modo prolongado a substâncias psicoativas, prosseguimos com este estudo usando um modelo de administração crónica de Meth. Neste estudo verificámos que a sinalização entre o CD47 e o SIRPα, um outro par regulador neuroimune, está alterada após a administração crónica de Meth e durante a abstinência. Os resultados demonstraram ainda que a alteração da sinalização CD47- SIRPα poderá estar relacionada com a alteração da homeostasia da microglia. Adicionalmente, também verificámos que a produção de IFN-γ pelas células T residentes nas meninges está diminuída após a administração crónica de Meth e que se mantém diminuída após um período curto de

abstinência. Sabendo que o IFN-γ é um modelador da expressão de CD47 em células cancerígenas, novos estudos serão realizados para compreender a relação entre o CD47 e o IFN-γ durante a exposição crónica a Meth.

Ainda no contexto deste trabalho, uma vez que a identificação de novos biomarcadores e alvos terapêuticos é uma forma de conceber terapias personalizadas, foi realizada uma revisão sistemática da literatura de forma a entender o perfil das citocinas e a relação imunológica central e periférica em diferentes fases do processo de adição a drogas de abuso. Os nossos resultados demonstraram que maioritariamente os estudos publicados avaliaram citocinas pró-inflamatórias clássicas (TNF-α; IL-6 e IL-1β) e quase exclusivamente a nível central. Esforços adicionais serão necessários para entender melhor a ligação entre agentes imunológicos periféricos e centrais nos perfis longitudinais e na dinâmica das citocinas durante o desenvolvimento de comportamentos aditivos.

Coletivamente, estes dados demonstram que as moléculas reguladoras neuroimunes podem ser alvos terapêuticos importantes na dependência de drogas. Porém, para intervenções terapêuticas futuras serão necessários mais estudos para encontrar moduladores dessas moléculas e a melhor estratégia modulatória precisará ser testada no comportamento aditivo.

Palavras-chave: CD200; CD47; contacto; IFN-γ; metanfetamina; neurónios-microglia.

Abstract

Exposure to methamphetamine (Meth), a powerful psychostimulant substance, has been classically associated with damage to neuronal terminals. However, it is now becoming clear that addiction may also result from the interplay between glial cells and neurons. Considering this, we hypothesized that limiting the inflammatory response could be relevant to control the addictive behavior and reduce relapse rates. Therefore, in this project we proposed several complementary approaches to better understand neuroinflammation under repeated drug exposure, focusing in the interplay between glial cells and neurons, in order to identify regulatory mechanisms of involved in this inflammatory process.

Recently, we demonstrated that binge Meth administration promotes microgliosis and microglia pro-inflammation via astrocytic glutamate release in a TNF/IP_3R2-Ca^{2+}-dependent manner. Herein, we further investigated the contribution of neuronal cells to this process.

To explore this issue, we first dissect at molecular level the neuronal modulation of microglia activation by Meth, using primary cell cultures. We found that neither indirect nor direct neuron-microglia contact was sufficient to promote an inflammatory response throughout neuronal cells under Meth exposure. Contrarily, we showed that contact-dependent mechanisms between neurons and microglia, namely through CD200/CD200r signaling, attenuated Meth-induced microglia reactivity and enhanced synaptic plasticity. Overall, these data indicated that neuronal cells may have an important role in the attenuation of microglia reactivity under Meth exposure.

In this scenario, aiming to understand the inflammatory process and the crosstalk between glial cells and neurons under drug addiction, we moved forward by resorting to a chronic model of Meth administration. We found that the signaling of CD47-SIRPα, another neuroimmune regulatory ligand-receptor pair, is disrupted both after chronic Meth administration and during Meth withdrawal. These results also indicate that CD47-SIRPα signaling disruption may be related with microglia homeostasis dysregulation. Additionally, we also found that the production of IFN-γ by meningeal T cells is reduced after chronic Meth administration and remains decreased at a short-term withdrawal. Considering that IFN-γ is a modulator of the expression of CD47 in cancer cells, further studies will be performed to understand the relationship between CD47 and IFN-γ under chronic Meth administration.

Still in this context, and since the identification of new biomarkers and therapeutic targets is a way to envision personalized immune-based therapeutics, we performed a

systematic review of the literature in order to understand the cytokine profile and the peripheral-central immune crosstalk in different stages of problematic drug use or addiction. Our results showed that, this far, the published studies mostly evaluated the classical pro-inflammatory cytokines (TNF-α; IL-6 and IL-1β) at central level. Additional efforts will be necessary to better understand the link between peripheral and central immune players in longitudinal profiles and the dynamics of cytokines during the buildup of addiction.

Collectively, these data showed that neuroimmune regulatory molecules may be important therapeutic targets in drug addiction. However, for therapeutic interventions further studies will be necessary to find modulators of these molecules and the best modulatory strategy needs to be tested in the addictive behavior.

Keywords: CD200; CD47; contact-dependent; IFN-γ; methamphetamine; neuron-microglia.

Table of contents

Resumo IX

Abstract XI

Abbreviations XV

Publications XXI

Thesis Layout XXIII

CHAPTER I ..... - 25 -

General introduction ..... - 25 -

1. Immune function in the Central Nervous System ..... - 27 -
2. CNS infiltrating immune cells ..... - 32 -
3. CNS resident immune cells - Microglia ..... - 33 -
4. Crosstalk between microglia and neurons in physiological conditions ..... - 40 -
5. Immune cells response in psychostimulants abuse ..... - 46 -

References ..... - 48 -

CHAPTER II ..... - 63 -

Thesis aims ..... - 63 -

1. General aims ..... - 65 -

CHAPTER III ..... - 67 -

Can The impact of psychostimulants on central and peripheral neuro-immune regulation: a scoping review cytokine profiles and their implications for addiction - 67 -

1. Introduction ..... - 69 -
2. Methods ..... - 70 -
3. Results ..... - 72 -
4. Discussion ..... - 94 -

References ..... - 99 -

Supplementary Information ..... - 110 -

CHAPTER IV ..... - 113 -

Neuron–Microglia Contact-Dependent Mechanisms Attenuate Methamphetamine-Induced Microglia Reactivity and Enhance Neuronal Plasticity ..... - 113 -
1. Introduction ..... - 115 -
2. Material and Methods ..... - 116 -
3. Results ..... - 121 -
4. Discussion ..... - 130 -
5. Conclusions ..... - 132 -
References ..... - 133 -
Supplementary Information ..... - 136 -
CHAPTER V ..... - 141 -
Effects of chronic Meth exposure ..... - 141 -
1. Introduction ..... - 143 -
2. Material and Methods ..... - 145 -
3. Results ..... - 152 -
4. Discussion ..... - 166 -
References ..... - 170 -
Supplementary Information ..... - 177 -
CHAPTER VI ..... - 188 -
General conclusion ..... - 188 -
Conclusion and future perspectives ..... - 190 -
References ..... - 194 -
APPENDIX ..... - 196 -

Abbreviations

Aβ – Amyloid beta

ACM – Astrocytic conditioned medium

AD – Alzheimer disease

AEA - Arachidonoylethanolamine

AGM – Aorta-gonad-mesonephros

ALS - Amyotrophic lateral sclerosis

Amph - Amphetamine

Arginase-1 – Arg1

ARM – Activated response microglia

ATP – Adenosine triphosphate

BAM - Border- associated macrophages

BBB – Blood brain barrier

BDNF – Brain-derived neurotrophic factor

CB1 - Type-1 cannabinoid receptors

CCL2 - C-C Motif Chemokine Ligand 2

CD - Cluster of differentiation

cLN – Cervical lymph node

CNS - Central nervous system

CPu – Caudate Putamen

CP – Choroid plexus

CPP – Conditioned place preference

CSF - Cerebrospinal fluid

CSF1R - Colony stimulating factor 1 receptor

Ctrl – Control

CUD – Cocaine use disorder

CVOs - Circumventricular organs

DAM - Disease-associated microglia

DAMPs - Damage-associated molecular patterns

DAPI - 4,6-diamidino-2-phenylindole

DC - Dendritic cell

dcLN – Deep cervical lymph node

DGAV – Direção Geral de alimentação e Veterinária

DID – Drinking in the Dark

DIV – Days *in vitro*

DSM - Diagnostic and statistical manual of mental disorders

ELISA – Enzyme-linked immunosorbent assay

EVs – Extracellular vesicles

FACS - Fluorescence-activated cell sorting

FR – Fixed ratio

FSC-A - Forward scatter area

FSC-H - Forward scatter height

FCRLS - Fc receptor-like S

GPR34 - G protein coupled receptor 34

HEXb - β-hexosaminidase subunit β

Iba1 - Ionized calcium-binding adapter molecule 1

IFN – Interferon

Ig - Immunoglobulin

IGF1 – Insulin-like growth factor 1

IL – Interleukin

I.m. - Intramuscular

iNOS - Inducible nitric oxide synthase

I.p. - Intraperitoneal

ISF – Interstitial fluid

I.v. - Intravenous

LPS – Lipopolysaccharide

KO – Knockout

MDD – Major depressive disorder

MDM – Monocyte-derived macrophages

MDMA - 3,4-methylenedioxy-methamphetamine

Meth - Methamphetamine

MGC – Mixed glial cell cultures

MGnD - Microglial neurodegenerative phenotype

mGluRs - Metabotropic glutamate receptors

MHC-II – Major histocompatibility complex-II

MIMs - Microglia inflamed in MS

mRNA – Messenger ribonucleic acid

MS – Multiple sclerosis

Nacc – Nucleus accumbens

NCM – Neuronal conditioned medium

NGF – Nerve growth factor

NK – Natural killer

NO – Nitric oxide

NT-3 – Neurotrophin 3

OLFML3 - Olfactomedin-like protein 3

PAMPs - Pathogen-associated molecular patterns

PBMCs – Peripheral blood mononuclear cells

PBS – Phosphate buffer saline

PD – Parkinson disease

PDL – Poly-d-lysine

PET – Positron emission tomography

PFA – Paraformaldehyde

PFC – Prefrontal cortex

PGE2 – Prostaglandins

PRRs – Pathogen recognition receptors

P2RY12 - P2Y purinoreceptor 12

P/S – Penicillin-Streptomycin

RNA – Ribonucleic acid

RNS – Reactive nitrogen species

ROS – Reactive oxygen species

RT-PCR – Real Time Polymerase Chain Reaction

SALL1 - Sal-like protein 1

SAS – Subarachnoid space

S.c. - Subcutaneous

SIGLECH - Sialic acid binding Ig-like lectin H

SIRPα - Signal regulatory protein alpha

SOCS3 - Suppressor of cytokine signalling 3

SVZ – Subventricular zone

TBI – Traumatic brain injury

T_{EM} cells - Effector memory T cells

TGF-β - Transforming growth factor-β

TLRs – Toll-like receptors

TMEM 119 - Transmembrane protein 119

TNF – Tumor necrosis factor

Treg – Regulatory T cells

TREM2 - Triggering receptor expressed on myeloid cells 2

Trk – Tyrosine kinase family

TSPO – Translocator protein

TSP-1 – Thrombospondin-1

UTP – Uridine triphosphate

VTA – Ventral tegmental area

WD - Withdrawal

YS – Yolk sac

Publications

Part of the results presented in this dissertation have been published in international peer-reviewed scientific journal:

- Bravo J., Ribeiro I., Terceiro A.F., Andrade E.B., Portugal C.C., Lopes I.M., Azevedo M.M., Sousa M., Lopes C.D.F., Lobo A.C., Canedo T., Relvas J.B., Summavielle T. Neuron-Microglia Contact-Dependent Mechanism Attenuate Methamphetamine Induced Microglia Reactivity and Enhance Neuronal Plasticity. Cells 11 2022. (Appendix I).

The following publications and book chapter were also obtained during the course of the candidate's doctoral thesis:

- Soares N.L., Paiva I., Bravo J., Queiroga C.S.F., Melo B.F., Conde S.V., Romão C.C., Summavielle T., Vieira H.L.A. Carbon Monoxide Modulation of Microglia Neuron Communication: Anti-Neuroinflammatory and Neurotrophic Role Molecular. Neurobiology 59 872-889 2022.

- Canedo T., Portugal C.C., Socodato R., Almeida T.O., Terceiro A.F., Bravo J., Silva A.I., Magalhães J.D., Guerra-Gomes S., Oliveira J.F., Sousa N., Magalhães A., Relvas J.B., Summavielle T. Astrocyte-derived TNF and glutamate critically modulate microglia activation by methamphetamine. Neuropsychopharmacology 46 2358-2370 2021.

- Brás J.P., Bravo J., Freitas J., Barbosa M.A., Santos S.G., Summavielle T., Almeida M.I. TNF-alpha-induced microglia activation requires miR-342: impact on NF-kB signaling and neurotoxicity. Cell Death and Disease 11 2020.

- Andrade E.B., Magalhães A., Puga A., Costa M., Bravo J., Portugal C.C., Ribeiro A., Correia-Neves M., Faustino A., Firon A., Trieu-Cuot P., Summavielle T., Ferreira P. A mouse model reproducing the pathophysiology of neonatal groupαB streptococcal infection. Nature Communications 9 2018.

Book Chapter

- Almeida A.C., Drpic D., Okada N., Bravo J., Madureira M., Maiato H. Functional dissection of mitosis using immortalized fibroblasts from the indian muntjac, a placental mammal with only three chromosomes. Methods in Molecular Biology 2101 247-266 2020.

Thesis Layout

This thesis is composed by six Chapters. In Chapter I is the general introduction, Chapter II describes the main goals of this thesis, Chapter III contains a systematic review of the literature, Chapters IV and V present the experimental work performed and Chapter VI comprehends the general discussion of this work. The systematic review of the literature included in Chapter III was submitted for publication and is under revision in the Frontiers in Cellular Neuroscience. The manuscript included in Chapter IV was published in a peer-reviewed scientific journal.

Chapter I presents a general introduction into the subjects that are part of this thesis, covering the immune function of the central nervous system, with particular focus in the immune cells responses to psychostimulants use.

Chapter II addresses de main goals of this dissertation.

Chapter III includes a systematic review of the literature regarding the state of the art of the cytokine profile and the peripheral-central immune crosstalk in different stages of drug addiction.

Chapter IV contains the research work conducted to dissect at molecular level the neuronal modulation of microglia activation by methamphetamine. This chapter is part of the publication entitled “Neuron-Microglia Contact-Dependent Mechanism Attenuate Methamphetamine Induced Microglia Reactivity and Enhance Neuronal Plasticity”, published on Cells journal.

Chapter V addresses the search for molecular critical players and pathways involved in different stages of the addictive process and its final validation as potential targets in addiction.

Chapter VI contains the general discussion, in which the major findings of this work are discussed in light of relevant literature and future perspectives are outlined for the remaining open questions.

CHAPTER I

General introduction

1. Immune function in the Central Nervous System

Under physiological conditions, the access to the central nervous system (CNS) by pathogens, circulating immune cells and other blood factors is tightly regulated [1]. This characteristic, which is considered an immune privilege, is attributable to several CNS tissue properties, including the endothelial blood brain barrier (BBB) and the epithelial blood-cerebrospinal fluid (CSF) barrier that regulate the transport of small molecules to CNS and restrict the entry of other macromolecules [2, 3]. However, under some circumstances, physiological conditions can be disrupted and the optimal functioning of the CNS may be compromised. Therefore, the CNS is continuously under immune surveillance in order to detect and eliminate potential infectious agents and damage, maintaining the homeostasis [1].

Whereas microglia, the brain resident immune cells, are the primary guardians of the brain, other peripheral immune cells are strategically located in specialized CNS compartments located outside the parenchyma [1, 4, 5]. Additionally, recent studies demonstrated that reciprocal communication between the CNS and the peripheral immune system also contributes to homeostasis [5].

CNS immune cell compartmentalization and its immune cells subsets

The CNS immune compartments contain infiltrating and resident immune cells residing both in the parenchyma and in nonparenchymal structures [5, 6]. The specialized immune compartments located outside the parenchyma are the choroid plexus (CP), the cerebrospinal fluid and the meninges [4, 5] **(Fig. 1)**.

Although other immune cells were identified in the brain parenchyma, microglia are clearly predominant [7, 8] **(Fig. 1A)**. Korin and colleagues demonstrated, using flow cytometry, that most of the infiltrating immune cells under homeostasis were located at meninges and CP (but not in the parenchyma) [7]. They found that the number of infiltrating cells in the parenchyma was approximately ten times lower when compared with the entire brain compartments (parenchyma, meninges and CP) [7]. It is important to note that by infiltrating cells, here, we are referring to immune cell populations present in the CNS, other than microglia.

Microglia are the resident myeloid cells in the CNS and therefore perform typical myeloid functions, such as sensing tissue damage and clearance of debris by phagocytosis [7, 9]. Beside these immune functions, microglia also have other important roles in the brain, such as in the neurogenesis [10], synaptic refinement [11] and synaptic plasticity [12].

The CP consist of a network of epithelial cells and blood vessels, which are located in the brain ventricles (one in each ventricle) and are responsible for producing the CSF [5, 13]. The CP provides an immunological interface between peripheral circulation and the CNS [13, 14]. Several immune cells, such as monocytes, neutrophils, natural killer (NK) cells, border- associated macrophages (BAM), dendritic, B and T cells, are present at the CP at steady state **(Fig. 1B)**. At the CP, dendritic cells (DC) are capable of presenting CNS antigens to effector memory T cells (T_{EM} cells) [5, 7, 15, 16].

The CSF is a clear watery fluid that baths the brain and provides some buoyancy for the CNS [17, 18]. It is produced by the choroid plexus of the lateral and fourth ventricles, flows through the lateral and third ventricles and reaches the subarachnoid spaces [19].

Under physiological conditions, 80% of the immune cells found in the CSF are T cells [1, 5] **(Fig. 1C)**. Small population of B cells, DCs, NK cells, neutrophils, monocytes and monocyte-derived macrophages (MDMs) were also found in the CSF of healthy individuals [5, 7] **(Fig. 1C)**. CSF also transports cytokines, hormones and neurotransmitters [17, 18].

The meninges consist of vascularized tissue membranes that envelop superficial CNS areas and enclose the parenchyma [14]. The meninges are composed of three layers, the inner layer is the pia mater, the middle layer or arachnoid mater (these two layers together constitute the leptomeninges) and the outer layer, the dura mater [14]. Lymphatic vessels are housed in the meninges, allowing the draining of soluble molecules derived from the brain parenchyma and CSF to the deep cervical lymph nodes (dcLNs) [20]. At steady state, the immune cells that are found in the meninges closely to the dural sinuses are DCs and BAMs, providing a local for antigen presentation to primed T_{EM} cells. In the dura mater, one can also detect regulatory T cells (Treg), γδ T cells, B cells, NK cells, monocytes, mast cells, neutrophils and plasma cells [5, 7] **(Fig. 1D)**. Importantly, dural T cells are able to modulate the CNS through the release of cytokines, which will affect parenchymal cells and impact on behavior control [21, 22].

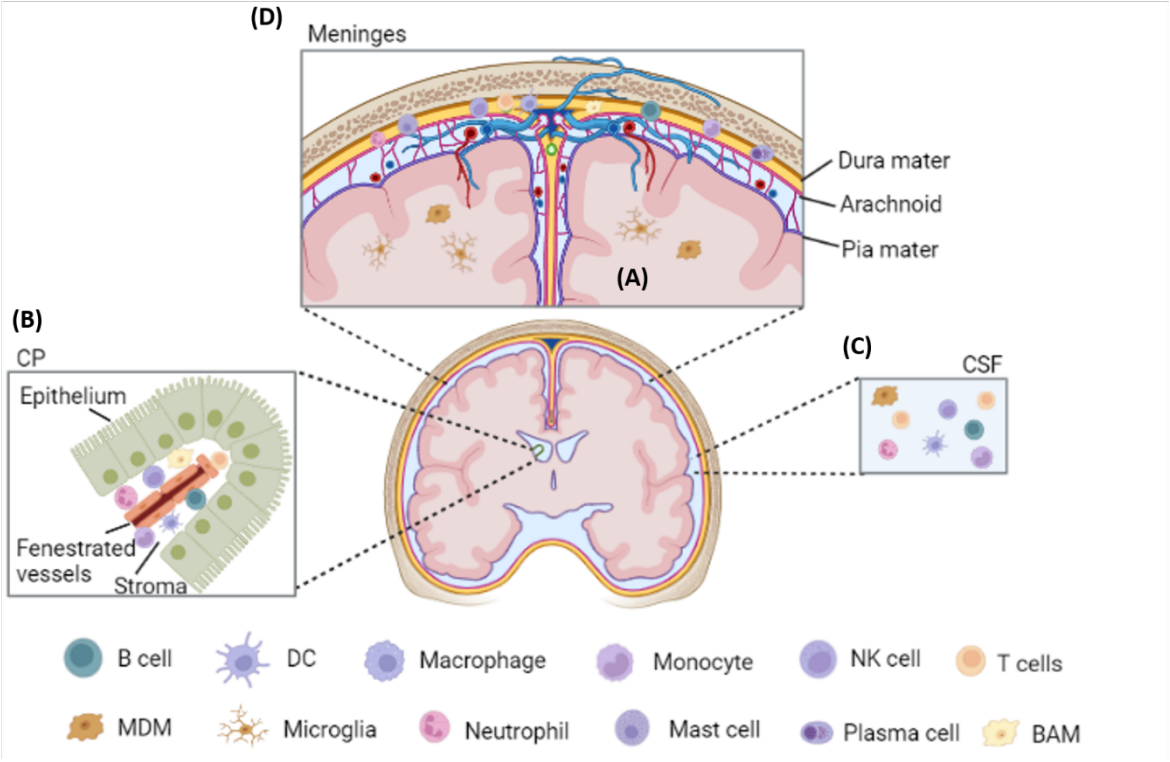

Figure 1: Immune cells in the CNS. The CNS immune cells reside in the parenchyma and in specialized compartments outside the parenchyma, the CP, CSF and meninges. **(A)** The predominant immune cells in the brain parenchyma is microglia. (B) At steady state monocytes, neutrophils, NK cells, BAM, dendritic, B and T cells are present in the stroma of the CP: **(C)** In the CSF, T cells are the predominant immune cells. In homeostasis, B cells, DCs, NK cells, neutrophils, monocytes and MDMs are also present in small proportions. **(D)** In the meninges, DCs and BAMS are present nearby dural sinuses. In the dura mater, T cells (Treg and γδ), B cells, NK cells, monocytes, mast cells, neutrophils and plasma cells are also found. Created in BioRender.com.

Immune cell trafficking to CNS

Although, immune cell migration into the CNS under physiological conditions is maintained at very low levels, during a variety of CNS pathological conditions, immune cells are able to cross the BBB and the CP to achieve the CSF spaces and/or the CNS parenchyma [3].
In physiological conditions, the access to the CNS by immune cells might occur through specific compartments in which the barrier properties and the vasculature itself are different from the BBB [23]. It is possible that immune cells entry into the CSF from blood across the fenestrated blood vessels of the choroid plexus [1, 23, 24]. Another possible route is the entry from blood to the subarachnoid space trough the perivascular or Virchow-Robin space, where meningeal blood vessels branch into the subarachnoid space [1, 24]. The

meningeal endothelial BBB in comparison with parenchymal BBB is more permissive to the entry of leukocytes, due to the lack of glia limitans astrocytic endfeet. Within these spaces, tight junctions might also be different from those present in the parenchymal vessels [3]. In addition, immune cells potentially may also gain access to parenchymal perivascular spaces through postcapillary venules that enter directly into the parenchyma [1, 23, 24]. In this route, immune cells need to migrate across the tightly regulated vascular endothelium [23]. Adhesion molecules might have an important role in this process [23].

Although the BBB structure limits the immune cells trafficking into CNS, is worth noting that even under physiological conditions, there are brain regions in which the tight junction barrier is reduced and consequently the number of immune cells surveilling those areas are higher [1, 4, 25]. Two examples are the area postrema of the circumventricular organs and the ventrorostral areas of the medulla oblongata [1, 4].

Upon to CNS injury, BBB integrity can be compromised due to endothelial cells and astrocytes activation, which may result in the reduction of tight junctions and in the formation of transendothelial cell channels, facilitating the migration of immune cells into the CNS [26-29]. Inflammatory cytokines are also able to disrupt BBB integrity and enhance the recruitment of leukocytes into CNS [30].

Lymphatic drainage from the CNS

Despite its role in immune surveillance, the CNS lymphatic system also has a role in waste clearance from the CNS [19]. Two extracellular fluids are associated with lymphatic drainage of the CNS, the interstitial fluid (ISF) in the CNS parenchyma and the CSF in the ventricles and in the subarachnoid space (SAS) [6, 31, 32]. The two fluids drain to lumbar and cervical lymph nodes, through different pathways [6]. The ISF and solutes from the CNS parenchyma drain along the walls of cerebral capillaries and arteries into cervical lymph nodes [6, 31]. The CSF drain to cervical lymph nodes or to lumbar lymph nodes, via the cribriform plate and nasal lymphatics or via spinal nerve roots, respectively [6, 33]. The drainage pathway for CSF allows the trafficking of immune cells, such as cluster of differentiation (CD) 4^+ T cells, monocytes and dendritic cells [34-36]. However, no evidence was found for direct immune cells drainage from parenchyma to the lymph nodes [31].

Additionally, the removal of macromolecules from CNS parenchyma may occurs via CSF-ISF exchange, also referred as the glymphatic system [19]. The exchange of CSF and ISF occurs at the brain surface, in which influx of CSF occurs through periarterial spaces and efflux through the paravenous spaces - back into the SAS [6, 19, 37]. ISF may also drain directly into the ventricular CSF from the periventricular white matter [38].

Communication between the CNS and the peripheral immune system

The communication between the CNS and the peripheral immune system takes place not only under a disease process, but also under homeostatic conditions [5, 39].

As described above, if on the one hand there are a few immune cells capable of entry into the CNS, on the other hand, the drainage of immune molecules and cells might occur from the CNS to the lymph nodes. Therefore, the communication between the immune system and the CNS is bidirectional and may occur through different ways.

Brain communication with the periphery can occur through the drainage of CNS antigens to the lymph nodes, via lymphatic vessels [5] **(Fig. 2A)**. These antigens, once inside the lymph nodes, might initiate an immune response [5].

Additionally, soluble factors from the CNS could reach the systemic circulation and peripheral organs **(Fig. 2B)**. One source of soluble mediators is the endocrine pathway, in which hormone release is mediated by the brain to the target peripheral tissues, via bloodstream [5, 40]. While in the target tissues, hormones impact on immune cells function and survival, and, in turn, peripheral inflammatory responses feedback to neurons responsible for hormone production [5, 40, 41].

The cytokines are also important players in the communication between the periphery and the CNS. The immune cells present in the CNS immunological niches produce cytokines that are able to modulate the cells in the CNS parenchyma. Although, it is not yet well established how cytokines reach the CNS parenchyma, there are a few studies showing that cytokines present at the meninges are capable of modulating neuronal activity and behavior [21, 22, 42]. Filiano and colleagues demonstrated that the interferon (IFN)-γ produced by meningeal T cells is crucial for social behavior in mice [22]. Moreover, another work from the same laboratory showed that meningeal γδ T cells regulate anxiety-like behavior via interleukin (IL)-17a [21].

Another important player in the bidirectional communication between the CNS and the periphery is the gut-brain axis [5] **(Fig. 2C)**. The nervous system innervates the gastrointestinal mucosa and many of these nerves appose local immune cells, forming neuroimmune cell units [43], that can be modulated by the gut microbiota, through bioactive neurotransmitters, and that ultimately are able to modulate the host nervous system activity and behavior and/or induce immunomodulatory effects [5, 44, 45].

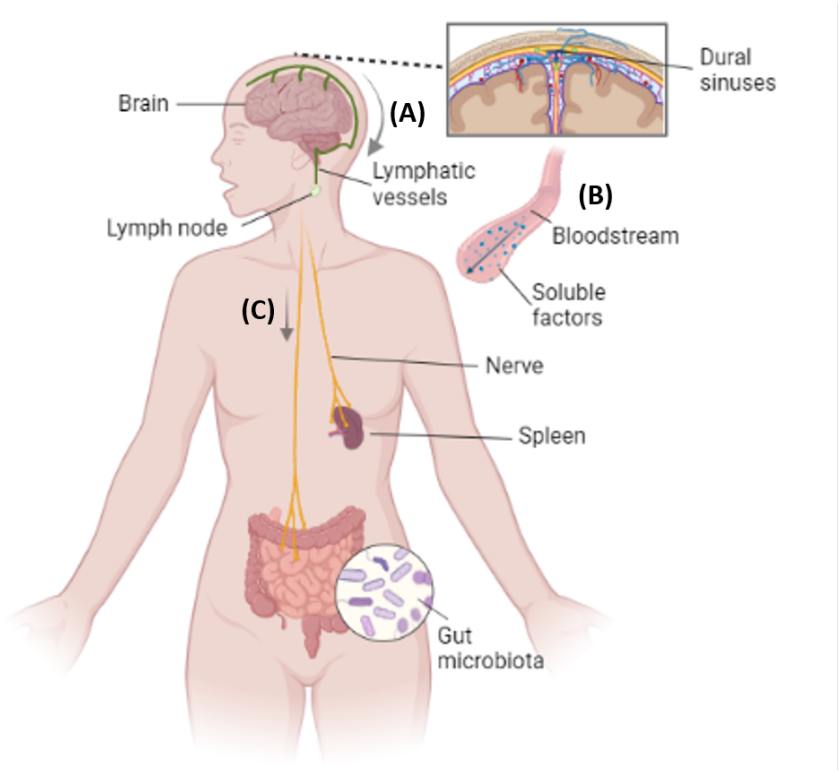

Figure 2: Communication between the CNS and the peripheral immune system. The communication between the CNS and the periphery can occur through: **(A)** the drainage of CNS antigens to the lymph nodes; **(B)** soluble factors that reach the systemic circulation and peripheral organs; and **(C)** the gut-brain axis, by CNS innervation of the gastrointestinal mucosa. Created in BioRender.com.

2. CNS infiltrating immune cells

Although several studies demonstrated that different lymphoid and myeloid populations are present in the parenchyma and boundaries of the brain, the infiltrating immune cells in the CNS comprises only specific immune cell populations [7]. Among the infiltrating cells the macrophages, monocytes, T- and B-lymphocytes are the most abundant cells in the CNS compartments [7]. Despite the importance of all infiltrating immune cells in the CNS, they will only be mentioned briefly, as they are not the main focus of the present study.

Different types of macrophages also referred as BAMs are present at the brain´s borders [46, 47]. Depending on their location, these macrophages are classified as perivascular macrophages, meningeal macrophages and CP macrophages [5]. As a consequence of their position at CNS barriers, BAMs may modulate the entry of immune cells and their

phenotype during inflammation [17]. Under a neuroinflammatory or neurodegenerative process, BAMs increase the expression of pro-inflammatory cytokines and are able to present antigens to circulating lymphocytes [5, 17, 48]. Moreover, BAMs support the BBB functionality and under homeostasis disruption are able to increase the permeability of pial and cortical blood vessels [5, 49, 50].

Infiltrating monocytes are capable of invading the brain and differentiate into MDMs [51]. In the context of injury, activated microglia may actively participate in monocyte recruitment [52, 53]. These immune cells have dual roles, contributing for CNS damage, while also supporting CNS repair [5]. Under certain circumstances, they act as anti-inflammatory mediators by producing of IL-10 [54], importantly participating in tissue repair and scar degradation, recruiting additional cells to the lesion site and removing apoptotic cells [5, 55-57].

Regarding lymphocytes, T cells are present in different CNS compartments and accordingly with their location, activation profile, number and persistence they can perform different functions [5, 58, 59]. Although, these immune cells are important for the control of pathogens, when excessively activated, T cells can contribute for neuroinflammation and neurodegeneration, through the release of pro-inflammatory cytokines [58-60]. Additionally, as mentioned above IFN-γ and IL-17a T-cells producers are crucial for normal social behavior and for the regulation of anxiety-like behavior, respectively [21, 22].

Lastly, B-lymphocytes numbers highly increase under CNS inflammatory processes and, depending on their functional state, are able to secrete IL-10 or tumor necrosis factor (TNF) [61]. Up on their function as antibody producers, these cells are also capable of secreting cytotoxic factors for oligodendrocytes, and releasing neurotrophins important for neuronal plasticity and neurogenesis [62, 63].

3. CNS resident immune cells - Microglia

In the CNS, astrocytes, oligodendrocytes, ependymal cells and microglia constitute glial cells population [64]. Microglia are the resident macrophages of the CNS and these cells are highly involved in brain homeostasis [65-67].

In the late nineteenth century Franz Nissl and W. Ford Robertson, using the Nissl staining, identified for the first time a different type of cells which were suggested to have mesodermal origin [66]. This was later supported by Ramon y Cajal. Pio Del Rio-Hortega introduced the term microglia in order to distinguish these cells, which presented phagocytic ability and migrating skills, from neuronal and astrocytic cells [66, 68].

Microglia represents around 10% of CNS total cells and are broadly distributed throughout the brain and the spinal cord [66, 69]. However, there are spatial heterogeneity regarding microglia density, morphology, turnover rate, molecular signatures, metabolism, clearance and ontogenesis (reviewed in [70]). There are also specie-specific differences in microglia number and distribution and sex-specific microglia phenotypes [66, 71].

Microglia cells are not only involved in the immune defense of the CNS and in the maintenance of its homeostasis, supporting tissue repair and remodeling, but are also involved in processes of CNS damage [66]. In the last years, the importance of microglia for the CNS development and its normal function has been extensively studied. Several studies demonstrated that these cells have fundamental roles in neurogenesis, mainly in neuronal differentiation and proliferation and are also involved in the formation and maturation of synaptic connections [72-74]. Microglia also contribute to the remodeling of post-natal neural circuits, through synaptic pruning and refinement [65, 74]. Additionally, several studies have shown evidences that some microglial states may contribute to the pathophysiology of several neurodegenerative diseases [69, 75, 76].

Microglia origin

The microglia ontogeny has been a matter of debate for many years, but now it is well established that microglia is a distinct macrophage population residing in the CNS with a well-defined development origin. The colonization of the CNS by microglial cells takes place before the formation of the neuroectodermally derived macroglia [77-79]. Using genetic fate mapping tools, several studies demonstrated that microglia derive from the yolk sac (YS), reside in the CNS throughout life and maintain their numbers trough a self-renewal process [80-84]. Additionally, microglia have the ability to completely restore their population in the adult brain. Elmore and colleagues demonstrated that less than 1% of microglial population was sufficient to restore the full microglia population 1 week after microglia elimination with colony stimulating factor 1 receptor (CSFR1) inhibitors [85].

The primitive hematopoiesis begins in the YS around embryonic stage E7 in mice and contributes to the generation of erythrocytes and tissue resident macrophages [86]. The definitive hematopoiesis, which takes place in aorta-gonad-mesonephros (AGM), replaces the primitive hematopoiesis around E10.5, giving rise to the progenitors that colonize the fetal liver [86, 87]. The primitive macrophages, which will originate microglia, initially appear in the blood islands of the YS [65, 66, 86]. The YS macrophages spread into the embryo through the blood after circulatory system has been established, around E8.5 to E10 and migrate to several areas, including the CNS [66, 88] **(Fig. 3)**. These cells enter into the brain

via the leptomeninges and lateral ventricles [79]. As referred most microglia migrate directly from the YS to the CNS, through the circulation, however De and colleagues demonstrated that a subpopulation of microglia that is Hoxb8+ has an alternative development [89]. These authors demonstrated that Hoxb8 microglia passage from the YS to the fetal liver before entering the developing brain at E12.5 [89]. Despite non-Hoxb8 microglia outnumber Hoxb8 microglia, they are not able to compensate the loss of Hoxb8 in Hoxb8 microglia [89].

After E11.5 the fetal liver serves as the major hematopoietic organ, but as the formation of BBB starts around E13.5, several authors suggested that it may isolate the developing brain from the contribution of fetal liver hematopoiesis for microglia population [66, 67]. Later, BBB isolates the CNS from potential contribution of bone marrow hematopoiesis to the microglial population [67] **(Fig. 3)**. The fetal macrophages have a high proliferative potential, so its numbers highly increase during the embryonic development and continue to increase also during early postnatal development [90, 91]. The proliferation declines progressively and is very low during the second postnatal week in rodents, maintaining a low level in the adult mature and healthy brain [92]. Concomitantly with the decrease of microglia proliferation, during the postnatal development, occurs microglial apoptosis, that overall contribute to microglia number reduction [92].

During development, microglial cells also follow migration pathways to colonize different brain layers. In a first phase, the cells have tangential migration, being distributed alongside to the surface in a uniform layer [65]. In a second phase the cells migrate radially, to reach all brain regions [65] **(Fig. 3)**. At early stages microglial cells have a morphology characteristic of immature cells that allows its migration, shown as amoeboid cells without or with few processes [93, 94]. After being located at their final destination, the cells gradually differentiate into ramified microglia [65]. In the adult brain, the microglia population is maintained in steady state, but during an inflammatory process they replicate, increasing in number [66]. Nevertheless, during an inflammatory process it is also possible that monocytes or other bone-marrow derived progenitor's are recruited, populating the cerebral tissue. It is not clear yet whether these cells are just temporary or if they become integrated in microglial population [66].

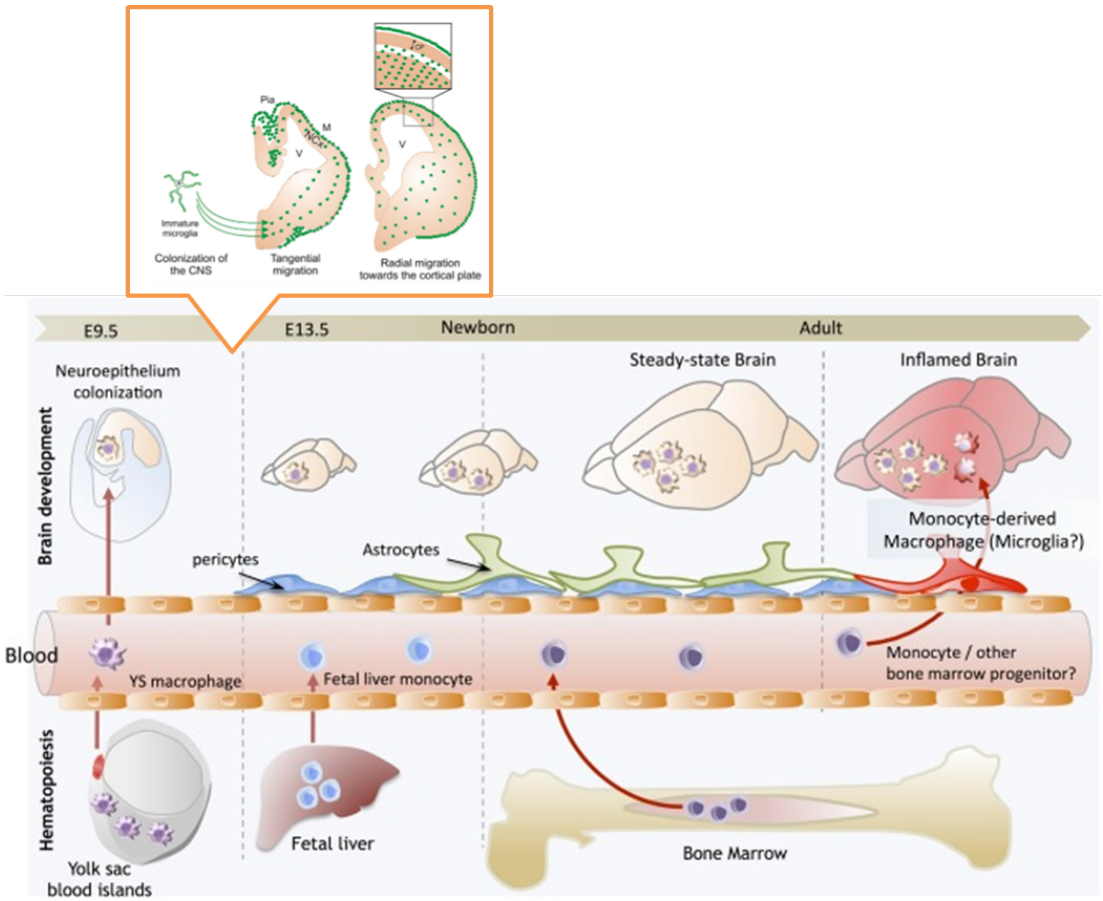

Figure 3: Development and establishment of microglia in the brain. Primitive macrophages exit at E9.5 from the yolk sac and colonize the neuroepithelium to give rise to microglia. Around E13.5 the BBB starts to be formed and may isolate the developing brain from the contribution of fetal liver hematopoiesis. The immature microglia to colonize the brain, first migrate tangentially, being distributed alongside to the surface and then the cells migrate radially, to reach all brain areas. Microglia proliferate during late gestation and post-natal development. During a brain injury, microglia proliferate and can also occur a recruitment of monocytes or other bone marrow-derived progenitors to supplement the microglial population. (Adapted from Ginhoux et al., 2013 and Mosser et al., 2017)

Homeostatic microglia

In a very recent publication, a group of multidisciplinary experts discussed the current understanding of microglial states and revised microglial nomenclature [95].

In agreement with these authors, the term “homeostatic” microglia used in this manuscript referred to microglia under physiological conditions. However, this does not necessarily

mean that microglia display a unique molecular profile. In fact, even in physiological conditions, microglia display several morphological and functional states, that are context-, space- and time-dependent. Taking this in mind and not willing to oversimplify, some general features of homeostatic microglia are described below. However, this does not mean that these characteristics are exclusive of homeostatic microglia.

In the mature healthy CNS, microglia display very active immune surveillance. These cells, in homeostatic conditions, are often characterized by a ramified morphology, with small cell body largely sessile with thin and long processes [96, 97]. Although this commonly ramified morphology, microglia can undergo massive and rapid morphological remodeling to engage with other CNS elements for synaptic pruning and clearance of tissue debris, not only, but also under physiological conditions [98]. Moreover, despite most brain regions present microglia with a ramified morphology, there are some morphological variations between them [70]. For instance, the cerebellum contains microglia with lower ramification complexity, when compared with the striatum, hippocampus and PFC [99]. Microglia in regions like circumventricular organs (CVOs) and subventricular zone (SVZ), displayed an amoeboid morphology under physiological conditions in adult mice [100, 101]. Additionally, older animals occasionally contain dystrophic, senescent, and gitter cell-like microglia [98].

Under physiological conditions, *in vivo* imaging studies demonstrated that microglia are highly motile, moving around surveilling the environment, under a continuous cycle of extension, retraction and formation of new processes [97, 102, 103]. In addition, Bernier and colleagues also demonstrated that microglia extend and retracts fine filopodia from the tip of the large processes to efficiently surveil the brain parenchyma [104]. In this study, it was shown that filopodia extensions and retractions occurred in random-direction pattern that was not aligned with the overall direction of an individual process, which suggest that filopodia are constantly searching for cues during the surveillance process [104]. Microglia filopodia allow increased surveillance, since amplify the number of contacts of microglia with neighboring cells and also amplify the number of exposed microglia receptors [104]. The homeostatic surveillance behavior of microglia is therefore, performed on two scales: large movements by processes and nanoscale probing by filopodia [104].

Due to its origin, microglia express several macrophages associated markers, such as CSF1R, fractalkine receptor (CX3CR1), cluster of differentiation-14 (CD14), integrin (CD11b), CD45, major histocompatibility complex-II (MHC-II) and the ionized calcium-binding adapter molecule 1 (Iba1) [105]. However, microglia in homeostatic conditions have distinct expression levels of CD45 and MHC-II, and if compared with brain macrophages, present lower levels of these molecules [106].

Additionally, some specific microglial markers were identified, such as transmembrane protein 119 (TMEM 119), Sal-like protein 1 (SALL1), P2Y purinoreceptor 12 (P2RY12), sialic acid binding Ig-like lectin H (SIGLECH), G protein coupled receptor 34 (GPR34), suppressor of cytokine signalling 3 (SOCS3), β-hexosaminidase subunit β (HEXb), olfactomedin-like protein 3 (OLFML3) and Fc receptor-like S, scavenger receptor (FCRLS) [107-110].

Many of the markers referred above are expressed either by microglia in homeostasis and in diseased states. However, the amount of protein levels can change due to the alteration of microglia homeostatic state and this enables the recognition of microglia profile, using a semi-quantitative analysis of more than one marker [105]. For example the homeostatic microglial signature markers are lost during the course of many diseases [110].

In the healthy brain, microglia are maintained in a homeostatic state by the signaling of the neighboring cells and by autocrine production of several factors [64]. Neurons, astrocytes and microglia locally release soluble factors such as neurotrophins, anti-inflammatory cytokines and prostaglandins that are important for the maintenance of microglia homeostasis [102]. Some of the neurotrophic factors secreted by microglia are insulin-like growth factor 1 (IGF1), nerve growth factor (NGF), transforming growth factor-β (TGF-β) and brain-derived neurotrophic factor (BDNF) [111]. They also express reduced levels of CD46, MHC-II and CD11b, which is also important to maintain the cells in a homeostatic state [112]. Moreover, the continuous crosstalk between microglia and neurons is required for microglia surveillance state and consequently contributes to brain homeostasis. As mentioned above, besides the key role of microglia in CNS immunity, these cells have important functions in sculpting neuronal connections. To enable microglia to execute their functions, they need to sense neuronal activity and therefore the microglia-neuron crosstalk communication is required.

Microglia states in disease

In order to efficiently perform its immune function, microglia express pathogen recognition receptors (PRRs), that sense signaling pathways activated or released by surrounding cells [113]. These PRRs are classified as pathogen-associated molecular patterns (PAMPs) and damage-associated molecular patterns (DAMPs), due to its affinity for molecules associated with pathogens or cellular damage, respectively [113].

After detection of harmful stimuli, microglia rapidly respond in accordance to the damage-signal received adopting an appropriated profile. Upon some stimuli, microglia have the ability to synthesize a broad spectrum of pro- and/or anti-inflammatory cytokines [114]. They

also undergo cytoskeletal rearrangements that alter the pattern of receptor expression and also alter their morphology, an important characteristic for cell motility and phagocytic ability [115]. Furthermore, microglia are able to upregulate many cell surface receptors, such as toll-like receptors (TLRs), phagocytic receptors (CR3 and CR4), scavenger receptors (CD36, CD91) and release several complement factors, a variety of factors such as ROS, reactive nitrogen species (RNS) and excitatory aminoacids [116-118].

Similarly to macrophages, microglia were also classified, for several years, in two different activation phenotypes, defined as classical activation or M1 phenotype and alternative activation or M2 phenotype [64]. In the M1 or pro-inflammatory phenotype, microglia used to be described as amoeboid cells with hypertrophic cell bodies, and shorter, thicker and fewer processes compared to the homeostatic state, with increased phagocytic capacity [119]. Moreover, in this characterization was described that microglia would release pro-inflammatory cytokines, such as TNF, IL-1, IL-6, IL-12 and IL-23. Contrary, in the M2 or anti-inflammatory profile microglia used to be characterized by hypertrophic bodies with thick and ramified processes, and a higher level of F-actin compared to the pro-inflammatory stage [119, 120]. Additionally, M2 microglia classically were associated to the release of anti-inflammatory cytokines such as IL-4, IL-5 IL-10, IL13 and TGF-β and has higher expression of arginase-1 (Arg1) [112]. However, this oversimplification is not suitable for the current state of knowledge, the use of single-cell technologies provided evidences that microglia often co-express M1 and M2 markers [95]. Moreover, based on microglia morphology and gene expressing signature, several altered microglial states have been described in diseased human brain and in animal models of brain diseases.

Using single cell ribonucleic acid (RNA) sequencing several studies identified different microglial transcriptional signatures in development, aging and in neurodegenerative diseases, such as Alzheimer disease (AD), Parkinson disease (PD), amyotrophic lateral sclerosis (ALS) and multiple sclerosis (MS) [121-125]. Some examples of these states are the disease-associated microglia (DAM) [121], microglial neurodegenerative phenotype (MGnD) [122], activated response microglia (ARM) [123] and microglia inflamed in MS (MIMS) [125]. One of microglial states that was initially identified in a mouse model of AD that expresses five human familial AD gene mutations (5xFAD) was the denominated disease-associated microglia (DAM) subtype [121]. DAM downregulate the unique transcriptional microglia signature and up-regulates genes like Lpl, Itgax, Apoe and Cst7, among many others [121]. The expression of genes encoding surface proteins like CD11c, MHCII, CD44, CD14, CD86, CD39, CD90 and CD274 is also increased in DAM, and this has been validated at protein level by mass cytometry [46, 126, 127]. Additionally, Keren-Shaul and colleagues indicate more diverse states during disease progression, grouping DAM into two different stages, the DAM stage 1 and 2 [121]. DAM are regulated through a

two-step mechanism, the shift from homeostatic state to DAM1 is triggering receptor expressed on myeloid cells 2 (TREM2)-independent, while the transition from DAM1 to DAM is TREM2-dependent [121]. Once DAM signature has been engaged, certain upregulated molecules might form an autocrine or paracrine loop to sustain it [127]. Further analysis identifies DAM in another mouse model of neurodegenerative disease, namely, ALS [121]. The large spectrum of diseases in which DAM is present, suggest that this microglia state appear in response to several challenges, which could mean that the same microglia state represents a benefit in certain contexts and might be detrimental in others. Taken this into consideration, a more comprehensive characterization of microglia in homeostasis and disease will benefit from the use of integrative methodological approaches and functional studies [95]. Ultimately, a better characterization of microglia states will be helpful to develop appropriate therapeutic strategies for neurodegenerative diseases. Ideally, the DAM concept should evolve to recognize that different diseases will display its own DAM signature.

4. Crosstalk between microglia and neurons in physiological conditions

The acquisition of different functions by microglia is regulated by intercellular interactions with neurons, astrocytes, oligodendrocytes, the blood brain barrier and T-cells infiltrating the CNS [128, 129]. Regardless the importance of all of these cell-to-cell interactions, as one of the key objectives of the present work was to better understand the crosstalk between microglia and neurons, this section will be focused in this interaction.

As previously mentioned, in the healthy brain the maintenance of homeostatic microglia is highly dependent on the dynamic crosstalk between neurons and microglia. Taking this into consideration, it has suggested that the inhibition of microglia-neuron crosstalk represents a type of “danger-signal” for microglia, leading to alterations in microglia state and function. There is large evidence that the reciprocal communication between neurons and microglia is mediated by contact-dependent mechanism, by several soluble factors, such as neurotransmitters, neuromodulators and neuropeptides, and by extracellular vesicles (EVs) [129-132].

Microglia-neuron communication through contact dependent mechanisms

Under physiological conditions, neurons have the ability to maintain microglia in a homeostatic state by releasing neuronal factors and through contact-dependent mechanisms; some of these neuronal factors are fractalkine, CD200, CD47, CD95 and CD22 **(Fig. 4A)**.

Fracktalkine, also known as CX3CL1, is the only chemokine that is constitutively expressed in neurons and signals to microglia through its receptor CX3CR1 [133, 134]. Although, CX3CL1 has been placed in this topic about microglia-neuron communication through contact dependent mechanism, in fact CX3CL1 can communicate with its receptor as membrane-bound into neurons or can be cleaved from it and communicate through the extracellular space [135]. These two ways of communications seem to have different functions, while when this molecule is anchored to the neuronal membrane is important for cell adhesion, in its soluble form acts as chemo-attractant, stimulating the recruitment of inflammatory cells [129, 136]. The CX3CL1-CX3CR1 signaling, between neurons and microglia has an important role in the regulation of synapses formation during the development and in synaptic plasticity in the adulthood (reviewed in [129]). In normal brain development, the CX3CL1 signaling was associated with microglial pruning of dendritic spines [74]. The absence of CX3CR1 receptor in microglia results in a reduction of synaptic pruning during development, affecting synaptic refinement [137, 138]. Moreover, a weakened signaling between CX3CL1-CX3CR1 in the adult brain affects synaptic transmission efficiency [138]. At behavior level, it was demonstrated that CX3CL1-CX3CR1 signaling plays an important role in learning and memory, once CX3CR1 knockout (KO) mice present deficits in associative learning and in hippocampal-dependent memory formation [138, 139]. In disease, it was demonstrated that maintaining or enhancing the communication between neurons and microglia through CX3CL1-CX3CR1 is neuroprotective in several PD rodent models [140-142]. Additionally, was found that the CX3CL1 signaling also plays variable roles in AD [129]. Interestingly, the level of soluble fracktalkine in plasma is inversely correlated with AD severity; its levels are higher in patients with mild to moderate pathology than in severe ones [143].

Another important molecule involved in the neuroimmune system in brain that has been highly studied is CD200 (OX2). CD200 is a glycoprotein expressed on the membrane surface of neurons, astrocytes and oligodendrocytes, which interacts with microglia or macrophages through the CD200 receptor (CD200r) [144-146]. When neurons interact with microglia through CD200-CD200r, microglia is maintained in a homeostatic state. CD200-deficient mice display severe progression of neuroinflammation [147]. In these mice,

microglial cells have an amoeboid-like shape, are less ramified and display shorter processes when compared with wild-type animals. Additionally, CD200-KO mice also have elevated levels of TNF and inducible nitric oxide synthase (iNOS) [148]. In addition, it was shown that antibody-mediated blockade of CD200R results in an increase of dopaminergic neuronal death in primary co-cultures of neurons and microglia [149]. CD200 overexpression decreases the accumulation of microglia in the CNS [150]. Moreover, defaults in CD200 signaling have been observed in several brain diseases, such as MS, PD and AD, and the same was also observed in aged brain [151-153]. In a 6-hydroxydopamine-induced rat model for PD, a blockade of CD200-CD200R interaction results in microglial activation, with TNF and IL-6 production [154]. Also, CD200/CD200r signaling was shown to be involved in the spontaneous recovery of synaptic plasticity after stroke via the inhibition of microglia activation and reduction of inflammatory factors release [155]. In animal models of Alzheimer´s disease, restoration of neuronal CD200 improved cognitive function and prevented further synaptic impairment [156].

CD47 is a receptor that belongs to the immunoglobulin (Ig) superfamily and are broadly expressed on cell membranes. CD47 and its receptor, the signal regulatory protein alpha (SIRPα) are possible co-expressed on a similar cell and their interaction could mediate the inter-cellular signaling in a bi-directional manner [157]. This pair of ligand-receptor was observed on the neuronal surface; whereas SIRPα was found on dendrites and axons, CD47 expression was limited to dendrites [157]. In microglia, the co-localization of CD47 and SIRPα has been described [158].

On neurons, CD47 is highly expressed on synapses and its expression is important in down-regulating immune responses in CNS [131]. The interaction between neurons and microglia, through CD47-SIRPα was demonstrated to regulate microglial phagocytosis, functioning as a “don´t-eat-me” signal [159-161]. Lehrman and colleagues showed that CD47-SIRPα signaling prevents excess microglial phagocytosis during developmental synaptic pruning [159]. Similarly, it was also demonstrated that microglial SIRPα regulates synaptic pruning in neurodegenerative conditions [160]. In AD pathology, microglial SIRPα signal is disrupted, resulting in excessive synapses elimination and increased cognitive impairment [160]. The down-regulation of CD47 in chronic MS was associated with microglia state alteration and may contribute to a proinflammatory predisposition in the area surrounding chronic active lesions [162]. Moreover, it was demonstrated that CD47 also reduces inflammation by interacting with thrombospondin-1 (TSP-1), leading to microglia apoptosis via CD95/CD95L pathway. CD95L (FasL) is expressed in neurons and is involved in the apoptosis of activated microglia, through the interaction with the receptor CD95 [163].

CD22 is another molecule that has been implicated in the regulation of immune responses by microglia. This molecule mediates neuron binding to microglia through CD45, which was already shown to prevent the LPS-induced microglial production of TNF [164].

Soluble factors mediating neuron-microglia bidirectional-communication

Neurons are able to modulate microglia state through the release of immune-related soluble factors that bind to cognate receptors on microglia. Some of those soluble factors are neurotrophins, neuropeptides, neurotransmitters, cytokines and chemokines [129, 161, 165]. In return, microglia influence and modulate neuronal function by the release of soluble factors, including cytokines, prostaglandins and neurotrophic factors, which bind to neuronal receptors [129] **(Fig. 4A)**.

The neurotrophins released by neurons act on microglia through their receptors that include the receptor tyrosine kinase family (TrkA, TrkB, and TrkC) and a receptor called p75 [130]. In hippocampal slice cultures, it was demonstrated that MHCII expression in microglia can be inhibited by specific neurotrophic factors, such as NGF, BDNF and neurotrophin 3 (NT-3) through the p75 [166]. Furthermore, NT-3 released by neurons has anti-inflammatory properties by decreasing the levels of IL1-β, TNF, iNOS and nitric oxide (NO) and by reducing the phagocytic activity (as seen after stimulation of microglia with lipopolysaccharide (LPS)) [130].

Among the neurotransmitters that have modulatory effects on microglia profile, the neurotransmitter glutamate is involved in this process via glutamate receptors, such as the metabotropic receptors [167]. At least mGlu2, mGlu3, mGlu4 and mGlu5 are expressed by microglia and these metabotropic glutamate receptors (mGluRs) subtypes have the ability to modulate microglial function differently. For example mGluRs that are part of group II, modulate microglia in different ways. The activation of mGlu2R in microglia results into a pro-inflammatory cytokine release, whether the activation of mGlu3R drives microglia to an anti-inflammatory state [168-170].

The purinergic system is also highly involved in the modulation of the microglia state [161]. Damaged or overactive neurons release or leak purines, including adenosine triphosphate (ATP) and uridine triphosphate (UTP) that will interact with microglial cells through its cognate receptors. There are several purinergic receptors in microglia, P2X4 and P2X7 are highly expressed, but P2Y2, P2Y6 and P2Y12 are also present in microglia [171]. It was demonstrated in mice that the extension of microglia processes in response to neuronal death is modulated by ATP through P2Y12. Also, P2Y6, which is involved in microglial phagocytosis, is upregulated after neuronal damage [172].

Some chemokines seem to be associated with attracting signals of microglia towards damaged neurons. At least, C-C Motif Chemokine Ligand 2 (CCL21) and CXCL10 are able to induce microglia migration, *in vitro* [173, 174]. Impaired migration and microglial activation were described in chemokine-deficient or chemokine-deficient-receptor animals [175].

In the opposite direction, microglia often released cytokines, such as IL-1β and TNF, prostaglandins (PGE2) and BDNF, which interact with neurons through its respective receptors [129].

The neurotrophin, BDNF, which is highly relevant in the bidirectional communication between microglia and neurons, has been related with several diseases [129]. Alterations in its gene have been pointed out as a responsible for the etiology of schizophrenia [176]. Moreover, this neurothrophin has also been linked to depression [177-179]. Ye and colleagues demonstrated that the infusion of BDNF partially reverse the depressive-like behavior in a rat model of chronic stress-induced depression [179].

Cytokines are also important modulators of the communication between microglia and neurons [180]. Several cytokines are expressed at low levels in the CNS, under physiological conditions, with important functions on the modulation of brain plasticity [181]. One example is the IL-6 family, which is involved in broad physiological functions, such as development and maturation of the brain [182]. Nevertheless, these signaling pathways when upregulated can mediate neurotoxicity [181].

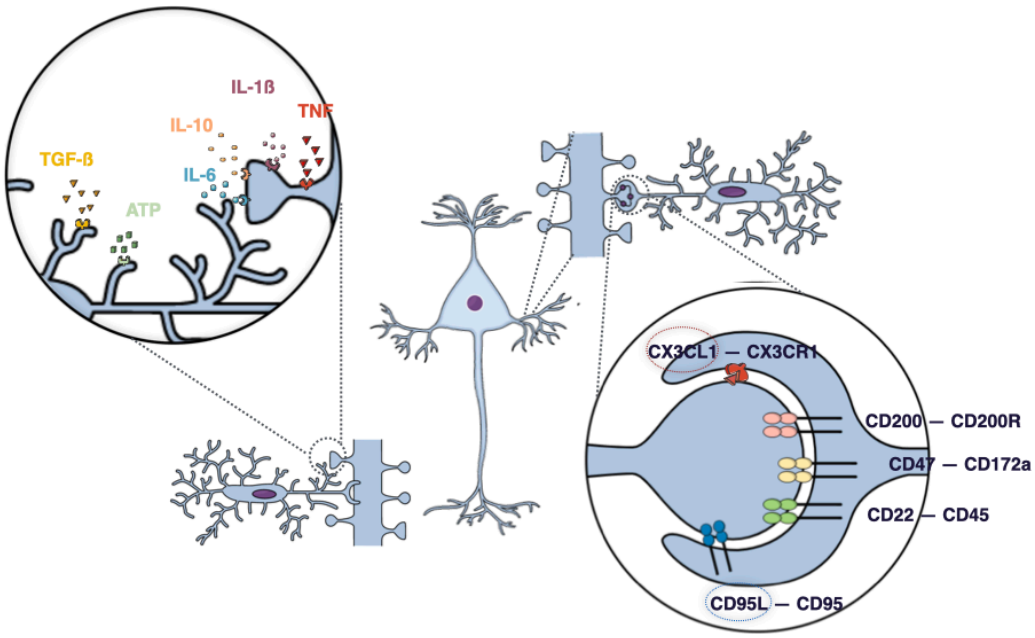

Figure 4: Microglia-neuron communication through contact-dependent mechanisms and soluble factors. (A) Under physiological conditions, neurons have the ability to maintain microglia in a homeostatic state through contact-dependent mechanisms. Some of those immune pairs are CD200-CD200r; CX3CL1-CX3CR1; CD47-Sirpα; CD95L-CD95 and CD22-CD45. **(B)** Neurons are also able to modulate microglia through soluble factors, such as cytokines.

Microglia-neuron communication by extracellular vesicles

Another type of bi-directional communication between microglia and neurons by contact-independent mechanism is through EVs, comprising ectosomes and exosomes (reviewed in [183]). These vesicles carry specific proteins, messenger ribonucleic acid (mRNA) and microRNA that in normal conditions have biological roles, but during a disease process the content of vesicles may switch to triggering inflammatory reactions [184]. Not only microglia and neurons communicate through these vesicles, but also astrocytes and oligodendrocytes [184, 185]. Due to their ability to diffuse, microglia-derived extracellular vesicles represent an efficient way to modulate the activity of neighboring microglial population as well as of different cell types in the surrounding environment [183].

At physiological level, EVs are able to modulate synaptic transmission, through the enhancement of sphingolipid metabolism [186]. It was demonstrated *in vitro* and *in vivo* that such enhancement positively affects the excitatory neurotransmission [186]. Additionally, EVs are also able to modulate synaptic transmission through the modulation of the endocannabinoid system [187]. EVs secreted by microglia carry the endocannabinoid *N*-arachidonoylethanolamine (AEA), which stimulates the type-1 cannabinoid receptors (CB1) present in GABAergic neurons, inhibiting presynaptic transmission [187].

EVs are also associated with neurodegenerative conditions. Among the contents of EVs, toxic protein aggregate such as α-synuclein, tau and amyloid beta (Aβ) were identified [188-190]. Several studies demonstrated that EVs may be responsible for the distribution of those protein aggregates, spreading AD disease [188-191]. Moreover, the shedding of microglia derived-EVs were observed after traumatic brain injury (TBI), ischemic stroke, spinal cord injury and in neuropathic pain [192-195].

This of course, does not exclude a role for tunneling nanotubules in also spreading these and other molecules, and in possibly contributing to cell-to-cell communication, which is still mostly unexplored [196].

5. Immune cells response in psychostimulants abuse

Addiction is a chronic complex disease characterized by compulsive drug seeking despite the harmful consequences. The latest World Drug Report estimated that in 2020, 284 million people worldwide aged 15–64 had used psychoactive substances within the last 12 months. The same report estimates the existence of 35.6M of problematic drug-users. Cannabis remains the most commonly used drug at global level, followed by opioids and by psychostimulant drugs, such as amphetamines, cocaine and ecstasy.

Despite the harmful consequences of drug abuse, successful treatments remains elusive. Treatments currently approved, primarily act on withdrawal symptoms reduction via partial receptor stimulation or act to prevent drug reinforcement through receptor inhibition [197]. Although these treatments are able to reduce drug cravings and promote abstinence, the relapse rates are even higher in people receiving such treatments.

The research that have been conducted for many years revealed distinct neural mechanisms involved in drug addiction disease [197]. Among psychostimulant drugs, it was demonstrated that methamphetamine (Meth) leads to dopaminergic system impairment, oxidative stress, mitochondrial dysfunction, BBB dysfunction and glutamate excitotoxicity [198-200]. More recently, growing evidence showed that immune cells within the CNS and in the periphery are able to modulate brain plasticity and behavior, suggesting that central and peripheral immune cells may be affected by drug use and may be involved in drug addiction progression [201-203].

At central level, psychostimulants have been described to induce microglia reactivity. Regarding Meth, it was demonstrated in animal models that this psychostimulant induces morphologic alterations in microglia and promote the release of pro-inflammatory cytokines in several brain regions [204, 205]. Recently, our group has shown that a binge administration of Meth leads to microgliosis and microglia activation in a process mediated by astrocytes *via* glutamate release in a TNF/IP_3R2-Ca^{2+}- dependent manner [206]. Additionally, cocaine was also reported to induce microgliosis in the nucleus accumbens (Nacc) [207]. In humans, the existent data is yet scarce. In abstinent Meth users, microgliosis was shown by positron emission tomography (PET) in different brain regions, such as the striatum, subsisting over long periods of abstinence [208, 209]. In abstinent cocaine abusers, however, PET imaging revealed no microgliosis in cortical and subcortical brain regions [210]. Lacagnina and colleagues suggested that these data discrepancies could be due to methodological or pharmacological differences related with the mechanisms triggered by each substance [211]. More recently, employing a second-generation translocator protein (TSPO) probe for estimating microglial status, Rathitharan and colleagues reported no evidence of microglia activation in chronic Meth users [212].

At the peripheral level, Meth impairs both innate and adaptive immunity, affecting macrophages, granulocytes, DCs, T cells, B cells and NK cells (reviewed in [213, 214]).
In mice, chronic Meth administration affects multiple subsets of immune cells, causing a reduction in absolute numbers and proportion of splenic NK cells, Gr-1(Ly-6C)^{high} monocytes/macrophages and DCs, which seems suggestive of immune suppression [215]. Similarly, Meth administration in mice altered cell distribution in thymus and spleen and modulates peripheral T-cell populations [216, 217]. Meth administration compromised T-cell function, diminishing the ability of T cells to control pathogens [218]. Additionally, Meth induces apoptosis of thymic and splenic lymphocytes [215, 219].
Available data also showed that cynomolgus monkeys administered with a single dose of Meth showed elevated activity of NK cells, 6h after the administration. However, 24h after the administration NK cells were reduced in 50%, compared with control animals [220]. Similarly, but in mice models, both single and repeated Meth dosing decreased splenic NK cells. Of note, this Meth effect in NK cells seems to occur particularly in females [221].
It was also reported that, in rodents, Meth alters antibody production by B cells during infection or antigenic challenge [216, 222]. Accumulating evidence indicates that psychostimulants, in particular Meth, exerts immunosuppressive effects at peripheral level, exacerbating infectious pathologies and increasing the risk of coinfections by drug users. Human immunodeficiency virus (HIV) pathogenesis usually presents a more severe profile in Meth users. Studies suggest that Meth increases immune cell dysfunction, facilitating HIV spread and exacerbating neurological complications associated with HIV infections [223].
Altogether, this demonstrates that psychostimulants exert a relevant effect in the peripheral-brain axis and dysregulate several tissue types. As such, understanding how exposure to psychostimulants impacts on the crosstalk between peripheral and central immune players, and how this may affect brain function and behavior, may be highly relevant to devise novel therapeutic approaches for addiction.
This subject will be further detailed in Chapter III.

References

1. Ousman, S.S. and P. Kubes, *Immune surveillance in the central nervous system.* Nat Neurosci, 2012. **15**(8): p. 1096-101.
2. Forrester, J.V., P.G. McMenamin, and S.J. Dando, *CNS infection and immune privilege.* Nat Rev Neurosci, 2018. **19**(11): p. 655-671.
3. Engelhardt, B., *Regulation of immune cell entry into the central nervous system.* Results Probl Cell Differ, 2006. **43**: p. 259-80.
4. Hickey, W.F., B.L. Hsu, and H. Kimura, *T-lymphocyte entry into the central nervous system.* J Neurosci Res, 1991. **28**(2): p. 254-60.
5. Croese, T., G. Castellani, and M. Schwartz, *Immune cell compartmentalization for brain surveillance and protection.* Nat Immunol, 2021. **22**(9): p. 1083-1092.
6. Engelhardt, B., P. Vajkoczy, and R.O. Weller, *The movers and shapers in immune privilege of the CNS.* Nat Immunol, 2017. **18**(2): p. 123-131.
7. Korin, B., et al., *High-dimensional, single-cell characterization of the brain's immune compartment.* Nat Neurosci, 2017. **20**(9): p. 1300-1309.
8. Pasciuto, E., et al., *Microglia Require CD4 T Cells to Complete the Fetal-to-Adult Transition.* Cell, 2020. **182**(3): p. 625-640 e24.
9. Prinz, M. and J. Priller, *Microglia and brain macrophages in the molecular age: from origin to neuropsychiatric disease.* Nat Rev Neurosci, 2014. **15**(5): p. 300-12.
10. Monje, M.L., H. Toda, and T.D. Palmer, *Inflammatory blockade restores adult hippocampal neurogenesis.* Science, 2003. **302**(5651): p. 1760-5.
11. Stephan, A.H., B.A. Barres, and B. Stevens, *The complement system: an unexpected role in synaptic pruning during development and disease.* Annu Rev Neurosci, 2012. **35**: p. 369-89.
12. Parkhurst, C.N., et al., *Microglia promote learning-dependent synapse formation through brain-derived neurotrophic factor.* Cell, 2013. **155**(7): p. 1596-609.
13. Lun, M.P., E.S. Monuki, and M.K. Lehtinen, *Development and functions of the choroid plexus-cerebrospinal fluid system.* Nat Rev Neurosci, 2015. **16**(8): p. 445-57.
14. Shechter, R., et al., *Recruitment of beneficial M2 macrophages to injured spinal cord is orchestrated by remote brain choroid plexus.* Immunity, 2013. **38**(3): p. 555-69.
15. Baruch, K., et al., *CNS-specific immunity at the choroid plexus shifts toward destructive Th2 inflammation in brain aging.* Proc Natl Acad Sci U S A, 2013. **110**(6): p. 2264-9.

16. Baruch, K. and M. Schwartz, *CNS-specific T cells shape brain function via the choroid plexus.* Brain Behav Immun, 2013. **34**: p. 11-6.
17. Prinz, M. and J. Priller, *The role of peripheral immune cells in the CNS in steady state and disease.* Nat Neurosci, 2017. **20**(2): p. 136-144.
18. Whedon, J.M. and D. Glassey, *Cerebrospinal fluid stasis and its clinical significance.* Altern Ther Health Med, 2009. **15**(3): p. 54-60.
19. Raper, D., A. Louveau, and J. Kipnis, *How Do Meningeal Lymphatic Vessels Drain the CNS?* Trends Neurosci, 2016. **39**(9): p. 581-586.
20. Norris, G.T. and J. Kipnis, *Immune cells and CNS physiology: Microglia and beyond.* J Exp Med, 2019. **216**(1): p. 60-70.
21. Alves de Lima, K., et al., *Meningeal gammadelta T cells regulate anxiety-like behavior via IL-17a signaling in neurons.* Nat Immunol, 2020. **21**(11): p. 1421-1429.
22. Filiano, A.J., et al., *Unexpected role of interferon-gamma in regulating neuronal connectivity and social behaviour.* Nature, 2016. **535**(7612): p. 425-9.
23. Wilson, E.H., W. Weninger, and C.A. Hunter, *Trafficking of immune cells in the central nervous system.* J Clin Invest, 2010. **120**(5): p. 1368-79.
24. Ransohoff, R.M., P. Kivisakk, and G. Kidd, *Three or more routes for leukocyte migration into the central nervous system.* Nat Rev Immunol, 2003. **3**(7): p. 569-81.
25. Huber, J.D., R.D. Egleton, and T.P. Davis, *Molecular physiology and pathophysiology of tight junctions in the blood-brain barrier.* Trends Neurosci, 2001. **24**(12): p. 719-25.
26. Stamatovic, S.M., R.F. Keep, and A.V. Andjelkovic, *Brain endothelial cell-cell junctions: how to "open" the blood brain barrier.* Curr Neuropharmacol, 2008. **6**(3): p. 179-92.
27. Wolburg, H., K. Wolburg-Buchholz, and B. Engelhardt, *Diapedesis of mononuclear cells across cerebral venules during experimental autoimmune encephalomyelitis leaves tight junctions intact.* Acta Neuropathol, 2005. **109**(2): p. 181-90.
28. Wolburg, H., K. Wolburg-Buchholz, and B. Engelhardt, *Involvement of tight junctions during transendothelial migration of mononuclear cells in experimental autoimmune encephalomyelitis.* Ernst Schering Res Found Workshop, 2004(47): p. 17-38.
29. Lossinsky, A.S. and R.R. Shivers, *Structural pathways for macromolecular and cellular transport across the blood-brain barrier during inflammatory conditions. Review.* Histol Histopathol, 2004. **19**(2): p. 535-64.
30. Blamire, A.M., et al., *Interleukin-1beta -induced changes in blood-brain barrier permeability, apparent diffusion coefficient, and cerebral blood volume in the rat brain: a magnetic resonance study.* J Neurosci, 2000. **20**(21): p. 8153-9.

31. Carare, R.O., et al., *Solutes, but not cells, drain from the brain parenchyma along basement membranes of capillaries and arteries: significance for cerebral amyloid angiopathy and neuroimmunology.* Neuropathol Appl Neurobiol, 2008. **34**(2): p. 131-44.
32. Szentistvanyi, I., et al., *Drainage of interstitial fluid from different regions of rat brain.* Am J Physiol, 1984. **246**(6 Pt 2): p. F835-44.
33. Kida, S., A. Pantazis, and R.O. Weller, *CSF drains directly from the subarachnoid space into nasal lymphatics in the rat. Anatomy, histology and immunological significance.* Neuropathol Appl Neurobiol, 1993. **19**(6): p. 480-8.
34. Kaminski, M., et al., *Migration of monocytes after intracerebral injection at entorhinal cortex lesion site.* J Leukoc Biol, 2012. **92**(1): p. 31-9.
35. Cserr, H.F., C.J. Harling-Berg, and P.M. Knopf, *Drainage of brain extracellular fluid into blood and deep cervical lymph and its immunological significance.* Brain Pathol, 1992. **2**(4): p. 269-76.
36. Goldmann, J., et al., *T cells traffic from brain to cervical lymph nodes via the cribroid plate and the nasal mucosa.* J Leukoc Biol, 2006. **80**(4): p. 797-801.
37. Iliff, J.J., et al., *A paravascular pathway facilitates CSF flow through the brain parenchyma and the clearance of interstitial solutes, including amyloid beta.* Sci Transl Med, 2012. **4**(147): p. 147ra111.
38. Spector, R., S. Robert Snodgrass, and C.E. Johanson, *A balanced view of the cerebrospinal fluid composition and functions: Focus on adult humans.* Exp Neurol, 2015. **273**: p. 57-68.
39. Marin, I.A. and J. Kipnis, *Central Nervous System: (Immunological) Ivory Tower or Not?* Neuropsychopharmacology, 2017. **42**(1): p. 28-35.
40. Bereshchenko, O., S. Bruscoli, and C. Riccardi, *Glucocorticoids, Sex Hormones, and Immunity.* Front Immunol, 2018. **9**: p. 1332.
41. Palin, K., et al., *Interleukin-6 activates arginine vasopressin neurons in the supraoptic nucleus during immune challenge in rats.* Am J Physiol Endocrinol Metab, 2009. **296**(6): p. E1289-99.
42. Derecki, N.C., et al., *Regulation of learning and memory by meningeal immunity: a key role for IL-4.* J Exp Med, 2010. **207**(5): p. 1067-80.
43. Jacobson, A., et al., *The intestinal neuro-immune axis: crosstalk between neurons, immune cells, and microbes.* Mucosal Immunol, 2021. **14**(3): p. 555-565.
44. O'Donnell, M.P., et al., *A neurotransmitter produced by gut bacteria modulates host sensory behaviour.* Nature, 2020. **583**(7816): p. 415-420.
45. Thaiss, C.A., et al., *The microbiome and innate immunity.* Nature, 2016. **535**(7610): p. 65-74.

46. Mrdjen, D., et al., *High-Dimensional Single-Cell Mapping of Central Nervous System Immune Cells Reveals Distinct Myeloid Subsets in Health, Aging, and Disease.* Immunity, 2018. **48**(2): p. 380-395 e6.
47. Goldmann, T., et al., *Origin, fate and dynamics of macrophages at central nervous system interfaces.* Nat Immunol, 2016. **17**(7): p. 797-805.
48. Kivisakk, P., et al., *Localizing central nervous system immune surveillance: meningeal antigen-presenting cells activate T cells during experimental autoimmune encephalomyelitis.* Ann Neurol, 2009. **65**(4): p. 457-69.
49. Kierdorf, K., et al., *Macrophages at CNS interfaces: ontogeny and function in health and disease.* Nat Rev Neurosci, 2019. **20**(9): p. 547-562.
50. Song, E., et al., *VEGF-C-driven lymphatic drainage enables immunosurveillance of brain tumours.* Nature, 2020. **577**(7792): p. 689-694.
51. Menezes, S., et al., *The Heterogeneity of Ly6C(hi) Monocytes Controls Their Differentiation into iNOS(+) Macrophages or Monocyte-Derived Dendritic Cells.* Immunity, 2016. **45**(6): p. 1205-1218.
52. Greenhalgh, A.D., S. David, and F.C. Bennett, *Immune cell regulation of glia during CNS injury and disease.* Nat Rev Neurosci, 2020. **21**(3): p. 139-152.
53. Fekete, R., et al., *Microglia control the spread of neurotropic virus infection via P2Y12 signalling and recruit monocytes through P2Y12-independent mechanisms.* Acta Neuropathol, 2018. **136**(3): p. 461-482.
54. Shechter, R., et al., *Infiltrating blood-derived macrophages are vital cells playing an anti-inflammatory role in recovery from spinal cord injury in mice.* PLoS Med, 2009. **6**(7): p. e1000113.
55. Raposo, C., et al., *CNS repair requires both effector and regulatory T cells with distinct temporal and spatial profiles.* J Neurosci, 2014. **34**(31): p. 10141-55.
56. Rolls, A., et al., *Two faces of chondroitin sulfate proteoglycan in spinal cord repair: a role in microglia/macrophage activation.* PLoS Med, 2008. **5**(8): p. e171.
57. Shichita, T., et al., *MAFB prevents excess inflammation after ischemic stroke by accelerating clearance of damage signals through MSR1.* Nat Med, 2017. **23**(6): p. 723-732.
58. Kipnis, J., et al., *T cell deficiency leads to cognitive dysfunction: implications for therapeutic vaccination for schizophrenia and other psychiatric conditions.* Proc Natl Acad Sci U S A, 2004. **101**(21): p. 8180-5.
59. Klein, R.S. and C.A. Hunter, *Protective and Pathological Immunity during Central Nervous System Infections.* Immunity, 2017. **46**(6): p. 891-909.
60. Pappalardo, J.L., et al., *Transcriptomic and clonal characterization of T cells in the human central nervous system.* Sci Immunol, 2020. **5**(51).

61. Duddy, M., et al., *Distinct effector cytokine profiles of memory and naive human B cell subsets and implication in multiple sclerosis.* J Immunol, 2007. **178**(10): p. 6092-9.
62. Lisak, R.P., et al., *Secretory products of multiple sclerosis B cells are cytotoxic to oligodendroglia in vitro.* J Neuroimmunol, 2012. **246**(1-2): p. 85-95.
63. Edling, A.E., et al., *Human and murine lymphocyte neurotrophin expression is confined to B cells.* J Neurosci Res, 2004. **77**(5): p. 709-17.
64. Kabba, J.A., et al., *Microglia: Housekeeper of the Central Nervous System.* Cell Mol Neurobiol, 2017.
65. Mosser, C.A., et al., *Microglia in CNS development: Shaping the brain for the future.* Prog Neurobiol, 2017. **149-150**: p. 1-20.
66. Ginhoux, F., et al., *Origin and differentiation of microglia.* Front Cell Neurosci, 2013. **7**: p. 45.
67. Ginhoux, F. and M. Prinz, *Origin of microglia: current concepts and past controversies.* Cold Spring Harb Perspect Biol, 2015. **7**(8): p. a020537.
68. Rezaie, P. and D. Male, *Mesoglia & microglia--a historical review of the concept of mononuclear phagocytes within the central nervous system.* J Hist Neurosci, 2002. **11**(4): p. 325-74.
69. Perry, V.H., *A revised view of the central nervous system microenvironment and major histocompatibility complex class II antigen presentation.* J Neuroimmunol, 1998. **90**(2): p. 113-21.
70. Tan, Y.L., Y. Yuan, and L. Tian, *Microglial regional heterogeneity and its role in the brain.* Mol Psychiatry, 2020. **25**(2): p. 351-367.
71. Villa, A., et al., *Sex-Specific Features of Microglia from Adult Mice.* Cell Rep, 2018. **23**(12): p. 3501-3511.
72. Graeber, M.B., *Changing face of microglia.* Science, 2010. **330**(6005): p. 783-8.
73. Hughes, V., *Microglia: The constant gardeners.* Nature, 2012. **485**(7400): p. 570-2.
74. Paolicelli, R.C., et al., *Synaptic pruning by microglia is necessary for normal brain development.* Science, 2011. **333**(6048): p. 1456-8.
75. Kettenmann, H., et al., *Physiology of microglia.* Physiol Rev, 2011. **91**(2): p. 461-553.
76. Kingwell, K., *Neurodegenerative disease: Microglia in early disease stages.* Nat Rev Neurol, 2012. **8**(9): p. 475.
77. Verney, C., et al., *Early microglial colonization of the human forebrain and possible involvement in periventricular white-matter injury of preterm infants.* J Anat, 2010. **217**(4): p. 436-48.

78. Schlegelmilch, T., K. Henke, and F. Peri, *Microglia in the developing brain: from immunity to behaviour.* Curr Opin Neurobiol, 2011. **21**(1): p. 5-10.
79. Swinnen, N., et al., *Complex invasion pattern of the cerebral cortex bymicroglial cells during development of the mouse embryo.* Glia, 2013. **61**(2): p. 150-63.
80. Ginhoux, F., et al., *Fate mapping analysis reveals that adult microglia derive from primitive macrophages.* Science, 2010. **330**(6005): p. 841-5.
81. Hoeffel, G., et al., *Adult Langerhans cells derive predominantly from embryonic fetal liver monocytes with a minor contribution of yolk sac-derived macrophages.* J Exp Med, 2012. **209**(6): p. 1167-81.
82. Hoeffel, G., et al., *C-Myb(+) erythro-myeloid progenitor-derived fetal monocytes give rise to adult tissue-resident macrophages.* Immunity, 2015. **42**(4): p. 665-78.
83. Schulz, C., et al., *A lineage of myeloid cells independent of Myb and hematopoietic stem cells.* Science, 2012. **336**(6077): p. 86-90.
84. Hashimoto, D., et al., *Tissue-resident macrophages self-maintain locally throughout adult life with minimal contribution from circulating monocytes.* Immunity, 2013. **38**(4): p. 792-804.
85. Elmore, M.R., et al., *Colony-stimulating factor 1 receptor signaling is necessary for microglia viability, unmasking a microglia progenitor cell in the adult brain.* Neuron, 2014. **82**(2): p. 380-97.
86. Bertrand, J.Y., et al., *Three pathways to mature macrophages in the early mouse yolk sac.* Blood, 2005. **106**(9): p. 3004-11.
87. Cumano, A. and I. Godin, *Ontogeny of the hematopoietic system.* Annu Rev Immunol, 2007. **25**: p. 745-85.
88. McGrath, K.E., et al., *Circulation is established in a stepwise pattern in the mammalian embryo.* Blood, 2003. **101**(5): p. 1669-76.
89. De, S., et al., *Two distinct ontogenies confer heterogeneity to mouse brain microglia.* Development, 2018. **145**(13).
90. Naito, M., et al., *Development, differentiation, and phenotypic heterogeneity of murine tissue macrophages.* J Leukoc Biol, 1996. **59**(2): p. 133-8.
91. Lichanska, A.M. and D.A. Hume, *Origins and functions of phagocytes in the embryo.* Exp Hematol, 2000. **28**(6): p. 601-11.
92. Nikodemova, M., et al., *Microglial numbers attain adult levels after undergoing a rapid decrease in cell number in the third postnatal week.* J Neuroimmunol, 2015. **278**: p. 280-8.
93. Monier, A., et al., *Distribution and differentiation of microglia in the human encephalon during the first two trimesters of gestation.* J Comp Neurol, 2006. **499**(4): p. 565-82.

94. Rigato, C., et al., *Microglia proliferation is controlled by P2X7 receptors in a Pannexin-1-independent manner during early embryonic spinal cord invasion.* J Neurosci, 2012. **32**(34): p. 11559-73.
95. Paolicelli, R.C., et al., *Microglia states and nomenclature: A field at its crossroads.* Neuron, 2022. **110**(21): p. 3458-3483.
96. Davalos, D., et al., *ATP mediates rapid microglial response to local brain injury in vivo.* Nat Neurosci, 2005. **8**(6): p. 752-8.
97. Nimmerjahn, A., F. Kirchhoff, and F. Helmchen, *Resting microglial cells are highly dynamic surveillants of brain parenchyma in vivo.* Science, 2005. **308**(5726): p. 1314-8.
98. Savage, J.C., M. Carrier, and M.E. Tremblay, *Morphology of Microglia Across Contexts of Health and Disease.* Methods Mol Biol, 2019. **2034**: p. 13-26.
99. Stowell, R.D., et al., *Cerebellar microglia are dynamically unique and survey Purkinje neurons in vivo.* Dev Neurobiol, 2018. **78**(6): p. 627-644.
100. Lawson, L.J., et al., *Heterogeneity in the distribution and morphology of microglia in the normal adult mouse brain.* Neuroscience, 1990. **39**(1): p. 151-70.
101. Ribeiro Xavier, A.L., et al., *A Distinct Population of Microglia Supports Adult Neurogenesis in the Subventricular Zone.* J Neurosci, 2015. **35**(34): p. 11848-61.
102. Loane, D.J. and A. Kumar, *Microglia in the TBI brain: The good, the bad, and the dysregulated.* Exp Neurol, 2016. **275 Pt 3**: p. 316-27.
103. Kettenmann, H., *Triggering the brain's pathology sensor.* Nat Neurosci, 2006. **9**(12): p. 1463-4.
104. Bernier, L.P., et al., *Nanoscale Surveillance of the Brain by Microglia via cAMP-Regulated Filopodia.* Cell Rep, 2019. **27**(10): p. 2895-2908 e4.
105. Jurga, A.M., M. Paleczna, and K.Z. Kuter, *Overview of General and Discriminating Markers of Differential Microglia Phenotypes.* Front Cell Neurosci, 2020. **14**: p. 198.
106. Li, Q. and B.A. Barres, *Microglia and macrophages in brain homeostasis and disease.* Nat Rev Immunol, 2018. **18**(4): p. 225-242.
107. Butovsky, O., et al., *Identification of a unique TGF-beta-dependent molecular and functional signature in microglia.* Nat Neurosci, 2014. **17**(1): p. 131-43.
108. Bennett, M.L., et al., *New tools for studying microglia in the mouse and human CNS.* Proc Natl Acad Sci U S A, 2016. **113**(12): p. E1738-46.
109. Buttgereit, A., et al., *Sall1 is a transcriptional regulator defining microglia identity and function.* Nat Immunol, 2016. **17**(12): p. 1397-1406.
110. Butovsky, O. and H.L. Weiner, *Microglial signatures and their role in health and disease.* Nat Rev Neurosci, 2018. **19**(10): p. 622-635.

111. Saijo, K. and C.K. Glass, *Microglial cell origin and phenotypes in health and disease.* Nat Rev Immunol, 2011. **11**(11): p. 775-87.
112. Orihuela, R., C.A. McPherson, and G.J. Harry, *Microglial M1/M2 polarization and metabolic states.* Br J Pharmacol, 2016. **173**(4): p. 649-65.
113. Varnum, M.M. and T. Ikezu, *The classification of microglial activation phenotypes on neurodegeneration and regeneration in Alzheimer's disease brain.* Arch Immunol Ther Exp (Warsz), 2012. **60**(4): p. 251-66.
114. Perry, V.H. and C. Holmes, *Microglial priming in neurodegenerative disease.* Nat Rev Neurol, 2014. **10**(4): p. 217-24.
115. Hanisch, U.K. and H. Kettenmann, *Microglia: active sensor and versatile effector cells in the normal and pathologic brain.* Nat Neurosci, 2007. **10**(11): p. 1387-94.
116. Akundi, R.S., et al., *Signal transduction pathways regulating cyclooxygenase-2 in lipopolysaccharide-activated primary rat microglia.* Glia, 2005. **51**(3): p. 199-208.
117. Takahashi, Y., et al., *Linking Activation of Microglia and Peripheral Monocytic Cells to the Pathophysiology of Psychiatric Disorders.* Front Cell Neurosci, 2016. **10**: p. 144.
118. Tian, L., et al., *Neuroimmune crosstalk in the central nervous system and its significance for neurological diseases.* J Neuroinflammation, 2012. **9**: p. 155.
119. Rojo, A.I., et al., *Redox control of microglial function: molecular mechanisms and functional significance.* Antioxid Redox Signal, 2014. **21**(12): p. 1766-801.
120. Xia, C.Y., et al., *Selective modulation of microglia polarization to M2 phenotype for stroke treatment.* Int Immunopharmacol, 2015. **25**(2): p. 377-82.
121. Keren-Shaul, H., et al., *A Unique Microglia Type Associated with Restricting Development of Alzheimer's Disease.* Cell, 2017. **169**(7): p. 1276-1290 e17.
122. Krasemann, S., et al., *The TREM2-APOE Pathway Drives the Transcriptional Phenotype of Dysfunctional Microglia in Neurodegenerative Diseases.* Immunity, 2017. **47**(3): p. 566-581 e9.
123. Sala Frigerio, C., et al., *The Major Risk Factors for Alzheimer's Disease: Age, Sex, and Genes Modulate the Microglia Response to Abeta Plaques.* Cell Rep, 2019. **27**(4): p. 1293-1306 e6.
124. Srinivasan, K., et al., *Alzheimer's Patient Microglia Exhibit Enhanced Aging and Unique Transcriptional Activation.* Cell Rep, 2020. **31**(13): p. 107843.
125. Absinta, M., et al., *A lymphocyte-microglia-astrocyte axis in chronic active multiple sclerosis.* Nature, 2021. **597**(7878): p. 709-714.
126. Ajami, B., et al., *Single-cell mass cytometry reveals distinct populations of brain myeloid cells in mouse neuroinflammation and neurodegeneration models.* Nat Neurosci, 2018. **21**(4): p. 541-551.

127. Song, W.M. and M. Colonna, *The identity and function of microglia in neurodegeneration.* Nat Immunol, 2018. **19**(10): p. 1048-1058.
128. Gonzalez, H., et al., *Neuroimmune regulation of microglial activity involved in neuroinflammation and neurodegenerative diseases.* J Neuroimmunol, 2014. **274**(1-2): p. 1-13.
129. Szepesi, Z., et al., *Bidirectional Microglia-Neuron Communication in Health and Disease.* Front Cell Neurosci, 2018. **12**: p. 323.
130. Chavarria, A. and G. Cardenas, *Neuronal influence behind the central nervous system regulation of the immune cells.* Front Integr Neurosci, 2013. **7**: p. 64.
131. Tian, L., H. Rauvala, and C.G. Gahmberg, *Neuronal regulation of immune responses in the central nervous system.* Trends Immunol, 2009. **30**(2): p. 91-9.
132. Posfai, B., et al., *New Insights into Microglia-Neuron Interactions: A Neuron's Perspective.* Neuroscience, 2019. **405**: p. 103-117.
133. Tarozzo, G., et al., *Fractalkine protein localization and gene expression in mouse brain.* J Neurosci Res, 2003. **73**(1): p. 81-8.
134. Paolicelli, R.C., K. Bisht, and M.E. Tremblay, *Fractalkine regulation of microglial physiology and consequences on the brain and behavior.* Front Cell Neurosci, 2014. **8**: p. 129.
135. Garton, K.J., et al., *Tumor necrosis factor-alpha-converting enzyme (ADAM17) mediates the cleavage and shedding of fractalkine (CX3CL1).* J Biol Chem, 2001. **276**(41): p. 37993-8001.
136. Mizoue, L.S., et al., *Molecular determinants of receptor binding and signaling by the CX3C chemokine fractalkine.* J Biol Chem, 2001. **276**(36): p. 33906-14.
137. Hoshiko, M., et al., *Deficiency of the microglial receptor CX3CR1 impairs postnatal functional development of thalamocortical synapses in the barrel cortex.* J Neurosci, 2012. **32**(43): p. 15106-11.
138. Zhan, Y., et al., *Deficient neuron-microglia signaling results in impaired functional brain connectivity and social behavior.* Nat Neurosci, 2014. **17**(3): p. 400-6.
139. Rogers, J.T., et al., *CX3CR1 deficiency leads to impairment of hippocampal cognitive function and synaptic plasticity.* J Neurosci, 2011. **31**(45): p. 16241-50.
140. Pabon, M.M., et al., *CX3CL1 reduces neurotoxicity and microglial activation in a rat model of Parkinson's disease.* J Neuroinflammation, 2011. **8**: p. 9.
141. Morganti, J.M., et al., *The soluble isoform of CX3CL1 is necessary for neuroprotection in a mouse model of Parkinson's disease.* J Neurosci, 2012. **32**(42): p. 14592-601.
142. Nash, K.R., et al., *Fractalkine over expression suppresses alpha-synuclein-mediated neurodegeneration.* Mol Ther, 2015. **23**(1): p. 17-23.

143. Kim, T.S., et al., *Changes in the levels of plasma soluble fractalkine in patients with mild cognitive impairment and Alzheimer's disease.* Neurosci Lett, 2008. **436**(2): p. 196-200.
144. Wright, G.J., et al., *The unusual distribution of the neuronal/lymphoid cell surface CD200 (OX2) glycoprotein is conserved in humans.* Immunology, 2001. **102**(2): p. 173-9.
145. Barclay, A.N., et al., *CD200 and membrane protein interactions in the control of myeloid cells.* Trends Immunol, 2002. **23**(6): p. 285-90.
146. Koning, N., et al., *Distribution of the immune inhibitory molecules CD200 and CD200R in the normal central nervous system and multiple sclerosis lesions suggests neuron-glia and glia-glia interactions.* J Neuropathol Exp Neurol, 2009. **68**(2): p. 159-67.
147. Gorczynski, R.M., *CD200:CD200R-Mediated Regulation of Immunity.* ISRN Immunology, 2012. **2012**: p. 18.
148. Deckert, M., et al., *Regulation of microglial cell responses in murine Toxoplasma encephalitis by CD200/CD200 receptor interaction.* Acta Neuropathologica, 2006. **111**(6): p. 548-558.
149. Wang, X.-J., et al., *Impaired CD200–CD200R-mediated microglia silencing enhances midbrain dopaminergic neurodegeneration: Roles of aging, superoxide, NADPH oxidase, and p38 MAPK.* Free Radical Biology and Medicine, 2011. **50**(9): p. 1094-1106.
150. Chitnis, T., et al., *Elevated neuronal expression of CD200 protects Wlds mice from inflammation-mediated neurodegeneration.* Am J Pathol, 2007. **170**(5): p. 1695-712.
151. Hernangomez, M., et al., *CD200R1 agonist attenuates glial activation, inflammatory reactions, and hypersensitivity immediately after its intrathecal application in a rat neuropathic pain model.* J Neuroinflammation, 2016. **13**: p. 43.
152. Varnum, M.M., et al., *The anti-inflammatory glycoprotein, CD200, restores neurogenesis and enhances amyloid phagocytosis in a mouse model of Alzheimer's disease.* Neurobiol Aging, 2015. **36**(11): p. 2995-3007.
153. Xie, X., et al., *Monocytes, microglia, and CD200-CD200R1 signaling are essential in the transmission of inflammation from the periphery to the central nervous system.* J Neurochem, 2017. **141**(2): p. 222-235.
154. Zhang, S., et al., *CD200-CD200R dysfunction exacerbates microglial activation and dopaminergic neurodegeneration in a rat model of Parkinson's disease.* J Neuroinflammation, 2011. **8**: p. 154.

155. Sun, H., et al., *The CD200/CD200R signaling pathway contributes to spontaneous functional recovery by enhancing synaptic plasticity after stroke.* J Neuroinflammation, 2020. **17**(1): p. 171.
156. Feng, D., et al., *CD200 dysfunction in neuron contributes to synaptic deficits and cognitive impairment.* Biochem Biophys Res Commun, 2019. **516**(4): p. 1053-1059.
157. Ohnishi, H., et al., *Differential localization of Src homology 2 domain-containing protein tyrosine phosphatase substrate-1 and CD47 and its molecular mechanisms in cultured hippocampal neurons.* J Neurosci, 2005. **25**(10): p. 2702-11.
158. Gitik, M., et al., *Myelin down-regulates myelin phagocytosis by microglia and macrophages through interactions between CD47 on myelin and SIRPalpha (signal regulatory protein-alpha) on phagocytes.* J Neuroinflammation, 2011. **8**: p. 24.
159. Lehrman, E.K., et al., *CD47 Protects Synapses from Excess Microglia-Mediated Pruning during Development.* Neuron, 2018. **100**(1): p. 120-134 e6.
160. Ding, X., et al., *Loss of microglial SIRPalpha promotes synaptic pruning in preclinical models of neurodegeneration.* Nat Commun, 2021. **12**(1): p. 2030.
161. Biber, K., et al., *Neuronal 'On' and 'Off' signals control microglia.* Trends in Neurosciences, 2007. **30**(11): p. 596-602.
162. Koning, N., et al., *Downregulation of macrophage inhibitory molecules in multiple sclerosis lesions.* Annals of Neurology, 2007. **62**(5): p. 504-514.
163. Choi, C. and E.N. Benveniste, *Fas ligand/Fas system in the brain: regulator of immune and apoptotic responses.* Brain Research Reviews, 2004. **44**(1): p. 65-81.
164. Mott, R.T., et al., *Neuronal expression of CD22: novel mechanism for inhibiting microglial proinflammatory cytokine production.* Glia, 2004. **46**(4): p. 369-79.
165. Kerschensteiner, M., E. Meinl, and R. Hohlfeld, *Neuro-immune crosstalk in CNS diseases.* Neuroscience, 2009. **158**(3): p. 1122-32.
166. Neumann, H., et al., *Neurotrophins inhibit major histocompatibility class II inducibility of microglia: involvement of the p75 neurotrophin receptor.* Proc Natl Acad Sci U S A, 1998. **95**(10): p. 5779-84.
167. Fazio, F., et al., *Targeting metabotropic glutamate receptors for the treatment of neuroinflammation.* Curr Opin Pharmacol, 2018. **38**: p. 16-23.
168. Murugan, M., E.A. Ling, and C. Kaur, *Glutamate receptors in microglia.* CNS Neurol Disord Drug Targets, 2013. **12**(6): p. 773-84.
169. Liang, J., et al., *Glutamate induces neurotrophic factor production from microglia via protein kinase C pathway.* Brain Res, 2010. **1322**: p. 8-23.
170. Kaushal, V. and L.C. Schlichter, *Mechanisms of microglia-mediated neurotoxicity in a new model of the stroke penumbra.* J Neurosci, 2008. **28**(9): p. 2221-30.

171. Inoue, K., *The function of microglia through purinergic receptors: neuropathic pain and cytokine release.* Pharmacol Ther, 2006. **109**(1-2): p. 210-26.
172. Koizumi, S., et al., *UDP acting at P2Y6 receptors is a mediator of microglial phagocytosis.* Nature, 2007. **446**(7139): p. 1091-5.
173. de Jong, E.K., et al., *Vesicle-mediated transport and release of CCL21 in endangered neurons: a possible explanation for microglia activation remote from a primary lesion.* J Neurosci, 2005. **25**(33): p. 7548-57.
174. Dijkstra, I.M., et al., *Cutting edge: activity of human adult microglia in response to CC chemokine ligand 21.* J Immunol, 2004. **172**(5): p. 2744-7.
175. Rappert, A., et al., *Secondary lymphoid tissue chemokine (CCL21) activates CXCR3 to trigger a Cl- current and chemotaxis in murine microglia.* J Immunol, 2002. **168**(7): p. 3221-6.
176. Zhang, X.Y., et al., *BDNF levels and genotype are associated with antipsychotic-induced weight gain in patients with chronic schizophrenia.* Neuropsychopharmacology, 2008. **33**(9): p. 2200-5.
177. Castren, E., *Neurotrophins and psychiatric disorders.* Handb Exp Pharmacol, 2014. **220**: p. 461-79.
178. Kishi, T., et al., *Brain-Derived Neurotrophic Factor and Major Depressive Disorder: Evidence from Meta-Analyses.* Front Psychiatry, 2017. **8**: p. 308.
179. Ye, Y., et al., *Brain-derived neurotrophic factor (BDNF) infusion restored astrocytic plasticity in the hippocampus of a rat model of depression.* Neurosci Lett, 2011. **503**(1): p. 15-9.
180. Marinelli, S., et al., *Microglia-neuron crosstalk: Signaling mechanism and control of synaptic transmission.* Semin Cell Dev Biol, 2019. **94**: p. 138-151.
181. Bourgognon, J.M. and J. Cavanagh, *The role of cytokines in modulating learning and memory and brain plasticity.* Brain Neurosci Adv, 2020. **4**: p. 2398212820979802.
182. Kummer, K.K., et al., *Role of IL-6 in the regulation of neuronal development, survival and function.* Cytokine, 2021. **144**: p. 155582.
183. Paolicelli, R.C., G. Bergamini, and L. Rajendran, *Cell-to-cell Communication by Extracellular Vesicles: Focus on Microglia.* Neuroscience, 2019. **405**: p. 148-157.
184. Brites, D. and A. Fernandes, *Neuroinflammation and Depression: Microglia Activation, Extracellular Microvesicles and microRNA Dysregulation.* Front Cell Neurosci, 2015. **9**: p. 476.
185. Fruhbeis, C., D. Frohlich, and E.M. Kramer-Albers, *Emerging roles of exosomes in neuron-glia communication.* Front Physiol, 2012. **3**: p. 119.

186. Antonucci, F., et al., *Microvesicles released from microglia stimulate synaptic activity via enhanced sphingolipid metabolism.* EMBO J, 2012. **31**(5): p. 1231-40.
187. Gabrielli, M., et al., *Active endocannabinoids are secreted on extracellular membrane vesicles.* EMBO Rep, 2015. **16**(2): p. 213-20.
188. Rajendran, L., et al., *Alzheimer's disease beta-amyloid peptides are released in association with exosomes.* Proc Natl Acad Sci U S A, 2006. **103**(30): p. 11172-7.
189. Ngolab, J., et al., *Brain-derived exosomes from dementia with Lewy bodies propagate alpha-synuclein pathology.* Acta Neuropathol Commun, 2017. **5**(1): p. 46.
190. Valdinocci, D., et al., *Potential Modes of Intercellular alpha-Synuclein Transmission.* Int J Mol Sci, 2017. **18**(2).
191. Zheng, T., et al., *Plasma Exosomes Spread and Cluster Around beta-Amyloid Plaques in an Animal Model of Alzheimer's Disease.* Front Aging Neurosci, 2017. **9**: p. 12.
192. Kumar, A., et al., *Microglial-derived microparticles mediate neuroinflammation after traumatic brain injury.* J Neuroinflammation, 2017. **14**(1): p. 47.
193. Huang, S., et al., *Increased miR-124-3p in microglial exosomes following traumatic brain injury inhibits neuronal inflammation and contributes to neurite outgrowth via their transfer into neurons.* FASEB J, 2018. **32**(1): p. 512-528.
194. Mondello, S., et al., *Extracellular vesicles: pathogenetic, diagnostic and therapeutic value in traumatic brain injury.* Expert Rev Proteomics, 2018. **15**(5): p. 451-461.
195. Osier, N., et al., *Exosomes in Acquired Neurological Disorders: New Insights into Pathophysiology and Treatment.* Mol Neurobiol, 2018. **55**(12): p. 9280-9293.
196. Dupont, M., et al., *Tunneling Nanotubes: Intimate Communication between Myeloid Cells.* Front Immunol, 2018. **9**: p. 43.
197. Namba, M.D., et al., *Neuroimmune Mechanisms as Novel Treatment Targets for Substance Use Disorders and Associated Comorbidities.* Front Neurosci, 2021. **15**: p. 650785.
198. Krasnova, I.N. and J.L. Cadet, *Methamphetamine toxicity and messengers of death.* Brain Res Rev, 2009. **60**(2): p. 379-407.
199. Shin, E.-J., et al., *Current understanding of methamphetamine-associated dopaminergic neurodegeneration and psychotoxic behaviors.* Archives of Pharmacal Research, 2017. **40**(4): p. 403-428.
200. Yu, S., et al., *Recent Advances in Methamphetamine Neurotoxicity Mechanisms and Its Molecular Pathophysiology.* Behavioural Neurology, 2015. **2015**: p. 103969.
201. Cui, C., D. Shurtleff, and R.A. Harris, *Neuroimmune mechanisms of alcohol and drug addiction.* Int Rev Neurobiol, 2014. **118**: p. 1-12.

202. Clark, K.H., C.A. Wiley, and C.W. Bradberry, *Psychostimulant abuse and neuroinflammation: emerging evidence of their interconnection.* Neurotox Res, 2013. **23**(2): p. 174-88.
203. Crews, F.T., J. Zou, and L. Qin, *Induction of innate immune genes in brain create the neurobiology of addiction.* Brain Behav Immun, 2011. **25 Suppl 1**: p. S4-S12.
204. Goncalves, J., et al., *Methamphetamine-induced neuroinflammation and neuronal dysfunction in the mice hippocampus: preventive effect of indomethacin.* Eur J Neurosci, 2010. **31**(2): p. 315-26.
205. Frank, M.G., et al., *The danger-associated molecular pattern HMGB1 mediates the neuroinflammatory effects of methamphetamine.* Brain Behav Immun, 2016. **51**: p. 99-108.
206. Canedo, T., et al., *Astrocyte-derived TNF and glutamate critically modulate microglia activation by methamphetamine.* Neuropsychopharmacology, 2021.
207. Lewitus, G.M., et al., *Microglial TNF-alpha Suppresses Cocaine-Induced Plasticity and Behavioral Sensitization.* Neuron, 2016. **90**(3): p. 483-91.
208. Sekine, Y., et al., *Brain serotonin transporter density and aggression in abstinent methamphetamine abusers.* Arch Gen Psychiatry, 2006. **63**(1): p. 90-100.
209. Sekine, Y., et al., *Methamphetamine causes microglial activation in the brains of human abusers.* J Neurosci, 2008. **28**(22): p. 5756-61.
210. Narendran, R., et al., *Cocaine abuse in humans is not associated with increased microglial activation: an 18-kDa translocator protein positron emission tomography imaging study with [11C]PBR28.* J Neurosci, 2014. **34**(30): p. 9945-50.
211. Lacagnina, M.J., P.D. Rivera, and S.D. Bilbo, *Glial and Neuroimmune Mechanisms as Critical Modulators of Drug Use and Abuse.* Neuropsychopharmacology, 2017. **42**(1): p. 156-177.
212. Rathitharan, G., et al., *Microglia imaging in methamphetamine use disorder: a positron emission tomography study with the 18 kDa translocator protein radioligand [F-18]FEPPA.* Addict Biol, 2021. **26**(1): p. e12876.
213. Papageorgiou, M., et al., *Methamphetamine and its immune-modulating effects.* Maturitas, 2019. **121**: p. 13-21.
214. Miller, D.R., et al., *Methamphetamine Dysregulation of the Central Nervous System and Peripheral Immunity.* J Pharmacol Exp Ther, 2021. **379**(3): p. 372-385.
215. Harms, R., et al., *Methamphetamine administration targets multiple immune subsets and induces phenotypic alterations suggestive of immunosuppression.* PLoS One, 2012. **7**(12): p. e49897.
216. In, S.W., et al., *Methamphetamine administration produces immunomodulation in mice.* J Toxicol Environ Health A, 2005. **68**(23-24): p. 2133-45.

217. Hernandez-Santini, A.C., et al., *Methamphetamine facilitates pulmonary and splenic tissue injury and reduces T cell infiltration in C57BL/6 mice after antigenic challenge.* Sci Rep, 2021. **11**(1): p. 8207.
218. Potula, R., et al., *Methamphetamine causes mitrochondrial oxidative damage in human T lymphocytes leading to functional impairment.* J Immunol, 2010. **185**(5): p. 2867-76.
219. Peerzada, H., et al., *Methamphetamine administration modifies leukocyte proliferation and cytokine production in murine tissues.* Immunobiology, 2013. **218**(8): p. 1063-8.
220. Saito, M., et al., *Effects of methamphetamine on cortisone concentration, NK cell activity and mitogen response of T-lymphocytes in female cynomolgus monkeys.* Exp Anim, 2006. **55**(5): p. 477-81.
221. Saito, M., et al., *Effects of single or repeated administrations of methamphetamine on immune response in mice.* Exp Anim, 2008. **57**(1): p. 35-43.
222. Martinez, L.R., et al., *Methamphetamine enhances histoplasmosis by immunosuppression of the host.* J Infect Dis, 2009. **200**(1): p. 131-41.
223. Salamanca, S.A., et al., *Impact of methamphetamine on infection and immunity.* Front Neurosci, 2014. **8**: p. 445.

CHAPTER II

Thesis aims

1. General aims

The existent literature suggests that the long-term adverse consequences occurring within the brain's reward circuitry under psychostimulant exposure may result, at least in part, from the underlying neuroinflammatory process. Considering this, we hypothesize that limiting the inflammatory response may be relevant to control the addictive behavior and reduce relapse rates. Therefore, in this project we proposed complementary approaches to better understand neuroinflammation under drug addiction, focusing on the interplay between glial cells and neurons in order to identify regulatory mechanisms of the this inflammatory process. The following aims were proposed in this project:

Aim I: **Understand the cytokine profile and the peripheral-central immune crosstalk in different stages of the drug addiction disease.** Since the identification of new biomarkers and therapeutic targets is a way to envision personalized immune-based therapeutics, the understanding of the cytokine profile and the peripheral-central immune crosstalk seems crucial to perspective successful translational therapeutic interventions. In this scenario, a scoping review of literature is reported in Chapter III.

Aim II: **Dissect at molecular level the neuronal modulation of microglia activation by Meth.** Previously we have demonstrated that Meth activates microglia through astrocytes. In this scenario, understanding how glial activation by Meth will affect the crosstalk between glial cells and neurons will provide a more comprehensive understanding of the mechanisms involved in modulation of psychostimulant-induced neuroinflammation. The data obtained to address this aim is mainly reported in Chapter IV.

Aim III: **Determine the proteome profile in key time points of the chronic process of drug intake and understand which molecular pathways are perturbed.** Using proteomic analysis, we aimed at knowing which proteins were more vulnerable to chronic Meth administration and different withdrawal periods. The data obtained to address this question is mainly reported in Chapter V.

Aim IV: **Validate the importance of the target proteins and pathways identified in "Aim II" in the addictive process.** After identifying proteins that could be promising candidates in Meth-addiction, we aimed at understanding the physiological mechanisms

in which these proteins were involved under Meth exposure and manipulated it to validate its relevance in the addictive behavior. The data obtained to address this aim is mainly reported in Chapter V.

CHAPTER III

The impact of psychostimulants on central and peripheral neuro-immune regulation: a scoping review cytokine profiles and their implications for addiction

(Under revision in the Frontiers in Cellular Neuroscience)

1. Introduction

Addiction is a chronic complex disease in which, after a period of episodic drug use, a subset of individuals develops problematic drug use and use related disorders, which will likely be followed by periods of abstinence and eventual relapse (1, 2). The latest World Drug Report estimates 35.6M of problematic drug-users, for whom there are limited, and often unspecific, treatment options (3).

Psychoactive substances are classically recognized by their neurotoxic effects on monoaminergic and glutamatergic systems (1). However, it is now evident that these substances also promote neuroinflammation and that seems to contribute to the establishment of problematic drug use and addiction (4, 5). Neuroinflammation can be described as an inflammatory response within the central nervous system (CNS), which is mediated through several cytokines, reactive oxygen species, chemokines, and other inflammatory markers (6). These mediators, in particular cytokines, are produced by resident CNS cells, such as microglia, astrocytes and oligodendrocytes, but also by endothelial and peripherally derived immune cells (6). Cytokines are regulatory peptides that orchestrate signal-dependent immune responses. Upon their essential role in the regulation of immune and inflammatory responses, cytokines are critical to maintain homeostasis, immune cell development and differentiation (7-9). Upon their function in immunity, cytokines play an important role in synaptic plasticity, impacting different behavioral responses, such as sickness behavior, social behavior, learning and anxiety-like behavior (reviewed in (10)). The production of cytokines in the CNS is under tight control and, usually, under physiological conditions, very low levels are detected (8). However, the disruption of homeostasis may significantly impact cytokine production and release (7, 8). Although, the initial cytokine release response, may be beneficial to counteract homeostatic imbalance, the production of cytokines over long periods of time may perpetuate an adverse environment and contribute to disease and neurodegenerative processes (7).

Cytokines' action on their target cells can be autocrine (signaling to self), paracrine (signaling to neighboring cells) or endocrine (signaling through the circulation) (11). Cytokines play also an important role in the communication between the peripheral and central nervous systems (12). This direct communication is more likely to occur under dysfunctional/disease states, in which the blood brain barrier (BBB) is disrupted (10, 12). However, there is growing evidence that even in the absence of higher BBB permeability, cytokines derived from immune cells residing in the immunological niches in CNS, reach the brain parenchyma and influence resident cells and behavior (10, 12, 13).

Several studies demonstrated that psychostimulants impact on cytokine production and release, both in the CNS and at the peripheral level (14-17). Still, little is yet known on the peripheral and central immune crosstalk under exposure to psychostimulants. Of note, one of the hallmarks of psychostimulants' neurotoxicity is BBB dysfunction (18), which most likely favors the entry of cytokines from the periphery into the brain parenchyma (10, 12).

In humans, a recent study addressed the associations between psychological distress linked to alcohol/drug use and circulating cytokines (19). Distress and anxiety are both recognized as important factors for drug relapse (20, 21), but the relation between cytokines and relapse was only investigated in problematic alcohol users, where stress-related suppression of tumour necrosis factor alpha (TNF-α) predicted drinking severity (22).

In this scenario, mapping the cytokine profile at each stage of exposure (acute or chronic), withdrawal and relapse, and understand the interplay between the peripheral and central immune system seems crucial to perspective new biomarkers, personalized immune-based therapeutics and more efficient treatments.

This scoping review aims at clarifying the current state of knowledge regarding the impact of psychostimulants on cytokine levels, both in the CNS and at the peripheral level, throughout the different phases of drug use. Simultaneously, it addresses a possible parallel between crucial immune players at central and peripheral compartments under exposure to psychostimulants.

2. Methods

The literature search was conducted following the PRSMA guidelines without a previous registered protocol (23). We have included studies meeting the following eligibility criteria: (a) published within the last ten years (from 2012 to June 2022); (b) redacted in English; (c) with an abstract available; (d) addressing cytokine levels either in humans or *in vivo* animal models; (e) published in journals from quartile (Q)1 or Q2, according to the Scimago Journal & Country Rank (SJR).

Our search was conducted using the Pubmed®, which is maintained by the National Center for Biotechnology Information (NCBI), at the U.S. National Library of Medicine (NLM), and is located at the National Institutes of Health (NIH). This database allows searching MEDLINE, PubMed Central (PCM) and Bookshelf databases and covers more than 35 million citations and abstracts of biomedical literature, providing liking access to the full-text. The following search equation was used: "(substance) AND (cytokine OR

interleukin OR interferon OR "tumor necrosis factor") NOT (culture)", where "substance" was replaced by amphetamine, cocaine or methylphenidate on three independent searches. A total of 200 publications for amphetamines, 153 for cocaine and 25 for methylphenidate were identified. Publications obtained in these searches were then checked to confirm that they met the eligibility criteria. Next, charting was conducted in parallel by two of the authors and differences in the initial selection were further discussed and compatibilized. At this stage, full abstracts and texts were read and the following exclusion criteria were adopted: (a) the study evaluated the conjugated effects of different psychoactive substances; (b) the study investigated drug effects after prenatal exposure; (c) the study was not empirical; (d) the study evaluated the effect of psychoactive substances in conjugation with other diseases or conditions. After this analysis a total of 50 articles for amphetamines, 20 for cocaine and 9 for methylphenidate were elected for full-text reading and further confirmation. A final list of 42 publications for amphetamines, 12 for cocaine and 8 for methylphenidate was used in this review. The complete selection process was represented in a flow diagram (**Fig.1**).

After full-text analysis, final items were further divided in three groups: the first group included articles that evaluated cytokines in the CNS; the second group included articles which evaluated peripheral cytokines; and the third group included articles that evaluated both central and peripheral cytokines. In each of these groups, data regarding: i) subjects studied; ii) drug dosing regimen, iii) time-point of evaluation; iv) type of tissues/samples evaluated; v) methodology used for evaluation; and vi) results obtained for the different cytokines were collected and organized by psychoactive substance in different Tables (**Tables 1-5 and Supplementary Tables 1-3**).

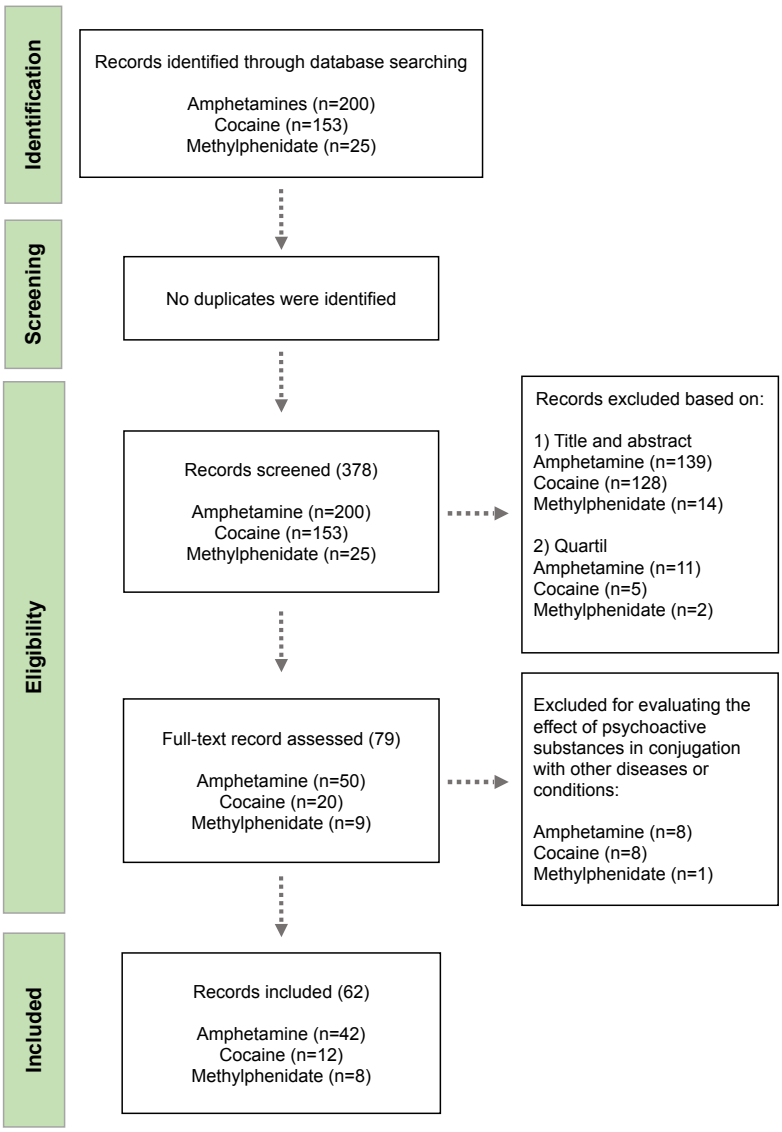

Figure 1: Flow diagram of the study selection process.

3. Results

Overview

The articles included in this study for full review cover a range of publications addressing the evaluation of several cytokines both at central and peripheral levels, in animal models and in studies conducted in patients with problematic drug use. These studies also cover different stages of the addictive process, extending from acute drug exposure, to short- or long-term administration/use, withdrawal and drug reinstatement. For a comprehensive understanding of the results, they were grouped according to the type of

substances administered/used and according to the type of administration and period evaluated.

After full-text analysis, a pool of 62 publications were considered eligible. Within these, we found 41 publication that evaluated cytokines in the CNS and 18 publications that evaluated cytokines at the peripheral level (**Fig. 2A**). Only three studies evaluated cytokines both at central and peripheral level (**Fig. 2A**). We also analyzed the distribution of cytokines in all the elected studies and found that 17 different cytokines had been evaluated in at least one study (**Fig. 2B**), while most studies addressed several cytokines simultaneously. As expected, the most studied cytokines were the classical pro-inflammatory cytokines TNF-α, IL-6 and IL-1β. The TNF-α profile was evaluated in 47 articles, while IL-6 and IL-1β were both evaluated in 34 articles. As for IL-10, IFN-γ, IL-4 and IL-2, they were evaluated in sixteen, ten, eight and five articles, respectively. The cytokines Il-1α, IL-5 and IL-17 were investigated in only two studies. The remaining cytokines - IL-7, IL-8, IL-9, IL-12, IL-15, IL-18 and IFN-α - were addressed in just one publication each **(Fig. 2B)**.

To analyze the results reported in the different studies, we have categorized them by type of exposure and/or evaluation timepoint, which allowed four different categories addressing: i) acute exposure (19 publications); ii) chronic (mid- or long-term) exposure (27 publications); iii) withdrawal/abstinence (nine publications); and iv) reinstatement (five publications) **(Fig. 2C)**. This categorization is reflected in **Tables 1-5 and Supplementary Table 1-3** and described in detail in the following subsections.

For reading simplification, significantly altered cytokines are referred to as increased/decreased (or equivalent adjectives), however, this implies always that a comparison to an adequate control group was verified.

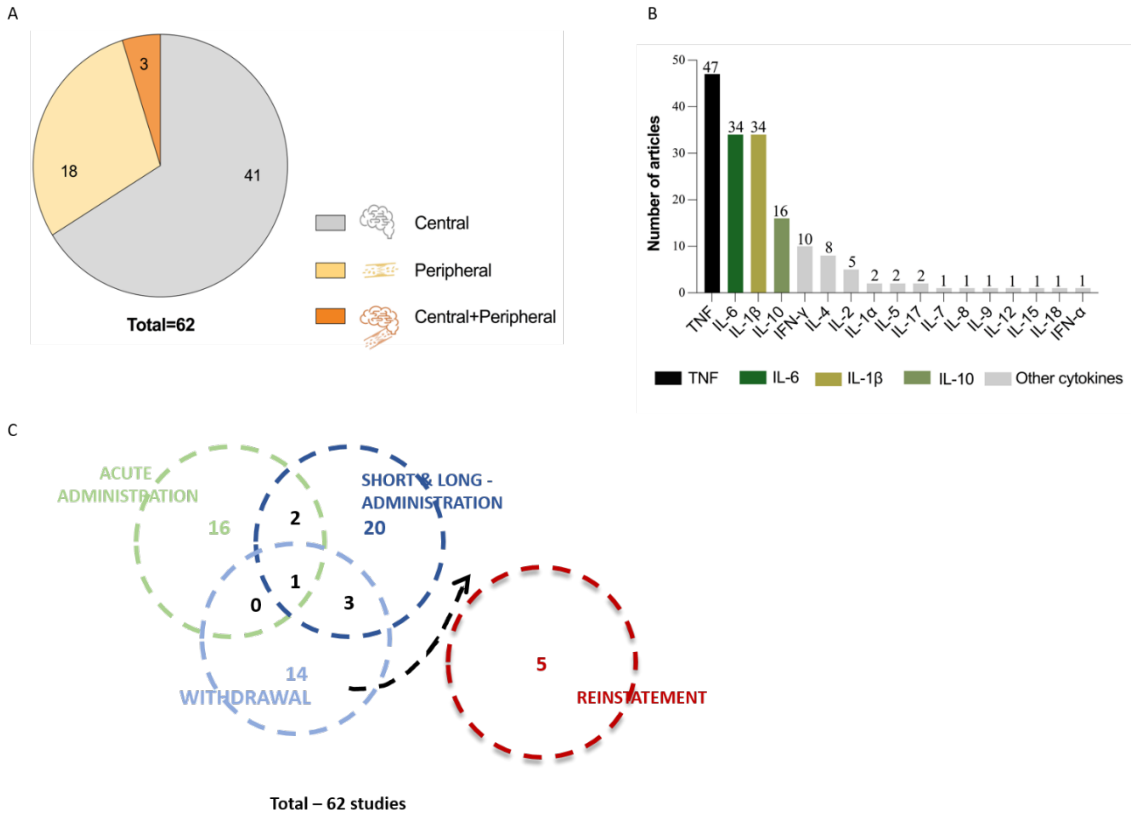

Figure 2: Overview of the 62 studies included for revision. (A) Pie chart representing the total number of articles included for revision and divided in three compartments that correspond to the number of articles that evaluated cytokines at central level (gray), at peripheral level (light orange) and at both central and peripheral level simultaneously (dark orange). (B) Graphic representation of all cytokines evaluated in the reviewed articles and the number of articles that evaluated each cytokine. (C) Venn diagram showing distribution of the number of studies performed at acute, short- and long-term administration, withdrawal and reinstatement, represented by circles. The circle overlapping shows the number of studies that evaluated cytokine levels in multiple timepoints or stages.

Cytokine profile in acute administration of psychostimulants

Drug use often refers to episodic or recreational administration of psychoactive substances (24). The effects of acute exposure to psychostimulants can either refer to the adverse effects that result from a single dose or from multiple dosing in a short period of time (i.e., binge drug exposure). Among the 19 studies that evaluated the acute effects of psychostimulants in the cytokine profile, nine used a protocol of a single dose administration (25-33) (**Tables 1-2 and Supplementary Table 1)** and ten used a binge pattern protocol (14, 15, 34-41) (**Tables 1-2 and Supplementary Table 1**). All these studies were conducted in rodent models.

The studies that used single exposure, evaluated only the central levels of cytokines. Upon methamphetamine (Meth) administration, several authors reported an increase in at least one of the classic pro-inflammatory cytokines TNF-α, IL-6 and IL-1β, in different brain regions (Nucleus accumbens (Nacc), the prefrontal cortex (PFC), the ventral tegmental area (VTA), the striatum and the hypothalamus) (25-29) **(Table 1)**. However, other studies reported that these cytokines were not altered in the hippocampus, PFC and Nacc, after a single administration of Meth or amphetamine (Amph) (25) **(Table 1)**, and a few other studies reported asymmetric results across brain regions (27, 30, 33) (**Tables 1 and Supplementary Table 1)**. Only two studies addressed central cytokines after a single dose of cocaine, showing unaltered TNF-α levels in the ventral striatum and unaltered IL-1β in the hippocampus (31, 32) **(Table 3)**. Collectively, these studies evidence that drug-induced cytokine changes are regional-dependent, which confirmed by studies that evaluated the same cytokine in different regions (26, 27, 30, 33) (see **Tables 1 and Supplementary Table 1)**. Of note, a number of other variables may also justify the differences observed between studies, such as differences in drug dosing, routes of administration, time-points of evaluation and the methodology used for cytokine quantification. These methodological differences are visible in **Tables 1, 3 and Supplementary Table 1**. Within these factors, dosing seems to strongly contribute to data heterogeneity, as studies that used low doses mostly showed no differences in cytokine levels (25, 30) **(Table 1)**, while studies that used higher doses showed increased TNF-α, IL-6 and IL-1β (26-29) **(Table 1)**.

Focusing on studies using binge patterns of administration, we found nine studies evaluating cytokines at the central level and just one evaluating circulating cytokine levels. In rodents, binge Meth administration resulted in cytokine changes similar to those reported for single dosing: i) one study observed increased expression of TNF-α and IL-1β in both the striatum and the hippocampus (14), ii) two studies reported increased TNF-α (15) or IL-6 in the striatum (34); and iii) another study showed increased IL-6 and TNF-α in the mPFC, caudate putamen (CPu) and hippocampus (41) **(Table 1)**. Additionally, two of the studies reviewed also reported persistently increased TNF-α levels past 7 and 12 days of Meth binge administration (38, 39) **(Table 1)**. However, other authors reported no differences in the expression of TNF-α and IL-6 in regions like the hippocampus, PFC, CPu and the Nacc (14, 36), as well as no differences in IL-1β in the striatum (14) **(Table 1)**.

Also, regarding binge administration but of MDMA, one work showed increased TNF-α and IL-1β levels in the CPu (40) **(Supplementary Table 1)**.

As verified in the studies using single dosing, the heterogeneity of results observed for TNF-α, IL-6 and IL-1β under binge schedules were impacted by the same variables. Also

in this case, studies using low doses mostly showed no impact in TNF-α, IL-6 and IL-1β levels (14, 36), while those using higher doses reported increased levels for these cytokines (15, 38, 39, 41) **(Table 1)**.

Additionally, two cytokines were evaluated in single studies (after Meth exposure): one study reported an increase in the expression of IL-15 in the striatum after binge administration (35) **(Table 1)** and one study reported no changes in IL-1α after single administration (25) **(Table 1)**.

A single study evaluated circulating cytokines after binge Meth administration, reporting augmented expression of IL-1β, IL-6 and IL-10 (37) (**Table 2)**. Of note, within the pool of studies reviewed in this section, none evaluated central and peripheral levels of cytokines simultaneously.

Taken together, these results revealed that: i) nine (out of thirteen) studies evaluating TNF-α, showed increased levels; ii) seven (out of nine) studies evaluating IL-1β reported increased levels; and iii) five (out of eight) reported increase IL-6 in at least one brain region. Based on this, one can concluded that IL-6, TNF-α and IL-1β were the most investigated cytokines in acute/binge exposure to psychoactive substances and that drug-induced variations in cytokines are region- and dose-dependent. As we found only a single study reporting on circulating cytokine levels, one can only concluded that more studies at the peripheral level are clearly necessary to understand how circulating cytokines vary with exposure to psychostimulants and how they relate to central cytokine level.

Table 1: Studies addressing the impact of methamphetamine in central cytokines

	References	Subjects	Dose regimen	Evaluation	Brain region	Results	Methodology
Acute	(14) Canedo et al., 2021	Adult male C57BL/6J mice	4x5 mg/Kg, 2 h apart, i.p.	24h after the last injection	Hippocampus Striatum	Hippocampus =TNF-α and IL-6 ↑IL1-β Striatum =IL-6 and IL-1β ↑TNF-α	RT-PCR
	(15) Coelho-Santos et al., 2015	Adult male C57BL/6J mice	4x10 mg/kg, 2 h apart, i.p.	2 h after the last injection	Striatum	↑TNF-α	Immunohistochemistry
	(24) DiCaro et al., 2019	Adult male C57BL/6J mice	5 mg/Kg, i.v.	4 h after administration	Brain	= IL1-α, IL-1β, IL-6 and TNF-α	RT-PCR
	(25) Frank et al., 2016	Adult male Sprague Dawley rats	10 mg/Kg, i.p.	2, 4 and 6 h after administration	Nacc VTA PFC	Nacc and PFC ↑IL-1β and TNF-α at 2h and IL-6 at 4h VTA ↑IL-1β, TNF-α and IL-6 at 2 h	RT-PCR
	(37) Ghanbari et al., 2019	Male Wistar rats	4x10 mg/Kg, 2 h apart, i.p.	7 days after administration	Hippocampus	↑TNF-α	ELISA
	(40) Gou et al., 2020	Male C57BL/6J mice	4x10 mg/Kg, 3 h apart, i.p.	(not reported)	mPFC CPu Hippocampus	mPFC, CPu and hippocampus ↑IL-6 and TNF-α	Flow Cytometric bead array
	(38) Hadizadeh-	Male Wistar rats	4x10 mg/Kg, 2 h apart, i.p.	12 days after administration	Hippocampus	↑TNF-α	ELISA

		Bazaz el al., 2021					
		(26) Kelly et al., 2012	Male C57BL/6J mice	20 mg/Kg, s.c.	12 h after Meth injection	Striatum, hippocampus and PFC	Striatum ↑ TNF-α ; IL-6 and IL-1β Hippocampus and PFC: = TNF-α ; IL-6 and IL-1β	RT-PCR
		(27) Nader et al., 2014	Male C57BL/6J mice	30 mg/Kg, i.p.	24 h after administration	Striatum	↑ TNF-α	ELISA
		(33) Robson et al., 2013	Male Swiss Webster mice	4x5 mg/Kg, 2 hours apart, i.p.	1.5; 3; 6; 12 and 24 h after administration	Striatum	↑ IL-6 (all timepoints)	RT-PCR
		(28) Seminerio et al., 2012	Male Swiss Webster mice	25; 35 or 45 mg/Kg, i.p.	45 min after administration.	Hypothalamus, striatum and PFC	Hypothalamus and striatum ↑ IL-1β (35 and 45 mg/ Kg) PFC ↑ IL-1β (45 mg/ Kg)	RT-PCR
		(34) Urrutia et al., 2014	C57BL/6J mice	3x4 mg/Kg, 3 h apart, i.p.	24 h after administration	Striatum	↑ IL-15	Immunohistochemistry
		(35) Wang et al., 2019a	Male C57BL/6J mice	4x5mg/Kg, 2 h apart, i.p.	24 h after the first administration	Hippocampus, PFC, CPU and Nacc	= IL-6 and TNF-α	ELISA
		(29) Wang et al., 2019b	Male Sprague-Dawley rats	A single injection of 1 mg/Kg, i.p.	30 min and 2 h after injection	VTA, Nacc and PFC	VTA ↑ TNF-α (at 30 min) and IL-6 (both time points) = TNF-α (at 2 h) Nacc and PFC = TNF-α and IL-6	RT-PCR

Short- and long-term administration	(42) Liskiewicz et al., 2019	Male C57BL/6NCrL mice	Escalating doses (0.2-2.4 mg/Kg, using an increase step-wise of 0.2 in each injection, 3x per day for 4 days). Then binge administration (3x4 mg/Kg, 3 h apart, i.p.)	24 h after last Meth dose	Hippocampus	↑ IL-1β = IL-6	ELISA
	(41) Gonçalves et al., 2017	Adult male Wistar rats	Self-administration (Meth 0.1mg/Kg per infusion. From day 1 to day 3, the sessions lasted 2 h or 25 infusions. From day 4 to day 10, the sessions lasted 6 h or 50 infusions)	24 h or 7 days after the last operant session	Hippocampus Striatum	<u>Hippocampus</u> ↑ TNF-α (at 24 h and 7 days) = IL-1β <u>Striatum.</u> ↑ TNF-α (at 24 h and 7 days) ↑ IL-1β (at 24 h) ↓ IL-1β (at 7 days)	Western blot
Withdrawal	(64) Beirami et al., 2017	Adult male Wistar rats	Escalating doses (1–10 mg/kg; twice a day, at 5-h intervals, for 10 consecutive days, i.p.)	2 weeks after last administration	Hippocampus	↑TNF-α and IL-6	Western Blot
	(65) Jiang et al., 2014	Adult male Wistar rats	20 mg/Kg for 5 days, i.p.	4, 6, 10 and 14 days after the initial injection.	Substantia nigra	Day 4: = IL1-β and TNF-α Day 6, 10 and 14: ↑IL-1β and TNF-α	ELISA
	(68) Loftis et al., 2013	Male C57BL/6J mice	4 mg/Kg once daily for 15 consecutive days, s.c.	6 days after last Meth dose	Hypothalamus	↑ IL-2 = IFN-γ, TNF-α, IL-6, IL-1β and IL-10	Multiplex immunoassay

	(66) Namyen et al., 2020	Wistar rats	Increasing doses (days 1 and 2 – 2.5, days 3 and 4 – 5 and days 5 to 11 – 10 mg/Kg	On day 15	Hippocampus and PFC	↑ IL-1β; IL-6 and TNF-α	Western blot and RT-PCR
	(67) Stolyarova et al., 2015	Long Evans rats	Increasing doses (0.3-6 mg/Kg with 0.3 increments/day, in 5 days per week for 4 weeks, s.c.)	17 days after the last administration	Frontal cortex; amygdala and striatum.	<u>Frontal cortex</u> ↓ IL-1β, IL-6, IL-10 and TNF-α <u>Amygdala</u> and <u>striatum</u> = IL-1β, IL-6, IL-10 and TNF-α	ELISA
Reinstatement	(78) Karimi-Haghighi et al., 2020	Male Wistar rats	Conditioned place preference paradigm (5 days of consecutive conditioning with 1mg/Kg, s.c.. Followed by 10 days of extinction and then a reinstatment day with Meth 0.25 mg/Kg or 0.5 mg/kg, s.c.)	Immediately after the reinstatement behavior test.	PFC and hippocampus	<u>PFC</u> Reinstatment with 0.25 = TNF-α, IL-6 and IL-10 ↑ IL-1β Reinstatment with 0.5 ↑ TNF-α, IL-1β and IL-10 = IL-6 <u>Hippocampus</u> Reinstatment with 0.25 = TNF-α, IL-1β, IL-6 and IL-10 Reinstatment with 0.5 ↑ TNF-α and IL-10 = IL-1β and IL-6	RT-PCR

Abbreviations: CPu – Caudate Putamen; ELISA - enzyme-linked immunosorbent assay; IFN – Interferon; IL - Interleukin i.p. – intraperitoneal; i.v. – intravenous; Meth – Methamphetamine; mPFC – medial Prefrontal cortex; Nacc – Nucleus accumbens; PFC – Prefrontal cortex; RT-PCR – Real Time Polymerase Chain Reaction; s.c. – subcutaneous; TNF-α – Tumor necrosis factor α; VTA – Ventral tegmental area. Results are expressed relative to control (↑ - increase; ↓ - decrease; = - unaltered).

Table 2: Studies addressing the impact of methamphetamine in peripheral cytokines

	References	Subjects	Dose regimen	Evaluation	Sample	Results	Methodology
Acute	(36) Kobeissy et al., 2022	Male Sprague Dawley rats	4x10 mg/Kg, 1 h apart, i.p.	24 h after injection	Serum	Cytokine antibody kit: ↑ IL-1β, IL-6 and IL-10 ELISA: ↑ IL-6 and IL-10	Cytokine antibody kit ELISA
Short- and long-term	(59) Jiang et al., 2016	Male and female Meth users (15) and healthy controls (15) from the same Chinese cities.	Chronic Meth use history longer than 1 year (use within 3 months and no other drugs use within 3 months)	Subjects with a positive result for recent Meth use (72h) and an history of at least an year.	PBMCs and plasma	PBMCs and plasma = IL-6 PBMCs ↑ IFN-α	RT-PCR ELISA
	(16) Mata et al., 2015	Sprague-Dawley rats	Self-administration (Meth 0.1mg/Kg per infusion. FR1 From day 1 to day 7. FR5 from day 8 to 14.)	One day after the last operant session.	Serum	= TNF-α, IL-6 and IFN-γ	ELISA
	(60) Shen et al., 2020	Meth-dependent patients (380 male and 27 female) from rehabilitation centers and hospital in Kunming (China).	Participants met criteria for Meth dependence. Mean duration of dependency: 114.37±106.752 months.	Before detoxification treatment.	Serum	↑ TNF-α	ELISA
	(57) Wang et al., 2022	Male C57BL/6J mice	8 Meth injections at a rate of 1.5 to 10 mg/Kg, i.p.	24 h after the last injection	Serum	↑ TNF-α, IL-1β and IL-18	ELISA
Withdrawal	(58) Kuo, et al., 2018	Female patients with amphetamine dependence from drug rehabilitation clinic in a detention center in Northern Taiwan (72); healthy controls (51).	Participants met DSM-IV criteria for Meth dependence.	Samples were collected less than 3 days after last drug use and after 4-week abstinence.	Plasma	At admission: ↑ IL-1β, IL-2, IL-4, IL-6, IL-10 = IFN-γ, TNF-α and IL-8 ↓ IL-5	Multiplex immunoassay

					At abstinence: ↑ IL-1β, IL-2, IL-4 and IL-6 = IFN-γ, TNF-α and IL-5 ↓ IL-8 and IL-10	
	(70) Kohno et al., 2018	Male and female Meth users (30) and healthy controls (20) recruited from the community and treatment centers.	Participants met DSM-IV criteria for Meth dependence and had been abstinent for > 1 month and < 6 months.	Abstinent from Meth for > 1 month and < 6 months	Plasma	= IL-1β and IL-10. ↑ IL-6	Multiplex immunoassay
	(73) Li et al., 2021	Male Sprague-Dawley rats	Conditioned place preference paradigm (2 mg/Kg daily for 10 days, i.m.)	18 days after Meth administration	Serum	↑ IL-1α and IL-2	ELISA
	(71) Luo et al., 2022	In patients (78) from voluntary drug rehabilitation hospital Guangzhou Baiyun (male and female); healthy controls (64)	Participants met DSM-IV criteria for Meth dependence	39.06 ±7.48 days from the last use	Serum	↑ TNF-α , IL-6 and IL-18	ELISA
	(72) Re et al., 2022	Meth users (67) recruited at the Yunnan drug rehabilitation center; 38 healthy matched controls.	Participants met DSM-V criteria for Meth dependence.	7 – 15 days (M-0.5); 3 months (M-3) and 12 months (M-12) after withdrawal	Plasma	↑ IL-6, IL-12p70, IFN-γ, TNF-α and IL-7 (showed a downward trend over the withdrawal time) ↓ IL-9 and IL-1β (M− 0.5 and M− 3) ↑ IL-2 and IL-5 (M-0.5 and M-3) ↑ IL-10, IL-4 and IL-5 (M-12)	Bio-Plex assay kit

Reinstatement	(109) Li et al., 2020	Male (9) and female (2) suffering from Meth use disorder.	Participants met DSM-IV criteria for Meth dependence and tested positive for Meth at least once prior to admission (urine tested). Patients received a 30 mg Meth intravenous (i.v.) challenge delivered over two minutes.	Blood was collected at 0, 60 and 360 min post-Meth infusion	Plasma	= TNF-α ↑ IL-6 after 360 min (but not 60 min)	Multiplex immunoassay

Abbreviations: DSM – Diagnostic and statistical manual of mental disorders; ELISA - enzyme-linked immunosorbent assay; FR – Fixed ratio; IFN – Interferon; IL – Interleukin; i.m – intramuscular; i.p. – intraperitoneal; i.v. – intravenous; Meth – Methamphetamine; PBMCs – Peripheral blood mononuclear cells; RT-PCR – Real Time Polymerase Chain Reaction; s.c. – subcutaneous; TNF-α – Tumor necrosis factor α. Results are expressed relative to control (↑- increase; ↓- decrease; = - unaltered).

Table 3: Studies addressing the impact of cocaine in central cytokines

		References	Subjects	Dose regimen	Evaluation	Brain region	Results	Methodology
Short- and long-term	Acute	(31) Montesinos et al., 2020	Male OF1 mice	Acute: single injection of 25 mg/Kg. Repeated: 25 mg/ Kg daily, for 7 days, i.p.	0, 30, 60, 120 and 240 min after cocaine injection	Hippocampus	↑ IL-1β (in repeated model, at 60 min). = IL-1β (in other time-points and in the acute model).	ELISA
		(30) * Lewitus et al., 2016	C57BL/6 mice	Single injection of 15 mg/Kg or 5 daily injections of 15 mg/Kg	24 h later after single injection or after the last injection. And 10 days after 5 daily injections	Ventral striatum	↑ TNF-α (24h later of 5 daily injections) = TNF-α (at single injection and after 10 days withdrawal)	Immuno-histochemistry RT-PCR
		(46) Chivero et al., 2021	C57BL/6 mice Cocaine users (postmortem)	20 mg/Kg daily, for 7 consecutive days Chronic cocaine dependence	1 h after the last administration	Striatum and cortex Frontal cortex	↑ IL-1β	Western Blot
		(47) Mai et al., 2018	C57BL/6 mice	45 mg/Kg/ day, for 5 days, i.p.	1 h, 6 h, 12 h, 1 day, 3 days, 7 days and 14 days after the last dose	Hippocampus	↑ IL-6 (all time points) ↓ IFN-γ (at 12h, 1 and 3 days) ↑ TNF-α (at 1,6 and 12 h)	RT- PCR Western Blot
Withdrawal		(69) Zhu et al., 2018	Male Sprague-Dawley adolescent rats	Single daily injection of 15 mg/Kg, during 15 days, i.p.	After 35 days.	mPFC	= IL-6, IL-1β and TNF-α	Western blot

Reinstatement	(79) Brown et al., 2018	Male Sprague-Dawley rats	Self-administration (0.5mg/Kg/infusion, during 2h daily sessions over 15 days). After self-administration rats received seven 2 h extinction sessions. After drug-extinction, rats received a drug priming stimulus of 15 mg/Kg, i.p.	2 h after cocaine challenge	VTA	↑ IL-1β = TNF-α	RT-PCR

Abbreviations: ELISA - enzyme-linked immunosorbent assay; IFN – Interferon; IL - Interleukin i.p. – intraperitoneal; mPFC – medial Prefrontal cortex; RT-PCR – Real Time Polymerase Chain Reaction; TNF-α – Tumor necrosis factor α; VTA – Ventral tegmental area. Results are expressed relative to control (↑- increase; ↓- decrease; = - unaltered). * Also report withdrawal data.

Cytokine profile under short and long-term administration of psychostimulants

In this section, we analyzed studies reporting on the effects of repeated administration (over a variable number of days) of psychoactive substances in cytokine levels, either at the central or peripherally. Importantly, repeated administration of psychostimulant may result in substance use disorder and unexpected system adaptations (1).

A total of 28 studies evaluating the short- and long-term effects of psychostimulant administration were considered. Eighteen reported on changes of cytokines in the brain, eight in the blood and two studies evaluated cytokines at both central and peripheral levels (**Table 1-5 and Supplementary Table 1-3**).

Gonçalves and colleagues showed an increase in the expression of TNF-α in the striatum and hippocampus after seven days of self-administration, but not of IL-1β (42) (**Table 1**). Other authors reported increased IL-1β in the hippocampus after 4 of days of an escalating regimen of Meth (43) (**Table 1**). All four studies that used protocols of short- or long-term administration of other amphetamines, reported an increase in several cytokines such as TNF-α, IL-1β, IL-6, IFN-γ, IL-4 and IL-10, in the striatum or the frontal cortex (44-46) (**Supplementary Table 1**). Gubert and colleagues (33) reported that IL-1β and TNF-α levels were unaltered in the PFC and hippocampus after repeated amphetamine administration, while in the striatum TNF-α was also unaltered, but IL-1β was increased (**Supplementary Table 1**).

Studies that evaluated changes in central cytokines as a result of repeated cocaine exposure consistently showed increased IL-1β, TNF-α and IL-6 (31, 32, 47, 48) and reduced IFN-γ (48) (**Table 3**). In these studies, performed in rodent models, the brain regions examined were the striatum, the cortex and the hippocampus (31, 32, 47, 48) (**Table 3**). Of note, Chivero and colleagues also showed higher IL-1β levels in human postmortem frontal cortices (47) (**Table 3**).

Consubstantiating the results already reported for cocaine and amphetamines, several studies using rodent models of long-term administration of methylphenidate, also reported increased IL-1β and TNF-α in the hippocampus (49-56). Schmitz and colleagues (55), further reported an increase in IL-6 levels in the hippocampus after methylphenidate administration (**Table 5**).

At the peripheral level, in rats, one study showed that TNF-α, IL-6 and IFN-γ levels were not affected by long-term Meth self-administration (16) (**Table 2**). Similarly, and also in rats, long-term administration of lisdexamfetamine, did not affect TNF-α, IL-1β and IL-10 serum levels (57) **(Supplementary Table 2)**. However, in mice, repeated Meth administration resulted in increased circulating levels of TNF-α, IL-1β and IL-18 (58) (**Table 2**).

Of note, Kuo and collaborators (59) analyzed several cytokines in patients that met the criteria for Meth dependence and reported an increase of IL-1β, IL-2, IL-4, IL-6 and IL-10, three days after the last dosing (**Table 2**). This same study reported that IFN-γ, TNF-α and IL-8 were not altered and that IL-5 was decreased (59) (**Table 2**). Opposing to these results, other authors reported that IL-6 was not altered in the plasma and PBMCs of Meth-dependent patients with a recent dosing (72h) (60), while a another study presented increased TNF-α levels in the serum of Meth-dependent patients that were about to start a detoxification treatment (61) (**Table 2**).

Also at the peripheral level, studies that investigated variations of circulating IL-6 and IL-10 in patients with cocaine dependency reported either an increase in both cytokines relative to healthy participants (17) or no changes in these two cytokines and TNF-α at the peripheral level (62) (**Table 4)** .

As already referred, only two studies addressed how psychostimulants affect cytokine levels at both peripheral and central levels. Both studies used a long-term administration of D-amphetamine in rats, and showed similar results for cortical, striatal (but not hippocampal) and circulating cytokines, i.e. increased levels of IL-4, IL-10, IL-6 and TNF-α (63, 64). IL-1β was unchanged either at central or peripheral level (63, 64) (**Supplementary Table 3**).

Taken together, these studies reveal that when evaluating short- and long-term effects of repeated exposure to psychostimulants, the target cytokines were again IL-6, TNF-α and IL-1β. At the central level: i) 13 out of 14 studies showed an increase in TNF-α levels in at least one brain region; ii) four out of five studies reported increased IL-6, and iii) all the twelve studies addressing IL-1β reported an increase. At the peripheral level: i) two out of five studies presented an increase in TNF-α and IL-6, and ii) two out of two studies reported an increase in IL-1β and IL-10. Interestingly, none of the two studies that evaluated the IFN-γ levels reported changes in this cytokine.

In summary, despite some variability, most of the cytokines evaluated seem to be increased in the brain after short and long-term exposure to psychostimulants, with more robust results for TNF-α, IL-6 and IL-1β. At the peripheral level there is a clear need for further investigation. Importantly, the few studies that analyzed cytokines both at the peripheral and central levels, reported similar results for the cytokines evaluated in both compartments.

Table 4: Studies addressing the impact of cocaine in peripheral cytokines

	References	Subjects	Dose regimen	Evaluation	Sample	Results	Methodology
Short- and long-term	(61) Ribeiro et al., 2021	Male (12) chronic users (or not) from a prison the State of Goias, Brazil.	Chronic users. Urine positive for cocaine.	In blood samples positive for cocaine.	Serum	= TNF-α, IL-6 and IL-10.	ELISA
	(17) Pianca et al., 2017	Adolescents aged 12-18 years	Participants met DSM-IV criteria for cocaine (crack) dependence.	On admission and 21 days later.	Serum	↑ IL-6 and IL-10 (on admission) = IL-6 and IL-10 (after 21 days)	Flow Cytometric bead array
Withdrawal	(76) Zaparte et al., 2019	Female (50) from an in patient unit from Southern Brazil suffering from CUD.	Participants met DSM-V criteria for cocaine (crack) dependence	4 days after the initiation of the detoxification treatment	PBMCs	↑ TNF-α, IFN-γ, IL-4 and IL-10 (low and high withdrawal) ↑ IL-2 and IL-17 (low withdrawal). ↑ IL-6 (high withdrawal)	Flow Cytometric bead array
	(75) Levandowski et al., 2016a	Women (36) recruited from therapeutic communities in Southern Brazil	Participants met DSM-IV criteria for cocaine (crack) dependence. No acute abstinence (>20 days).	At admission	Serum	↑ IL-6	Flow Cytometric bead array
	(74) Levandowski et al., 2016b	Women (108) recruited from therapeutic communities in Southern Brazil	Participants met DSM-IV criteria for cocaine (crack) dependence.	On day 4, 11 and 18 of the 3-week detoxification period.	Serum	↓ TNF-α and IL-6 (day 4 and 11) = TNF-α and IL-6 (day 18) ↓ IFN-γ, IL-2 and IL-17A ↑ IL-4 and IL-10	Flow Cytometric bead array

Reinstatement	(80) Gupta et al., 2018	Male adults (11) with current cocaine use	Cocaine users within the past 4 weeks. After 24 h of admission, subjects received a cocaine bolus at 0.18 mg/Kg and if tolerated then 90 min later another cocaine bolus at 0.36 mg/Kg, i.v.	Before cocaine injection and 6 h, 24 h and 6 days after cocaine challenge	Serum	= IL-6	ELISA

Abbreviations: CUD – Cocaine use disorder; DSM – Diagnostic and statistical manual of mental disorders; ELISA - enzyme-linked immunosorbent assay; FACS - Fluorescence activated cell sorting; IFN – Interferon; IL – Interleukin; i.v. – intravenous; PBMCs – Peripheral blood mononuclear cells; TNF-α – Tumor necrosis factor α. Results are expressed relative to control (↑-increase; ↓- decrease; = - unaltered).

Table 5: Studies addressing the impact of methylphenidate in central cytokines

	References	Subjects	Dose regimen	Evaluation	Brain region	Results	Methodology
Short- and long-term	(55) Ebrahimzadeh A. et al, 2019	Male Wistar rats	10 mg/Kg for 21 days, i.p.	On day 22	Hippocampus	↑ IL-1β and TNF-α	ELISA
	(50) Motaghinejad and Motevalian, 2016	Male rats	10 mg/Kg for 21 days, i.p.	On day 22	Hippocampus	↑ IL-1β and TNF-α	ELISA
	(49) Motaghinejad and Motevalian, 2022	Male Wistar rats	10 mg/Kg for 21 days, i.p.	On day 22	Hippocampus	↑ IL-1β and TNF-α	ELISA
	(48) Motaghinejad et al., 2016a	Male Wistar rats	2, 5,10 or 20 mg/Kg for 21 days, i.p.	On day 22	Hippocampus	↑ IL-1β and TNF-α (using 10 or 20 mg/Kg for 21 days)	ELISA
	(53) Motaghinejad et al., 2016b	Male Wistar rats	10 mg/Kg for 21 days, i.p.	On day 22	Hippocampus	↑ IL-1β and TNF-α	ELISA
	(52) Motaghinejad et al., 2017	Male Wistar rats	2, 5,10 or 20 mg/Kg, i.p.	On day 22	Hippocampus	↑ TNF-α ↑ IL-1β (with 10 and 20 mg/Kg dose regimen)	ELISA
	(51) Motaghinejad et al., 2016c	Male Wistar rats	10 mg/Kg for 28 days, i.p.	24h after the last administration	Hippocampus	↑ IL-1β and TNF-α	ELISA
	(54) Schmitz et al., 2017	Juvenile male Wistar rats	2 mg/Kg for 30 days, i.p.	24h after the last administration	Hippocampus	↑ IL-6 and TNF-α	ELISA

Abbreviations: ELISA - enzyme-linked immunosorbent assay; IL – Interleukin; i.p. – intraperitoneal; TNF-α – Tumor necrosis factor α. Results are expressed relative to control (↑ - increase).

Central and peripheral cytokine profiles at the withdrawal from psychostimulants

The withdrawal period encompasses a disruption in drug intake, in which one develops distressing feelings and strong physiologic reactions (24). A correct management of this period is critical to prevent drug relapse (24). In this context, understanding how cytokine levels impact on anxiety and impulsivity, critical factors for relapse, may contribute to more successful therapeutic approaches.

Within the pool of studies obtained for review that addressed the cytokine profile at the withdrawal from psychostimulants, we found ten studies reporting on central cytokine levels, nine studies analyzing circulating levels, and one evaluating them both at central and peripheral levels (**Tables 1- 4 and Supplementary Tables 1 and 3**).

When considering studies that evaluated cytokines, at the central level, during withdrawal from Meth, five publications reported increased TNF-α in the hippocampus, striatum, substantia nigra and PFC (42, 45, 65-67), while one publication showed decreased TNF-α in the frontal cortex and unaltered TNF-α in the amygdala and striatum (68) **(Table 1 and Supplementary Table 1)**. Other authors, also found unaltered TNF-α in the hypothalamus (69) **(Table 1)**. Of note, differently from the other publications that resorted to shorter administration periods, i.e. 5 to 15 days (42, 65-67), Stolyarova and colleagues administered Meth for 4 weeks and evaluated cytokine levels 17 days after the last Meth administration (68), which may justify the divergences in reported data **(Table 1)**.

Focusing on IL-1β, we identified two studies showing an increased expression in the substancia nigra, hippocampus and PFC (66, 67), and two studies showing decreased IL-1β in the striatum and frontal cortex (42, 68) **(Table 1)**. Additionally, three studies reported that IL-1β was unaltered in the hippocampus, hypothalamus, amygdala and striatum at the withdrawal from Meth (42, 68, 69) **(Table 1)**. Again, these studies used different Meth doses (ranging from 0.3 to 20 mg/kg) and different administration periods, which invalidates direct comparisons.

Within the studies that evaluated the pro-inflammatory cytokine IL-6, one work showed increased levels in the hippocampus and PFC during the Meth withdrawal period (65) **(Table 1)** and another showed its increase in striatum during withdrawal from para-methoxy-methamphetamine (45) **(Supplementary Table 1)**. Other two studies reported that at Meth withdrawal IL-6 was unaltered in the hypothalamus, amygdala and striatum (67, 68) **(Table 1)**. Again, Stolyarova and colleagues reported the opposite effect in the PFC, showing a decrease in IL-6 expression during the withdrawal period (68) **(Table 1)**.

In addition, one of the publications analyzed, revealed unaltered levels of IFN-γ in the hypothalamus (69) **(Table 1)**, while Shin and colleagues (45) **(Supplementary Table 1)** reported an increase in this cytokine in the striatum. Upon that, two studies reported

unaltered IL-10 in the hypothalamus, amygdala and striatum (69) and decreased IL-10 in the PFC after Meth withdrawal (68) **(Table 1)**. Lastly, IL-2 levels were seen increased in the hypothalamus (69) **(Table 1)**.

When addressing studies that evaluated cytokines during withdrawal from cocaine: i) three studies reported unaltered TNF-α levels in the ventral striatum, hippocampus and mPFC (31, 48, 70) **(Table 3)**; ii) one study reported that IL-6 was increased in the hippocampus (48); iii) another that it was unaltered in the mPFC (70); and this last one also study showed that IL-1β levels were unaltered in the mPFC (70) **(Table 3)**. The levels of IFN-γ were described as decreased at earlier cocaine withdrawal (3 days after last administration) and as unaltered in longer periods of withdrawal (7 and 14 days after last administration) in the hippocampus (48) **(Table 3)**.

At the peripheral level, opposing results were reported. In Meth abstinent patients, one study showed that IL-1β levels were unaltered in the plasma (71), while another showed that IL-1β was increased (59) **(Table 2)**. The same was observed for TNF-α, one study reported unaltered levels (59) and two studies reported an increase (72, 73) **(Table 2)**. Opposing results were also described for IL-10, with Kohno and colleagues claiming that IL-10 was unaltered in Meth abstinent patients (71), and Kuo and colleagues reporting that IL-10 was decreased in the plasma of Meth abstinent patients (59) **(Table 2)**. Interestingly, Re and colleagues (73), showed that IL-10 levels were unaltered in the plasma of patients in early periods of withdrawal (7-15 days and 3 months), but increased after one year of Meth withdrawal **(Table 2)**.

For IL-6 and IL-2 reported data were consistent, showing an increase in these cytokines in three studies that evaluating Meth abstinent patients (59, 71, 73) **(Table 2).** Furthermore, for IL-2, similar results were observed in rats (74) **(Table 2)**.

Other cytokines were also evaluated in Meth abstinent patients, showing an increase in IL-4, IL-1α, IL-18, IL-12, IL-7 and IL-5, a decrease in IL-8 and IL-9, and unaltered levels of IFN-γ and IL-5 as measured in the serum (59, 72, 73) (**Table 2**). The strong level of variation observed among different studies may be attributable to differences in the target populations, since most were recruited from rehabilitation centers in China and Taiwan.

Regarding the studies performed in cocaine abstinent patients, one study evaluated the serum cytokine levels in adolescents, at different time-points of the withdrawal period, and observed that initially the levels of TNF-α and IL-6 were decreased, but after a longer period of abstinence, the levels of both cytokines were reestablished (75) **(Table 4)**. Another study, also in adolescents, showed unaltered IL-6 after a similar period of cocaine withdrawal in the serum (17), and two studies reported an increase in IL-6 at a similar time-point, but in women meeting the criteria for cocaine (crack) dependence (76, 77). **(Table 4)**. Yet in cocaine abstinent patients, different studies addressing circulating

levels reported: i) an increase in TNF-α (77); ii) increased IL-10 in adults (75, 77); iii) unaltered IL-10 in adolescents (17); iv) increased IFN-γ, IL-2 and IL-17 in PBMCs (77); v) decrease IFN-γ, IL-2 and IL-17 in the serum (75); and vi) augmented IL-4 in two studies (75, 77) **(Table 4**).

A single study addressed cytokines both at central and peripheral levels at withdrawal, using a binge protocol of amphetamine (3x1mg/kg, 3 h apart) for six consecutive days, and reporting increased TNF in the striatum and in serum, and unaltered TNF-α in the hippocampus (78) **(Supplementary Table 3)**.

Taken together, at central level: i) five out of ten studies showed an increase in TNF-α and only one reported decreased levels; ii) four out of seven showed increased IL-6 and IL-1β; and iii) one out of two presented a decrease in IL-10 levels. At the peripheral level, i) three out of six studies reported an increase in TNF-α: ii) six out of eight showed an increase in IL-6; iii) one out of three reported increased IL-1β; iv) two out of seven presented increased IL-10; v) two out of four showed an increase in IFN-γ; vi) three out of four presented increased IL-2; and vii) one out of two reported increased IL-17 (see also **Fig. 3**). Up on that, four studies evaluated peripheral levels of IL-4, and all reported increased levels. For all the cytokines evaluated at peripheral level, with an exception of IL-4, only one study reported decreased levels.

As described above, the pool of studies that reported data on how withdrawal from psychostimulants affect the cytokine profile, described very heterogeneous results. These may be influenced by several parameters that differ between the studies such as dosing, age of use, or other unreported pathologies; however, the period of withdrawal in which cytokines were evaluated seems to be a powerful modulator of the outcome. This is confirmed in studies that evaluated cytokine profiles in different withdrawal periods and timepoints (48, 66, 73, 75).

Central and peripheral cytokines profiles after psychostimulant reinstatement

The high rates of relapse are a major obstacle in the treatment of drug addiction (24). Therefore, it is important to address also how relapse itself impacts on cytokines. This can be nicely investigated using animal models of reinstatement (24), which are considered a measure of relapse in drug intake.

Among the four studies that evaluated cytokines after psychostimulants reinstatement, two studies measured cytokines in the brain (79, 80) and two studies in the blood (74, 81) (**Tables 1-4**). No studies evaluating simultaneously cytokines at central and peripheral level were found.

One of the reviewed studies evaluated the levels of TNF-α, IL-10, IL-1β and IL-6 in the PFC and hippocampus of rodents, after reinstatement with two different doses of Meth (0.25 or 0.5 mg/Kg) (79) **(Table 1)**. The levels of TNF-α and IL-10 were increased in both brain regions after reinstatement following the highest Meth dose. The levels of IL-1β were increased with both reinstatement doses, but only in the PFC. No changes were reported for IL-6. At the central level, another study, also in rodents, showed increased IL-1β in the VTA after a cocaine challenge, but no differences in TNF-α levels (80) **(Table 3)**.

Lastly, Li and colleagues showed that in patients suffering from Meth use disorder, a Meth challenging-dose increased IL-6 levels within 360 min of Meth infusion (82) **(Table 2)**. The same study showed that TNF-α levels were not affected at that time point (82). Gupta and colleagues, on the other hand, showed in adult cocaine users, that a cocaine challenging does not seem to affect IL-6 levels in the serum at 6h, 24h and 6 days past cocaine (81) **(Table 4)**.

Based on the reduced number of studies addressing cytokines at reinstatement and the variability on reported data, the only possible conclusion is that a strong research effort is yet necessary in the field.

4. Discussion

There is robust evidence confirming that psychostimulants strongly impact on cytokine production and release both at central and peripheral level. However, a number of important matters remain unclear, of which we highlight that: i) there is a clear lack of information regarding the temporal course of cytokines dysregulation along the transition from episodic to problematic use and progression to addiction; ii) the crosstalk between central and peripheral immune players, under exposure to psychostimulants, and whether this crosstalk could be a valuable therapeutic target, remains elusive. The present scoping review aimed at providing a comprehensive compilation of the cytokine profile at central and peripheral level in the different stages of the addictive process, envisioning the understanding of the crosstalk between the two immune systems during the disease progression and, eventually the use of cytokines as biomarkers. From the present analysis, it is possible to conclude that the available data are mostly focused on the classical pro-inflammatory cytokines TNF-α, IL-6 and IL-1β. This was not an unexpected result since, in general, psychoactive substances have been described to activate pro-inflammatory immune responses and inflammation has been associated with drug-seeking, craving and withdrawal (83-85).

Focusing on the studies that evaluated TNF-α in the brain, all of them conducted in animal models, and looking into the results longitudinally, throughout the different phases of the addictive process, this cytokine was seen increased at central level, mainly after

acute exposures and during the short- and long-term administration of psychostimulants (**Fig. 3**). Contrarily, during the withdrawal period, the results were heterogeneous, with studies showing changes in TNF-α levels in opposite directions (**Fig. 3**). Additionally, the results for TNF-α levels at the periphery were less robust, which can simply be a consequence of the fewer studies having evaluated this cytokine in the blood, or because they were evaluated in different human populations (such adult women vs adolescents) (**Fig. 3**). Only further research will clarify this issue. The differences observed for TNF-α levels after either acute or after short- and long-term exposure to psychostimulants, may be justified by several variables, such as differences in drug dosing and route of administration or time-point of evaluation. Furthermore, at the central level, these differences were highly dependent on the brain region evaluated. At the withdrawal period, however, one can speculate that the heterogeneous results reported were mostly due differences in timepoints of analysis (86).

Over the past few years, cytokines have been described as modulators of behavior (reviewd in 10) and in problematic drug use they seem to vary according to the stage of the disease and consequently differently impact on behavior throughout disease progression. In particular, TNF-α has been described as an important modulator of different behaviors, such as sickness behavior, depressive-like behavior and cognitive dysfunction (10, 87-89). Moreover, several studies suggest that TNF-α produced by peripheral immune cells, may signal CNS cells and impact on different behaviors (10, 87, 89). Recently, it was demonstrated that circulating TNF-α levels were positively associated with depression scores in people with drug use disorder (19), while dampened TNF-α and TNFR1 levels were associated with stress response in abstinent alcohol-dependent individuals (90). Additionally, the severity of withdrawal symptoms was positively associated with TNF-α levels (90). As such, it possible that under psychostimulants, increased TNF-α, acutely and after longer periods of exposure, may be positively related with depressive mood. Likewise, TNF-α variable levels during abstinent periods may also be associated with variable withdrawal symptoms and possible increased likelihood of relapse. However, the scarcity of results regarding TNF-α levels at drug reinstatement averts a deeper understanding of its possible role in relapse.

The pro-inflammatory cytokine IL-6 was investigated in fewer studies than TNF-α, but looking into the results longitudinally, allows perceiving that these two cytokines display similar variations across the different phases of exposure to psychostimulants (**Fig. 3**). Centrally, the levels of IL-6 were reported, in animal models, as mainly increased under acute exposure or short- to long-term administration of psychostimulants; while during the withdrawal period the results were more heterogeneous (**Fig. 3**). When a addressing

the variation of circulating IL-6, again, in different human populations results were variable. Furthermore, there is, to some extent, higher heterogeneity in the levels of IL-6 reported within each period, which may be explained by the factors already mentioned for TNF-α.

In the CNS, IL-6 signaling modulates a variety of stress-related and sickness-like behaviors (10, 91). A growing body of evidence suggests that IL-6 has a crucial role in the pathogenesis of depression (91) and recent studies, both pre-clinical and clinical, demonstrated a functional role for IL-6 in the development of major depressive disorder (MDD) (92). In MDD patients, IL-6 is the most consistently increased cytokine in the blood (91, 93, 94), which was also reported as increased at the central level (95). This cytokine has been suggested as a promising potential target to treat depression (92). In pathological alcohol use, IL-6 was positively associated with depression and psychological distress scores (19). Moreover, elevated concentrations of IL-6 at peripheral level have been associated with cognitive decline (96, 97) and with Meth-induced mesocorticolimbic deficits (71). Nevertheless, further studies are still necessary to understand the role of IL-6 in depressive behavior and impaired cognition, which are also hallmarks of the problematic use psychostimulants.

Focusing into the results obtained for IL-1β, we observe that, centrally (and therefore mostly in animal models), the levels of this cytokine were reported as increased in at least one brain region, in most studies using acute administration of psychostimulants and in all studies performed after short- or long-term administration. At peripheral level, IL-1β was augmented in the few studies performed. When evaluated at the withdrawal, most studies also so showed higher levels of IL-1β in at least one brain region, but circulating levels were very inconsistent, calling for further research. This inconsistency is again driven by a reduced number of studies, conducted in very different groups of patients.

IL-1β has been described as an important modulator of sickness behavior and cognition and seems to be critical for maintaining homeostatic sleep behavior (10). Regarding cognition, in a mice model for Alzheimer disease, a chronic systemic administration of anti-IL-1R, in mice, resolved brain inflammation and reversed cognitive deficits (98). Another study suggested that increased serum levels of IL-1β were a stage marker for brain neurodegenerative progression (99). In accordance, one of the articles reviewed reported that cognitive decline after Meth exposure could be associated with IL-1 levels in the hippocampus (43). Additionally, blockade of IL-1β signaling can lead to sleep disruption (100, 101), which will also affect memory consolidation. As such, further studies focusing on IL-1β levels at the periphery and its contribution for behavioral disruption in drug context will be highly relevant.

Considering the results for the classical pro-inflammatory cytokines, TNF-α, IL-6 and IL-1β, one could conclude that the majority of the studies showed an increase in these cytokines at central level. However, peripheral results are scarcer and much less consistent. Therefore, further studies will be necessary to understand the crosstalk between the two immune compartments in the context of disease progression. Moreover, there is a demand for longitudinal studies with measurements, starting in the acute phase of psychostimulant exposure, covering different moments of long-term exposure, and addressing several time-points of withdrawal and reinstatement. Such data sets will finally clarify how TNF-α, IL-6 and IL-1β vary across the progression from occasional use to addiction.

Although, most studies included in this scoping review were focused on pro-inflammatory cytokines, a considerable number of studies also evaluated the anti-inflammatory cytokine IL-10. In the reviewed literature, IL-10 levels were mainly evaluated at the periphery and the results were heterogeneous. Contrary to what one could expect, acute, short- and long-term administration of psychostimulants resulted in increased levels of IL-10. The same was seen after reinstatement. Augmented IL-10 may be justified as a response to the elevation of pro-inflammatory cytokines (17), in particular to IFN- γ as recently described (102). On the other hand, the heterogeneous results observed during the withdrawal period may be a consequence of sampling cytokines at variable time points, as already discussed.

Variations in IL-10 expression are associated with alterations in depressive-like behavior, but do not seem to influence cognitive performance (103). Importantly, in users diagnosed with alcohol disorder, IL-10 was negatively associated with anxiety scores (19). Moreover, overexpressing IL-10, specifically in the NAcc, reduced self-administration of remifentanil in rats (104), and injections of recombinant IL-10 into the basolateral amygdala during a Drinking in the Dark (DID) paradigm attenuated binge-like ethanol consumption in mice (105). These observations suggest that IL-10 could be an important target for the treatment of addiction.

Despite some of the reviewed studies having evaluated IFN-γ and IL-4, available data is still very limited, which difficult a better understanding of the role of these cytokines in the addictive process. However, further studies focusing on the role of both cytokines will be of great importance. IFN-γ was described as an important modulator of social behavior (106), which is impaired during the psychostimulant abstinent period (107). Additionally, IL-4 was described as a critical player in learning and memory (108) and also participating in the regulation of depressive-like behavior (109).

Limitations – As already discussed this scoping review is limited by a reduced number of studies addressing cytokines simultaneously at central and peripheral levels and by

methodology differences. However, it is also important to highlight that drug users are highly heterogenous populations, not always sufficiently characterized, and most likely suffering from stress and mood disorders that can also affect the cytokine profile and impact on the data reported (110). Sex differences can also strongly affect cytokine profiles, which was not explored. Upon that, several studies have also identified chemokines as possible immunoregulators and this is not addressed in the present study.

In summary, a wide use of arrays for several cytokines should be strongly considered to better determine which cytokines, upon the classical ones, may be involved in the progression from episodic use to the development of addiction. Additionally, a concerted effort should be accomplished to better understand the link between peripheral and central immune players in longitudinal expression profiles of cytokines and its dynamics under exposure to different psychoactive substances.

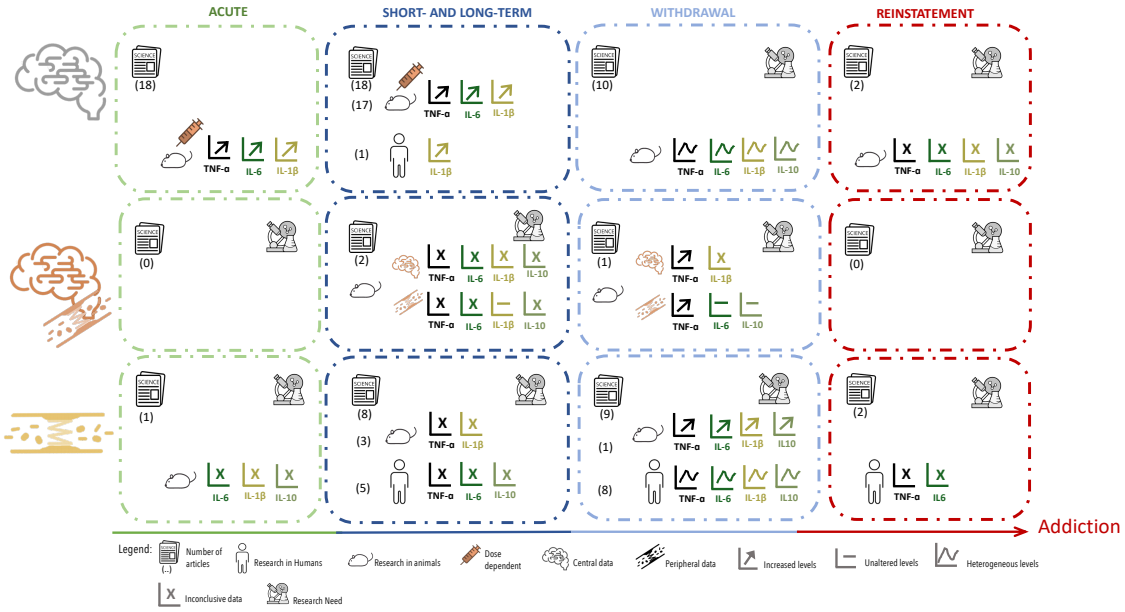

Fig. 3: Summary of data distribution according to cytokines measurement, showing the number, type and major results of manuscripts that evaluated cytokines in brain tissue, brain tissue plus blood or serum. Manuscripts were further divided according to the type of exposure and timepoint of evaluation.

References

1. Nestler EJ, Luscher C. The Molecular Basis of Drug Addiction: Linking Epigenetic to Synaptic and Circuit Mechanisms. Neuron. 2019;102(1):48-59.

2. Koob GF, Volkow ND. Neurocircuitry of addiction. Neuropsychopharmacology. 2010;35(1):217-38.

3. UNODC. Global Overview: Drug demand, drug supply. World drug report. 2021;Booklet 2.

4. Kohno M, Link J, Dennis LE, McCready H, Huckans M, Hoffman WF, et al. Neuroinflammation in addiction: A review of neuroimaging studies and potential immunotherapies. Pharmacol Biochem Behav. 2019;179:34-42.

5. Miguel-Hidalgo JJ. The role of glial cells in drug abuse. Curr Drug Abuse Rev. 2009;2(1):72-82.

6. DiSabato DJ, Quan N, Godbout JP. Neuroinflammation: the devil is in the details. J Neurochem. 2016;139 Suppl 2:136-53.

7. Becher B, Spath S, Goverman J. Cytokine networks in neuroinflammation. Nat Rev Immunol. 2017;17(1):49-59.

8. Hofer MJ, Campbell IL. Immunoinflammatory diseases of the central nervous system - the tale of two cytokines. Br J Pharmacol. 2016;173(4):716-28.

9. Deverman BE, Patterson PH. Cytokines and CNS development. Neuron. 2009;64(1):61-78.

10. Salvador AF, de Lima KA, Kipnis J. Neuromodulation by the immune system: a focus on cytokines. Nat Rev Immunol. 2021;21(8):526-41.

11. Altan-Bonnet G, Mukherjee R. Cytokine-mediated communication: a quantitative appraisal of immune complexity. Nat Rev Immunol. 2019;19(4):205-17.

12. Croese T, Castellani G, Schwartz M. Immune cell compartmentalization for brain surveillance and protection. Nat Immunol. 2021;22(9):1083-92.

13. Alves de Lima K, Rustenhoven J, Kipnis J. Meningeal Immunity and Its Function in Maintenance of the Central Nervous System in Health and Disease. Annu Rev Immunol. 2020;38:597-620.

14. Canedo T, Portugal CC, Socodato R, Almeida TO, Terceiro AF, Bravo J, et al. Astrocyte-derived TNF and glutamate critically modulate microglia activation by methamphetamine. Neuropsychopharmacology. 2021;46(13):2358-70.

15. Coelho-Santos V, Leitao RA, Cardoso FL, Palmela I, Rito M, Barbosa M, et al. The TNF-alpha/NF-kappaB signaling pathway has a key role in methamphetamine-induced blood-brain barrier dysfunction. J Cereb Blood Flow Metab. 2015;35(8):1260-71.

16. Mata MM, Napier TC, Graves SM, Mahmood F, Raeisi S, Baum LL. Methamphetamine decreases CD4 T cell frequency and alters pro-inflammatory cytokine production in a model of drug abuse. Eur J Pharmacol. 2015;752:26-33.

17. Pianca TG, Rosa RL, Cereser KMM, de Aguiar BW, de Abrahao RC, Lazzari PM, et al. Differences in biomarkers of crack-cocaine adolescent users before/after abstinence. Drug Alcohol Depend. 2017;177:207-13.

18. Sajja RK, Rahman S, Cucullo L. Drugs of abuse and blood-brain barrier endothelial dysfunction: A focus on the role of oxidative stress. J Cereb Blood Flow Metab. 2016;36(3):539-54.

19. Martinez P, Lien L, Zemore S, Bramness JG, Neupane SP. Circulating cytokine levels are associated with symptoms of depression and anxiety among people with alcohol and drug use disorders. J Neuroimmunol. 2018;318:80-6.

20. Engel K, Schaefer M, Stickel A, Binder H, Heinz A, Richter C. The Role of Psychological Distress in Relapse Prevention of Alcohol Addiction. Can High Scores on the SCL-90-R Predict Alcohol Relapse? Alcohol Alcohol. 2016;51(1):27-31.

21. Willinger U, Lenzinger E, Hornik K, Fischer G, Schönbeck G, Aschauer HN, et al. ANXIETY AS A PREDICTOR OF RELAPSE IN DETOXIFIED ALCOHOL-DEPENDENT PATIENTS. Alcohol and Alcoholism. 2002;37(6):609-12.

22. Fox HC, Milivojevic V, MacDougall A, LaVallee H, Simpson C, Angarita GA, et al. Stress-related suppression of peripheral cytokines predicts future relapse in alcohol-dependent individuals with and without subclinical depression. Addiction Biology. 2020;25(6):e12832.

23. Kuhar M. The Addicted Brain: Why We Abuse Drugs, Alcohol, and Nicotine2012.

24. DiCaro D, Lee HH, Belisario C, Ramos RL, Martinez LR. Combination of acute intravenous methamphetamine injection and LPS challenge facilitate leukocyte

infiltration into the central nervous system of C57BL/6 mice. Int Immunopharmacol. 2019;75:105751.

25. Frank MG, Adhikary S, Sobesky JL, Weber MD, Watkins LR, Maier SF. The danger-associated molecular pattern HMGB1 mediates the neuroinflammatory effects of methamphetamine. Brain Behav Immun. 2016;51:99-108.

26. Kelly KA, Miller DB, Bowyer JF, O'Callaghan JP. Chronic exposure to corticosterone enhances the neuroinflammatory and neurotoxic responses to methamphetamine. J Neurochem. 2012;122(5):995-1009.

27. Nader J, Rapino C, Gennequin B, Chavant F, Francheteau M, Makriyannis A, et al. Prior stimulation of the endocannabinoid system prevents methamphetamine-induced dopaminergic neurotoxicity in the striatum through activation of CB2 receptors. Neuropharmacology. 2014;87:214-21.

28. Seminerio MJ, Robson MJ, McCurdy CR, Matsumoto RR. Sigma receptor antagonists attenuate acute methamphetamine-induced hyperthermia by a mechanism independent of IL-1beta mRNA expression in the hypothalamus. Eur J Pharmacol. 2012;691(1-3):103-9.

29. Wang X, Northcutt AL, Cochran TA, Zhang X, Fabisiak TJ, Haas ME, et al. Methamphetamine Activates Toll-Like Receptor 4 to Induce Central Immune Signaling within the Ventral Tegmental Area and Contributes to Extracellular Dopamine Increase in the Nucleus Accumbens Shell. ACS Chem Neurosci. 2019;10(8):3622-34.

30. Lewitus GM, Konefal SC, Greenhalgh AD, Pribiag H, Augereau K, Stellwagen D. Microglial TNF-alpha Suppresses Cocaine-Induced Plasticity and Behavioral Sensitization. Neuron. 2016;90(3):483-91.

31. Montesinos J, Castilla-Ortega E, Sanchez-Marin L, Montagud-Romero S, Araos P, Pedraz M, et al. Cocaine-induced changes in CX3CL1 and inflammatory signaling pathways in the hippocampus: Association with IL1beta. Neuropharmacology. 2020;162:107840.

32. Gubert C, Fries GR, Pfaffenseller B, Ferrari P, Coutinho-Silva R, Morrone FB, et al. Role of P2X7 Receptor in an Animal Model of Mania Induced by D-Amphetamine. Mol Neurobiol. 2016;53(1):611-20.

33. Robson MJ, Turner RC, Naser ZJ, McCurdy CR, Huber JD, Matsumoto RR. SN79, a sigma receptor ligand, blocks methamphetamine-induced microglial activation and cytokine upregulation. Exp Neurol. 2013;247:134-42.

34. Urrutia A, Granado N, Gutierrez-Lopez MD, Moratalla R, O'Shea E, Colado MI. The JNK inhibitor, SP600125, potentiates the glial response and cell death induced by methamphetamine in the mouse striatum. Int J Neuropsychopharmacol. 2014;17(2):235-46.

35. Wang B, Chen T, Xue L, Wang J, Jia Y, Li G, et al. Methamphetamine exacerbates neuroinflammatory response to lipopolysaccharide by activating dopamine D1-like receptors. Int Immunopharmacol. 2019;73:1-9.

36. Kobeissy FH, Shakkour Z, Hayek SE, Mohamed W, Gold MS, Wang KKW. Elevation of Pro-inflammatory and Anti-inflammatory Cytokines in Rat Serum after Acute Methamphetamine Treatment and Traumatic Brain Injury. J Mol Neurosci. 2022;72(1):158-68.

37. Ghanbari F, Khaksari M, Vaezi G, Hojati V, Shiravi A. Hydrogen Sulfide Protects Hippocampal Neurons Against Methamphetamine Neurotoxicity Via Inhibition of Apoptosis and Neuroinflammation. J Mol Neurosci. 2019;67(1):133-41.

38. Hadizadeh-Bazaz M, Vaezi G, Khaksari M, Hojati V. Curcumin attenuates spatial memory impairment by anti-oxidative, anti-apoptosis, and anti-inflammatory mechanism against methamphetamine neurotoxicity in male Wistar rats: Histological and biochemical changes. Neurotoxicology. 2021;84:208-17.

39. Frau L, Costa G, Porceddu PF, Khairnar A, Castelli MP, Ennas MG, et al. Influence of caffeine on 3,4-methylenedioxymethamphetamine-induced dopaminergic neuron degeneration and neuroinflammation is age-dependent. J Neurochem. 2016;136(1):148-62.

40. Gou H, Sun D, Hao L, An M, Xie B, Cong B, et al. Cholecystokinin-8 attenuates methamphetamine-induced inflammatory activation of microglial cells through CCK2 receptor. Neurotoxicology. 2020;81:70-9.

41. Goncalves J, Leitao RA, Higuera-Matas A, Assis MA, Coria SM, Fontes-Ribeiro C, et al. Extended-access methamphetamine self-administration elicits neuroinflammatory response along with blood-brain barrier breakdown. Brain Behav Immun. 2017;62:306-17.

42. Liskiewicz A, Przybyla M, Park M, Liskiewicz D, Nowacka-Chmielewska M, Malecki A, et al. Methamphetamine-associated cognitive decline is attenuated by neutralizing IL-1 signaling. Brain Behav Immun. 2019;80:247-54.

43. El-Sayed El-Sisi A, Sokkar SS, El-Sayed El-Sayad M, Sayed Ramadan E, Osman EY. Celecoxib and omega-3 fatty acids alone and in combination with risperidone affect the behavior and brain biochemistry in amphetamine-induced model of schizophrenia. Biomed Pharmacother. 2016;82:425-31.

44. Shin EJ, Dang DK, Tran HQ, Nam Y, Jeong JH, Lee YH, et al. PKCdelta knockout mice are protected from para-methoxymethamphetamine-induced mitochondrial stress and associated neurotoxicity in the striatum of mice. Neurochem Int. 2016;100:146-58.

45. Valvassori SS, Resende WR, Varela RB, Arent CO, Gava FF, Peterle BR, et al. The Effects of Histone Deacetylase Inhibition on the Levels of Cerebral Cytokines in an Animal Model of Mania Induced by Dextroamphetamine. Mol Neurobiol. 2018;55(2):1430-9.

46. Chivero ET, Thangaraj A, Tripathi A, Periyasamy P, Guo ML, Buch S. NLRP3 Inflammasome Blockade Reduces Cocaine-Induced Microglial Activation and Neuroinflammation. Mol Neurobiol. 2021;58(5):2215-30.

47. Mai HN, Chung YH, Shin EJ, Sharma N, Jeong JH, Jang CG, et al. IL-6 knockout mice are protected from cocaine-induced kindling behaviors; possible involvement of JAK2/STAT3 and PACAP signalings. Food Chem Toxicol. 2018;116(Pt B):249-63.

48. Motaghinejad M, Motevalian M, Shabab B. Effects of chronic treatment with methylphenidate on oxidative stress and inflammation in hippocampus of adult rats. Neurosci Lett. 2016;619:106-13.

49. Motaghinejad M, Motevalian M. Neuroprotective Properties of Minocycline Against Methylphenidate-Induced Neurodegeneration: Possible Role of CREB/BDNF and Akt/GSK3 Signaling Pathways in Rat Hippocampus. Neurotox Res. 2022;40(3):689-713.

50. Motaghinejad M, Motevalian M. Involvement of AMPA/kainate and GABAA receptors in topiramate neuroprotective effects against methylphenidate abuse sequels involving oxidative stress and inflammation in rat isolated hippocampus. Eur J Pharmacol. 2016;784:181-91.

51. Motaghinejad M, Seyedjavadein Z, Motevalian M, Asadi M. The neuroprotective effect of lithium against high dose methylphenidate: Possible role of BDNF. Neurotoxicology. 2016;56:40-54.

52. Motaghinejad M, Motevalian M, Shabab B. Possible involvements of glutamate and adrenergic receptors on acute toxicity of methylphenidate in isolated hippocampus and cerebral cortex of adult rats. Fundam Clin Pharmacol. 2017;31(2):208-25.

53. Motaghinejad M, Motevalian M, Shabab B. Neuroprotective effects of various doses of topiramate against methylphenidate induced oxidative stress and inflammation in rat isolated hippocampus. Clin Exp Pharmacol Physiol. 2016;43(3):360-71.

54. Schmitz F, Pierozan P, Rodrigues AF, Biasibetti H, Grunevald M, Pettenuzzo LF, et al. Methylphenidate Causes Behavioral Impairments and Neuron and Astrocyte Loss in the Hippocampus of Juvenile Rats. Mol Neurobiol. 2017;54(6):4201-16.

55. Ebrahimzadeh A, Moghadam SY, Rahimi H, Motaghinejad M, Motevalian M, Safari S, et al. Crocin acts as a neuroprotective mediator against methylphenidate-induced neurobehavioral and neurochemical sequelae: Possible role of the CREB-BDNF signaling pathway. Acta Neurobiol Exp (Wars). 2019;79(4):352-66.

56. Bristot G, Ascoli BM, Scotton E, Gea LP, Pfaffenseller B, Kauer-Sant'Anna M. Effects of lithium on inflammatory and neurotrophic factors after an immune challenge in a lisdexamfetamine animal model of mania. Braz J Psychiatry. 2019;41(5):419-27.

57. Wang LB, Xu LL, Chen LJ, Zhang KK, Zhang QY, Chen YK, et al. Methamphetamine induces intestinal injury by altering gut microbiota and promoting inflammation in mice. Toxicol Appl Pharmacol. 2022;443:116011.

58. Kuo SC, Yeh YW, Chen CY, Huang CC, Ho PS, Liang CS, et al. Differential effect of the DRD3 genotype on inflammatory cytokine responses during abstinence in amphetamine-dependent women. Psychoneuroendocrinology. 2018;97:37-46.

59. Jiang J, Wang M, Liang B, Shi Y, Su Q, Chen H, et al. In vivo effects of methamphetamine on HIV-1 replication: A population-based study. Drug Alcohol Depend. 2016;159:246-54.

60. Shen S, Zhao J, Dai Y, Chen F, Zhang Z, Yu J, et al. Methamphetamine-induced alterations in intestinal mucosal barrier function occur via the microRNA-181c/ TNF-alpha/tight junction axis. Toxicol Lett. 2020;321:73-82.

61. Ribeiro CB, Castro FOF, Dorneles GP, de Sousa Barros JB, Silva JM, Tavares C, et al. The concomitant use of cannabis and cocaine coexists with increased LPS levels and systemic inflammation in male drug users. Cytokine. 2021;141:155472.

62. Valvassori SS, Dal-Pont GC, Tonin PT, Varela RB, Ferreira CL, Gava FF, et al. Coadministration of lithium and celecoxib attenuates the behavioral alterations and inflammatory processes induced by amphetamine in an animal model of mania. Pharmacol Biochem Behav. 2019;183:56-63.

63. Valvassori SS, Tonin PT, Varela RB, Carvalho AF, Mariot E, Amboni RT, et al. Lithium modulates the production of peripheral and cerebral cytokines in an animal model of mania induced by dextroamphetamine. Bipolar Disord. 2015;17(5):507-17.

64. Beirami E, Oryan S, Seyedhosseini Tamijani SM, Ahmadiani A, Dargahi L. Intranasal insulin treatment alleviates methamphetamine induced anxiety-like behavior and neuroinflammation. Neurosci Lett. 2017;660:122-9.

65. Jiang W, Li J, Zhang Z, Wang H, Wang Z. Epigenetic upregulation of alpha-synuclein in the rats exposed to methamphetamine. Eur J Pharmacol. 2014;745:243-8.

66. Namyen J, Permpoonputtana K, Nopparat C, Tocharus J, Tocharus C, Govitrapong P. Protective Effects of Melatonin on Methamphetamine-Induced Blood-Brain Barrier Dysfunction in Rat Model. Neurotox Res. 2020;37(3):640-60.

67. Stolyarova A, Thompson AB, Barrientos RM, Izquierdo A. Reductions in frontocortical cytokine levels are associated with long-lasting alterations in reward valuation after methamphetamine. Neuropsychopharmacology. 2015;40(5):1234-42.

68. Loftis JM, Wilhelm CJ, Vandenbark AA, Huckans M. Partial MHC/neuroantigen peptide constructs: a potential neuroimmune-based treatment for methamphetamine addiction. PLoS One. 2013;8(2):e56306.

69. Zhu W, Ge X, Gao P, Li M, Guan Y, Guan X. Adolescent cocaine exposure induces prolonged synaptic modifications in medial prefrontal cortex of adult rats. Brain Struct Funct. 2018;223(4):1829-38.

70. Kohno M, Loftis JM, Huckans M, Dennis LE, McCready H, Hoffman WF. The relationship between interleukin-6 and functional connectivity in methamphetamine users. Neurosci Lett. 2018;677:49-54.

71. Luo Y, He H, Ou Y, Zhou Y, Fan N. Elevated serum levels of TNF-alpha, IL-6, and IL-18 in chronic methamphetamine users. Hum Psychopharmacol. 2022;37(1):e2810.

72. Re GF, Jia J, Xu Y, Zhang Z, Xie ZR, Kong D, et al. Dynamics and correlations in multiplex immune profiling reveal persistent immune inflammation in male drug users after withdrawal. Int Immunopharmacol. 2022;107:108696.

73. Li Z, Qi Y, Liu K, Cao Y, Zhang H, Song C, et al. Effect of Chaihu-jia-Longgu-Muli decoction on withdrawal symptoms in rats with methamphetamine-induced conditioned place preference. Biosci Rep. 2021;41(8).

74. Levandowski ML, Viola TW, Prado CH, Wieck A, Bauer ME, Brietzke E, et al. Distinct behavioral and immunoendocrine parameters during crack cocaine abstinence in women reporting childhood abuse and neglect. Drug Alcohol Depend. 2016;167:140-8.

75. Levandowski ML, Hess AR, Grassi-Oliveira R, de Almeida RM. Plasma interleukin-6 and executive function in crack cocaine-dependent women. Neurosci Lett. 2016;628:85-90.

76. Zaparte A, Schuch JB, Viola TW, Baptista TAS, Beidacki AS, do Prado CH, et al. Cocaine Use Disorder Is Associated With Changes in Th1/Th2/Th17 Cytokines and Lymphocytes Subsets. Front Immunol. 2019;10:2435.

77. You MJ, Bang M, Park HS, Yang B, Jang KB, Yoo J, et al. Human umbilical cord-derived mesenchymal stem cells alleviate schizophrenia-relevant behaviors in amphetamine-sensitized mice by inhibiting neuroinflammation. Transl Psychiatry. 2020;10(1):123.

78. Karimi-Haghighi S, Dargahi L, Haghparast A. Cannabidiol modulates the expression of neuroinflammatory factors in stress- and drug-induced reinstatement of methamphetamine in extinguished rats. Addict Biol. 2020;25(2):e12740.

79. Brown KT, Levis SC, O'Neill CE, Northcutt AL, Fabisiak TJ, Watkins LR, et al. Innate immune signaling in the ventral tegmental area contributes to drug-primed reinstatement of cocaine seeking. Brain Behav Immun. 2018;67:130-8.

80. Gupta K, Sharma R, Singh V, Masoomi R, Dileepan KN, He J, et al. Intravenous Cocaine Results in an Acute Decrease in Levels of Biomarkers of Vascular Inflammation in Humans. Cardiovasc Toxicol. 2018;18(4):295-303.

81. Crews FT, Zou J, Qin L. Induction of innate immune genes in brain create the neurobiology of addiction. Brain Behav Immun. 2011;25 Suppl 1:S4-S12.

82. Cui C, Shurtleff D, Harris RA. Neuroimmune mechanisms of alcohol and drug addiction. Int Rev Neurobiol. 2014;118:1-12.

83. Coller JK, Hutchinson MR. Implications of central immune signaling caused by drugs of abuse: mechanisms, mediators and new therapeutic approaches for prediction and treatment of drug dependence. Pharmacol Ther. 2012;134(2):219-45.

84. Harricharan R, Abboussi O, Daniels WMU. Addiction: A dysregulation of satiety and inflammatory processes. Prog Brain Res. 2017;235:65-91.

85. Clinical Guidelines for Withdrawal Management and Treatment of Drug Dependence in Closed Settings. WHO Guidelines Approved by the Guidelines Review Committee. Geneva2009.

86. Hennessy E, Gormley S, Lopez-Rodriguez AB, Murray C, Murray C, Cunningham C. Systemic TNF-alpha produces acute cognitive dysfunction and exaggerated sickness behavior when superimposed upon progressive neurodegeneration. Brain Behav Immun. 2017;59:233-44.

87. Fourrier C, Bosch-Bouju C, Boursereau R, Sauvant J, Aubert A, Capuron L, et al. Brain tumor necrosis factor-alpha mediates anxiety-like behavior in a mouse model of severe obesity. Brain Behav Immun. 2019;77:25-36.

88. Kaster MP, Gadotti VM, Calixto JB, Santos AR, Rodrigues AL. Depressive-like behavior induced by tumor necrosis factor-alpha in mice. Neuropharmacology. 2012;62(1):419-26.

89. Fox HC, Milivojevic V, Angarita GA, Stowe R, Sinha R. Peripheral immune system suppression in early abstinent alcohol-dependent individuals: Links to stress and cue-related craving. J Psychopharmacol. 2017;31(7):883-92.

90. Barney TM, Vore AS, Gano A, Mondello JE, Deak T. The influence of central interleukin-6 on behavioral changes associated with acute alcohol intoxication in adult male rats. Alcohol. 2019;79:37-45.

91. Roohi E, Jaafari N, Hashemian F. On inflammatory hypothesis of depression: what is the role of IL-6 in the middle of the chaos? J Neuroinflammation. 2021;18(1):45.

92. Miranda DO, Anatriello E, Azevedo LR, Cordeiro JFC, Peria FM, Floria-Santos M, et al. Elevated serum levels of proinflammatory cytokines potentially correlate with depression and anxiety in colorectal cancer patients in different stages of the antitumor therapy. Cytokine. 2018;104:72-7.

93. Dowlati Y, Herrmann N, Swardfager W, Liu H, Sham L, Reim EK, et al. A meta-analysis of cytokines in major depression. Biol Psychiatry. 2010;67(5):446-57.

94. Kern S, Skoog I, Borjesson-Hanson A, Blennow K, Zetterberg H, Ostling S, et al. Higher CSF interleukin-6 and CSF interleukin-8 in current depression in older women. Results from a population-based sample. Brain Behav Immun. 2014;41:55-8.

95. Tegeler C, O'Sullivan JL, Bucholtz N, Goldeck D, Pawelec G, Steinhagen-Thiessen E, et al. The inflammatory markers CRP, IL-6, and IL-10 are associated with cognitive function--data from the Berlin Aging Study II. Neurobiol Aging. 2016;38:112-7.

96. Mooijaart SP, Sattar N, Trompet S, Lucke J, Stott DJ, Ford I, et al. Circulating interleukin-6 concentration and cognitive decline in old age: the PROSPER study. J Intern Med. 2013;274(1):77-85.

97. Kitazawa M, Cheng D, Tsukamoto MR, Koike MA, Wes PD, Vasilevko V, et al. Blocking IL-1 signaling rescues cognition, attenuates tau pathology, and restores neuronal beta-catenin pathway function in an Alzheimer's disease model. J Immunol. 2011;187(12):6539-49.

98. Forlenza OV, Diniz BS, Talib LL, Mendonca VA, Ojopi EB, Gattaz WF, et al. Increased serum IL-1beta level in Alzheimer's disease and mild cognitive impairment. Dement Geriatr Cogn Disord. 2009;28(6):507-12.

99. Opp MR, Krueger JM. Anti-interleukin-1 beta reduces sleep and sleep rebound after sleep deprivation in rats. Am J Physiol. 1994;266(3 Pt 2):R688-95.

100. Takahashi S, Fang J, Kapas L, Wang Y, Krueger JM. Inhibition of brain interleukin-1 attenuates sleep rebound after sleep deprivation in rabbits. Am J Physiol. 1997;273(2 Pt 2):R677-82.

101. Cardoso A, Martins AC, Maceiras AR, Liu W, Castro I, Castro AG, et al. Interleukin-10 induces interferon-gamma-dependent emergency myelopoiesis. Cell Rep. 2021;37(4):109887.

102. Mesquita AR, Correia-Neves M, Roque S, Castro AG, Vieira P, Pedrosa J, et al. IL-10 modulates depressive-like behavior. J Psychiatr Res. 2008;43(2):89-97.

103. Lacagnina MJ, Kopec AM, Cox SS, Hanamsagar R, Wells C, Slade S, et al. Opioid Self-Administration is Attenuated by Early-Life Experience and Gene Therapy for Anti-Inflammatory IL-10 in the Nucleus Accumbens of Male Rats. Neuropsychopharmacology. 2017;42(11):2128-40.

104. Marshall SA, McKnight KH, Blose AK, Lysle DT, Thiele TE. Modulation of Binge-like Ethanol Consumption by IL-10 Signaling in the Basolateral Amygdala. J Neuroimmune Pharmacol. 2017;12(2):249-59.

105. Filiano AJ, Xu Y, Tustison NJ, Marsh RL, Baker W, Smirnov I, et al. Unexpected role of interferon-gamma in regulating neuronal connectivity and social behaviour. Nature. 2016;535(7612):425-9.

106. Favrod-Coune T, Broers B. The Health Effect of Psychostimulants: A Literature Review. Pharmaceuticals (Basel). 2010;3(7):2333-61.

107. Gadani SP, Cronk JC, Norris GT, Kipnis J. IL-4 in the brain: a cytokine to remember. J Immunol. 2012;189(9):4213-9.

108. Wachholz S, Knorr A, Mengert L, Plumper J, Sommer R, Juckel G, et al. Interleukin-4 is a participant in the regulation of depressive-like behavior. Behav Brain Res. 2017;326:165-72.

109. Li MJ, Briones MS, Heinzerling KG, Kalmin MM, Shoptaw SJ. Ibudilast attenuates peripheral inflammatory effects of methamphetamine in patients with methamphetamine use disorder. Drug Alcohol Depend. 2020;206:107776.

Supplementary Information

Supplementary Table 1: Studies addressing the impact of amphetamines (other than Meth) in central cytokines

		References	Subjects	Substance	Dose regimen	Evaluation	Tissue	Results	Methodology
	Acute	(39) Frau et al, 2016	Adult and adolescent male C57BL/6J mice	MDMA	4x20 mg/Kg, 2 h apart, i.p.	48 h after administration	CPu	Adults ↑ IL-1β and TNF (no differences in the adolescent mice group)	Immuno-histochemistry
Short- and long term	Acute	(32) Gubert et al., 2016	Adult male C57BL/6J mice	Amphetamine	Acute – 2 mg/Kg, i.p. Chronic – 2 mg/Kg once a day for 7 days, i.p.	After last injection	PFC Striatum Hippocampus	**Acute and chronic treatment** PFC and hippocampus = IL-1β and TNF Striatum ↑ IL-1β = TNF	Flow Cytometric bead array
		(43) El-Sayed El-Sisi et al., 2016	Adult male rats	Amphetamine	2 mg/Kg, for 5 days, s.c.	24 h after the last injection	Brain	↑ TNF	ELISA
		(45) Valvassori et al., 2018	Male Wistar rats	Dextroamphetamine	2mg/Kg once a day for 14 days, i.p.	At day 15	Frontal cortex and striatum	Cortex and striatum ↑ IL-4; IL-6, IL-10 and TNF	ELISA
		(44) Shin et al., 2016	C57BL/6J mice	Para-methoxy -methamphetamine	60mg/Kg, twice a day for 4 consecutive days.	1 h; 2 h; 1 day and 7 days	Striatum	↑ IL-6 (at 1h; 12h and 7 days) ↑ IFN-γ and TNF	RT-PCR and western blot

Abbreviations: CPu – Caudate putamen; ELISA - enzyme-linked immunosorbent assay; IFN – Interferon; IL – Interleukin; i.p. – intraperitoneal; PFC – Prefrontal cortex; RT-PCR – Real Time Polymerase Chain Reaction; s.c. – subcutaneous; TNF – Tumor necrosis factor. Results are expressed relative to control (↑ - increase; = - unaltered).

Supplementary Table 2: Studies addressing the impact of amphetamines (other than Meth) in peripheral cytokines

	References	Subjects	Substance	Dose regimen	Evaluation	Tissue	Results	Methodology
Short- and long-term	(56) Bristot et al., 2019	Adult male Wistar rats	Lisdexamfetamine	One daily administration of 10 mg/Kg, for 14 days, gavage	On the day 14	Serum	= TNF, IL-1β and IL-10	Milliplex Map Kit

Abbreviations: IL – Interleukin; TNF – Tumor necrosis factor. Results are expressed relative to control (= - unaltered).

Supplementary Table 3: Studies addressing the impact of amphetamines (other than Meth) in both peripheral and central cytokines

	References	**Subjects**	**Substance**	**Dose regimen**	**Evaluation**	**Tissue**	**Results**	**Methodology**
Short- and long-term	(62) Valvassori et al., 2019	Male Wistar rats	Dextroamphetamine	2mg/Kg once a day for 14 days, i.p.	At day 15	Serum, cortex and striatum	Serum, cortex and striatum = IL1-β ↑ IL-4 and IL-10	ELISA
	(63) Valvassori et al., 2015	Male Wistar rats	Dextroamphetamine	2mg/Kg once a day for 14 days, i.p.	At day 15	Serum, CSF, frontal cortex, hippocampus and striatum	Serum, cortex and striatum = IL1-β ↑ IL-4, IL-6, IL-10 and TNF Hippocampus and CSF = IL1-β, IL-4, IL-6, IL-10 and TNF	ELISA

Withdrawal	(77) You et al., 2020	Male C57BL/6J mice	Amphetamine	Binge amphetamine 3x1 mg/kg (3h apart, 3xAMP) for 6 consecutive days, or 3 daily administrations, using an escalating dose regimen, consisting of 60 administrations ranging from 1 to 10 mg/Kg.	21 days past 6 days of Meth or 21 days past 20 days of escalating Meth (both with stressful behavioral evaluation in between).	Striatum, hippocampus, lymph nodes and serum.	3xAMP: <u>Striatum</u> ↑ TNF and IL-1β <u>Hippocampus</u> = TNF and IL-1β Serum ↑ TNF = IL-10, IL-6, IL-4 and IFN-γ Escalating: <u>Striatum</u> ↑ TNF = IL-1β <u>Hippocampus</u> ↑ TNF = IL-1β	RT-PCR and Bio-Plex®

Abbreviations: AMP – Amphetamine; CSF - Cerebrospinal fluid; IFN – Interferon; ELISA - enzyme-linked immunosorbent assay; IL – Interleukin; i.p. – intraperitoneal; RT-PCR – Real Time PCR. Results are expressed relative to control (= - unaltered; ↑ - increased).

CHAPTER IV

Neuron–Microglia Contact-Dependent Mechanisms Attenuate Methamphetamine-Induced Microglia Reactivity and Enhance Neuronal Plasticity

(Published in Cells in 2022)

1. Introduction

Methamphetamine (Meth) is a potent and widely abused synthetic stimulant, classically recognized by its impact on the monoaminergic and glutamatergic neuronal systems [1]. Nevertheless, it has become increasingly accepted that the interplay between neuronal and glial cells is also a relevant mechanism for addiction [2, 3]. Using human cerebral organoids, it was recently demonstrated by single-cell resolution that upon exposure to Meth, most upregulated pathways were associated with immune response and oxidative stress [4]. In accordance, in rats, a single dose of Meth was sufficient to increase the levels of pro-inflammatory cytokines in several brain regions [5].

Recently, we have shown that a binge administration of Meth leads to microgliosis and microglia activation in a process mediated by astrocytes *via* glutamate release in a TNF/IP_3R2-Ca^{2+}- dependent manner [6]. In addition, we also showed increased levels of the pro-inflammatory cytokines IL-1ß and TNF in the striatum and hippocampus [6]. However, how Meth-induced glial reactivity may affect neurons is yet unknown.

The neuronal ability to sense their surrounding environment is crucial for maintaining homeostasis in the brain parenchyma [7]. There is now considerable evidence showing that immune and neuronal systems communicate through contact-dependent regulatory molecules or over soluble factors, such as neurotransmitters, neuromodulators, cytokines, neuropeptides and miRNAs [7-9]. The communication between these two types of cells critically regulates the inflammatory response [8, 10, 11]. Indeed, it has been previously shown in other neurological disorders that neurons might attenuate microglia reactivity resorting to various different neuroprotective mechanisms [11, 12].

Several neuroimmune regulatory proteins, highly expressed in neurons, were already shown to modulate microglial activation, including CD200, CD22, CX3CL1 and CD95, among others [7]. Notably, receptors to these ligands are mostly restricted to myeloid cells. In particular, the interaction of CD200 and its receptor (CD200r) seems to act as a potent immune suppressor, promoting microglia quiescence [7]. In accordance, CD200-deficient mice display severe progression of neuroinflammation [13]. Also, CD200/CD200r signaling was shown to be involved in the spontaneous recovery of synaptic plasticity after stroke *via* the inhibition of microglia activation and reduction of inflammatory factors release [12]. Corroborating this, in animal models of Alzheimer´s disease, restoration of neuronal CD200 improved cognitive function and prevented further synaptic impairment [14].

In this scenario, understanding how glial activation by Meth will affect the crosstalk between glial cells and neurons will provide a more comprehensive understanding of the

mechanisms involved in modulation of psychostimulant-induced neuroinflammation. Here, we investigated how neurons affect microglia activation under Meth exposure. Our results revealed that contact-dependent mechanisms between neurons and microglia, namely through CD200/CD200r signaling, attenuate Meth-induced microglia reactivity and enhance synaptic plasticity.

2. Material and Methods

Animals

Timely pregnant Wistar dams were necessary to obtain both 18 days embryos (E18) and postnatal day one or two pups (P1-P2). All procedures were conducted following the Directive 2010/63/EU and approved by the competent authorities Direcção Geral de Alimentação e Veterinária (DGAV) and i3S Animal Ethical Committee (ref.2018-13-TS and DGAV 003891/2019-02-15). Researchers involved in animal experimentation were FELASA certified. All efforts were made to minimize animal suffering and the number of dams/pups used. Dams were housed under specific pathogen-free conditions and controlled environment (20°C, 45–55% humidity) with free access to food and water.

Neuronal cell culture

Hippocampal neurons were obtained from Wistar rat embryos (E18) as described before [15]. Briefly, brain rat embryos were dissected in Hank's buffer solution (HBSS) (Gibco, ThermoFisher Scientific) and enzymatically treated with trypsin (1.5mg/mL) (Gibco, ThermoFisher Scientific) for 15 min [15]. The tissue was dissociated in serum-free Neurobasal medium (Gibco, ThermoFisher Scientific), supplemented with B27 (Gibco, ThermoFisher Scientific), glutamine (0.5 mM, Sigma-Aldrich), glutamate (25 µM, Sigma-Aldrich) and gentamycin (0.12 mg/ml) (Gibco, ThermoFisher Scientific) [15]. The cells were seeded on cell culture plates coated with 0.1mg/ml of poly-d-lysine (PDL) (Sigma-Aldrich) at a density of 0.75x105/cm2 and kept at 37 °C in a humidified incubator with 5% CO2/95% air, for 12 days in vitro (DIV). At DIV8, the medium was partially replaced.

Microglia and astrocytes purified cultures obtained from mixed glial cell cultures

The mixed glial cell cultures (MGC) were obtained from newborn Wistar pups (P1-P2) [6, 16]. The pups' brains were dissected in HBSS with 1% *Penicillin-Streptomycin* (P/S)

(Gibco, ThermoFisher Scientific). The meninges were removed, and the cortex and hippocampi were collected. After complete tissue dissociation, DNAse I (0.1U/ml) (Irvine) and 0.25% of trypsin (Gibco, Life Technologies) were added and incubated 15 min at 37ºC. The cells were suspended in Dulbecco's Modified Eagle Medium (DMEM) (1x)/Glutamax (Gibco, ThermoFisher Scientific) supplemented with 10% of FBS and 1% of P/S. The cell suspension was distributed by T-75 flasks coated with 0.01mg/ml of PDL at a density of two brains/flask. The cell cultures were maintained for 10 days at 37ºC in a humidified incubator with 5% CO_2/95% air; the medium was partially replaced at DIV 4 and then totally replaced every 2 days.

To prepare the purified microglial cultures, MGCs were shaken at 200 rpm for 2h in iNFORS HT Minitron incubator with a radius of 2.5 cm at 37ºC. The cell suspension obtained was centrifuged at 1200 rpm for 10 min and suspended in Dulbecco's Modified Eagle Medium: Nutrient Mixture F-12 (DMEM/F-12) (Gibco, ThermoFisher Scientific) supplemented with 10% of FBS and 1% of P/S. Purified microglia were plated at a density of $0.5x10^5/cm^2$. Purity of microglia cell cultures was 99% as previously reported [17].

To obtain purified astrocytic cultures, the MGCs were shaken at 220 rpm overnight to remove non-astrocytic cells, and adherent cells were detached with 0.25% trypsin. The cell suspension was centrifuged at 1200 rpm for 10 min and partially split in DMEM/Glutamax supplemented with 10% of FBS and 1% of P/S, in a non-coated flask. Purified astrocytes were obtained after two consecutive splits. Cells were plated for the experiment at a density of $0.5x10^5/cm^2$.

Microglia incubation with neuronal-conditioned medium

At DIV12, the neuronal cell cultures were treated with 100 µM Meth (Sigma-Aldrich) for 24h. Untreated neuronal conditioned medium (NCM Ctrl) and conditioned medium from Meth treated neurons (NCM Meth) were collected, centrifuged (1200rpm, 1min) and added to microglial cultures (Experimental design I, Fig. 1A).

Co-cultures of neurons and microglia in microfluidic devices

Co-cultures of neurons and microglia were performed in an Axon Investigation System, adapted from [18] (AXIS150, Millipore). The microfluidic devices were placed on the top of a glass coverslips (22 x 22 mm) coated with 0.1 mg/ml PDL, channel side down, creating a microfluidic chamber composed of two compartments separated by 150 µm length × 5 µm height × 10 µm width microgrooves. Neuronal cells were plated in one of

the compartments at a density of $1x10^5$/device. At DIV 12 for neurons, microglial cells were plated in the opposite chamber at a density of $1x10^5$/device.

Astrocytic-conditioned medium

At DIV2, purified astrocytes were incubated with Meth 100 µM for 24h. The medium from untreated astrocytes (ACM Ctrl) or from Meth treated astrocytes (ACM Meth) was collected and centrifuged at 1200 rpm, 1min.

Co-cultures treatments

To carry out this study, three different conditions were used: 1) Meth 100 µM was added to the neuronal side in the microfluidic device for 24 h (Experimental design II, Fig. 2A); 2) the conditioned media obtained from astrocytes treated with Meth 100 µM for 24 h (ACM Meth) or from control astrocytes cultures (ACM Ctrl) were added to the microglial/axonal compartment for 24 h (Experimental design III, Fig. 3A); 3) ACM Ctrl or ACM Meth were added to the microglia/axonal compartment, and Meth 100 µM was added to the neuronal compartment for 24 h (Experimental design IV, Suppl. Fig. 1).

Immunocytochemistry and image acquisition

Cells were fixed with 4% PFA, permeabilized with 0.25% Triton X-100 and blocked with 3% BSA. Next, cells were incubated overnight, at 4ºC, with the primary antibody under the manufacture's recommendations, washed, and incubated with the secondary antibody for 1h at RT. Then, cells were incubated with DAPI for 5min, and coverslips were mounted with fluorescent mounting media (Dako). Imaging was done using a Zeiss AxioImager Z1 fluorescence microscope equipped with an Axiocam MR v3.0 camera, an HXP 120 light source, and a 40x/1.30 objective. The following filter sets were used to image DAPI, Alexa 488, Alexa 568 and DyLight 650, respectively: 49 - Excitation: G 365 Beam Splitter: FT 395 Emission: BP 445/50; 38HE - Excitation: BP 470/40 (HE) Beam Splitter: FT 495 (HE) Emission: BP 525/50 (HE); 43HE - Excitation: BP 550/25 (HE) Beam Splitter: FT 570 (HE) Emission: BP 605/70 (HE); 50 - Excitation: BP 640/30 Beam Splitter: FT 660 Emission: BP 690/50 . Antibodies are detailed in Supplementary Table I.

Phagocytic assay

Microglial cultures were incubated with fluorescent latex beads 0.5μm diameter (Sigma-Aldrich), for 30 min at 37ºC. Briefly, the beads were diluted in cell culture medium (1:1000) and then cells were washed, fixed with 4% PFA and the staining for iba1 (Wako) was performed. The number of beads per cell was counted.

Fluorescence intensity quantification

The fluorescence intensity of microglial cells was quantified using the ImageJ software [19], as previously reported [6]. Fluorescence channels were separated, image converted to 32-bit and the background subtracted using 50%-off pixels radius by the rollerball algorithm. Then, cells were segmented using the Triangle algorithm with automatic complementation for both the bottom and upper threshold ramps with background values set to black and foreground values set to red. Individual segmented cells were transposed to ImageJ's ROI manager using the *analyse particles* tool. A range between 1000-to-infinity of non-calibrated pixels defined each segmented cell. Mean gray values for the intensities were returned for each cell individually using the multi-measure function on ImageJ`s ROI manager.

RNA extraction, cDNA synthesis, and qRT-PCR

RNA from cell cultures was isolated from the PureLink®RNA Mini-Kit (ThermoFisher Scientific) according to the manufacturer's specifications, and its quality was checked by Experion automated electrophoresis system (Bio-Rad). Of note, in the microglia and neuronal cell cultures, the microfluidic device was removed and the RNA was extracted from total cell culture .

The synthesis of cDNA was performed using 500 ng of RNA through SuperScript® III First-Strand Synthesis SuperMix (Invitrogen). The qRT-PCR reactions, using equal amounts of total RNA from each sample, were performed on the CFX96 Touch™ Real-Time PCR Detection System (Bio-Rad), using the iTaq™ universal SYBR® Green supermix (Bio-Rad). All primers (Sigma-Aldrich) are described in Supplementary Table II. Raw data were analyzed using the $2^{-\Delta CT}$ method with S18 serving as the internal control.

Flow cytometry of microglia

Cells were collected from microfluidic devices using accutase (Gibco, ThermoFisher Scientific) for 5 min, centrifuged at 1200rpm for 5 min, washed with PBS 1x and incubated with Zombie Aqua (Biolegend), for dead cell exclusion. After washing, cells

were fixed with 2% PFA, resuspended in FACS buffer (2% BSA in PBS) and incubated with the antibodies described in Supplementary Table III, for 20 min, at 4 °C. Data were acquired in a FACSCanto II flow cytometer (BD Biosciences). Post-acquisition analysis was performed using FlowJo software v10 (Tree Star).

Quantification of synaptic proteins

The acquired images were analyzed using ImageJ, as described elsewhere [20]. The puncta were analyzed for number, area and intensity in the selected region, per dendritic length. Briefly, neurite isolated segments containing both PSD95 and VGlut1 stainings were thresholded using Li and Moments algorithms, respectively. The obtained mask was applied on the original images to determine the fluorescence intensity and area. The background value was then subtracted from the obtained intensity value, and this result was multiplied by the puncta area, obtaining the intensity per area. The thresholded signals were then used to determine the co-localization. For this, VGlut1 channel was set as binary, and PSD95 channel was used to define the total puncta. The puncta positive for VGlut1 and PSD95 were defined as colocalized.

Statistical analysis

Data presentation is described in figure legends. Identification and removal of outliers were performed with the automatic GraphPad Prism® software (version 9.1.2. for macOS), using the ROUT (robust non-linear regression) method, with a $Q = 5\%$, for removing outliers.

Statistical analyses for qRT-PCR and flow cytometry data were performed in the GraphPad Prism® software, using paired Student´s t-test. For immunocytochemistry data, a linear mixed model analysis was performed using SAS® Visual Statistics with REML function, followed by Tukey–Kramer multiple comparison test, using the culture as a random variable. The data of PSD95 positive for VGlut1 intensity does not follow the normal distribution, so a transformation of the data was carried out, using the square root function, before the linear mixed model application. Adjusted p-value was considered for these data. Differences were considered at the significance level of $p<0.05$.

3. Results

Neurons exposed to Meth do not promote microglial activation through contact-dependent or independent mechanisms

We have previously shown that the conditioned media of astrocytes (ACM) exposed to Meth can activate microglia cells [6]. Thus, we started by evaluating the role of neurons in the activation of microglia under the same conditions of Meth exposure. To this end, we incubated primary microglial cultures with conditioned media obtained from neuronal cultures treated with Meth (NCM Meth) or with conditioned media obtained from control neuronal cultures (NCM Ctrl) (Fig. 1A) for 24 h. We found that NCM Meth did not promote increased expression of classical microglial activation markers, such as iNOS (Fig. 1B) and iba 1 (Fig. 1C). The phagocytic capacity of microglia exposed to NCM Meth was decreased (F (1,540) = 4.35, $p<0.05$) (Fig. 1D). We also observed no differences in the mRNA levels of the pro-inflammatory cytokines TNF, IL-1β and IL-6 (Fig. 1E), or the anti-inflammatory cytokines IL-10 and TGF-β (Fig. 1F). These results suggest that upon Meth exposure, neurons do not induce microglia activation through contact-independent mechanisms.

Since the conditioned media of neurons exposed to Meth did not induce microglia activation, and taking into consideration that microglia and neurons also communicate through cell-to-cell contact *via* several regulatory molecules [7, 8], we tested the hypothesis that the crosstalk between neurons and microglia under Meth exposure could be contact-dependent. To test this hypothesis, we used co-cultures of microglia and neurons in microfluidic devices, that allow direct contact between microglia and axons, and exposed neurons to Meth for 24 h (Fig. 2A). Our findings revealed that neurons exposed to Meth do not significantly impact iNOS expression (Fig. 2B) or microglia phagocytic capacity (Fig. 2C). Since arginase 1 can outcompete iNOS to downregulate production of nitric oxide, and is, therefore, considered a good anti-inflammatory marker for microglia [21], we also evaluated the expression of arginase 1 in these co-cultures. We found that in the presence of Meth, arginase 1 was decreased (F (1,892) = 24.71, $p<0.0001$) (Fig. 2D). These results suggest that exposing neurons to Meth was not sufficient to promote a pro-inflammatory state in microglia, despite the decrease in arginase 1. To further confirm this, the mRNA expression levels of the pro-inflammatory cytokines TNF-α, IL-1β and IL-6, and the anti-inflammatory cytokines Il-10 and TGF-β were evaluated. No differences were found between groups (Fig. 2E and 2F). Together, these data indicate that neurons exposed to Meth do not trigger a pro-inflammation in

microglia in a cell-autonomous way, either through contact-dependent or -independent mechanisms

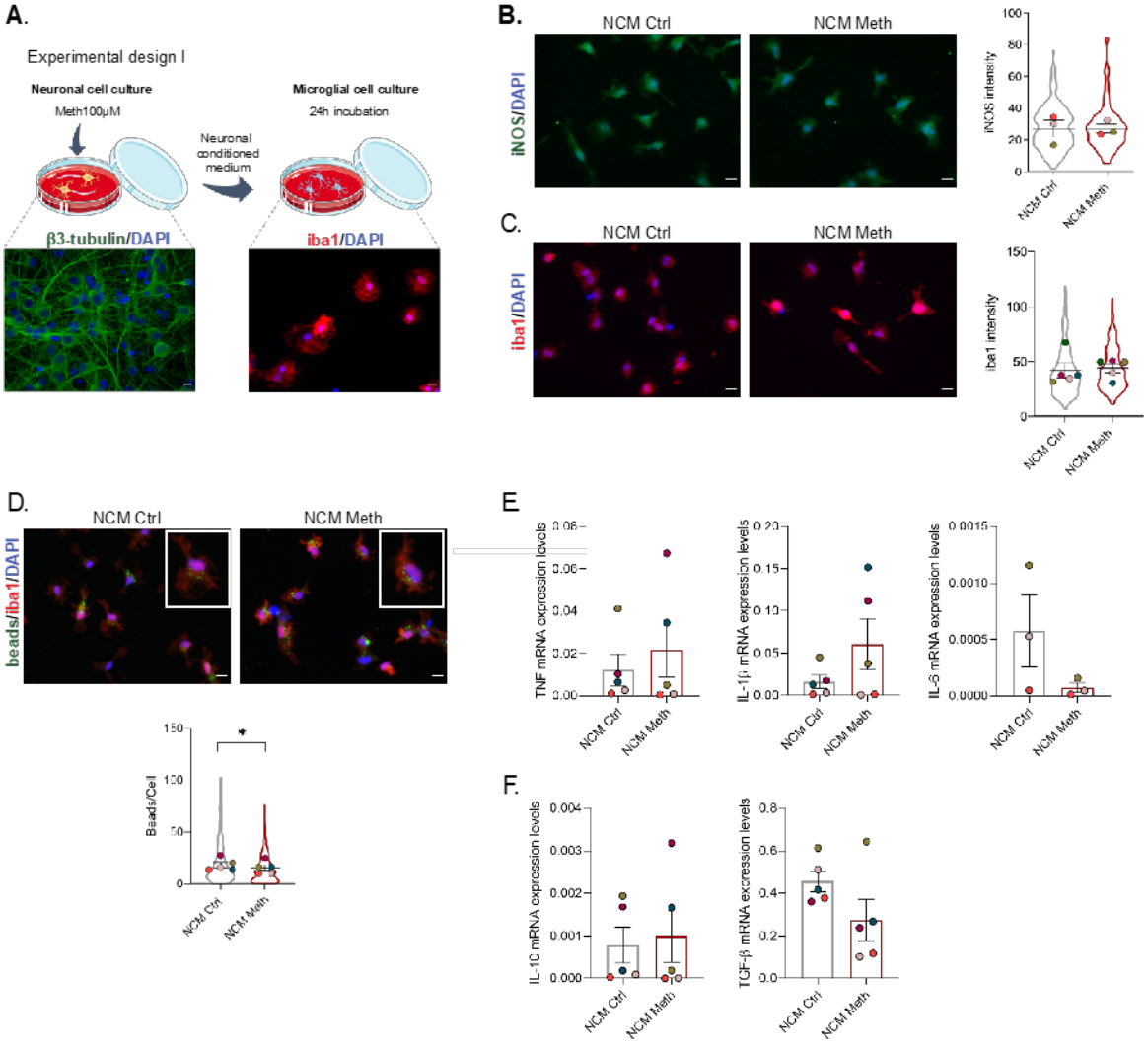

Figure 1: Neurons exposed to Meth do not promote microglial activation through contact-independent mechanisms. (A) Experimental design I – Neuronal cell cultures from the hippocampus were incubated with 100 µM Meth for 24 h. Following that, primary microglial cell cultures were incubated for 24 h with the conditioned media obtained from neurons treated with Meth (NCM Meth) or from control neuronal cell cultures (NCM Ctrl). **(B)** Fluorescence imaging of microglia cells immunolabeled for iNOS (green) incubated with NCM Ctrl or NCM Meth for 24 h. Results express the iNOS intensity (average ±SEM) of three

independent cultures. Symbol colors represent the mean of each independent cell culture, and the violin plots the variability of all cells quantified (NCM Ctrl – 132 cells; NCM Meth – 143 cells). Statistical analysis was performed using a linear mixed model followed by Tukey–Kramer comparison test. Scale bar 10 µm. **(C)** Fluorescence imaging of microglia cells immunolabeled for iba1 (red) incubated with NCM Ctrl or NCM Meth for 24 h. Results express iba1 intensity (average ±SEM) of five independent cultures. Symbol colors represent the mean of each independent cell culture and the violin plots the variability of all cells quantified (NCM Ctrl – 252 cells; NCM Meth – 265 cells). Statistical analysis was performed using a linear mixed model followed by Tukey–Kramer comparison test. Scale bar 10 µm. **(D)** Fluorescence imaging of microglia cells immunolabeled for iba1 (red) incubated with microbeads (green) and treated with NCM Ctrl or NCM Meth for 24 h. Results represent the number of beads per cell (average ±SEM) of five independent cultures. Symbol colors represent the mean of each independent cell culture and the violin plots the variability of all cells quantified (NCM Ctrl – 267 cells; NCM Meth – 264 cells). Statistical analysis was performed using a linear mixed model followed by Tukey–Kramer comparison test (*$p<0.05$). Scale bar 10 µm. **(E)** RT-qPCR for TNF, Il-1β and Il-6 from microglia exposed to NCM Ctrl and NCM Meth for 24h. Results were normalized to the S18 gene and are expressed as the average ±SEM of three or five independent cultures. Symbol colors represent the mean of each independent cell culture. Statistical analysis was performed using paired Student's *t*-test. **(F)** RT-qPCR for Il-10 and TGFβ from microglia exposed to NCM Ctrl and NCM Meth for 24h. Results were normalized to the S18 gene and are expressed as the average ±SEM of five independent cultures. Symbol colors represent the mean of each independent cell culture. Statistical analysis was performed using paired Student's *t*-test.

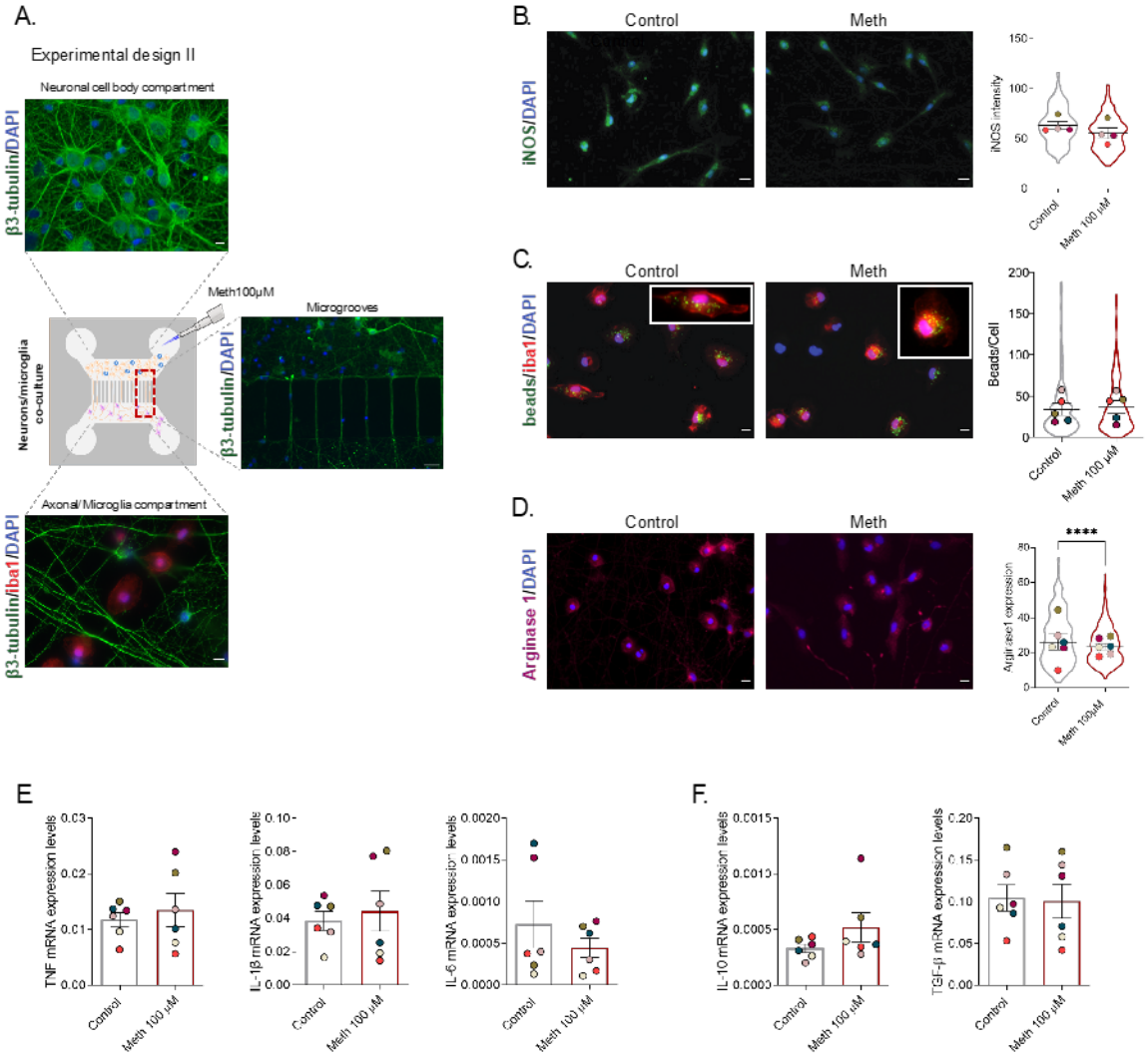

Figure 2. Neurons exposed to Meth and in direct contact with microglia do not promote its activation. (A) Experimental design II – Neuronal cell culture from the hippocampus were seeded in one side of a microfluidic device, and the axons were allowed to extend to the other compartment for 12 days. On DIV12, microglia cells were seeded in the axonal compartment. On DIV13, Meth 100 µM was added to the neuronal compartment for 24 h. **(B)** Fluorescence imaging of microglial cells cultured in a microfluidic device with neurons exposed to Meth 100 µM for 24 h. Microglia cells were immunolabeled for iNOS (green) and the results express the iNOS intensity (mean ±SEM) of four independent cultures. Symbol colors represent the mean of each independent cell culture and the violin plots the variability of all cells quantified (Ctrl – 297 cells; Meth – 325 cells). Statistical analysis was performed using a linear mixed model followed by Tukey–Kramer comparison test. Scale bar 10 µm. **(C)** Fluorescence imaging of microglia cells cultured in a microfluidic device with neurons exposed to Meth 100 µM for 24 h. Microglia were incubated with microbeads (green) and immunolabeled for iba1 (red). Results represent the number of beads per cell (mean ±SEM) of five independent cultures. Symbol colors represent the mean of each independent cell culture and the violin plots the variability of all cells quantified (Ctrl

– 268 cells; Meth – 211 cells). Statistical analysis was performed using a linear mixed model followed by Tukey–Kramer comparison test. Scale bar 10 µm. **(D)** Fluorescence imaging of microglial cells cultured in a microfluidic device with neurons exposed to Meth 100 µM for 24 h. Microglia cells were immunolabeled for arginase 1 (magenta), and results express the arginase 1 intensity (mean±SEM) of six independent cultures. Symbol colors represent the mean of each independent cell culture and the violin plots the variability of all cells quantified (Ctrl – 489 cells; Meth –410 cells). Statistical analysis was performed using a linear mixed model followed by Tukey–Kramer comparison test (****p<0.0001). Scale bar 10 µm. **(E)** RT-qPCR for TNF, Il-1β and Il-6 from microglia and neuron co-culture cells, cultured in a microfluidic device where neurons were exposed to Meth 100 µM for 24 h. The results were normalized to the S18 gene and are expressed as the mean±SEM of six independent cultures. Symbol colors represent the mean of each independent cell culture. Statistical analysis was performed using paired Student's t-test. **(F)** RT-qPCR for Il-10 and TGFβ from microglia and neuron co-cultured cells, in a microfluidic device where neurons were exposed to Meth 100 µM for 24 h. The results were normalized to the S18 gene and are expressed as the mean ±SEM of six independent cultures. Symbol colors represent the mean of each independent cell culture. Statistical analysis was performed using paired Student's t-test.

Microglia activation induced by Meth-exposed astrocytes is partially prevented by neurons

Since we have recently shown that Meth-induced microglial reactivity requires both astrocyte-released TNF and glutamate [6], we next sought to verify if this was also the case in co-cultures of neurons and microglia. To do so, co-cultures of neurons and microglia were performed in microfluidic devices, and the conditioned media of primary astrocytes, treated with Meth (ACM Meth) or untreated (ACM Ctrl) was added to the microglial/axonal compartment (Fig. 3A). Confirming our previous results [6], ACM Meth led to increased iNOS levels in microglia (F (1,729) = 120.67, p<0.0001), independently of the presence of primary neurons (Fig. 3B). No significant effect was observed in microglia phagocytic capacity (Fig. 3C). Of note, arginase 1 was concomitantly increased in ACM Meth treated microglia (F (1,591) = 59.30, p<0.0001) (Fig. 3D). Because we previously reported that ACM Meth increased the transcript expression of pro-inflammatory cytokines in microglia cultures [6], we also evaluated the mRNA levels of the pro-inflammatory cytokines TNF, IL-1β and IL-6. Interestingly, no significant alterations were observed (Fig. 3E). The mRNA expression levels of the anti-inflammatory cytokines Il-10 and TGF-β were also unaltered (Fig. 3F). Next, we repeated

these experiments adding also Meth to the neuronal compartment, while still exposing microglia to ACM Meth (Suppl. Fig. 1A). In these conditions, we also observed an increase in both iNOS (F (1,942) = 53.45, p<0.0001) and arginase 1 expression (F (1,942) =53.45, p<0.0001) (Suppl. Fig. 1B and 1D), while the phagocytic capacity (Suppl. Fig. 1C) and the cytokines mRNA expression levels were not affected (Suppl. Fig. 1E and F). Importantly, these results suggest that Meth-induced microglia activation via astrocytes is attenuated by neuronal action.

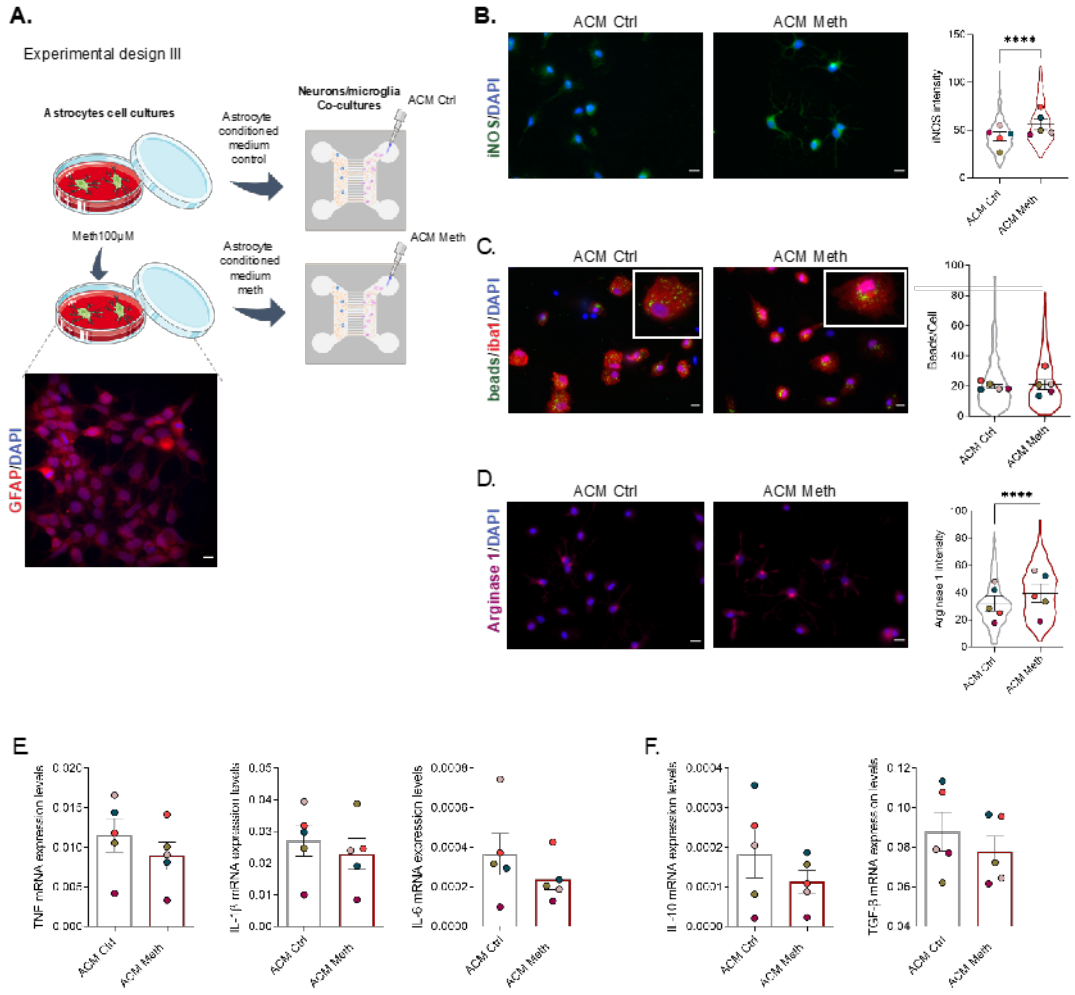

Figure 3. Neurons partially prevented microglia activation via Meth exposed astrocytes. **(A)** Experimental design III – Primary cell cultures of astrocytes were incubated with Meth 100 µM for 24 h. Neuronal cells from the hippocampus were seeded in one side of a microfluidic device and the axons were allowed to extend to the other compartment for 12 days. On DIV 12, microglia cells were seeded in the axonal compartment. The conditioned media obtained from astrocytes treated with Meth (ACM Meth) or from control astrocytes cultures (ACM Ctrl) was added to the microglia/axonal compartment for 24h. **(B)** Fluorescence imaging of microglial cells

co-cultured with neurons and exposed to the ACM Ctrl or ACM Meth for 24h. Microglia cells were immunolabeled for iNOS (green) and results express the iNOS intensity (mean±SEM) of five independent cultures. Symbol colors represent the mean of each independent cell culture and the violin plots the variability of all cells quantified (ACM Ctrl – 405 cells; ACM Meth – 329 cells). Statistical analysis was performed using a linear mixed model followed by Tukey–Kramer comparison test (****p<0.0001). Scale bar 10 µm. **(C)** Fluorescence imaging of microglia cells co-cultured with neurons and incubated with ACM Ctrl or ACM Meth for 24h. Microglia were incubated with microbeads (green) and immunolabeled for iba1 (red). The results represent the number of beads per cell (mean ±SEM) of five independent cultures. Symbol colors represent the mean of each independent cell culture and the violin plots the variability of all cells quantified (ACM Ctrl –183 cells; ACM Meth –248 cells). Statistical analysis was performed using a linear mixed model followed by Tukey–Kramer comparison test. Scale bar 10 µm. **(D)** Fluorescence imaging of microglial cells co-cultured with neurons and exposed to ACM Ctrl or ACM Meth for 24h. Microglia cells were immunolabeled for arginase 1 (magenta) and results express the arginase 1 intensity (mean±SEM) of six independent cultures. Symbol colors represent the mean of each independent cell culture and the violin plots the variability of all cells quantified (ACM Ctrl –310 cells; ACM Meth –287 cells). Statistical analysis was performed using a linear mixed model followed by Tukey–Kramer comparison test (****p<0.0001). Scale bar 10 µm. **(E)** RT-qPCR for TNF, Il-1β and Il-6 from microglia and neurons co-culture cells, cultured in a microfluidic device with microglia exposed to ACM Ctrl or ACM Meth for 24 h. The results were normalized to the S18 gene and are expressed as the mean±SEM of five independent cultures. Symbol colors represent the mean of each independent cell culture. Statistical analysis was performed using paired Student's t-test. **(F)** RT-qPCR for Il-10 and TGFβ from microglia and neurons co-culture cells, cultured in a microfluidic device with microglia exposed to ACM Ctrl or ACM Meth for 24 h. The results were normalized to the S18 gene and are expressed as mean ±SEM of five independent cultures. Symbol colors represent the mean of each independent cell culture. Statistical analysis was performed using paired Student's t-test.

Neurons increased self-protection from Meth-induced activation of microglia through contact-dependent mechanisms

Because neurons can use several contact-dependent mechanisms to protect themselves from reactive microglia [8, 10], we next evaluated the expression of neuroimmune regulatory molecules known to downregulate microglial pro-inflammatory response. To do so, co-cultures of neurons and microglia were performed in microfluidic devices, and ACM Meth or ACM Ctrl were added to the axonal/microglial side. After 24 h, the mRNA levels of ligand-receptor pairs relevant for the crosstalk between neurons and microglia were determined in the axonal/microglial compartment. We found a

significant increase in CD200 mRNA levels ($p<0.05$), without significant changes in its receptor CD200r (Fig. 4A). The expression of CD22 and its receptor CD45 were not altered (Fig. 4B). We observed an increase in the mRNA levels of CX3CL1 that was close to reaching significance ($p=0.0565$), but no differences were found for its receptor CX3CR1 (Fig. 4C). Concerning the pair CD95-CD95L, the mRNA expression levels of CD95 were not altered (Fig. 4D), and CD95L mRNA levels were not detectable. To further confirm these results, we also evaluated the protein expression of CD95 and CD200r specifically in microglia by flow cytometry and no differences were observed neither in CD95 (Fig. 4E), nor in CD200r levels (Fig. 4F). These results indicate that neurons in contact with microglia activated via Meth-exposed astrocytes increased the expression of CD200, which is a well described self-protection mechanism.

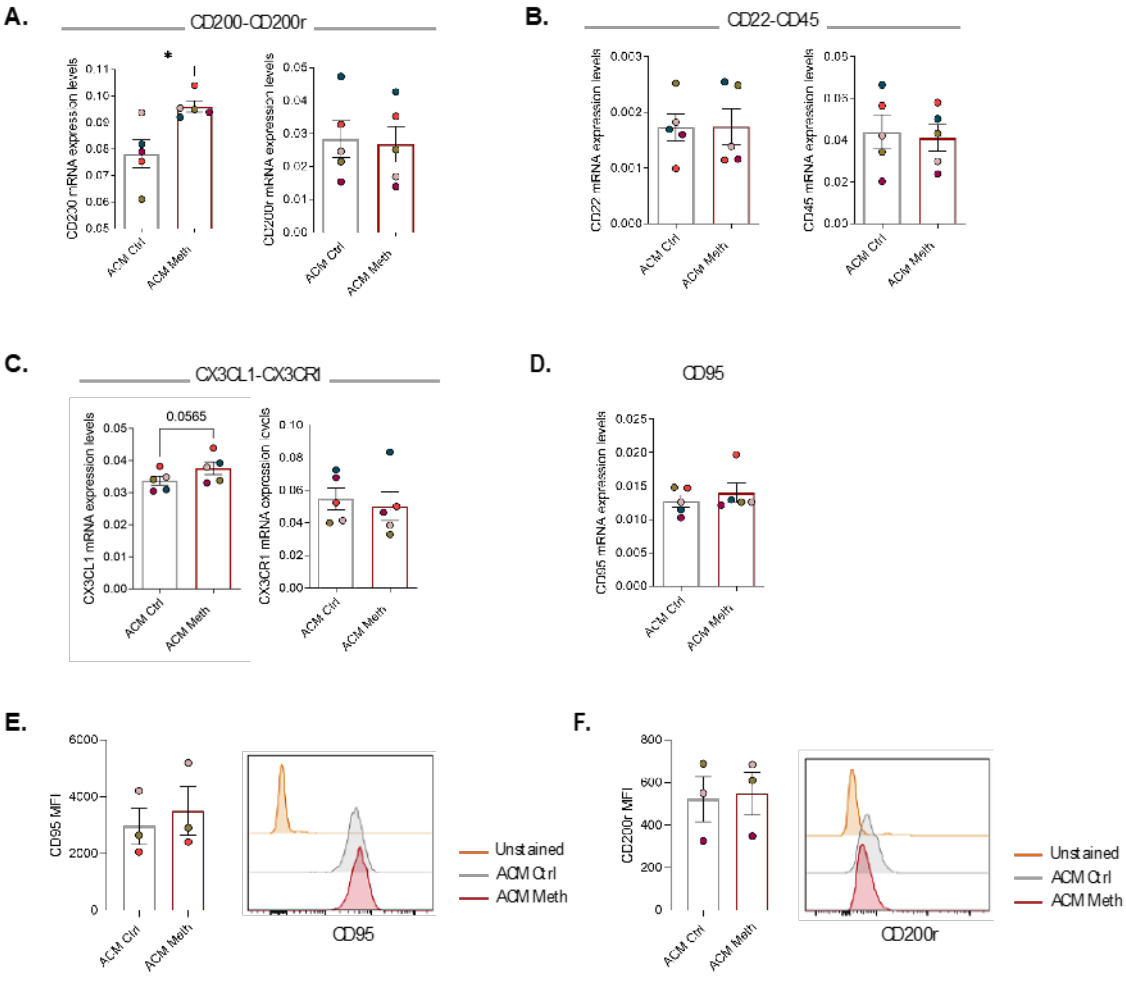

Figure 4. Neurons increased self-protection through contact-dependent mechanisms. RT-qPCR for ligand-receptor immunoregulatory pairs from microglia and neurons co-cultured cells in microfluidic devices, where microglial cells were exposed to ACM Ctrl or ACM Meth for 24 h. **(A)** Results for CD200 and CD200r, **(B)** CD22 and CD45, **(C)** CX3CL1 and CX3CR1 and **(D)** CD95. The results were normalized to the S18 gene and are expressed as the mean ±SEM of five

independent cultures. Symbol colors represent the mean of each independent cell culture. Statistical analysis was performed using paired Student's t-test (*p<0.05). Quantification of **(E)** CD95 and **(F)** CD200r on microglia by flow cytometry, presented as median fluorescence intensity (MFI). Results are expressed as mean ±SEM of three independent cultures. Symbol colors represent the mean of each independent cell culture. Statistical analysis was performed using paired Student's t-test. Representative histograms are shown; orange histogram represents unstained cells, gray the ACM Ctrl group and red the ACM Meth group.

Synaptic proteins expression was increased in co-cultures of neurons and ACM Meth-microglia

Since we found increased CD200 levels and the signaling of CD200/CD200r has been associated with the modulation of microglia activation and synaptic plasticity in other neurological diseases [12, 14], we evaluated how exposure to ACM Meth was affecting synaptic proteins. For that, we used the same co-cultures of neurons and microglia in microfluidic devices with ACM Meth or ACM Ctrl added to the axonal/microglial side, and evaluated the expression of the postsynaptic marker PSD95 and of the presynaptic marker VGlut1. We observed an increase in PSD95 puncta number (F (1,254) = 11.92, p<0.001), area (F (1,252) =29.38, p<0.0001) and intensity (F (1,251) = 51.97, p<0.0001) (Fig. 5A, B, C, D) when ACM Meth was added to the axonal/microglial compartment, while VGlut1 puncta number was decreased (F (1,258) = 5.71, p<0.05) (Fig. 5E and 5F) in comparison with to the ACM Ctrl condition. However, no significant differences were observed in VGlut1 puncta area nor intensity (Fig. 5E, G, H). As the co-localization between both markers is accepted as an indicator of active synapses (since both pre- and postsynaptic terminals are present) [22], we also evaluated their co-localization. We observed a significant increase in the PSD95/VGlut1 positive puncta area (F (1,247) =17.53, p<0.0001) and intensity (F (1,244) =49, adj p<0.0001) (Fig. 5I, K and L), reflecting an increase in synapses area when ACM Meth was used, but no significant differences in PSD95/VGlut1 positive puncta number (Fig. 5I, J). Collectively, these data show that neuronal/microglial co-cultures present higher levels of synaptic proteins and active synapses when exposed to the ACM of Meth-treated astrocytes.

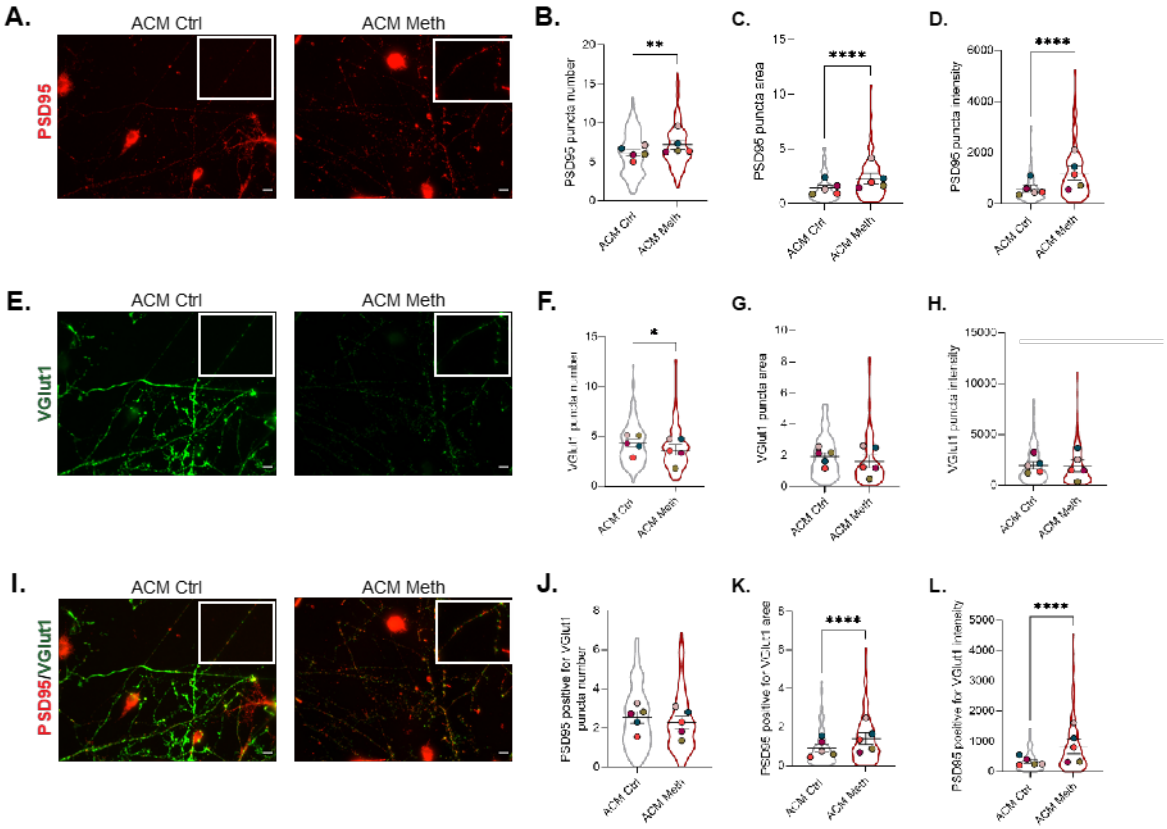

Figure 5. Synaptic plasticity was concomitantly increased. (A) Fluorescence imaging of microglial cells co-cultured with neurons and exposed to ACM Ctrl or ACM Meth for 24h. Cells were immunolabeled for PSD95 (red) and results represent the PSD95 puncta B) number, (C) area and (D) intensity. (E) Fluorescence imaging of microglial cells co-cultured with neurons and exposed to ACM Ctrl or ACM Meth for 24h. Microglia cells were immunolabeled for vGlut1 (green) and results represent the Vglut1 puncta (F) number, (G) area and (H) intensity. (I) Fluorescence imaging of microglial cells co-cultured with neurons and exposed to ACM Ctrl or ACM Meth for 24h. Cells were immunolabeled for PSD95 (red) and VGlut1 (green) and results represent the (J) PSD95 plus vGlut1 positive puncta number, (G) puncta area and (H) puncta intensity. Symbol colors of each graph represent the mean of each independent cell culture (n=5) and the violin plots the variability of all neuronal segments quantified (ACM Ctrl – 149; ACM Meth – 111 segments). Statistical analysis was performed using a linear mixed model followed by Tukey–Kramer comparison test. Scale bar 10 µm.

4. Discussion

We have recently demonstrated that acute Meth exposure requires astrocytes to induce microglia activation, which happens *via* glutamate release in a TNF/IP_3R2-Ca^{2+}-dependent manner [6]. Herein, we explored, *in vitro*, how neurons contribute to modulate microglia under Meth. We demonstrate contact-dependent mechanisms between

neurons and microglia attenuated Meth-induced microglia activation and increased PSD95 related synaptic plasticity.

Multiple mechanisms mediating Meth-induced neurotoxicity have been widely described, such as impairment of the dopaminergic system, increased oxidative stress, mitochondrial dysfunction and glutamate excitotoxicity [23-25]. The primary goal of this study was to further contribute to clarify the mechanisms involved in Meth-induced neurotoxicity through microglia activation. As the crosstalk between microglia and neurons can occur by contact-dependent and/or independent mechanisms, we first investigated if contact independent mechanisms were sufficient to mediate microglia activation by Meth-exposed neurons. Using a strategy similar the one we have used to explore the contribution of astrocytes in Meth-induced microglia activation [6], we verified that the neuronal conditioned media obtained from neurons exposed to Meth failed to induce a pro-inflammatory profile in primary microglia. Since these results could be explained because direct contact was necessary to promote microglia activation, we explored if under direct contact with microglia, Meth-exposed neurons could use contact-dependent mechanisms to promote their activation. Interestingly, we found only a decrease in arginase 1 expression in microglia cells, that differently from what could be expected, since arginase outcompetes iNOS and limits NO production [26], did not result in increased iNOS levels. These results clarified that neither direct nor indirect neuron-microglia contact was sufficient to promote an inflammatory response under Meth exposure, indicating that astrocyte mediation was in fact necessary, as previously reported [6]. Confirming this, when we added ACM Meth to the axonal/microglial compartment, microglia exhibited increased iNOS expression.

Previous studies demonstrated that neurons may induce an anti-inflammatory profile in microglial cells to protect themselves from excessive microglia activation [8, 10]. Several neuronal membrane proteins, including CD200, CD22, CD95, CD47 and other proteins like NCAM or ICAM-5, were shown to modulate microglial activation through specific counter-receptors [8]. As an example, neurons can contribute to inhibit the lipopolysaccharide (LPS)-induced release of NO and pro-inflammatory cytokines by glial cells [27]. As such, understanding the role of these ligand-receptor pairs has gained increased relevance over the last few years. Among the most explored, CD200 is highly expressed in neurons and other cells, but its receptor, CD200R, is found predominantly in myeloid cells. Interestingly, knocking out CD200 in mice leads to robust activation of microglia [28], while overexpressing it seems to protect from different pro-inflammatory events [8]. Likewise, the interaction of CD22 and its microglial receptor CD45 was shown to prevent LPS-induced neuroinflammation [29]. It was also reported that neurons may induce microglial apoptosis through increased expression of CD95L (or Fas ligand) [30],

while CD95L expression in hippocampal neurons protected them against reactive T cells [31]. In the present work, we found increased expression of CD200 when ACM Meth was added to the axonal/microglial compartment, which likely reflects a neuronal defense strategy against astrocyte-driven activation of microglia when exposed to Meth. Interestingly, activating the CD200/CD200R signaling pathway was reported to increase dendritic spine density and PSD95 [12] an essential indicator of synaptic plasticity [32, 33]. ACM Meth increased the number of PSD95 puncta that might be correlated with increased dendritic spine density [34] and an increase in the area and intensity of PSD95 puncta colocalized with VGLUT1. PSD95, by coupling with stargazing, regulates a dynamic pool of AMPA receptors and has a direct role in regulating synaptic strength and maturation [33]. Of note, the dynamics of PSD95 seem to respond also to glutamate variations, which we have reported to be increased in ACM Meth [6]. On the other hand, we found decreased VGlut1 puncta numbers, a major player in vesicular glutamate uptake, which dysregulation in response to Meth was previously reported [35]. Acute exposure to psychoactive substances, such as Meth, has long been associated with high levels of synaptic plasticity, contributing to the drug-driven effects in neuronal function [36, 37]. Although the exact mechanisms regulating Meth-associated changes in synaptic plasticity and their direct link to CD200, require further exploration, it was reported that the CD200/CD200R signaling involvement in suppressing inflammatory responses might be exerted through reduced activation of MAPK [12], which is involved in the regulation of classic RhoGTPases such as RhoA, Rac1 and Cdc42 that are well known for their roles in spine formation and maintenance [38, 39].

5. Conclusions

In summary, using microfluidic chambers as an effective tool to explore contact-dependent mechanisms between neurons and microglia, we report that hippocampal neurons in direct contact with primary microglia counteract microglia activation by increasing the expression of the neuroimmune regulatory molecule CD200. Furthermore, our data also suggests that the activation of the CD200-CD200r signaling pathway is likely contributing to increase synaptic plasticity. These results highlight CD200 and its receptor as molecules with promising therapeutic potential in the field of addiction.

References

1. Nestler, E.J. and C. Luscher, *The Molecular Basis of Drug Addiction: Linking Epigenetic to Synaptic and Circuit Mechanisms.* Neuron, 2019. **102**(1): p. 48-59.
2. Cadet, J.L. and V. Bisagno, *Glial-neuronal ensembles: partners in drug addiction-associated synaptic plasticity.* Front Pharmacol, 2014. **5**: p. 204.
3. Miguel-Hidalgo, J.J., *The role of glial cells in drug abuse.* Curr Drug Abuse Rev, 2009. **2**(1): p. 72-82.
4. Dang, J., et al., *Glial cell diversity and methamphetamine-induced neuroinflammation in human cerebral organoids.* Mol Psychiatry, 2021. **26**(4): p. 1194-1207.
5. Frank, M.G., et al., *The danger-associated molecular pattern HMGB1 mediates the neuroinflammatory effects of methamphetamine.* Brain Behav Immun, 2016. **51**: p. 99-108.
6. Canedo, T., et al., *Astrocyte-derived TNF and glutamate critically modulate microglia activation by methamphetamine.* Neuropsychopharmacology, 2021.
7. Chavarria, A. and G. Cardenas, *Neuronal influence behind the central nervous system regulation of the immune cells.* Front Integr Neurosci, 2013. **7**: p. 64.
8. Tian, L., H. Rauvala, and C.G. Gahmberg, *Neuronal regulation of immune responses in the central nervous system.* Trends Immunol, 2009. **30**(2): p. 91-9.
9. Bras, J.P., et al., *TNF-alpha-induced microglia activation requires miR-342: impact on NF-kB signaling and neurotoxicity.* Cell Death Dis, 2020. **11**(6): p. 415.
10. Biber, K., et al., *Neuronal 'On' and 'Off' signals control microglia.* Trends Neurosci, 2007. **30**(11): p. 596-602.
11. Hernangomez, M., et al., *CD200R1 agonist attenuates glial activation, inflammatory reactions, and hypersensitivity immediately after its intrathecal application in a rat neuropathic pain model.* J Neuroinflammation, 2016. **13**: p. 43.
12. Sun, H., et al., *The CD200/CD200R signaling pathway contributes to spontaneous functional recovery by enhancing synaptic plasticity after stroke.* J Neuroinflammation, 2020. **17**(1): p. 171.
13. Denieffe, S., et al., *Classical activation of microglia in CD200-deficient mice is a consequence of blood brain barrier permeability and infiltration of peripheral cells.* Brain Behav Immun, 2013. **34**: p. 86-97.
14. Feng, D., et al., *CD200 dysfunction in neuron contributes to synaptic deficits and cognitive impairment.* Biochem Biophys Res Commun, 2019. **516**(4): p. 1053-1059.

15. Braz, S.O., et al., *Expression of Rac1 alternative 3' UTRs is a cell specific mechanism with a function in dendrite outgrowth in cortical neurons.* Biochim Biophys Acta Gene Regul Mech, 2017. **1860**(6): p. 685-694.
16. Chen, Y., et al., *Isolation and culture of rat and mouse oligodendrocyte precursor cells.* Nat Protoc, 2007. **2**(5): p. 1044-51.
17. Socodato, R., et al., *c-Src function is necessary and sufficient for triggering microglial cell activation.* Glia, 2015. **63**(3): p. 497-511.
18. Lopes, C.D., et al., *Microfluidic-based platform to mimic the in vivo peripheral administration of neurotropic nanoparticles.* Nanomedicine (Lond), 2016. **11**(24): p. 3205-3221.
19. Schindelin, J., et al., *Fiji: an open-source platform for biological-image analysis.* Nat Methods, 2012. **9**(7): p. 676-82.
20. Santos, S.D., et al., *Contactin-associated protein 1 (Caspr1) regulates the traffic and synaptic content of alpha-amino-3-hydroxy-5-methyl-4-isoxazolepropionic acid (AMPA)-type glutamate receptors.* J Biol Chem, 2012. **287**(9): p. 6868-77.
21. Cherry, J.D., J.A. Olschowka, and M.K. O'Banion, *Neuroinflammation and M2 microglia: the good, the bad, and the inflamed.* J Neuroinflammation, 2014. **11**: p. 98.
22. McLeod, F., et al., *Evaluation of Synapse Density in Hippocampal Rodent Brain Slices.* J Vis Exp, 2017(128).
23. Krasnova, I.N. and J.L. Cadet, *Methamphetamine toxicity and messengers of death.* Brain Res Rev, 2009. **60**(2): p. 379-407.
24. Yu, S., et al., *Recent advances in methamphetamine neurotoxicity mechanisms and its molecular pathophysiology.* Behav Neurol, 2015. **2015**: p. 103969.
25. Shin, E.J., et al., *Current understanding of methamphetamine-associated dopaminergic neurodegeneration and psychotoxic behaviors.* Arch Pharm Res, 2017. **40**(4): p. 403-428.
26. Krystofova, J., et al., *The Arginase Pathway in Neonatal Brain Hypoxia-Ischemia.* Dev Neurosci, 2018. **40**(5-6): p. 437-450.
27. Chang, R.C., et al., *Immune modulatory effects of neural cell adhesion molecules on lipopolysaccharide-induced nitric oxide production by cultured glia.* Brain Res Mol Brain Res, 2000. **81**(1-2): p. 197-201.
28. Hoek, R.M., et al., *Down-regulation of the macrophage lineage through interaction with OX2 (CD200).* Science, 2000. **290**(5497): p. 1768-71.
29. Mott, R.T., et al., *Neuronal expression of CD22: novel mechanism for inhibiting microglial proinflammatory cytokine production.* Glia, 2004. **46**(4): p. 369-79.

30. Beier, C.P., et al., *FasL (CD95L/APO-1L) resistance of neurons mediated by phosphatidylinositol 3-kinase-Akt/protein kinase B-dependent expression of lifeguard/neuronal membrane protein 35.* J Neurosci, 2005. **25**(29): p. 6765-74.
31. Medana, I., et al., *Fas ligand (CD95L) protects neurons against perforin-mediated T lymphocyte cytotoxicity.* J Immunol, 2001. **167**(2): p. 674-81.
32. Taft, C.E. and G.G. Turrigiano, *PSD-95 promotes the stabilization of young synaptic contacts.* Philos Trans R Soc Lond B Biol Sci, 2014. **369**(1633): p. 20130134.
33. El-Husseini, A.E., et al., *PSD-95 involvement in maturation of excitatory synapses.* Science, 2000. **290**(5495): p. 1364-8.
34. Berry, K.P. and E. Nedivi, *Spine Dynamics: Are They All the Same?* Neuron, 2017. **96**(1): p. 43-55.
35. Mark, K.A., et al., *Dynamic changes in vesicular glutamate transporter 1 function and expression related to methamphetamine-induced glutamate release.* J Neurosci, 2007. **27**(25): p. 6823-31.
36. Dietz, D.M., et al., *Molecular mechanisms of psychostimulant-induced structural plasticity.* Pharmacopsychiatry, 2009. **42 Suppl 1**: p. S69-78.
37. Kutlu, M.G. and T.J. Gould, *Effects of drugs of abuse on hippocampal plasticity and hippocampus-dependent learning and memory: contributions to development and maintenance of addiction.* Learn Mem, 2016. **23**(10): p. 515-33.
38. Nakahata, Y. and R. Yasuda, *Plasticity of Spine Structure: Local Signaling, Translation and Cytoskeletal Reorganization.* Front Synaptic Neurosci, 2018. **10**: p. 29.
39. Murakoshi, H., H. Wang, and R. Yasuda, *Local, persistent activation of Rho GTPases during plasticity of single dendritic spines.* Nature, 2011. **472**(7341): p. 100-4.

Supplementary Information

Supplementary Table 1. Antibodies for immunocytochemistry

Antibody	Dilution	Company
Anti-Arginase 1	1:100	Santa Cruz Biotechnology
Anti-β3-tubulin	1:1000	Biolegend
Anti-GFAP	1:500	abcam
Anti-Iba1	1:500	Wako
Anti-iNOS	1:200	Santa Cruz Biotechnology
Anti-PSD95	1:500	Life Technologies
Anti-VGlut1	1:1000	Synaptic Systems
Anti-GAD67	1:100	Santa Cruz Biotechnology
Anti-Tyrosine hydroxylase	1:200	Merck Millipore
Anti-mouse Alexa 488	1:1000	Life Technologies
Anti-rabbit Alexa 568	1:1000	Life Technologies
Anti-goat DyLight 650	1:1000	abcam

Supplementary Table 2. Primer sequences used in qRT-PCR

Gene	Forward Sequence	Reverse Sequence
TNF	TTCTCATTCCTGCTTGTGGC	CTACAGGCTTGTCACTCGAATTT
Il1-β	AGGAGAACCAAGCAACGACA	CTTGGGATCCACACTCTCCAG
Il-6	GGAGCCCACCAAGAACGATA	CAACTGGATGGAAGTCTCTTGC
Il-10	GTTGCCAAGCCTTATCGGAA	GAAATCGATGACAGCGCCT
TGF-β	TGGAAATCAACGGGATCAGC	AGTTGGTATCCAGGGCTCTC
CD200	ATGGGCAGTCCGGTATTCA	AAGGATGCAGTTGTGTGCAG
CD200R	CTTCGCGGCTGAGTCAAGTT	AGGCTGTCCTCTGAGGGTTA
CD22	CTAGGCACGGGAAAGTCACC	CTGGCCACTGGAATTGTCCT
CD45	AACAACCGACGATGGTGCC	ACGCACAGTAACGTTCCCAA
CX3CL1	CCATCATCCTGGAGACGAGA	GCCGAGGTGATCCTAGGTGT
CX3CR1	GCCCTTCTGGACTCACTACC	TGCACTGTCCGGTTGTTCAT
CD95	TATCACTGCACCTCGTGTGG	GTTGCCTCTTCCGGTACCTT
S18	CTTCCACAGGAGGCCTACAC	ACCACATGAGCGTATCTCC

Supplementary Table 3. Antibodies for flow cytometry

Antibody	Dilution	Company
APC anti-rat CD11b/c	1:100	Biolegend
Pacific Blue™ anti-rat CD45	1:100	Biolegend
FITC anti-rat CD200 Receptor	1:50	Biolegend
Anti-CD95	1:100	abcam
Anti-mouse Alexa 488	1:1000	Life Technologies

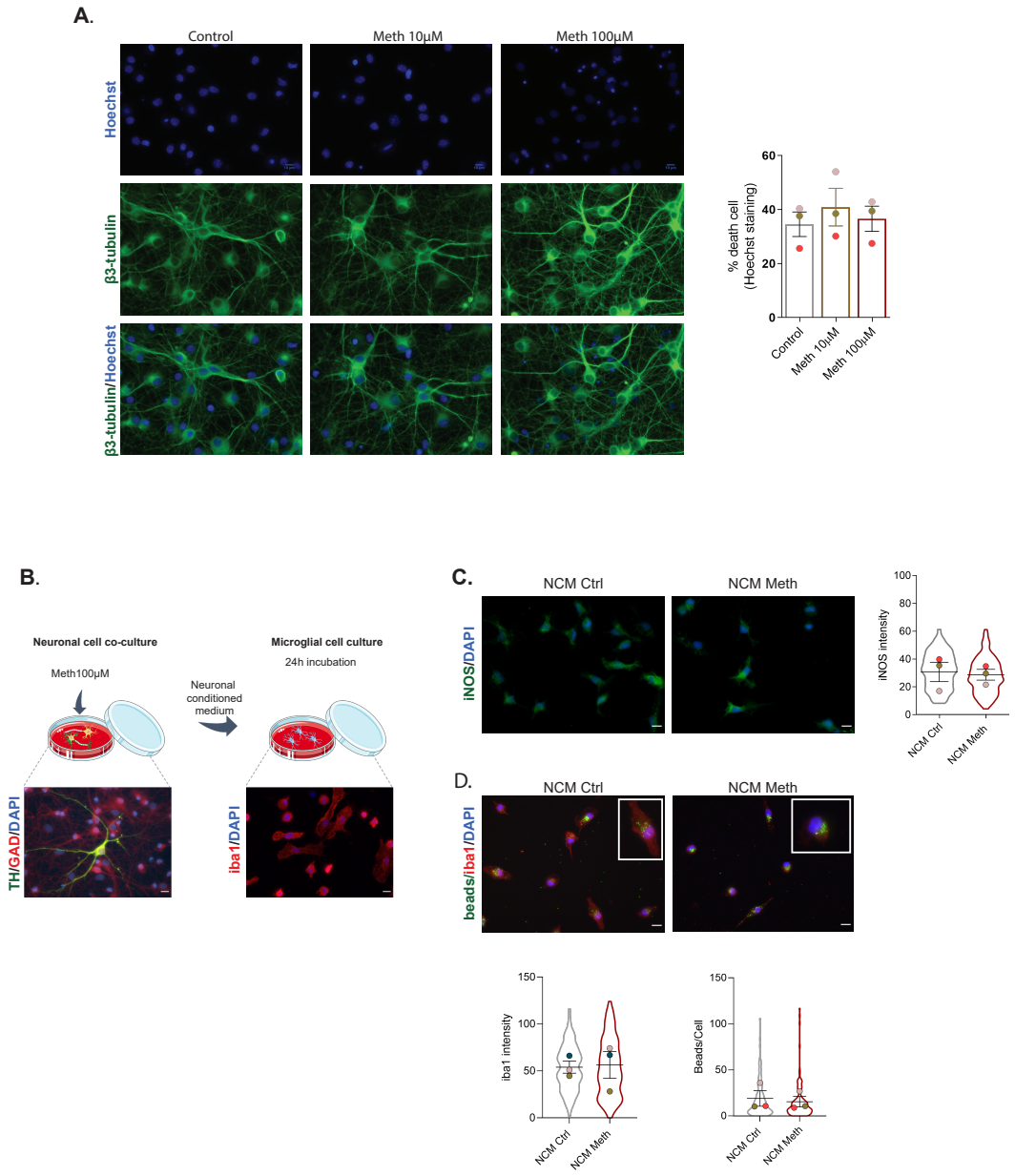

Supplementary Figure S1. **(A)** Fluorescence imaging of neuronal cells labeled for β3-tubulin (green) and Hoechst (blue) incubated with Meth 10 and 100 µM for 24 h. Results are expressed as mean ± SEM of the percentage of neuronal death for three independent experiments. Statistical analysis was performed using one-way ANOVA, followed by Tukey multiple comparisons test. **(B)** Neuronal cell cultures from striatum and mesencephalon were incubated with 100 µM Meth for 24 h. Following that, primary microglia cell cultures were incubated for 24 h with the conditioned media obtained from neurons treated with Meth (NCM Meth) or from control neuronal cell cultures (NCM Ctrl). **(C)** Fluorescence imaging of microglia cells immunolabeled for iNOS (green) incubated with NCM Ctrl or NCM Meth for 24 h. Results express the iNOS intensity (average ±SEM) of three independent cultures (NCM Ctrl – 146 cells; NCM Meth – 178 cells). **(D)** Fluorescence imaging of microglia cells immunolabeled for iba1 (red) incubated with microbeads

(green) and treated with NCM Ctrl or NCM Meth for 24 h. Results express iba1 intensity and the number of beads per cell (average ±S EM) of three independent cultures (NCM Ctrl – 142 cells; NCM Meth – 131 cells). Symbol colors represent the mean of each independent cell culture and the violin plots the variability of all cells quantified. Statistical analysis was performed using a linear mixed model followed by Tukey–Kramer comparison test. Scale bar 10 µm.

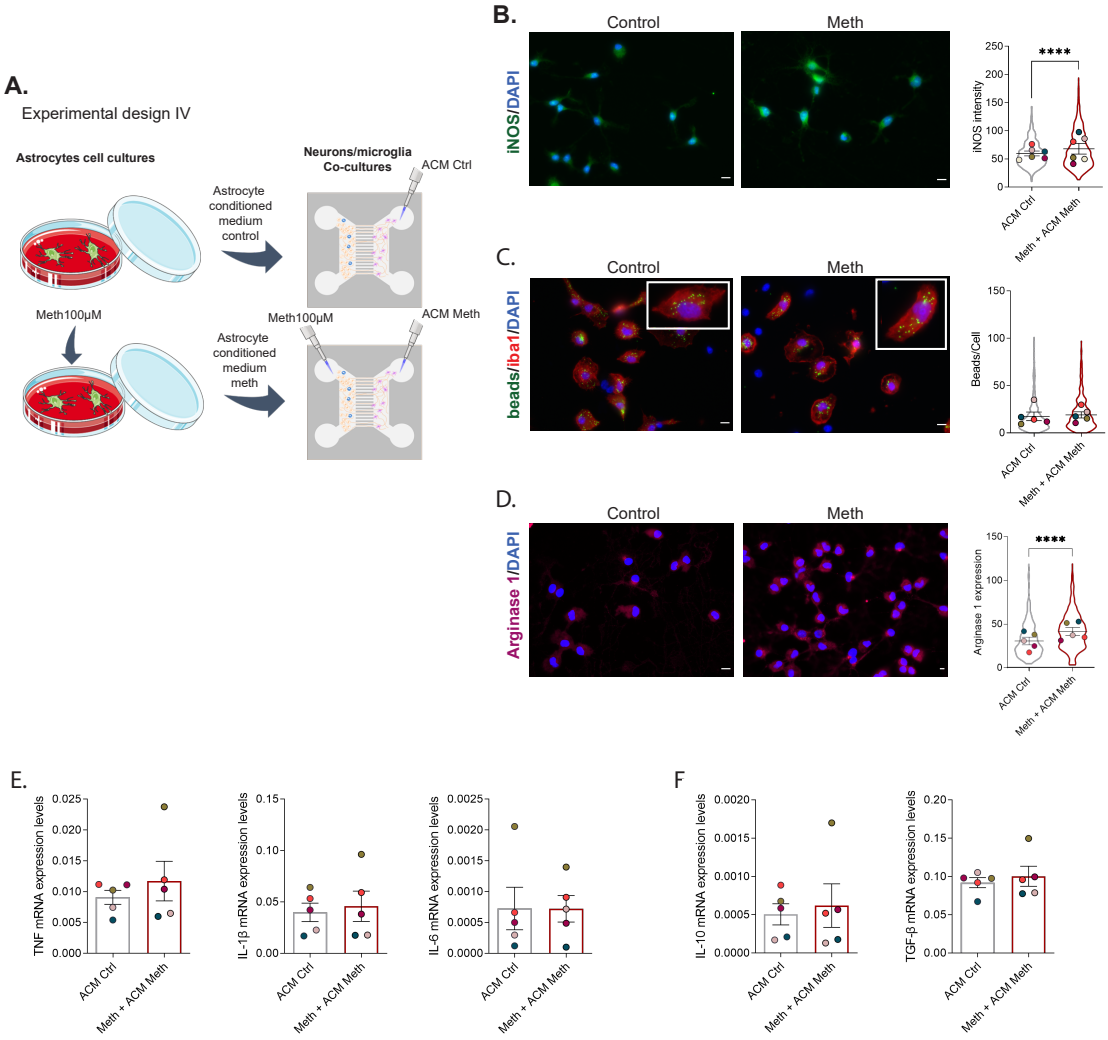

Supplementary Figure S2. (A) Experimental design IV – Primary cell cultures of astrocytes were incubated with Meth 100 µM for 24 h. Neuronal cells from the hippocampus were seeded in one side of a microfluidic device, the axons grew to the other compartment for 12 days and microglia cells were seeded in the axonal compartment. The conditioned media obtained from astrocytes treated with Meth (ACM Meth) or from control astrocytes cultures (ACM Ctrl) was added to the microglia/axonal compartment and Meth 100 µM was added to the neuronal compartment for 24 h. **(B)** Fluorescence imaging of microglial cells co-cultured with neurons and exposed to ACM Ctrl or ACM Meth + Meth for 24 h. Microglia cells were immunolabeled for iNOS (green) and results express the iNOS intensity (mean ±SEM) of five independent cultures (ACM Ctrl – 480 cells; ACM

Meth + Meth - 459 cells). **(C)** Fluorescence imaging of microglia cells co-cultured with neurons and exposed to ACM Ctrl or ACM Meth + Meth for 24 h. Microglia were incubated with microbeads (green) and immunolabeled for iba1 (red). The results represent the number of beads per cell (mean ±SEM) of five independent cultures (ACM Ctrl – 460 cells; ACM Meth + Meth - 430 cells). **(D)** Fluorescence imaging of microglial cells co-cultured with neurons and exposed to ACM Ctrl or ACM Meth + Meth for 24 h. Microglia cells were immunolabeled for arginase 1 (magenta) and results express the arginase 1 intensity (mean ±SEM) of six independent cultures (ACM Ctrl – 395 cells; ACM Meth + Meth - 403 cells). Symbol colors represent the mean of each independent cell culture and the violin plots the variability of all cells quantified. Statistical analysis for B, C and D was performed using a linear mixed model followed by Tukey–Kramer comparison test (****p<0.0001). Scale bar 10 µm. **(E)** RT-qPCR for TNF, Il-1β and Il-6 from microglia and neurons co-cultured cells in a microfluidic device, where microglia were exposed to ACM Ctrl or ACM Meth + Meth for 24 h. **(F)** RT-qPCR for Il-10 and TGFβ from microglia and neurons co-cultured cells in a microfluidic device, where microglia were exposed to ACM Ctrl or ACM Meth + Meth for 24 h. In both cases, results were normalized to the S18 gene and are expressed as the mean ±SEM of five independent cultures. Symbol colors represent the mean of each independent cell culture. Statistical analysis was performed using paired Student's *t*-test.

CHAPTER V

Effects of chronic Meth exposure

1. Introduction

Addiction is a chronic, relapsing disease characterized by compulsive drug seeking and use, despite the harmful consequences [1]. The latest World Drug Report estimates that in 2020, 284 million (M) people aged 15–64 made use of psychoactive substances within the last 12 months [2]. This report estimates 35.6M of problematic drug-users of which only one in six has access to treatment [2]. Among those enrolled in treatment programs, relapse rates are usually higher than 40% [3], which is justified by an unfortunate conjugation between the complexity of substance disorders and lack of therapeutic efficacy.

The complexity of addiction is patent in the many distinct neural mechanisms involved in this condition [4]. Among psychostimulant substances, methamphetamine (Meth), due to its high potency and wide use, is likely one of the most studied substances. Meth has been associated with impairment of the dopaminergic system, high oxidative stress, mitochondrial dysfunction, blood brain barrier dysfunction and glutamate excitotoxicity [5-7]. More recently, a growing body of evidence shows that immune cells, either within the CNS or in the periphery, are also strongly affected by psychoactive substances [8-10] Once these cells can modulate brain plasticity and behavior , it is fair to assume that they can also be involved in drug addiction progression. In fact, exposure to psychostimulant substances was already seen to induce morphologic alterations in microglia cells and promote the release of pro-inflammatory cytokines in several brain regions [11, 12]. Adding to this, we have reported that a binge administration of Meth leads to microgliosis and microglia activation in a process mediated *via* astrocytic glutamate release, in a TNF/IP_3R2-Ca^{2+}- dependent manner [13]. In accordance, in Meth abstinent users, persistent microgliosis was observed by positron emission tomography (PET) over long periods of abstinence [14, 15].

Under physiological conditions, the maintenance of microglia in a homeostatic state is highly dependent on the dynamic crosstalk between neurons and microglia [16]. There is large evidence that the reciprocal communication between neurons and microglia is mediated by contact-dependent mechanisms, by several soluble factors, such as neurotransmitters, neuromodulators and neuropeptides, and by extracellular vesicles (EVs) [17-20]. Previously, using *in vitro* microfluidic primary cultures, we have reported that contact-dependent mechanisms between neurons and microglia, such as the CD200/CD200 receptor signaling, counteract microglia activation and likely contributing to increase synaptic plasticity under Meth exposure [21]. Another neuroimmune regulatory ligand-receptor pair that has been described as important player in CNS is the cluster differentiation 47 (CD47) and its receptor signal-regulatory protein alpha (SIRPα)

[22-24]. CD47 is a transmembrane protein broadly expressed in different cell types, while its receptor (SIRPα) is mostly expressed on phagocytic cells [25, 26]. The binding of CD47 to SIRPα functions as a “don´t eat me” signal, inhibiting phagocytosis [27]. In neurons, CD47 is highly expressed at the synapse and its expression seems to be relevant for down-regulating central immune responses [18], while SIRPα is mostly expressed in microglia[28]. The interaction CD47-SIRPα seems to regulate microglial phagocytosis and synaptic pruning [24, 29, 30]. Of note, various cancer cells promote the expression of CD47 to bind SIRPα in professional phagocytes and escape their action [31-34]. In cancer cells, the expression of CD47 can be modulated by interferon gamma (IFN-γ) [35, 36], a cytokine whose role in addiction needs to be clarified (as reviewed in Chapter III).

As already mentioned, despite the heavy consequences of drug use for our society and for individuals with use disorders, successful treatments remains elusive. Treatments currently approved, primarily act by reducing withdrawal symptoms, via partial receptor stimulation, or act to prevent drug reinforcement through receptor inhibition [4]. Although these treatments are able to reduce drug cravings and promote abstinence, the relapse rates are still very high. Therefore, a better understanding of the inflammatory response dynamics during the different periods of the addictive process is of prime importance. In this sense, the study of the interplay between glial cells and neurons to identify microglial regulatory mechanisms may be helpful to counterbalance the inflammatory response and unveil new targets to treat addictive disorders.

In the present study, a proteomic analysis allowed us to identify proteins potentially involved in novel drug related mechanisms. Our results showed that CD47 is decreased after chronic Meth administration and that this is concomitant with an increase in microglia numbers and homeostasis dysregulation. The CD47 receptor, SIRPα, is downregulated in microglia cells during Meth-withdrawal. Down-regulation of this neuro-immune-regulatory pair may promote synaptic pruning and contribute to the behavioral changes elicited by Meth. Moreover, we also observe decreased meningeal T cells and lower production of IFN-γ after chronic Meth exposure, which remained after short-term withdrawal. Further studies will be necessary to further understand the possible correlation between CD47 and IFN-γ under Meth exposure.

2. Material and Methods

Mice and treatment

All procedures were conducted following the Directive 2010/63/EU and approved by the competent authorities Direcção Geral de Alimentação e Veterinária (DGAV) and i3S Animal Ethical Committee (ref.2018-13-TS and DGAV 003891/2019-02-15). Researchers involved in animal experimentation were FELASA certified. All efforts were made to minimize animal suffering and the number of animals used. Mice were housed under specific pathogen-free conditions and controlled environment (20°C, 45–55% humidity) with an inverted cycle 12h/12h light/dark cycle, and with free access to food and water. C57BL/6 male mice were obtained from the i3S animal facility. Animals were randomly assigned to four different groups: i) Control group (Ctrl); ii) Chronic group – animals administered intraperitoneally with increasing doses of Meth for ten days and euthanized 24 h after the last administration; iii) Two days withdrawal group (2d WD) - animals administered with increasing doses of Meth during ten days and euthanized 72 h after the last administration; iv) Ten days withdrawal group (10d WD) – animals administered with increasing doses of Meth during ten days and euthanized ten days after the last administration (**Fig. 1A**). Methamphetamine hydrochloride was imported from Sigma-Aldrich under a special INFARMED license (ref. 290-13).

Conditioned place preference

In order to validate the Meth administration protocol, vulnerability to drug abuse was assessed by the conditioned place preference (CPP) test adapted from Alves and colleagues [37]. The CPP apparatus consisted of a wide acrylic box divided into three compartments (two 33 × 33 cm side compartments and one 12 × 12 cm central compartment) connected by doors. One side compartment displayed black walls, while the other side compartment presented black and white striped walls. The floor of both compartments had different textures. A video camera was installed 1 m above the apparatus to record the animals in the first day of the testing, and then 24 h, two days and ten days after the last administration of Meth. In the first test day (pre-conditioning day), each animal was placed in the central compartment with open doors and allowed to freely explore all the apparatus for 30 min. The time spent in each compartment was measured, using the software Tiselius (www.tiselius.es). The non-preferred side was paired with Meth and the preferred side was paired with a saline solution. During 10 days (conditioning phase), mice were injected intraperitoneally with a saline solution and with

Meth after 4 hours, following the schematized protocol of administration in **Suppl. Fig. 1A**. Each training session lasted 30 min, in which mice stayed in the compartment paired with saline or Meth in accordance to the substance administered. In day twelve (post-conditioning day), mice were individually placed in the central compartment with the doors opened and they were able to freely explore all the CPP apparatus, as already experienced during the pre-conditioning. The amount of time spent in each side compartment was determined as in the pre-conditioning day. Each animal was tested once more in the apparatus at days 14 and 22, sessions were recorded as in the post-conditioning day. CPP score was calculated accordingly with the following formula: CPP-score = [(percentage of time in Meth compartment − percentage of time in saline compartment)$_{post\text{-}conditioning}$ − (percentage of time in Meth compartment − percentage of time in saline compartment)$_{pre\text{-}conditioning}$].

Brain protein extraction

At each evaluated time point, animals were anesthetized and perfused intracardially with ice-cold phosphate buffer saline (PBS). The brains were removed, the hippocampi collected, frozen in dry ice and stored at -80°C until further processing. Frozen tissue was then transferred into lysing matrix D beads for FastPrep®-24 and incubated in RIPA buffer (Thermo Scientific) with cOmplete™ protease inhibitor cocktail (Roche) and PhosSTOP™ (Roche). Samples were homogenized on FastPrep®-24 at speed 6 for 30 s and the homogenate was centrifuged for 5 min at 13400 rpm. The supernatant was collected and cell lysis was performed at 95°C, 1000rpm, for 10 min. Afterwards, samples were sonicated with two cycles of 5 s, with 15 s of interval. Cell debris were pelleted by centrifugation at 13,400 rpm for 5 min. Protein concentration was determined using the Pierce™ BCA protein assay kit (Thermo Scientific) and one-hundred micrograms of protein from each sample (n=5/group) were processed for proteomic analysis.

Proteomics data acquisition

Each sample was processed for proteomic analysis following the solid-phase-enhanced sample-preparation (SP3) protocol and enzymatically digested with Trypsin/LysC as previously described [38].

Protein identification and quantitation were performed by nanoLC-MS/MS. This equipment is composed of an Ultimate 3000 liquid chromatography system coupled to a Q-Exactive Hybrid Quadrupole-Orbitrap mass spectrometer (Thermo Scientific,). Five

hundred nanograms of peptides of each sample were loaded onto a trapping cartridge (Acclaim PepMap C18 100 Å, 5 mm × 300 µm i.d., 160454, Thermo Scientific) in a mobile phase of 2% ACN, 0.1% FA at 10 µL/min. After 3 min loading, the trap column was switched in-line to a 50 cm × 75 µm inner diameter EASY- Spray column (ES803, PepMap RSLC, C18, 2 µm, Thermo Scientific) at 250 nL/min. Separation was achieved by mixing A: 0.1% FA and B: 80% ACN, 0.1% FA with the following gradient: 5 min (2.5% B to 10% B), 120 min (10% B to 30% B), 20 min (30% B to 50% B), 5 min (50% B to 99% B), and 10 min (hold 99% B). Subsequently, the column was equilibrated with 2.5% B for 17 min. Data acquisition was controlled by Xcalibur 4.0 and Tune 2.11 software (Thermo Scientific).

The mass spectrometer was operated in the data-dependent (dd) positive acquisition mode alternating between a full scan (m/z 380-1580) and subsequent HCD MS/MS of the 10 most intense peaks from a full scan (normalized collision energy of 27%). The ESI spray voltage was 1.9 kV. The global settings were as follows: use lock masses best (m/z 445.12003), lock mass injection Full MS and chrom. peak width (FWHM) of 15 s. The full scan settings were as follows: 70 k resolution (m/z 200), AGC target 3×10^6, maximum injection time 120 ms; dd settings: minimum AGC target 8×10^3, intensity threshold 7.3×10^4, charge exclusion: unassigned, 1, 8, >8, peptide match preferred, exclude isotopes on, and dynamic exclusion 45 s. The MS2 settings were as follows: microscans 1, resolution 35 k (m/z 200), AGC target 2×10^5, maximum injection time 110 ms, isolation window 2.0 m/z, isolation offset 0.0 m/z, dynamic first mass, and spectrum data type profile.

Proteomics data analysis

The raw data was processed using the Proteome Discoverer 2.5.0.400 software (Thermo Scientific) and searched against the UniProt database for the *Mus musculus* Proteome (2020_04 with 55471 entries). A common protein contaminant list from MaxQuant was also considered in the analysis. The Sequest HT search engines was used to identify tryptic peptides. The ion mass tolerance was 10 ppm for precursor ions and 0.02 Da for fragmentfor-fragment ions. Maximum allowed missing cleavage sites was set to two. Cysteine carbamidomethylation was defined as constant modification. Methionine oxidation, deamidation of glutamine and asparagine, peptide terminus glutamine to pyroglutamate, and protein N-terminus acetylation, Met-loss, and Met-loss+acetyl were defined as variable modifications. Peptide confidence was set to high. The processing node Percolator was enabled with the following settings: maximum delta Cn 0.05; decoy

database search target false discovery rate 1%, validation based on *q*-value. Protein label-free quantitation was performed with the Minora feature detector node at the processing step. Precursor ions quantification was performed at the consensus step with the following parameters: unique plus razor peptides were considered, precursor abundance based on intensity, and normalization based on total peptide amount. For hypothesis testing, protein ratio calculation was pairwise ratio-based and a t-test (background based) hypothesis test was performed.

Bioinformatics analysis and visualization of proteomic data

For determination of differentially expressed proteins between the different experimental groups (Chronic vs Ctrl; 2d WD vs Ctrl; 10d WD vs Ctrl; 2d WD vs Chronic; 10d WD vs Chronic and 2d WD vs 10d WD), the following filters were additionally considered: (1) the minimum number of samples that a protein must be detected to be used was set to 3 samples per experimental group; (2) the use of at least two unique peptides; (3) the ratio considered between groups was the abundance ratio adjusted p-value settled to ≤0.05 for altered proteins.

Proteome Discoverer-generated output table was loaded into R (version 4.2.2, http://www.R-project.org/) for further analysis. The generation of the different plots was made as following: heatmaps were performed using the Pheatmap package; volcano plots were done using the EnhancedVolcano package; venn diagrams with the VennDiagram package; and any other plots were created using the ggplot2 package.

For the determination of the pathways and GO-biological terms associated with the significantly altered proteins, the list of protein names was loaded onto Panther classification system (http://www.pantherdb.org/) and the results downloaded and further processed in R.

Previously published single-cell RNA sequencing data from the adult mouse brain [39] were download from http://dropviz.org and analyzed using R. For our analysis, only the metadata and annotations referring to data derived from the hippocampus were used. To predict the cell-cell communications between all the different cell types using CD47 signaling pathway, we used the R toolkit Cellchat [40] as previously performed [41]. The dataset was analyzed using the original pipeline described by Jin et al., 2021, including the default method for the computation of the communication probability and the use of 10 cells as the threshold for the minimum number of cells needed expressing the ligand or receptor.

The identification of which significant altered proteins are involved and/or located in synapses was done by matching them with a previously generated resource synapse proteome [42], filtered to include only the synapse proteome derived from mouse hippocampus.

Immunohistochemistry

Brains isolated from perfused mice were post-fixed overnight with 4% of paraformaldehyde (PFA), crioprotected using 30% of sucrose, then cryo-embedded and sectioned coronally at 30 µm thick. Brain sections were collected in PBS and preserved in a cryoprotection solution (30% of sucrose and 30% of ethylene glycol in 0.1M phosphate buffer) at - 20°C until further use.

For immunostaining, sections at the level of dorsal hippocampus were processed in free floating. Brain sections were permeabilized (0.25% Triton X-100 in PBS) for 10 min, blocked (0.1% Triton X-100, 5% BSA in PBS) for 1 h at room temperature and incubated overnight at 4°C with the relevant primary antibodies diluted in 0.1% Triton X-100, 5% BSA in PBS. The following primary antibodies were used: rabbit anti-Iba 1 (1:500, Wako); rabbit anti- PSD95 (1:500, Cell Signaling); mouse anti-VGlut1 (1:1000, Synaptic Systems); mouse anti-VGlut2 (1:1000, Synaptic Systems); Alexa Fluor 647 anti- mouse CD47 (Biolegend). Corresponding secondary antibodies conjugated to Alexa Fluor 488 or 568 (1:1000, Thermo Fisher Scientific) were used. Brain sections were incubated with secondary antibodies diluted in 0.1% Triton X-100, 5% BSA in PBS for 1 h at room temperature. Nuclei were counterstained with 4,6-diamidino-2-phenylindole (DAPI, 1:5000, Sigma). Slices were mounted using fluorescence mounting medium (Dako).

Microscope images acquisition

Images were acquired with an inverted Leica SP8 single point scanning confocal microscope equipped with a fully motorized DMi8 microscope, a HC PL APO CS2 63x / 1.3 glycerol immersion objective lens. A tunable Argon laser AOBS modulated, a 405 Diode laser line, 561 DPSS laser line and/or a 594 HeNe laser line, and Leica PMT and HyD GaASP detectors were used. Images were acquired sequentially by line scanning unidirectionally at 600 Hz for microglia analysis and at 1000 Hz for synapses quantification, using the galvanometer-based imaging mode. A line average of 3 was used, with a pixel size of 0.361 µm for microglia or 0.075 µm for synapses analysis and a z step-size of 0.333 µm, for an area size of 184.52 um x 184.52 µm or 38.44 um x

38.44 µm in Leica LasX software, and saved as LIF files. For all images the pinhole size was 102.9 um, calculated at 1 AU for 580 nm emission.
In image acquisition for microglia analysis: DAPI was excited with 405 nm laser line with laser power of 6 %, and emission was collected on a Leica PMT detector with a collection window of 415 nm – 478 nm with 845 V. AlexaFluor 488 was excited with 488 nm laser line with laser power of 2.198 % (Argon at 9.4828 %), and emission was collected on a Leica HyD2 (BrightR mode) detector with a collection window of 498 nm- 551 nm with a smart gain of 100 %.
In image acquisition for synapses quantification: AlexaFluor 488 was excited with 488 nm laser line with laser power of 10.0013 % (Argon at 9.4828 %), and emission was collected on a Leica PMT2 detector with a collection window of 498 nm- 557 nm with a smart gain of 562 V, and an offset of -0.06. AlexaFluor 594 was excited with 594 nm laser line with laser power of 12.0035 %, and emission was collected on a Leica HyD3 (standard mode) detector with a collection window of 604 nm- 623 nm and smart gain of 109.2 %.

Microglia density quantification and 3D reconstruction

Microglia cell density quantification was performed in the hippocampus regions CA1, CA2, CA3 and DG. For each animal (n=5 per group), 3 images per region and per section were acquired (n=3/animal).
Microglia cells were counted using ImageJ software [43] and microglia density was calculated taking into consideration the volume of each slice analyzed. Three-dimensional microglia reconstruction, using the surface and filaments modules from Imaris software (version 9.1.1, Bitplane) was performed in CA1 hippocampus and different microglia morphologic parameters (filament length, number of dendritic segments and number of dendritic terminals) were extracted. Morphologic analysis was performed in 20 cells/group (n=5 per group).

Synapses quantification

Synapses quantification was performed in the hippocampus CA1 region. Ten images per slice (3 slices/animal) were acquired (n=2 or 3/group).
Deconvolution was applied to images using Huygens Professional software (version 22.04.0p0 64b, SVI, Scientific Volume Imaging). The deconvolution express module was used, applying the aggressive profile. Imaris software was subsequently used to quantify

the number of pre- and postsynaptic puncta and the number of pre- and postsynaptic puncta colocalized, in order to quantify the number of synapses. To segment the pre-synaptic puncta (VGlut1 and VGlut2) the surface module in the Imaris software was used and to segment the postsynaptic puncta (PSD95) the spot module was used.

Flow cytometry

For mononuclear cell isolation, mice were anesthetized and perfused intracardially with ice cold PBS. Brain or the hippocampi were dissected, and tissue was mechanically homogenized in HBSS supplemented with HEPES (15mM, Lonza), glucose (0.6%, Sigma) and EDTA (1mM, ThermoFisher Scientific). The homogenate was filtered through a 70 µm cell strainer and cells were pelleted by centrifugation at 300 rcf for 10 min at 4°C. Cells were resuspended with 24% Percoll buffer, prepared from a previous dilution of Percoll (GE Healthcare) in 1× HBSS (9:1 Percoll: 10× HBSS). Carefully PBS was added on the top of 24% Percoll buffer and a centrifugation at 950 rcf for 20 min at RT was performed. The supernatant was discarded, pelleted cells were resuspendend in ice-cold FACS buffer (2 mM EDTA; 25 mM HEPES; 2% FBS and 0.01% NaN_3 in DPBS) and counted. Meningeal tissue was carefully removed from the skullcaps under a dissecting microscope and were incubated in digestion solution (1.4U/mL collagenase D (Roche); 35 U/mL DNase I (Roche); 2% FBS; 2mM L-glutamine; 10 mM HEPES in RPMI 1640 medium) and incubated at 37°C for 30 min. Then, meninges were passed through a 25G needle and subsequently through a 70 µm cell strainer. Cell suspension was collected and centrifuged at 500 g, for 7 min at 4° C. Cells were resuspended in in FACS buffer and counted. Spleens and cLNs were homogenized and washed in RPMI 1640 medium containing 2% FBS and resuspended in FACS buffer. Thereafter, cells were incubated with Zombie Aqua™ (Biolegend) to further dead cells exclusion in the analysis. Before antibody incubation, cells were incubated with FcBlock (1:100, Biolegend) for 10 min on ice to reduce non-specific antibody binding. For extracellular staining, cells were stained with appropriate surface anti-mouse antibodies. Cells were fixed in PFA 2% and ressuspended in FACS buffer. For intracellular staining, cells were stimulated in complete RPMI 1640 medium with PMA (Phorbol 12-Myristate 13-Acetate; 50 ng/mL, Sigma-Aldrich) and Ionomycin (1 µg/mL, Sigma-Aldrich) in presence of Brefeldin A (BFA; 10 µg/mL, Sigma-Aldrich), for 4 h at 37 °C 5% CO_2. Cells were surface stained as described above and fixed/permeabilized with a Foxp3/Transcription Staining Buffer kit (eBioscience™) supplemented with BFA for 30 min. Then, cells were permeabilized in Permeabilization Buffer with rat IgG (1:100, Sigma-Aldrich) and FcBlock (1:500, Biolegend). Intracellular staining mix containing the appropriate antibodies was

added and the cells were incubated for 1 h, at RT. Samples were washed and resuspended in FACS buffer.

The following antibodies anti-mouse were used (all from Biolegend): CD45 PE or FITC (Clone 30-F11); CD11b Pe-Cy7 (Clone M1/70); CD3 APC-Cy7 (Clone 17A2); CD4 Pacific blue (Clone RM4-5); CD8 PerCP-Cy5.5 (Clone 53-6.7); SIRPα FITC (Clone P84); TCR γδ PECy7 (Clone GL3); and IFN-γ PE (Clone XMG1.2).

Mono labels were performed either with cells (for Zombie Aqua™) or compensation beads (Invitrogen) to achieve clear positive and negative populations for compensation. Data were acquired in a FACSCanto II flow cytometer (BD Biosciences). Post-acquisition analysis was performed using FlowJo software v10 (Tree Star).

Statistical analysis

Data presentation is described in figure legends. Identification and removal of outliers were performed with the automatic GraphPad Prism® software (version 9.1.2. for macOS), using the ROUT (robust non-linear regression) method, with a $Q = 5\%$, for removing outliers.

Statistical analyses, with exception of microglia density quantification and morphology analysis, were performed in the GraphPad Prism® software, using repeated measure one-way ANOVA Sidak´s post hoc test for CPP or one-way ANOVA Tukey´s post hoc test for the remaining statistical analysis. For microglia density quantification and morphology analysis by immunocytochemistry, a linear mixed model analysis was performed using SAS® Visual Statistics with REML function, followed by Tukey–Kramer multiple comparison test, using the animal as a random variable. Differences were considered at the significance level of $p<0.05$ .and are indicated by*; those at $p<0.01$ are indicated by **; those at $p<0.001$ are indicated by ***; and those at $p<0.001$ are indicated by ****.

3. Results

Profiling the proteome of mouse hippocampus after chronic Meth administration and withdrawal

To understand how chronic Meth administration altered the hippocampal proteome and how this could impact the addictive behavior, we used an escalating Meth dosing and evaluated mice at 10 days of Meth administration (chronic group), 2 and 10 days of Meth withdrawal (2d WD and 10d WD**, Fig. 1A**). The CPP test was performed to confirm the

rewarding effects of this Meth administration schedule (**Suppl. Fig. 1A**). CPP resulted in the conditioning of 75 % of Meth administered mice. **Suppl. Fig. 1B** displays CPP scores for the animals that were conditioned after Meth administration, and shows that they still presented preference for the Meth compartment after 2 or 10 days WD

Among the 6007 proteins identified in the proteomic analysis, 124 proteins were differentially expressed in at least one of the performed comparisons, which were presented as a heatmap (**Fig. 1B and Suppl. Table 1**). Considering the Chronic vs Ctrl comparison, 32 proteins were differentially expressed, 10 of them downregulated and 22 upregulated (**Fig. 1C**). In the comparisons 2d WD vs Ctrl and 10d WD vs Ctrl, we found 25 and 23 proteins differentially expressed (respectively), including 18 proteins upregulated in both comparisons, 7 downregulated in the 2d WD vs Ctrl comparison and 5 downregulated in the 10d WD vs Ctrl comparison (**Fig. 1C**). The 2d WD vs Chronic comparison is the comparison with higher number of differentially expressed proteins: a total of 66 proteins, with 56 proteins upregulated and 10 downregulated (**Fig. 1C**). Regarding the 10d WD vs Chronic comparison, a total of 47 proteins were differentially expressed: 39 proteins were upregulated and 8 downregulated (**Fig. 1C**). Finally, in the 10d WD vs 2d WD comparison, 27 proteins were differentially expressed: 9 proteins upregulated and 18 downregulated (**Fig. 1C**). None of the differentially expressed proteins was altered in all the comparisons performed. However, 3 proteins were differentially expressed in all experimental groups when compared to the control group (**Fig. 1D**). Those proteins were Ppp1cb, Gap43 and Glg1. Additionally, we sought to determine the proteins that were altered after chronic Meth exposure when compared with the control group and after short- and long-term of Meth withdrawal (**Fig. 1E**). The proteins Hbb-bs, CD47, Hspa1a, Hba-a1 and H4c were altered in these comparisons (**Fig. 1E**). Of these proteins, with exception of Hspa1a, all presented lower levels of expression after chronic Meth, were again increased during withdrawal.

We then determined the ten most relevant pathways and GO-biological terms associated with significantly altered proteins. This analysis revealed alterations in several neurotransmission-related pathways, such as metabotropic glutamate receptor group III, ionotropic glutamate receptor, muscarinic acetylcholine receptor 1 and 3 signaling, 5HT2 receptor mediated signaling and dopamine receptor signaling (**Fig. 1F**). Additionally, proteins related with Parkinson disease, WNT signaling, apoptosis signaling and cadherin signaling pathways were also found differentially expressed in the comparisons performed (**Fig. 1F**).

Together these data showed that chronic Meth exposure and short- or long-term Meth withdrawal highly affect the mouse hippocampus proteome, with a strong impact in

proteins that are part of neurotransmission-related pathways. Importantly, this is concordant with the classical hallmarks of Meth use [5, 44, 45] .

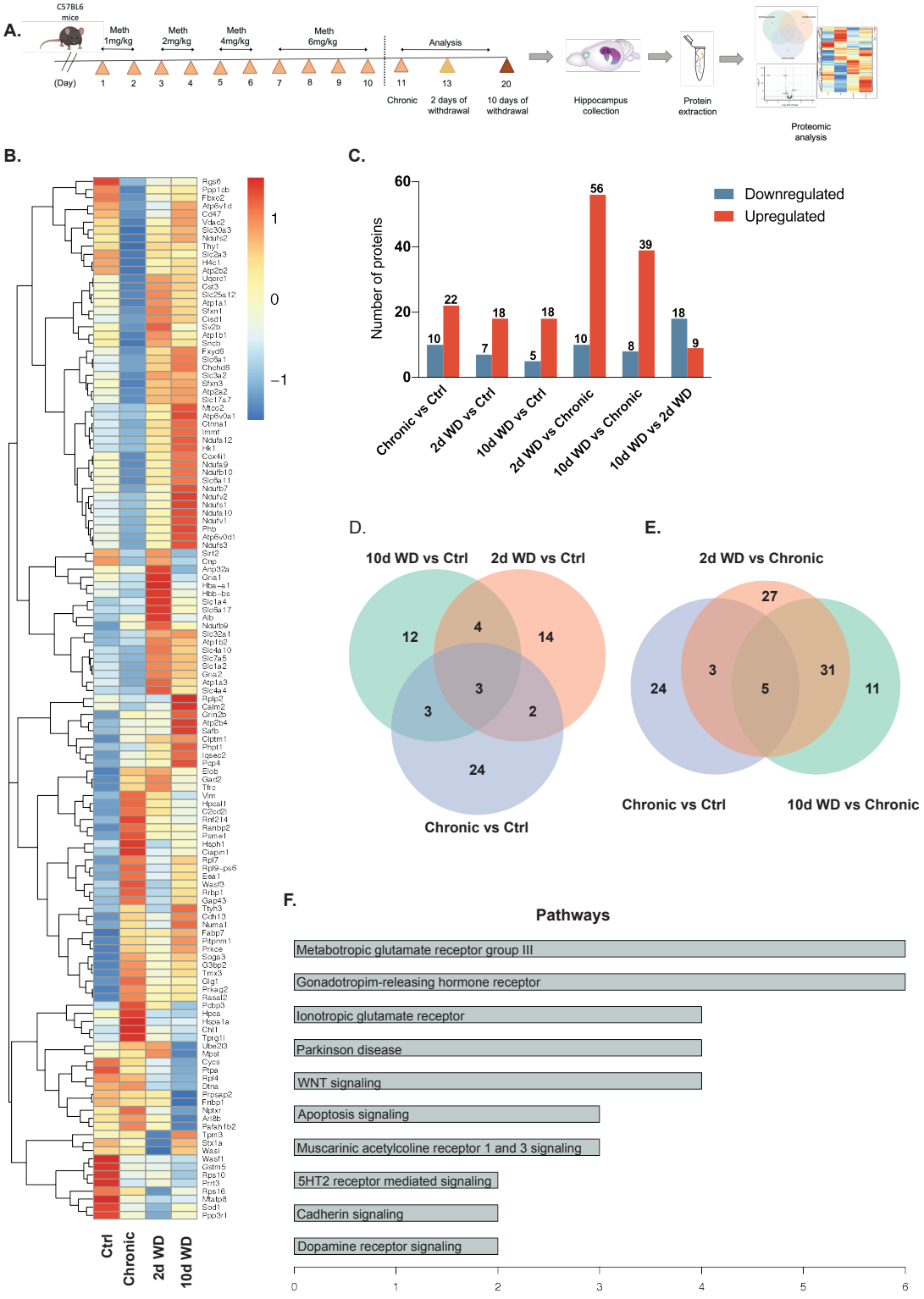

Figure 1: Impacts of chronic Meth exposure and short- and long-term withdrawal in the mouse hippocampal proteome. **(A)** Schematic representation of the chronic escalating Meth

administration schedule used. Data analysis time-points and workflow for hippocampal proteome analysis **(B)** Heatmap of differentially expressed proteins at the different time-points **(C)** Graphic representation of the number of proteins up- (red colored) and down-regulated (blue colored) in all the comparisons performed. **(D)** Venn's diagrams representing the proteins that were differentially expressed in the following comparisons: 10d WD vs Ctrl; 2d WD vs Ctrl and Chronic vs Ctrl.**(E)** Venn's diagrams representing the proteins that were differentially expressed in the following comparisons: 2d WD vs Chronic, 10d WD vs Chronic and Chronic vs Ctrl. **(F)** Significant enriched pathways and GO-biological terms associated with the significantly altered proteins.

CD47 was downregulated after chronic Meth exposure

Since proteomic data pointed to changes in neurotransmission-related pathways and because there is strong accumulated evidence that addictive substances modify synaptic activity [46], we them focused our analysis on synaptic proteins. To do so, proteins differentially expressed and involved and/or located in synapses were identified using a previously generated resource synapse proteome [42]. In fact, 114 out 124 proteins, identified as differentially expressed in each of the comparisons described in the previous section, matched the synapse proteome (**Fig. 2A-C** and **Suppl. Fig. 2A-C**). One of the synaptic-related proteins that grabbed our attention was CD47, since it was differentially expressed in three of the comparisons performed (**Fig. 1E** and **Fig 2A-C**). We found that this protein was downregulated after chronic Meth exposure (**Fig. 2A**) and that its levels were then increased after 2 and 10d WD when compared with the chronic experimental group (**Fig. 2B and C**). No differences in CD47 protein levels were observed in the remaining comparisons performed (**Suppl. Fig. 2A-C**). We previously demonstrated that contact-dependent mechanisms between neurons and microglia attenuate Meth-induced microglia reactivity and enhance synaptic plasticity [21]. CD47 is one of the several neuroimmune regulatory proteins, highly expressed in neurons, that modulate microglia homeostasis [17]. The interaction between neurons and microglia, through CD47 and its receptor SIRPα was previously seen to regulate microglial phagocytosis, functioning as a "don´t-eat-me" signal [24, 29, 30]. Although, CD47 is mostly expressed in neuronal cells and its receptor in microglia, this ligand-receptor pair is possibly co-expressed in other cells and their interaction could, in theory, mediate the inter-cellular signaling in a bi-directional manner [47]. So, we asked whether neurons could be a major cell type contributor to our proteomic CD47 results and if the communication between neurons and microglia using CD47 could be affected by chronic Meth exposure. To do so, we first analyzed the expression of CD47 and SIRPα on cells of the hippocampus, using an available single-cell sequencing dataset [39]. CD47 was expressed on several cell types,

still, the population of cells with higher percentage expressing this protein were neurons (**Fig. 2D**), which was also the population with higher expression levels of CD47 (**Fig. 2E**). To predict the cell-cell communications between different cell types using CD47 signaling pathway, the Cellchat tool [40] was used. The prediction showed that, through CD47, neurons were able to communicate with microglia, oligodendrocyte, astrocytes and self-interact (**Fig. 2F**). The predicted communication between neurons and microglia was bidirectional (**Fig. 2F**). Additionally, communications between microglia and oligodendrocytes and between astrocytes and oligodendrocytes were also predicted (**Fig. 2F**). In silico analysis of potential strength in ligand-receptor interaction, predicted a predominant communication of CD47 to Sirpα from neurons-to-microglia (**Fig. 2G**), or microglia-to-neurons through Sirpα to CD47 (**Fig. 2H**). Together these data demonstrated that chronic Meth administration resulted in a decrease of CD47 protein levels, which may impact the CD47-SIRPα neuron-to-microglia signaling.

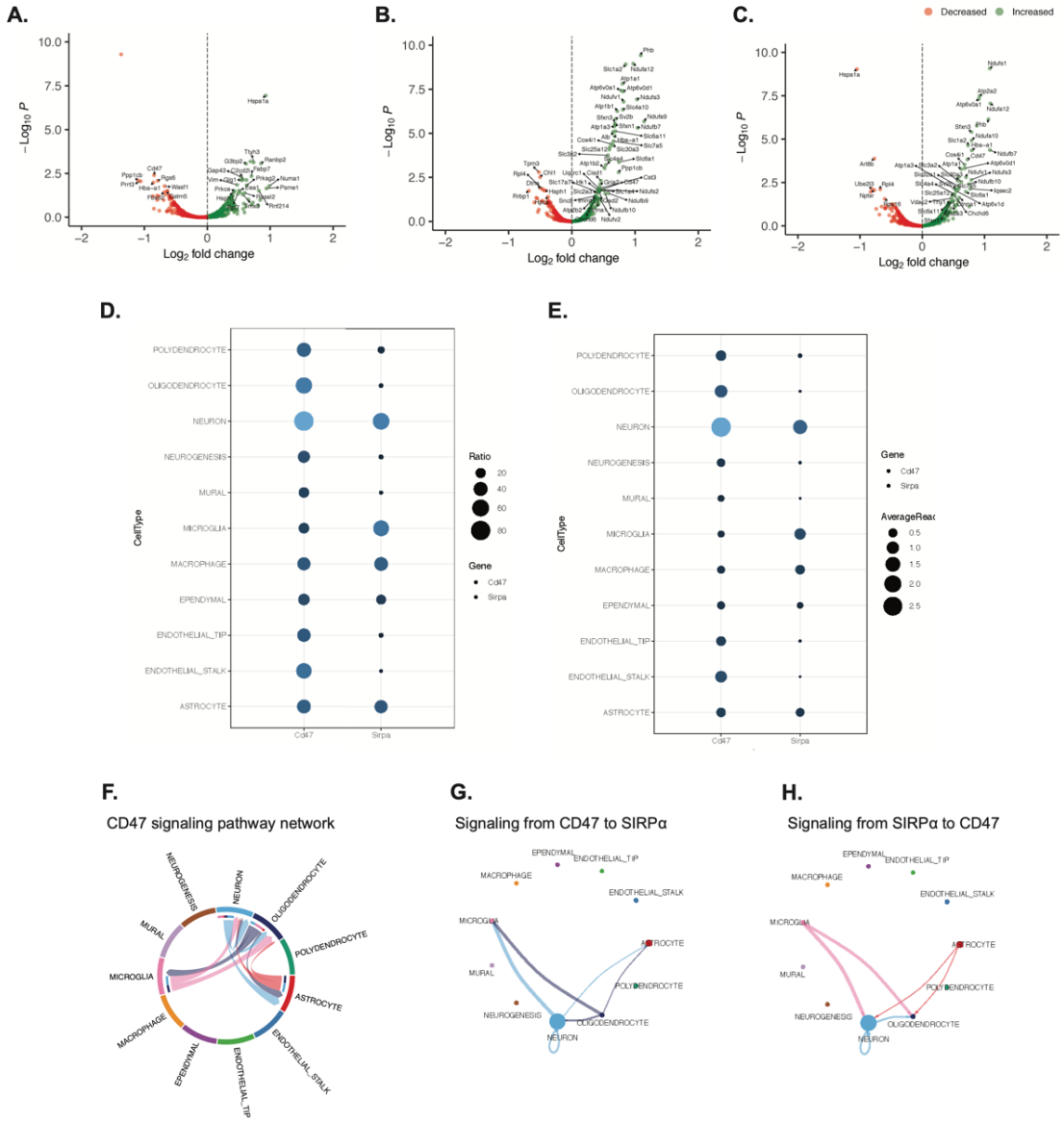

Figure 2: **CD47 protein levels are decreased after chronic Meth administration. (A)** Volcano Plot highlighting the synaptic-related proteins differentially expressed between Chronic and Ctrl groups. **(B)** Volcano Plot highlighting the synaptic-related proteins differentially expressed between 2d WD and Chronic groups. **(C)** Volcano Plot highlighting the synaptic-related proteins differentially expressed between 10d WD and Chronic groups. In the Volcano Plot the upregulated proteins are plotted in green and downregulated proteins in red. (**D** and **E**) Predicted percentage of different cell types expressing CD47 or SIRPα **(D)** or predicted expression levels of CD47 or SIRPα in different cells types **(E)**, using previously published single-cell RNA-seq data [39]. **(F)** Graph showing the interaction between the different cell types using the CD47 signaling pathway network. **(G)** Graph showing the predicted signaling from CD47 to SIRPα. **(H)** Graph showing the predicted signaling from SIRPα to CD47.

Chronic Meth administration and withdrawal lead to dysregulation of microglia homeostasis

To evaluate whether the communication between neurons and microglia, through CD47-SIRPα was compromised by chronic Meth administration and taking into consideration that we previously reported that binge Meth exposure impacts on microglia profile [13], we next evaluated microglia after chronic Meth exposure and at WD.

The evaluation of microglia cells in the hippocampus by fluorescence-activated cell sorting (FACS) (gating strategy - **Fig. 3A**) revealed no significant alterations in the percentage of microglia among the CD45+ cells after chronic Meth administration nor after 2d or 10d WD (**Fig. 3B**). However, the evaluation of morphologic parameters by FACS revealed an enlargement of microglia cells after chronic Meth administration (**Fig. 3D**), with no significant alterations in microglia granularity (**Fig. 3C**). Microglia enlargement could represent a shift into a more amoeboid profile after Meth administration, likely characterized by reduced branching and increased soma size [48]. Microglia size was reestablished after 2d WD (**Fig. 3D**). The expression of CD11b and CD45, key markers of microglia [49], was also found significantly reduced after 2d WD when compared with the Ctrl and Chronic groups and remained decreased at 10d WD (**Fig. 3E and 3F**). Functionally, CD11b regulates leukocytes adhesion and migration to mediate the inflammatory response [50]. Whereas, CD45 is a negative regulator of microglia activation by several proinflammatory stimuli [51]. The decrease of CD11b and CD45 in microglia during the WD period further confirmed that microglia homeostasis was dysregulated.

To strength our proteomica data, we used FACS to evaluate SIRPα on microglia and found decreased expression after 2d WD when compared with Ctrl and Chronic groups. SIRPα remained reduced at 10d WD (**Fig. 3G**). Of note, reduced SIRPα microglial levels at WD may indicate increased microglia phagocytic activity [24].

Next, we evaluated microglial density and morphology through immunohistological analysis. Because of our previous data [13], microglia were evaluated in the dorsal hippocampus subregions CA1, CA2, CA3 and DG. Our results showed lower microglia density in the CA3 when compared with CA1, CA2 or DG (**Fig. 3H and 3J** and **Suppl. Fig 3A-C)**. In addition, the comparison between experimental groups showed a significant increase in microglia density after chronic Meth administration and 2d WD when compared with the Ctrl group. However, after 10d WD, the microglia density was decreased when compared with 2d WD and the microglia numbers were reestablished to the Ctrl group levels (**Fig. 3H and 3J and Suppl. Fig. 3A-C**). These hippocampal subregional differences in microglia density, may justify why in the FACS analysis we

found no difference in microglia levels in the whole hippocampus. Because we have previously reported that under Meth microglia undergo cytoskeletal rearrangements and alter their morphology [13], an important characteristic for cell motility and phagocytic ability [48], next, based on our previous results [13] we evaluated microglia morphology, in the CA1, using IMARIS 3D reconstruction. We observed a reduction in filament length (**Fig. 3H, 3I and 3K**), in the number of dendritic segments (**Fig. 3H, 3I and 3L**) and in the number of dendritic terminals (**Fig. 3H, 3I and 3M**) after chronic Meth administration when compared with Ctrl. During the Meth withdrawal period, the microglia cells regained the initial phenotype. Together with the morphologic parameter evaluated by FACS, one can conclude that microglia cells after chronic Meth administration acquired a more amoeboid profile.

Taken together, these data show that microglia are increased in number and acquired a more amoeboid profile after chronic Meth administration. Additionally, after 2d WD the microglia number remains increased and its homeostatic state is altered even after 10d WD. Of note, during the Meth WD period a reduction in SIRPα levels on microglia was also observed.

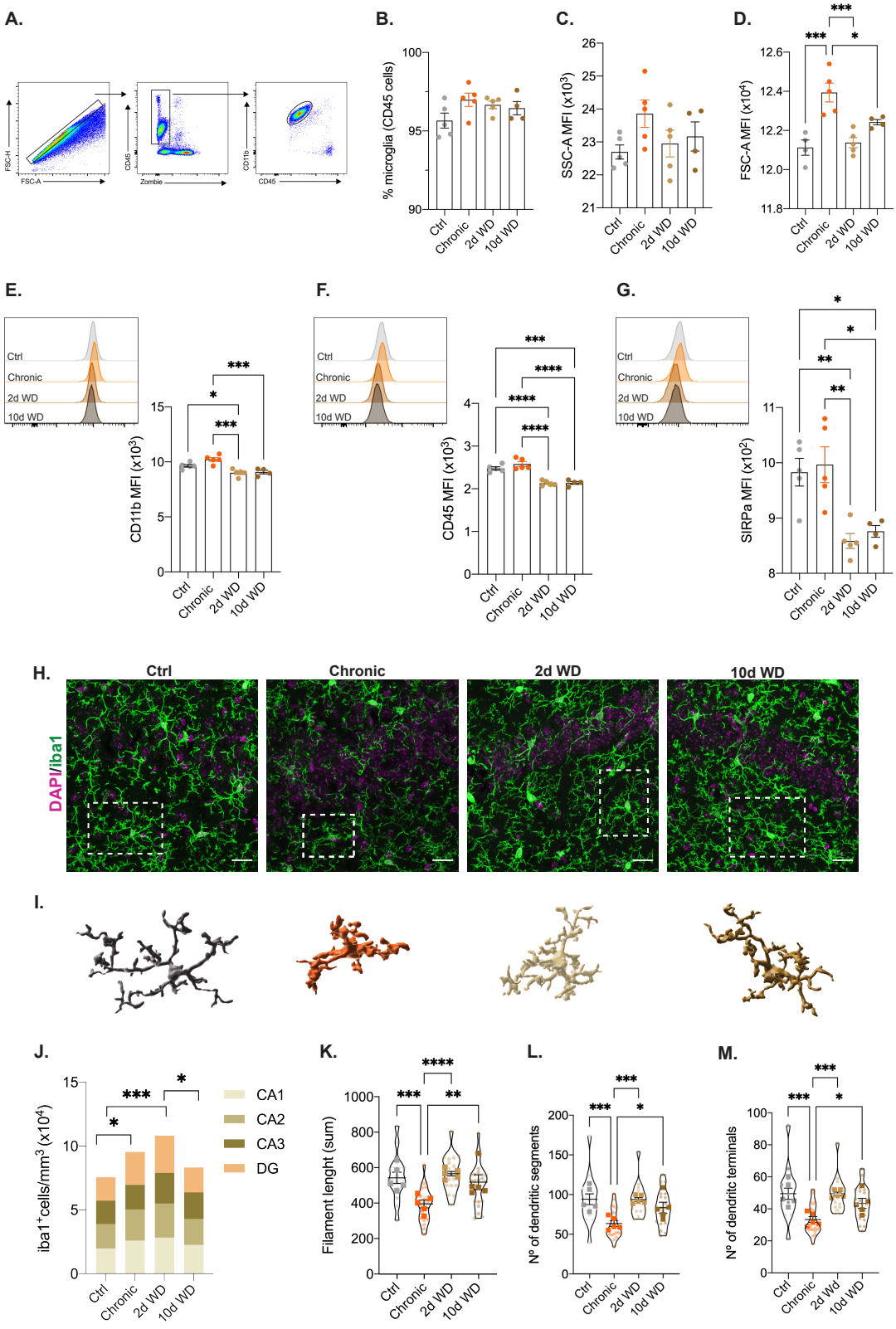

Figure 3: Chronic Meth administration and withdrawal led to different microglia non-homeostatic profiles. (A) Representative flow cytometry plot showing gating strategy for microglia cells (CD45 $^{low/int}$CD11b^{+}) upon doublet discrimination and death cell exclusion. FSC-H:

Forward scatter height. FSC-A: Forward scatter area. Flow cytometry analysis of hippocampal **(B)** microglia cells in $CD45^+$ cells ; **(C)** microglia granularity; and **(D)** microglia cell size, for the following experimental groups Ctrl, Chronic, 2d WD and 10d WD (n =5 mice/group). Graphs displays (mean and SEM) the percentage of microglial cells among $CD45^+$ cells, MFI of microglia side scatter area (SSC-A) and MFI of microglia FSC-A, respectively. Statistical analysis was performed using one-way ANOVA Tukey´s post hoc test. **(E, F, G)** Quantification of CD11b **(E),** CD45 **(F)** and SIRPα **(G)** on microglia isolated from the hippocampus of mice from the Ctrl, Chronic, 2d WD and 10d WD experimental groups (n =5 mice/group). Graphs displays MFI (mean and SEM). Representative histograms are shown. **(H)** Representative confocal images of CA1 hippocampus region from mice of the Ctrl, Chronic, 2d WD and 10d WD experimental groups, immunostained for Iba1 (green). Dashed rectangles highlight microglia cells that were three-dimensionally reconstructed in **(I)**, scale bar 10 µm. **(I)** Imaris (Bitplane)- based three-dimensional reconstructions of representative microglia from morphological analysis of CA1 region from the hippocampus of Ctrl, Chronic, 2d WD and 10d WD experimental groups. **(J)** Quantification of microglia density in CA1, CA2, CA3 and DG hippocampal regions of Ctrl, Chronic, 2d WD and 10d WD experimental groups (n =5 mice/group). Each column represents microglia-accumulated density in the CA1, CA2, CA3 and DG. Hippocampal subregions are represented by different colors. Statistical analysis was performed using a linear mixed model followed by Tukey–Kramer comparison test. Statistical main effect hippocampal subregion ***p<0.001. Statistical main effect experimental group ***p<0.001**.** Statistical interaction hippocampus region x experimental groups revealed no significant effect. Statistical analysis displayed in graphs is representative of comparisons between experimental groups. **(K, L, M)** Graph display the quantification of Imaris-based automated quantification of microglial total filament length **(K)**, number of dendritic branches **(L)** and number of dendritic terminals **(M)**. Symbol colors represent the mean of each animal (n=5 mice/group) and the violin plots the variability of all cells quantified 18-20 cells/group). Statistical analysis was performed using a linear mixed model followed by Tukey–Kramer comparison test.*p<0.05; **p<0.01; ***p<0.001 and ****p<0.0001.

Synaptic density after chronic Meth administration and withdrawal

As a decrease in CD47 [29] or in the microglial SIRPα [24] potentiate synaptic pruning, we further assessed synaptic structures. To do so, synaptic density was evaluated in the CA1 hippocampus region, performing a co-localization of the postsynaptic marker PSD95 [52] and one of the presynaptic markers, VGlut1 or VGlut2 [29]. Our results seem to indicate that chronic Meth administration resulted in decreased $VGlut2^+$ synapses (**Fig. 4E, 4F, 4G and 4H**), but not $VGlut1^+$ synapses (**Fig. 4A, 4B, 4C and 4D**). At WD, VGlut2 synapse numbers seem to be reestablished (**Fig. 4E, 4F, 4G and 4H**).
Further analysis, of synapses number will be necessary to confirm these results.

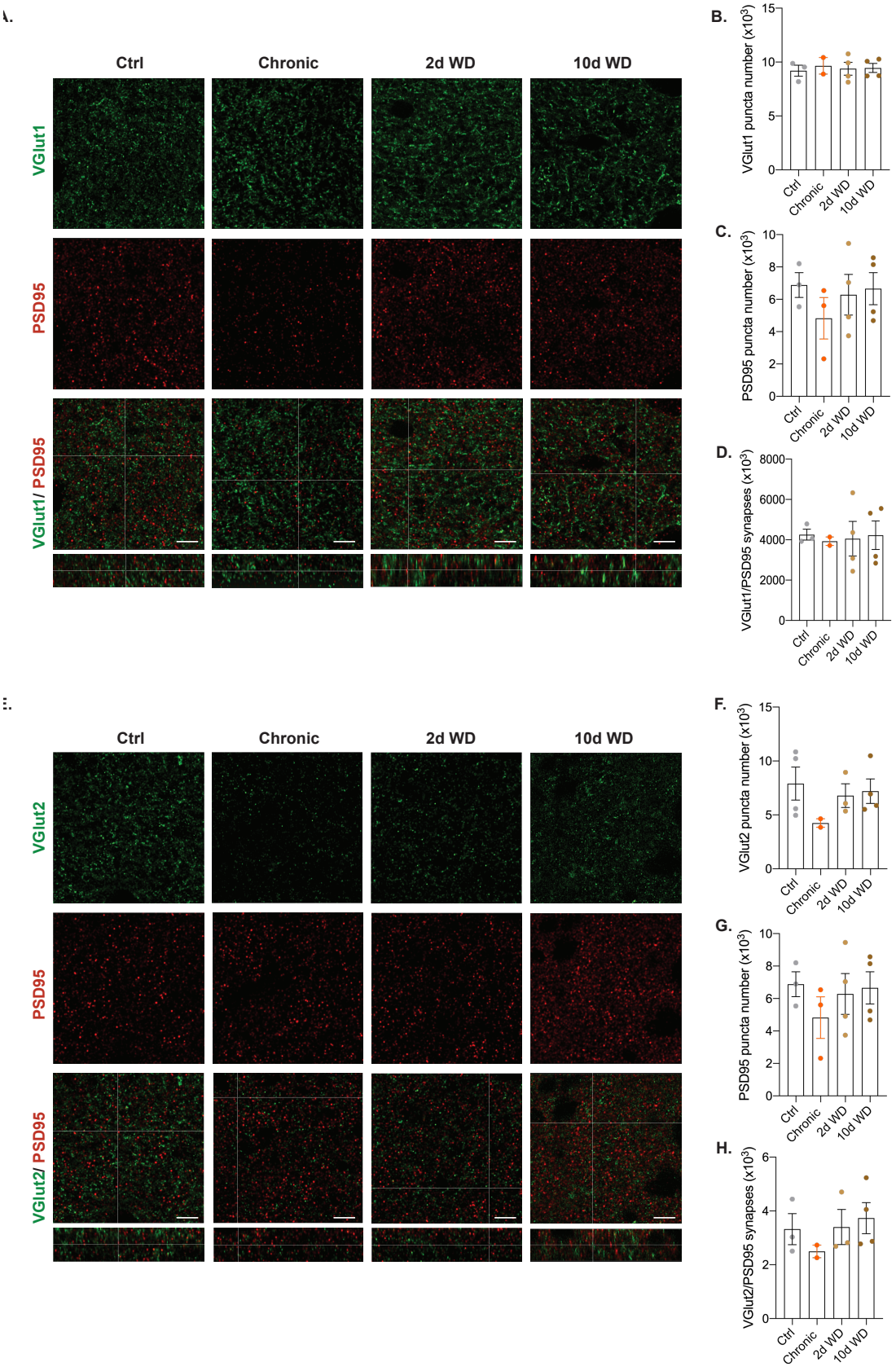

Figure 4: Assessment of Vglut1- and VGlut2-positive synapses after chronic Meth administration and Meth withdrawal. (A) Representative confocal images depicting synaptic

staining for presynaptic marker VGlut1 (green) and postsynaptic marker PSD95 (red) separately or colocalized in CA1 region of the hippocampus of mice from the Ctrl, Chronic, 2d WD and 10d WD experimental groups. Scale bars 10 μm. **(B)** Graph depicting the number of VGlut1 puncta in the Ctrl, Chronic, 2d WD and 10d WD experimental groups (mean and SEM). **(C)** Graph depicting the number of PSD95 puncta in the Ctrl, Chronic, 2d WD and 10d WD experimental groups (mean and SEM).**(D)** Graph depicting the number of VGlut1-positive synapses in the Ctrl, Chronic, 2d WD and 10d WD experimental groups. n=2-3 animals/group. **(E)** Representative confocal images depicting synaptic staining for presynaptic marker VGlut2 (green) and postsynaptic marker PSD95 (red) separately or colocalized in CA1 region of the hippocampus of mice from the Ctrl, Chronic, 2d WD and 10d WD experimental groups. Scale bars 10 μm. **(F)** Graph depicting the number of VGlut2 puncta in the Ctrl, Chronic, 2d WD and 10d WD experimental groups (mean and SEM). **(G)** Graph depicting the number of PSD95 puncta in the Ctrl, Chronic, 2d WD and 10d WD experimental groups (mean and SEM).**(H)** Graph depicting the number of VGlut2-positive synapses in the Ctrl, Chronic, 2d WD and 10d WD experimental groups. n=2-3 animals/group.

Regulation of CD47 by IFN-γ after chronic Meth administration

We next sought to deep our understanding of the regulatory mechanisms of CD47 expression during chronic Meth exposure. The fact that in cancer cells, IFN-γ is strongly correlated with the expression of CD47 [35, 36] made us question whether, in the case of chronic Meth administration, IFN-γ could also be regulating CD47. In line with the existing evidence in cancer cells, we hypothesized that the decrease of CD47 after chronic Meth administration was correlated with IFN-γ. This cytokine is predominantly secreted by lymphoid cells such as $CD4^+$ T cells, $CD8^+$ T cells, γδ T cells and group 1 innate lymphoid cells, including natural killer (NK) cells [53-56]. Moreover, it has been demonstrated that T cells are scattered across the brain parenchyma under steady-state conditions and that both $CD4^+$ T cells and $CD8^+$ T cells are major IFN-γ producers in the CNS [57, 58]. Thus, we asked whether these cells were altered after chronic Meth exposure, and if Meth was affecting their production of IFN-γ. The analysis of total $CD45^+$ infiltrating cells in the hippocampus revealed no significant differences in the percentage and numbers of these cells in any of the comparisons performed between experimental groups, indicating that chronic Meth exposure does not lead to leukocyte infiltration in this brain region (**Sup. Fig. 4A**). Regarding T cells, no significant differences were found in their frequency or absolute numbers (**Sup. Fig. 4B**). Among T cell subsets, also no differences were found neither in CD4+ T cells (**Sup. Fig. 4C**) nor in CD8+ T cells between experimental groups (**Sup. Fig. 4D**).

Although it is not yet well established how cytokines reach the CNS parenchyma, there are a few studies showing that cytokines from the meninges are able to modulate neuronal activity and behavior [59-61]. In particular, it was proposed that IFN-γ produced by meningeal T cells could have a critical role in mediating both neural function and social behavior [59]. Thus, we hypothesized that chronic Meth administration and/or Meth WD could also impact meningeal T cells and the production of IFN-γ. Therefore, we analyzed this population and the phenotype of IFN-γ producing cells in the meninges (**Fig. 5**). We observed a significant decrease in T cell numbers after chronic Meth administration compared with the Ctrl group and these differences remained until 2d WD (**Fig. 5A**)**.** At 10d of WD T cell numbers in the meninges were reestablished to the control levels (**Fig. 5A**). Importantly, this decrease in T cells affected both T cell subsets, $CD4^+$ and $CD8^+$ T cells (**Fig. 5B and 5C**). When analyzing IFN-γ production (**Fig. 5D**), we found a significant decrease in the absolute numbers of IFN-γ^+ cells in animals exposed to chronic Meth and 2d WD, compared with controls, but not in its percentage among CD45+ cells (**Fig. 5D and 5E**). As expected,, both $CD4^+$ and $CD8^+$ T cells contributed to this decrease, as the numbers of IFN-γ-producing $CD4^+$ and $CD8^+$ T cells significantly decreased in the meninges after chronic Meth administration and 2d WD (**Fig. 5G and 5H**). Of note, no differences were observed in IFN-γ-producing $\gamma\delta$ T cells nor $CD3^-$ cells population (**Sup Fig. 5A and 5B**). As such, within the CNS, the decrease in IFN-γ producing T cells after chronic Meth exposure and early WD, seems to be restricted to the meninges. As IFN-γ is normally expressed in draining cervical lymph nodes (cLN) and also in the spleen, we evaluated also IFN-γ production at these peripheral structures (**Sup. Fig. 6**). Our results for the spleen, revealed a significant increase in IFN-γ^+ cells, at 10d of Meth WD, when compared to the control group (**Sup. Fig. 6E**), which was both contributed by $CD4^+$ (**Fig. 6F**) and $CD8^+$ (**Fig. 6G**) T cells.

Together, these findings showed a decrease of meningeal T cells and reduced production of IFN-γ by these cells after chronic Meth exposure, a reduction that remained until 2d WD. Although the decrease of CD47 protein levels in the hippocampus and the decrease of IFN-γ T cells producers after chronic Meth was concomitant, the CD47 levels were recovered after 2d WD, while IFN-γ T cells producers were only reestablished after 10d WD. Further studies will be necessary to understand if there is a correlation between CD47 and IFN-γ under Meth exposure.

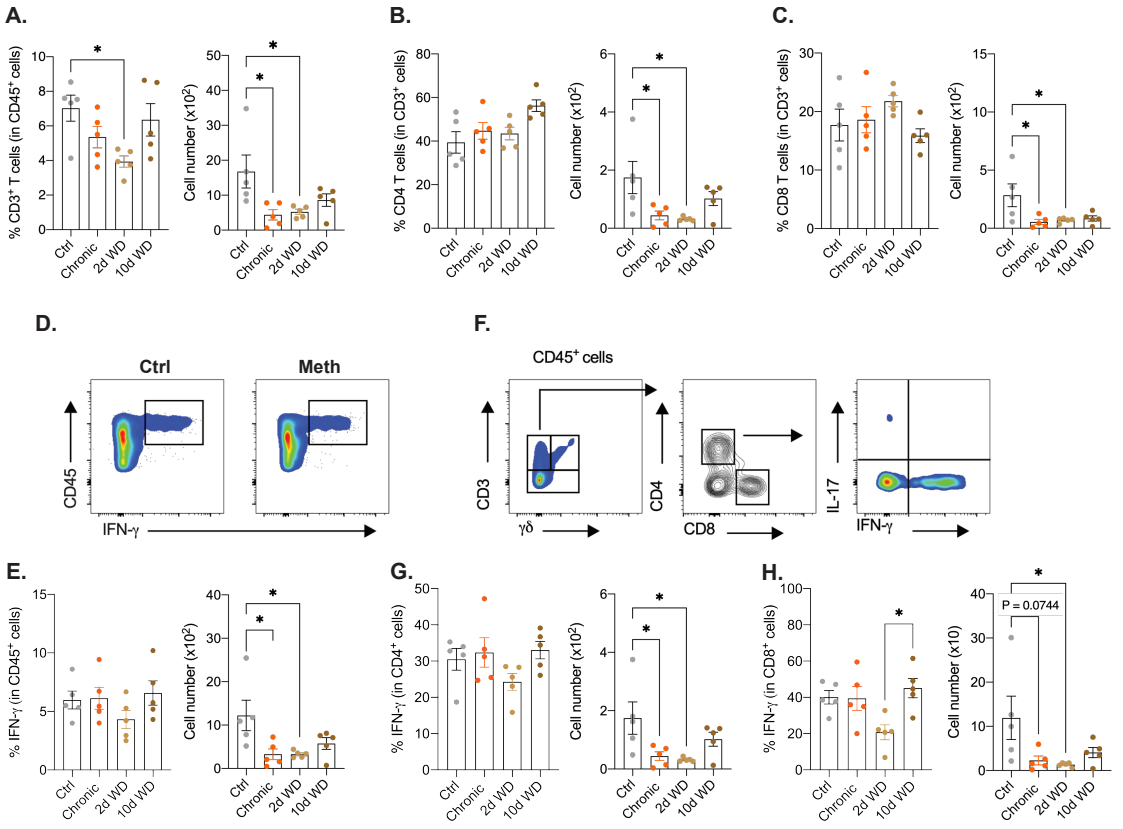

Figure 5: Meningeal T cells and the production of IFN-γ by meningeal T cells is decreased after chronic Meth exposure and short-term withdrawal. Flow cytometry analysis of T cells isolated from the meninges of mice from the Ctrl, Chronic, 2d WD and 10d WD experimental groups (n =5 mice/group). **(A**) The graphs display the percentage of $CD3^+$ T cells among $CD45^+$ cells and the number of $CD3^+$ T (mean and SEM). **(B)** The graphs display the percentage of CD4 T cells among $CD3^+$ cells and the number of CD4 T (mean and SEM). **(C)** The graphs display the percentage of CD8 T cells among $CD3^+$ cells and the number of CD8 T (mean and SEM). **(D)** Representative flow cytometry plot schemes showing gating strategy for IFN-γ^+ cells, from cells isolated from the meninges of Ctrl or Chronic Meth exposure experimental groups. **(E)** The graphs display the percentage of IFN-γ^+ cells among $CD45^+$ cells and the number of IFN-γ^+ producers $CD45^+$ cells (mean and SEM). **(F)** Representative flow cytometry plot scheme showing gating strategy for IFN-γ^+ cells, from cells isolated from the meninges of Ctrl or Chronic Meth exposure experimental groups. **(G and H)** Flow cytometry analysis of IFN-γ^+ producers T cells subsets, CD4 and CD8 T cells: **(G)** The graphs display the percentage of IFN-γ^+ producer cells among $CD4^+$ cells and the absolute number of IFN-γ^+ producers $CD4^+$ T cells (mean and SEM). **(H)** The graphs display the percentage of IFN-γ^+ producer cells among $CD8^+$ cells and the absolute number of IFN-γ^+ producers $CD8^+$ T cells (mean and SEM). Statistical analysis was performed using one-way ANOVA Tukey´s post hoc test. *p<0.05

4. Discussion

Multiple mechanisms mediating Meth-induced neurotoxicity, such as impairment of the dopaminergic system, increased oxidative stress, mitochondrial dysfunction and glutamate excitotoxicity, have been widely described [5, 62, 63]. Growing evidence also shows that glial cells in the CNS, particularly microglia, are highly impacted by Meth exposure [8-10]. Exposure to Meth induces alterations in microglia and results in a more pro-inflammatory profile in several brain regions [11, 12], which together with the interplay between neuronal and glial cells seems to be critical for developing and maintaining addiction [64-66]. However, the dynamics of the inflammatory response and the crosstalk between glia and neurons throughout different stages of the addictive process is yet poorly understood. Herein, we used a chronic model of Meth administration and evaluated its impact at the end of the Meth-exposure period and during a short- and long- withdrawal periods. We found that CD47-SIRPα signaling was disrupted after chronic Meth exposure and during WD. Simultaneously, we also showed that important pathways related with neurotransmission were strongly altered.

While this was an interesting confirmation of the hallmarks of Meth, as powerful disruptor of many neurotransmitter systems [5, 44, 45], as we simultaneously identified a robust decrease in CD47-SIRPα signaling and microglia homeostasis dysregulation, this may indicate that the classical depletion in neurotransmitters may well be related with exacerbated phagocytosis. To our knowledge, this is entirely new, and allows looking into an old problem from completely new perspective. Depletion of the “don´t eat me” signal provided by CD47-SIRPα [24, 29] may facilitate synaptic pruning by Meth-activated microglia. Of note, we have previously reported that in binge Meth administration, microglia are activated by TNF-mediated astrocytic glutamate release [13], which neurons seem to counterbalance through the action of neuroimmune regulatory pairs as CD200 and its receptor (CD200r) [21]. The present results, further confirm the relevance of contact depend communication in the neuron-to-microglia crosstalk under Meth exposure.

Our profiling of the hippocampal proteome after chronic Meth exposure and during Meth withdrawal revealed 124 proteins differentially expressed. The number of proteins differentially expressed was particularly large when comparing chronic Meth exposure with early WD, suggesting that the drug WD had a strong impact in the hippocampus proteome. This highlights the importance of a correct management of the WD to prevent drug relapse, since the disrupted drug intake is accompanied by development of distress feelings and strong physiologic reactions that can result in drug reinstatement [67].

The determination of the most relevant pathways related with the altered proteins revealed several alterations in neurotransmission-related pathways. These results match the long-lasting accumulated evidence that shows drug use a powerful modifier of synaptic transmission in many brain regions [46]. Acute and chronic exposure to psychoactive substances has been repeatedly associated with high levels of synaptic plasticity, contributing to the drug-driven effects in neuronal function [68-70]. While, in most cases, acute exposure is not sufficient to induce disease, repeated drug use of psychostimulants holds a strong addictive potential that is indissociable from synaptic remodelling [71, 72].

Our data also revealed alterations in the WNT signaling. The WNT pathways are important regulators of cell proliferation, migration and differentiation [73]. Recent studies in the CNS demonstrated that WNT signaling also has regulatory effects on microglia [74]. When dysfunctional, this pathway impairs microglia driven synapse modification and promotes microglial inflammation [75-77]. Recent findings pointed out that these pathways might be relevant during the neurodegenerative process involving inflammation, as in Alzheimer disease [74, 78]. Although, we did not further explore the WNT signaling pathway, we cannot exclude that the proteins that belong to this pathway and that are altered in our work, are also involved in the alterations of the microglia profile observed after chronic Meth exposure.

Since our proteomic results showed that several neurotransmission-related pathways were altered by chronic Meth exposure and/or by Meth WD, we next focused on synaptic proteins. One of the synaptic-related proteins that we found altered after chronic Meth exposure was CD47. The protein levels of CD47 were decreased after chronic Meth administration and reestablished to the control levels during the withdrawal period. In chronic multiple sclerosis (MS) lesions, one study found that CD47 was downregulated, suggesting that this may contribute to the activation of microglia and macrophages, resulting in a proinflammatory predisposition in MS lesions [79]. In our study, we observed an alteration in microglia profile after chronic Meth exposure, the same period in which CD47 levels were decreased. Interestingly, Wang and colleagues demonstrated that CD47 signaling may modulate astrocytic activation [23] and previously we have reported that microglia activation after binge Meth administration was mediated by astrocytes [13]. This potential relation requires further investigation and may add complementary data to what we have already described [13].

Although, the CD47 expression was reestablished during the Meth WD period, CD47-SIRPα signaling seems to be also compromised during this period, since we found that SIRPα was decreased in microglia cells. Additionally, during this period microglia cells also recovered a more ramified morphology. Wang and colleagues reported that SIRPα

deficient microglia, upon LPS stimuli, display a stronger inflammatory response then wild-type microglia [23], which suggest that SIRPα deficient microglia acquired a priming profile [80, 81]. In line with this, one can hypothesize that, after drug relapse, an exaggerated or heightened microglial response, stronger than after chronic Meth administration, may also occur. Despite the apparent recovery of the microglia morphologic phenotype at WD, CD11b and CD45 expression were decreased, meaning that microglial homeostasis was not fully rescued during this period. CD11b inhibition by specific antibodies reduced myeloid cells recruitment into irradiated tumors [82] and similar results were observed in CD11b deficient mice [83], meaning that reduced CD11b seems to decreases the severity of inflammatory responses [84, 85]. On the other hand, CD45, is seen as a negative regulator of cytokine receptor signaling [86]. CD45-deficient mice brains were shown to have increased levels of potentially neurotoxic cytokines such as TNF-α [51]. Taken together, these results seem to point to a primed microglia profile at early WD, which we will confirm by evaluation of cytokine production.

The CD47-SIRPα crosstalk is an important “don´t eat me” signal, regulating. phagocytosis [27]. Several studies demonstrated that this neuroimmmune pair regulates synaptic pruning [24, 29, 30]. Lehrman and colleagues showed that CD47-SIRPα signaling prevents excess microglial phagocytosis during developmental synaptic pruning [29]. Similarly, it was also demonstrated that microglial SIRPα regulates synaptic pruning in neurodegeneration [24]. In AD pathology, microglial SIRPα signal is disrupted, resulting in excessive synaptic elimination and cognitive impairment [24]. Still preliminary results, we observed decreased VGlut2-positive synapses after chronic Meth exposure (but not in VGlut1-positive synapses). Corroborating our data, Lehrman and colleagues demonstrated that CD47 KO mice display reduced numbers of VGlut2-positive synapses, but not VGlut1 synapses [29]. Recently, a developmental study has shown that neuronal SIRPα drives microglial phagocytosis by limiting the crosstalk between neurons and microglia through CD47-SIRPα [87]. Herein, neuronal SIRPα was not evaluated, however, after synapses evaluation at all time points, if justified, this will be considered.

Of note, cancer cells use the CD47-SIRPα signaling to escape to the immune system [88]. These cells promote the expression of CD47 and bind to its receptor SIRPα in the immune cells, escaping to phagocytosis [31-34]. Interestingly, in cancer cells, the expression of CD47 can be modulated by IFN-γ [35, 36]. To the best of our knowledge, the modulation of CD47 by IFN-γ was not yet described in the CNS, as such, we decided to investigate the involvement of IFN-γ in the modulation of CD47 after chronic Meth exposure. We observed a decrease in meningeal T cells and in their production of IFN-γ after chronic Meth exposure. Despite, the concomitant decrease of CD47 and IFN-γ-

producing T cells, at this time point, the same was not observed after short-term WD, where the expression of CD47 was reestablished, while the number of meningeal IFN-γ-producing T cells remained decreased. Further studies are already ongoing to clarify the role of IFN-γ in this context.

Of note, the decrease in IFN-γ producing T cells after chronic Meth, that lasts into a short-period of WD, was restricted to the meninges. At peripheral level, we only observed increased IFN-γ producing T cells after a long-period of WD. In Meth users, the plasma levels of IFN-γ were found unaltered both after Meth use and in abstinence [89, 90]. However, a recent study demonstrated that opioids drive the expansion of fragile-like T regulatory cells, favoring peripheral Treg diapedesis across the BBB [91]. Relevantly, these authors describe that IFN-γ mediates synaptic instability and subsequent withdrawal symptoms.

Collectively, our findings provide evidences that CD47-SIRPα signaling is disrupted during different addiction stages. Although further studies will be necessary, this signaling disruption may be related with the inflammatory process under psychostimulant use. Interestingly, further confirmation of the CD47 modulation by IFN-γ will increase the translational significance not only in drug addiction, but also in other CNS pathologies.

References

1. NIDA. *Drug Misuse and Addiction* 2020 [cited 2023 January 17]; Available from: https://nida.nih.gov/publications/drugs-brains-behavior-science-addiction/drug-misuse-addiction.
2. (UNODC), U.N.O.o.D.a.C., *World drug report 2022*. 2022.
3. McLellan, A.T., et al., *Drug dependence, a chronic medical illness: implications for treatment, insurance, and outcomes evaluation.* JAMA, 2000. **284**(13): p. 1689-95.
4. Namba, M.D., et al., *Neuroimmune Mechanisms as Novel Treatment Targets for Substance Use Disorders and Associated Comorbidities.* Front Neurosci, 2021. **15**: p. 650785.
5. Krasnova, I.N. and J.L. Cadet, *Methamphetamine toxicity and messengers of death.* Brain Res Rev, 2009. **60**(2): p. 379-407.
6. Shin, E.-J., et al., *Current understanding of methamphetamine-associated dopaminergic neurodegeneration and psychotoxic behaviors.* Archives of Pharmacal Research, 2017. **40**(4): p. 403-428.
7. Yu, S., et al., *Recent Advances in Methamphetamine Neurotoxicity Mechanisms and Its Molecular Pathophysiology.* Behavioural Neurology, 2015. **2015**: p. 103969.
8. Cui, C., D. Shurtleff, and R.A. Harris, *Neuroimmune mechanisms of alcohol and drug addiction.* Int Rev Neurobiol, 2014. **118**: p. 1-12.
9. Clark, K.H., C.A. Wiley, and C.W. Bradberry, *Psychostimulant abuse and neuroinflammation: emerging evidence of their interconnection.* Neurotox Res, 2013. **23**(2): p. 174-88.
10. Crews, F.T., J. Zou, and L. Qin, *Induction of innate immune genes in brain create the neurobiology of addiction.* Brain Behav Immun, 2011. **25 Suppl 1**: p. S4-S12.
11. Goncalves, J., et al., *Methamphetamine-induced neuroinflammation and neuronal dysfunction in the mice hippocampus: preventive effect of indomethacin.* Eur J Neurosci, 2010. **31**(2): p. 315-26.
12. Frank, M.G., et al., *The danger-associated molecular pattern HMGB1 mediates the neuroinflammatory effects of methamphetamine.* Brain Behav Immun, 2016. **51**: p. 99-108.
13. Canedo, T., et al., *Astrocyte-derived TNF and glutamate critically modulate microglia activation by methamphetamine.* Neuropsychopharmacology, 2021.
14. Sekine, Y., et al., *Brain serotonin transporter density and aggression in abstinent methamphetamine abusers.* Arch Gen Psychiatry, 2006. **63**(1): p. 90-100.

15. Sekine, Y., et al., *Methamphetamine causes microglial activation in the brains of human abusers.* J Neurosci, 2008. **28**(22): p. 5756-61.
16. Kabba, J.A., et al., *Microglia: Housekeeper of the Central Nervous System.* Cell Mol Neurobiol, 2017.
17. Chavarria, A. and G. Cardenas, *Neuronal influence behind the central nervous system regulation of the immune cells.* Front Integr Neurosci, 2013. **7**: p. 64.
18. Tian, L., H. Rauvala, and C.G. Gahmberg, *Neuronal regulation of immune responses in the central nervous system.* Trends Immunol, 2009. **30**(2): p. 91-9.
19. Szepesi, Z., et al., *Bidirectional Microglia-Neuron Communication in Health and Disease.* Front Cell Neurosci, 2018. **12**: p. 323.
20. Posfai, B., et al., *New Insights into Microglia-Neuron Interactions: A Neuron's Perspective.* Neuroscience, 2019. **405**: p. 103-117.
21. Bravo, J., et al., *Neuron-Microglia Contact-Dependent Mechanisms Attenuate Methamphetamine-Induced Microglia Reactivity and Enhance Neuronal Plasticity.* Cells, 2022. **11**(3).
22. Koning, N., et al., *Downregulation of macrophage inhibitory molecules in multiple sclerosis lesions.* Annals of Neurology, 2007. **62**(5): p. 504-514.
23. Wang, J., et al., *SIRPalpha deficiency accelerates the pathologic process in models of Parkinson disease.* Glia, 2019. **67**(12): p. 2343-2359.
24. Ding, X., et al., *Loss of microglial SIRPalpha promotes synaptic pruning in preclinical models of neurodegeneration.* Nat Commun, 2021. **12**(1): p. 2030.
25. Oldenborg, P.A., et al., *Role of CD47 as a marker of self on red blood cells.* Science, 2000. **288**(5473): p. 2051-4.
26. Okazawa, H., et al., *Negative regulation of phagocytosis in macrophages by the CD47-SHPS-1 system.* J Immunol, 2005. **174**(4): p. 2004-11.
27. Bian, Z., et al., *Cd47-Sirpalpha interaction and IL-10 constrain inflammation-induced macrophage phagocytosis of healthy self-cells.* Proc Natl Acad Sci U S A, 2016. **113**(37): p. E5434-43.
28. Ohnishi, H., et al., *Differential localization of Src homology 2 domain-containing protein tyrosine phosphatase substrate-1 and CD47 and its molecular mechanisms in cultured hippocampal neurons.* J Neurosci, 2005. **25**(10): p. 2702-11.
29. Lehrman, E.K., et al., *CD47 Protects Synapses from Excess Microglia-Mediated Pruning during Development.* Neuron, 2018. **100**(1): p. 120-134 e6.
30. Biber, K., et al., *Neuronal 'On' and 'Off' signals control microglia.* Trends in Neurosciences, 2007. **30**(11): p. 596-602.

31. Chao, M.P., R. Majeti, and I.L. Weissman, *Programmed cell removal: a new obstacle in the road to developing cancer.* Nat Rev Cancer, 2011. **12**(1): p. 58-67.
32. Chao, M.P., I.L. Weissman, and R. Majeti, *The CD47-SIRPalpha pathway in cancer immune evasion and potential therapeutic implications.* Curr Opin Immunol, 2012. **24**(2): p. 225-32.
33. Majeti, R., et al., *CD47 is an adverse prognostic factor and therapeutic antibody target on human acute myeloid leukemia stem cells.* Cell, 2009. **138**(2): p. 286-99.
34. Zhao, H., et al., *CD47 Promotes Tumor Invasion and Metastasis in Non-small Cell Lung Cancer.* Sci Rep, 2016. **6**: p. 29719.
35. Sockolosky, J.T., et al., *Durable antitumor responses to CD47 blockade require adaptive immune stimulation.* Proc Natl Acad Sci U S A, 2016. **113**(19): p. E2646-54.
36. Basile, M.S., et al., *Differential modulation and prognostic values of immune-escape genes in uveal melanoma.* PLoS One, 2019. **14**(1): p. e0210276.
37. Alves, R.L., et al., *Early-life stress affects drug abuse susceptibility in adolescent rat model independently of depression vulnerability.* Sci Rep, 2020. **10**(1): p. 13326.
38. Osorio, H., et al., *Proteomics Analysis of Gastric Cancer Patients with Diabetes Mellitus.* J Clin Med, 2021. **10**(3).
39. Saunders, A., et al., *Molecular Diversity and Specializations among the Cells of the Adult Mouse Brain.* Cell, 2018. **174**(4): p. 1015-1030 e16.
40. Jin, S., et al., *Inference and analysis of cell-cell communication using CellChat.* Nat Commun, 2021. **12**(1): p. 1088.
41. Vieira, J.R., et al., *Endothelial PlexinD1 signaling instructs spinal cord vascularization and motor neuron development.* Neuron, 2022. **110**(24): p. 4074-4089 e6.
42. Sorokina, O., et al., *A unified resource and configurable model of the synapse proteome and its role in disease.* Sci Rep, 2021. **11**(1): p. 9967.
43. Schindelin, J., et al., *Fiji: an open-source platform for biological-image analysis.* Nat Methods, 2012. **9**(7): p. 676-82.
44. Mark, K.A., et al., *Dynamic changes in vesicular glutamate transporter 1 function and expression related to methamphetamine-induced glutamate release.* J Neurosci, 2007. **27**(25): p. 6823-31.
45. Mark, K.A., J.J. Soghomonian, and B.K. Yamamoto, *High-dose methamphetamine acutely activates the striatonigral pathway to increase striatal*

glutamate and mediate long-term dopamine toxicity. J Neurosci, 2004. **24**(50): p. 11449-56.

46. Kauer, J.A. and R.C. Malenka, *Synaptic plasticity and addiction.* Nat Rev Neurosci, 2007. **8**(11): p. 844-58.
47. Gaikwad, S., et al., *Signal regulatory protein-beta1: a microglial modulator of phagocytosis in Alzheimer's disease.* Am J Pathol, 2009. **175**(6): p. 2528-39.
48. Hanisch, U.K. and H. Kettenmann, *Microglia: active sensor and versatile effector cells in the normal and pathologic brain.* Nat Neurosci, 2007. **10**(11): p. 1387-94.
49. Li, Q. and B.A. Barres, *Microglia and macrophages in brain homeostasis and disease.* Nat Rev Immunol, 2018. **18**(4): p. 225-242.
50. Hynes, R.O., *Integrins: bidirectional, allosteric signaling machines.* Cell, 2002. **110**(6): p. 673-87.
51. Tan, J., et al., *CD45 opposes beta-amyloid peptide-induced microglial activation via inhibition of p44/42 mitogen-activated protein kinase.* J Neurosci, 2000. **20**(20): p. 7587-94.
52. Yoo, K.S., et al., *Postsynaptic density protein 95 (PSD-95) is transported by KIF5 to dendritic regions.* Mol Brain, 2019. **12**(1): p. 97.
53. Mosmann, T.R. and R.L. Coffman, *TH1 and TH2 cells: different patterns of lymphokine secretion lead to different functional properties.* Annu Rev Immunol, 1989. **7**: p. 145-73.
54. Sad, S., R. Marcotte, and T.R. Mosmann, *Cytokine-induced differentiation of precursor mouse CD8+ T cells into cytotoxic CD8+ T cells secreting Th1 or Th2 cytokines.* Immunity, 1995. **2**(3): p. 271-9.
55. Ribot, J.C., et al., *CD27 is a thymic determinant of the balance between interferon-gamma- and interleukin 17-producing gammadelta T cell subsets.* Nat Immunol, 2009. **10**(4): p. 427-36.
56. Martin-Fontecha, A., et al., *Induced recruitment of NK cells to lymph nodes provides IFN-gamma for T(H)1 priming.* Nat Immunol, 2004. **5**(12): p. 1260-5.
57. Pasciuto, E., et al., *Microglia Require CD4 T Cells to Complete the Fetal-to-Adult Transition.* Cell, 2020. **182**(3): p. 625-640 e24.
58. Ribeiro, M., et al., *Meningeal gammadelta T cell-derived IL-17 controls synaptic plasticity and short-term memory.* Sci Immunol, 2019. **4**(40).
59. Filiano, A.J., et al., *Unexpected role of interferon-gamma in regulating neuronal connectivity and social behaviour.* Nature, 2016. **535**(7612): p. 425-9.
60. Alves de Lima, K., et al., *Meningeal gammadelta T cells regulate anxiety-like behavior via IL-17a signaling in neurons.* Nat Immunol, 2020. **21**(11): p. 1421-1429.

61. Derecki, N.C., et al., *Regulation of learning and memory by meningeal immunity: a key role for IL-4.* J Exp Med, 2010. **207**(5): p. 1067-80.
62. Yu, S., et al., *Recent advances in methamphetamine neurotoxicity mechanisms and its molecular pathophysiology.* Behav Neurol, 2015. **2015**: p. 103969.
63. Shin, E.J., et al., *Current understanding of methamphetamine-associated dopaminergic neurodegeneration and psychotoxic behaviors.* Arch Pharm Res, 2017. **40**(4): p. 403-428.
64. Cadet, J.L. and V. Bisagno, *Glial-neuronal ensembles: partners in drug addiction-associated synaptic plasticity.* Front Pharmacol, 2014. **5**: p. 204.
65. Miguel-Hidalgo, J.J., *The role of glial cells in drug abuse.* Curr Drug Abuse Rev, 2009. **2**(1): p. 72-82.
66. Beardsley, P.M. and K.F. Hauser, *Glial modulators as potential treatments of psychostimulant abuse.* Adv Pharmacol, 2014. **69**: p. 1-69.
67. Kuhar, M., *The Addicted Brain: Why We Abuse Drugs, Alcohol, and Nicotine*. 2012.
68. Dietz, D.M., et al., *Molecular mechanisms of psychostimulant-induced structural plasticity.* Pharmacopsychiatry, 2009. **42 Suppl 1**: p. S69-78.
69. Kutlu, M.G. and T.J. Gould, *Effects of drugs of abuse on hippocampal plasticity and hippocampus-dependent learning and memory: contributions to development and maintenance of addiction.* Learn Mem, 2016. **23**(10): p. 515-33.
70. Liu, Q.S., L. Pu, and M.M. Poo, *Repeated cocaine exposure in vivo facilitates LTP induction in midbrain dopamine neurons.* Nature, 2005. **437**(7061): p. 1027-31.
71. Luscher, C. and R.C. Malenka, *Drug-evoked synaptic plasticity in addiction: from molecular changes to circuit remodeling.* Neuron, 2011. **69**(4): p. 650-63.
72. Nestler, E.J. and C. Luscher, *The Molecular Basis of Drug Addiction: Linking Epigenetic to Synaptic and Circuit Mechanisms.* Neuron, 2019. **102**(1): p. 48-59.
73. Nusse, R. and H. Clevers, *Wnt/beta-Catenin Signaling, Disease, and Emerging Therapeutic Modalities.* Cell, 2017. **169**(6): p. 985-999.
74. Yang, Y. and Z. Zhang, *Microglia and Wnt Pathways: Prospects for Inflammation in Alzheimer's Disease.* Front Aging Neurosci, 2020. **12**: p. 110.
75. Halleskog, C., et al., *WNT signaling in activated microglia is proinflammatory.* Glia, 2011. **59**(1): p. 119-31.
76. Song, D., et al., *Wnt canonical pathway activator TWS119 drives microglial anti-inflammatory activation and facilitates neurological recovery following experimental stroke.* J Neuroinflammation, 2019. **16**(1): p. 256.

77. Van Steenwinckel, J., et al., *Decreased microglial Wnt/beta-catenin signalling drives microglial pro-inflammatory activation in the developing brain.* Brain, 2019. **142**(12): p. 3806-3833.
78. Jia, L., J. Pina-Crespo, and Y. Li, *Restoring Wnt/beta-catenin signaling is a promising therapeutic strategy for Alzheimer's disease.* Mol Brain, 2019. **12**(1): p. 104.
79. Koning, N., et al., *Downregulation of macrophage inhibitory molecules in multiple sclerosis lesions.* Ann Neurol, 2007. **62**(5): p. 504-14.
80. Niraula, A., J.F. Sheridan, and J.P. Godbout, *Microglia Priming with Aging and Stress.* Neuropsychopharmacology, 2017. **42**(1): p. 318-333.
81. Raj, D.D., et al., *Enhanced microglial pro-inflammatory response to lipopolysaccharide correlates with brain infiltration and blood-brain barrier dysregulation in a mouse model of telomere shortening.* Aging Cell, 2015. **14**(6): p. 1003-13.
82. Ahn, G.O., et al., *Inhibition of Mac-1 (CD11b/CD18) enhances tumor response to radiation by reducing myeloid cell recruitment.* Proc Natl Acad Sci U S A, 2010. **107**(18): p. 8363-8.
83. Zhang, Q.Q., et al., *CD11b deficiency suppresses intestinal tumor growth by reducing myeloid cell recruitment.* Sci Rep, 2015. **5**: p. 15948.
84. Coxon, A., et al., *A novel role for the beta 2 integrin CD11b/CD18 in neutrophil apoptosis: a homeostatic mechanism in inflammation.* Immunity, 1996. **5**(6): p. 653-66.
85. Maiguel, D., et al., *Small molecule-mediated activation of the integrin CD11b/CD18 reduces inflammatory disease.* Sci Signal, 2011. **4**(189): p. ra57.
86. Irie-Sasaki, J., et al., *CD45 is a JAK phosphatase and negatively regulates cytokine receptor signalling.* Nature, 2001. **409**(6818): p. 349-54.
87. Jiang, D., et al., *Neuronal signal-regulatory protein alpha drives microglial phagocytosis by limiting microglial interaction with CD47 in the retina.* Immunity, 2022. **55**(12): p. 2318-2335 e7.
88. Willingham, S.B., et al., *The CD47-signal regulatory protein alpha (SIRPa) interaction is a therapeutic target for human solid tumors.* Proc Natl Acad Sci U S A, 2012. **109**(17): p. 6662-7.
89. Kuo, S.C., et al., *Differential effect of the DRD3 genotype on inflammatory cytokine responses during abstinence in amphetamine-dependent women.* Psychoneuroendocrinology, 2018. **97**: p. 37-46.

90. Re, G.F., et al., *Dynamics and correlations in multiplex immune profiling reveal persistent immune inflammation in male drug users after withdrawal.* Int Immunopharmacol, 2022. **107**: p. 108696.
91. Zhu, Y., et al., *Opioid-induced fragile-like regulatory T cells contribute to withdrawal.* Cell, 2023. **186**(3): p. 591-606 e23.

Supplementary Information

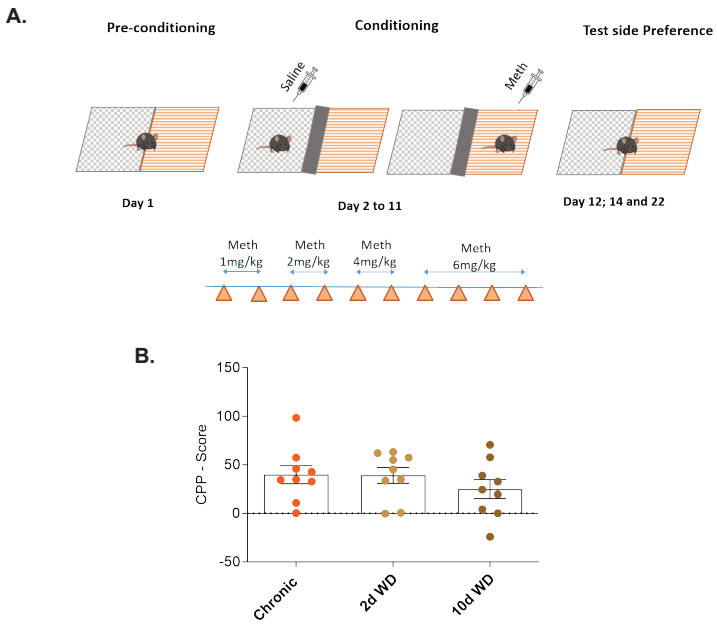

Supplementary figure S1: Chronic exposure to increasing doses of Meth results in prolonged a drug reward effect. (A) Schematic representation of conditioned place preference (CPP) after administration of escalating Meth doses for ten days. After the Meth-conditioning phase, side preference was tested after chronic Meth exposure (Chronic), 2 days of withdrawal (2d WD) and 10 days of withdrawal (10d WD). **(B)** Graph displays the CPP score (mean and SEM) of mice conditioned to chronic Meth exposure, tested at 24h after the last administration, 2 days and 10 days of withdrawal (n=8 animals). Statistical analysis was performed using repeated measure one-way ANOVA Sidak´s post hoc test. CPP-score = [(percentage of time in Meth compartment − percentage of time in saline compartment)$_{\text{post-conditioning}}$ − (percentage of time in Meth compartment − percentage of time in saline compartment)$_{\text{pre-conditioning}}$].

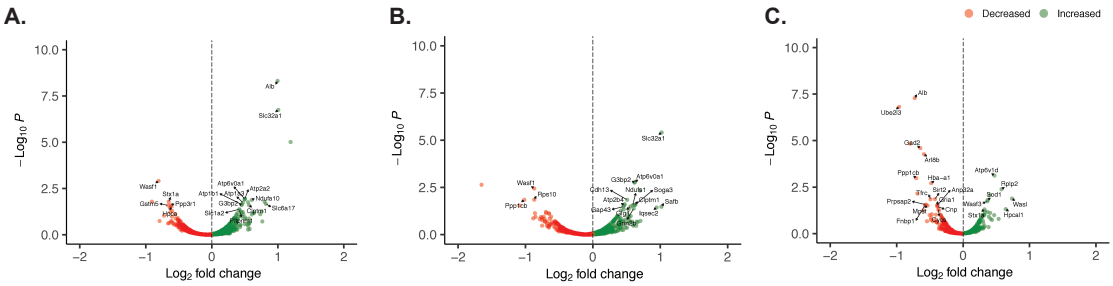

Supplementary figure S2: A) Volcano Plot highlighting the synaptic-related proteins differentially expressed between 2d WD and Ctrl groups. **(B)** Volcano Plot highlighting the synaptic-related proteins differentially expressed between 10d WD and Ctrl groups. **(C)** Volcano Plot highlighting the synaptic-related proteins differentially expressed between 10d WD and 2d WD groups. In the Volcano Plot the upregulated proteins are plotted in green and downregulated proteins in red.

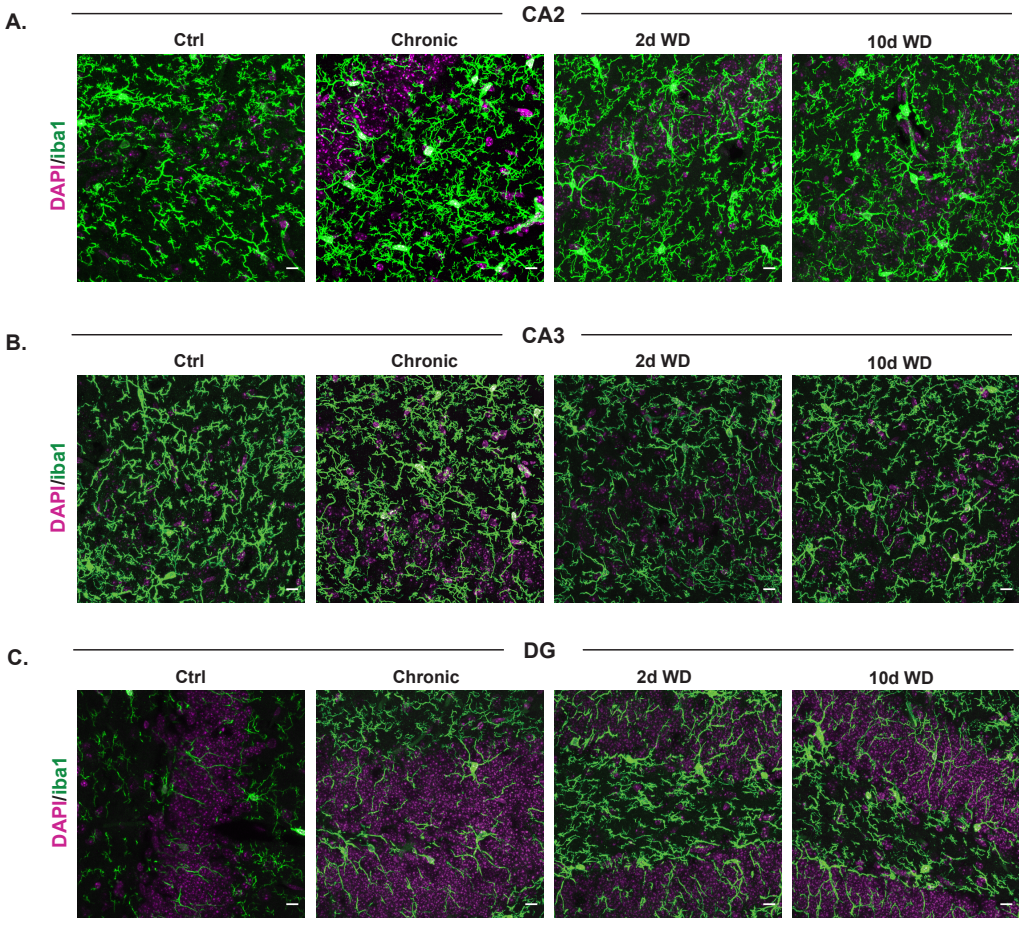

Supplementary figure S3: Representative confocal images of **(A)** CA2, **(B)** CA3 and **(C) DG** hippocampal subregions from mice of the Ctrl, Chronic, 2d WD and 10d WD experimental groups, immunostained for Iba1 (green). Scale bar 10 µm.

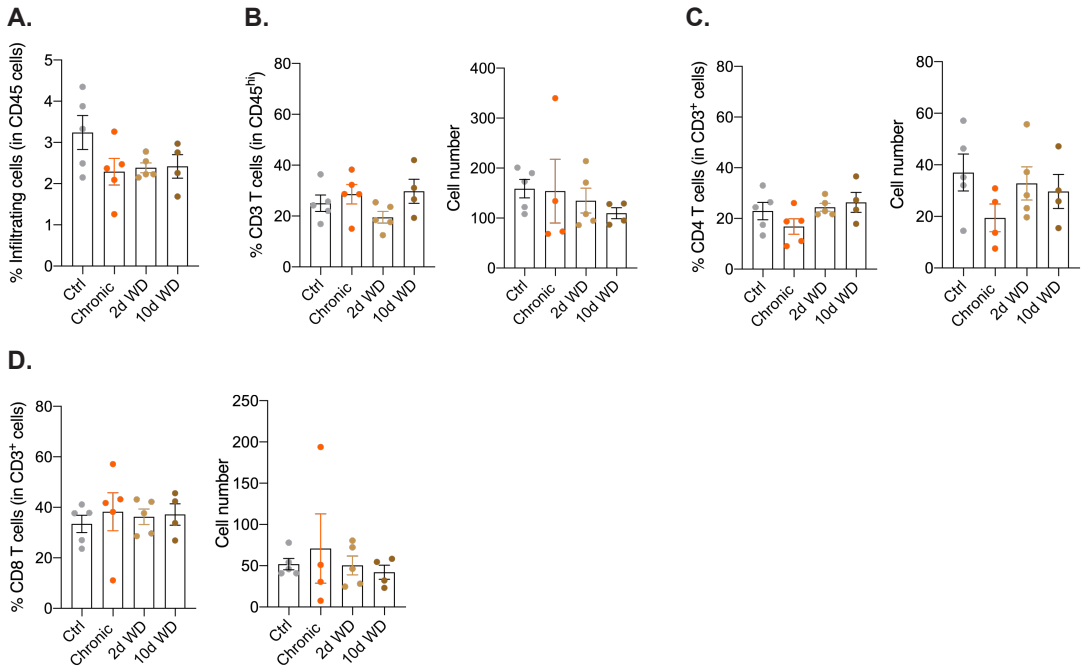

Supplementary figure S4: **Hippocampal T cells are not altered after chronic Meth exposure or withdrawal. (A)** Flow cytometry analysis of infiltrating cells from the hippocampus of mice from the Ctrl, Chronic, 2d WD and 10d WD experimental groups (n =5 mice/group). The graph displays the percentage of infiltrating cells among $CD45^+$ cells T (mean and SEM). Statistical analysis was performed using one-way ANOVA Tukey´s post hoc test. **(B)** Flow cytometry analysis of T cells isolated from the hippocampus of mice from the Ctrl; Chronic; 2d WD and 10d WD experimental groups (n =5 mice/group). The graphs display the percentage of $CD3^+$ T cells among $CD45^{hi}$ cells and the number of $CD3^+$ T (mean and SEM). Statistical analysis was performed using one-way ANOVA Tukey´s post hoc test. **(C and D)** Flow cytometry analysis of T cells subsets, CD4 and CD8 T cells, isolated from the hippocampus of mice from the Ctrl; Chronic; 2d WD and 10d WD experimental groups (n =5 mice/group). **(C)** The graphs display the percentage of CD4 T cells among $CD3^+$ cells and the number of CD4 T (mean and SEM). **(D)** The graphs display the percentage of CD8 T cells among $CD3^+$ cells and the number of CD8 T (mean and SEM). Statistical analysis was performed using one-way ANOVA Tukey´s post hoc test.

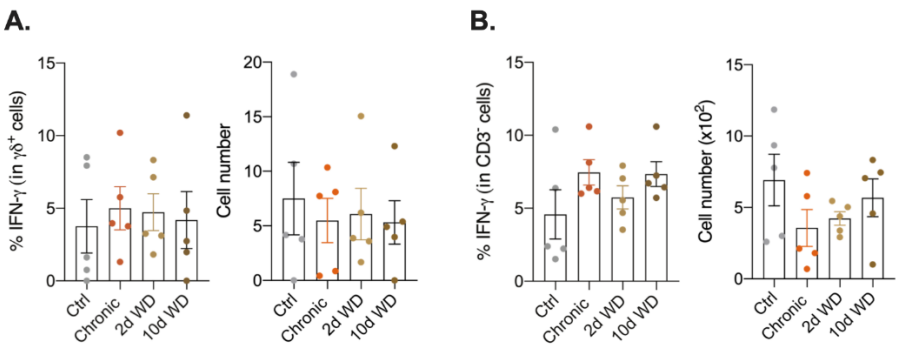

Supplementary figure S5: **(A)** Flow cytometry analysis of IFN-γ$^+$ producers γδ T cells, isolated from the hippocampus of mice from the Ctrl, Chronic, 2d WD and 10d WD experimental groups (n =5 mice/group). The graphs display the percentage of IFN-γ$^+$ producers cells among γδ T cells and the absolute number of IFN-γ$^+$ producers γδ T cells (mean and SEM). Statistical analysis was performed using one-way ANOVA Tukey´s post hoc test. **(B)** Flow cytometry analysis of IFN-γ$^+$ cells isolated from the hippocampus of mice from the Ctrl, Chronic, 2d WD and 10d WD experimental groups (n =5 mice/group). The graphs display the percentage of IFN-γ$^+$ cells among CD3$^-$ cells and the number of CD3$^-$ IFN-γ$^+$ producers cells (mean and SEM). Statistical analysis was performed using one-way ANOVA Tukey´s post hoc test.

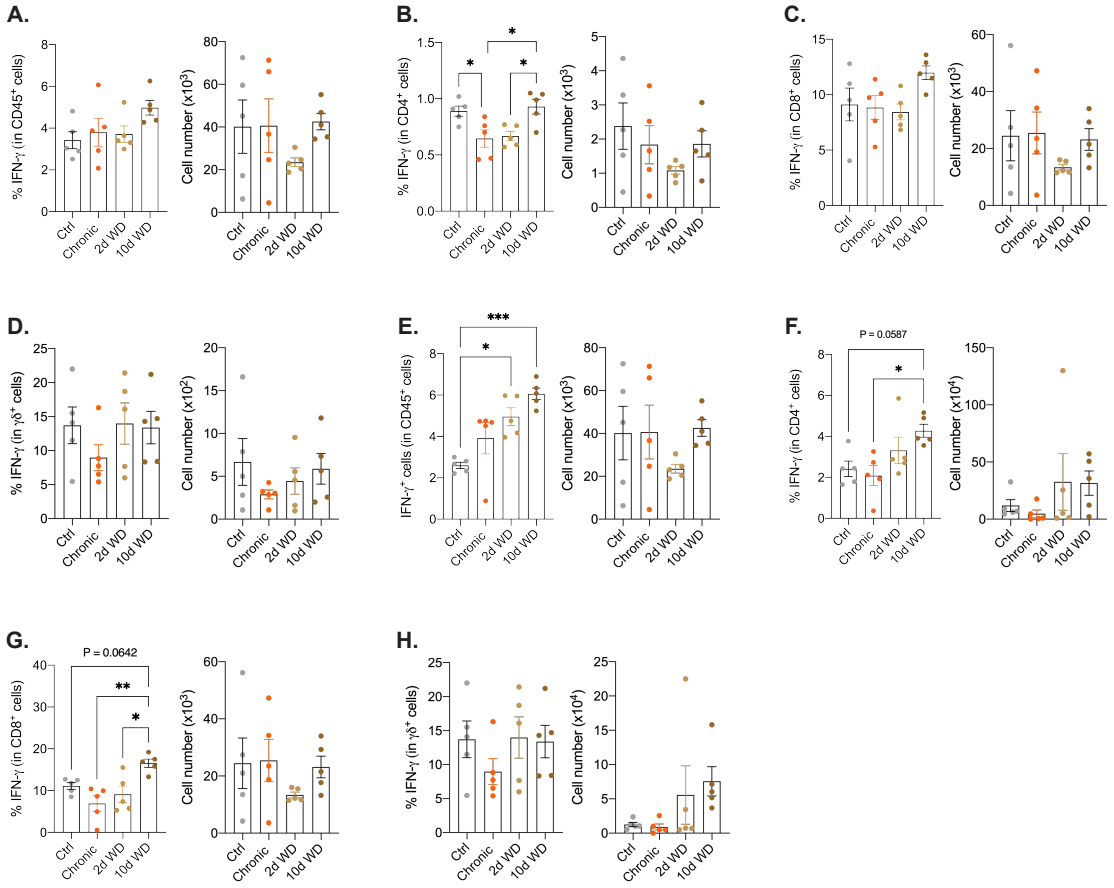

Supplementary figure S6: **(A**)Flow cytometry analysis of IFN-γ$^+$ cells isolated from the draining cervical lymph nodes (cLN) of mice from the Ctrl, Chronic, 2d WD and 10d WD experimental groups (n =5 mice/group). The graphs display the percentage of IFN-γ$^+$ cells among CD45$^+$ cells and the number of IFN-γ producers CD45$^+$ cells (mean and SEM). Statistical analysis was performed using one-way ANOVA Tukey´s post hoc test. **(B, C and D)** Flow cytometry analysis of IFN-γ$^+$ producers T cells subsets, CD4, CD8 and γδ T cells, isolated from cLN of mice from the Ctrl, Chronic, 2d WD and 10d WD experimental groups (n =5 mice/group). Statistical analysis was performed using one-way ANOVA Tukey´s post hoc test. **(B)** The graphs display the percentage of IFN-γ$^+$ producers cells among CD4$^+$ cells and the absolute number of IFN-γ producers CD4$^+$ T cells (mean and SEM). **(C)** The graphs display the percentage of IFN-γ$^+$ producers cells among CD8$^+$ cells and the absolute number of IFN-γ producers CD8$^+$ T cells (mean and SEM). **(D)** The graphs display the percentage of IFN-γ$^+$ producers cells among γδ$^+$ cells and the absolute number of IFN-γ producers γδ$^+$ T cells (mean and SEM). **(E**)Flow cytometry analysis of IFN-γ$^+$ cells isolated from the spleen of mice from the Ctrl; Chronic; 2d WD and 10d WD experimental groups (n =5 mice/group). The graphs display the percentage of IFN-γ$^+$ cells among CD45$^+$ cells and the number of IFN-γ producers CD45$^+$ cells (mean and SEM). **(F, G and H)** Flow cytometry analysis of IFN-γ$^+$ producers T cells subsets, CD4, CD8 and γδ T cells, isolated from the spleen of mice from the Ctrl, Chronic, 2d WD and 10d WD experimental groups (n =5

mice/group). Statistical analysis was performed using one-way ANOVA Tukey´s post hoc test. **(F)** The graphs display the percentage of IFN-γ$^+$ producers cells among CD4$^+$ cells and the absolute number of IFN-γ producers CD4$^+$ T cells (mean and SEM). **(G)** The graphs display the percentage of IFN-γ$^+$ producers cells among CD8$^+$ cells and the absolute number of IFN-γ producers CD8$^+$ T cells (mean and SEM). **(H)** The graphs display the percentage of IFN-γ$^+$ producers cells among γδ$^+$ cells and the absolute number of IFN-γ producers γδ$^+$ T cells (mean and SEM).*p<0.05; **p<0.01; ***p<0.001.

Supplementary table1: Differentially expressed proteins at the different time-points.

Protein acession	Gene symbol	Descripton
A0A087WQG6	Rgs6	Regulator of G-protein-signaling 6
P62141	Ppp1cb	Serine/threonine-protein phosphatase PP1-beta catalytic subunit
Q80UW2	Fbxo2	F-box only protein 2
P57746	Atp6v1d	V-type proton ATPase subunit D
A0A2R8VI94	Cd47	Leukocyte surface antigen CD47
G3UX26	Vdac2	Outer mitochondrial membrane protein porin 2
Q91WD5	Ndufs2	NADH dehydrogenase [ubiquinone] iron-sulfur protein 2, mitochondria
A0A1L1SUX8	Thy1	Thy-1 antigen
P32037	Slc2a3	Solute carrier family 2, facilitated glucose transporter member 3
P62806	H4c1	Histone H4
Q3UHH0	Atp2b2	Calcium-transporting ATPase
Q9CZ13	Uqcrc1	Cytochrome b-c1 complex subunit 1, mitochondrial
A2APX3	Cst3	Cystatin-C (fragment)
Q8BH59	Slc25a12	Calcium-binding mitochondrial carrier protein Aralar1
Q8VDN2	Atp1a1	Sodium/potassium-transporting ATPase subunit alpha-1
Q99JR1	Sfxn1	Sideroflexin-1
Q91WS0	Cisd1	CDGSH iron-sulfur domain-containing protein 1
Q8BG39	Sv2b	Synaptic vesicle glycoprotein 2B
P14094	Atp1b1	Sodium/potassium-transporting ATPase subunit beta-1
Q91ZZ3	Sncb	Beta-synuclein
Q9D164	Fxyd6	FXYD domain-containing ion transport regulator 6
P31648	Slc6a1	Sodium- and chloride-dependent GABA transporter 1
Q91VN4	Chchd6	MICOS complex subunit Mic25
P10852	Slc3a2	4F2 cell-surface antigen heavy chain
Q3U4F0	Sfxn3	Sideroflexin-3
O55143	Atp2a2	Sarcoplasmic/endoplasmic reticulum calcium ATPase 2
A0A1B0GRU0	Slc17a7	Vesicular glutamate transporter 1
P00405	Mtco2	Cytochrome c oxidase subunit
Q9Z1G4	Atp6v0a1	V-type proton ATPase 116 kDa subunit a1
P26231	Ctnna1	Catenin alpha-1
Q8CAQ8	Immt	MICOS complex subunit Mic60
Q7TMF3	Ndufa12	NADH dehydrogenase [ubiquinone] 1 alpha subcomplex subunit 12
G3UVV4	Hk1	Hexokinase
P19783	Cox4i1	Cytochrome c oxidase subunit 4 isoform 1, mitochondrial
A0A0R3P9C8	Ndufa9	NADH dehydrogenase [ubiquinone] 1 alpha subcomplex subunit 9, mitochondrial

Q9DCS9	Ndufb10	NADH dehydrogenase [ubiquinone] 1 beta subcomplex subunit 10
P31650	Slc6a11	Sodium- and chloride-dependent GABA transporter 3
Q9CR61	Ndufb7	NADH dehydrogenase [ubiquinone] 1 beta subcomplex subunit 7
Q9D6J6	Ndufv2	NADH dehydrogenase [ubiquinone] flavoprotein 2, mitochondria
Q91VD9	Ndufs1	NADH-ubiquinone oxidoreductase 75 kDa subunit, mitochondrial
Q99LC3	Ndufa10	NADH dehydrogenase [ubiquinone] 1 alpha subcomplex subunit 10, mitochondrial
D3Z1U9	Ndufv1	NADH dehydrogenase [ubiquinone] flavoprotein 1, mitochondrial
P67778	Phb	Prohibitin
P51863	Atp6v0d1	V-type proton ATPase subunit d 1
Q9DCT2	Ndufs3	NADH dehydrogenase [ubiquinone] iron-sulfur protein 3, mitochondrial
Q8VDQ8	Sirt2	NAD-dependent protein deacetylase sirtuin-2
P16330	Cnp	2',3'-cyclic-nucleotide 3'-phosphodiesterase
D3YYE1	Anp32a	Acidic leucine-rich nuclear phosphoprotein 32 family member A (Fragment)
P23818	Gria1	Glutamate receptor 1
Q91VB8	Hba-a1	Alpha globin 1
A8DUK4	Hbb-bs	Beta-globin
O35874	Slc1a4	Neutral amino acid transporter A
A0A0R4J087	Slc6a17	Transporter
P07724	Alb	Albumin
Q9CQJ8	Ndufb9	NADH dehydrogenase [ubiquinone] 1 beta subcomplex subunit 9
O35633	Slc32a1	Vesicular inhibitory amino acid transporter
P14231	Atp1b2	Sodium/potassium-transporting ATPase subunit beta-2
Q5DTL9	Slc4a10	Sodium-driven chloride bicarbonate exchanger
Q9Z127	Slc7a5	Large neutral amino acids transporter small subunit 1
P43006	Slc1a2	Excitatory amino acid transporter 2
P23819	Gria2	Glutamate receptor 2
A0A0G2JGX4	Atp1a3	Sodium/potassium-transporting ATPase subunit alpha
E9Q8N8	Slc4a4	Anion exchange protei
P99027	Rplp2	60S acidic ribosomal protein P2
P0DP27	Calm2	Calmodulin-2
G3X9V4	Grin2b	Glutamate receptor ionotropic, NMDA 2B
E9Q828	Atp2b4	Calcium-transporting ATPase
D3YXK2	Safb	Scaffold attachment factor B1
Q8VBZ3	Clptm1	Cleft lip and palate transmembrane protein 1
Q9DAK9	Phpt1	14 kDa phosphohistidine phosphatase
Q5DU25	Iqsec2	IQ motif and SEC7 domain-containing protein 2
P63054	Pcp4	Calmodulin regulator protein PCP4
P48320	Gad2	Glutamate decarboxylase 2
Q8C872	Tfrc	Transferrin receptor protein 1

A0A0A6YWC8	Vim	Vimentin
E9PV73	Hpca	Neuron-specific calcium-binding protein hippocalcin (Fragment)
Q80X80	C2cd2l	Phospholipid transfer protein C2CD2L
Q9ERU9	Ranbp2	E3 SUMO-protein ligase RanBP2
P97371	Psme1	Proteasome activator complex subunit 1
Q61699	Hsph1	Heat shock protein 105 kDa
Q8WTY4	Ciapin1	Anamorsin
P14148	Rpl7	60S ribosomal protein L7
A0A140T8T4	Rpl9-ps6	60S ribosomal protein L9
Q8BL66	Eea1	Early endosome antigen 1
Q8VHI6	Wasf3	Wiskott-Aldrich syndrome protein family member 3
A2AVJ7	Rrbp1	Ribosome-binding protein 1
P06837	Gap43	Neuromodulin
Q6P5F7	Ttyh3	Protein tweety homolog 3
Q9WTR5	Cdh13	Cadherin-13
E9Q7G0	Numa1	Nuclear mitotic apparatus protein 1
E9Q0H6	Fabp7	Fatty acid-binding protein, brain
O35954	Pitpnm1	Membrane-associated phosphatidylinositol transfer protein 1
P16054	Prkce	Protein kinase C epsilon type
Q6NZL0	Soga3	Protein SOGA3
P97379	G3bp2	Ras GTPase-activating protein-binding protein 2
Q8BXZ1	Tmx3	Protein disulfide-isomerase TMX3
F8WHM5	Glg1	Golgi apparatus protein 1 (Fragment)
Q91WG5	Prkag2	5'-AMP-activated protein kinase subunit gamma-2
E9PW37	Rasal2	RAS protein activator-like 2
E9PV73	Hpca	Neuron-specific calcium-binding protein hippocalcin (Fragment)
Q61696	Hspa1a	Heat shock 70 kDa protein 1A
P70232	Chl1	Neural cell adhesion molecule L1-like protein
Q9DBS2	Tprg1l	Tumor protein p63-regulated gene 1-like protein
A0A338P786	Ube2l3	Ubiquitin-conjugating enzyme E2 L3 (Fragment)
Q99J99	Mpst	3-mercaptopyruvate sulfurtransferase
P62897	Cycs	Cytochrome c, somatic
P58389	Ptpa	Serine/threonine-protein phosphatase 2A activator
Q9D8E6	Rpl4	60S ribosomal protein L4
A0A1Y7VL34	Dtna	Dystrobrevin
Q8R574	Prpsap2	Phosphoribosyl pyrophosphate synthase-associated protein 2
Q99J85	Nptxr	Neuronal pentraxin receptor
Q9CQW2	Arl8b	ADP-ribosylation factor-like protein 8B
A0A1L1SVK0	Pafah1b2	Platelet-activating factor acetylhydrolase IB subunit beta (Fragment)
D3Z6I8	Tpm3	Tropomyosin alpha-3 chain
O35526	Stx1a	Syntaxin-1A
Q91YD9	Wasl	Neural Wiskott-Aldrich syndrome protein

Q8R5H6	Wasf1	Wiskott-Aldrich syndrome protein family member 1
P48774	Gstm5	Glutathione S-transferase Mu 5
P63325	Rps10	40S ribosomal protein S10
A0A0N4SVB5	Prrt3	Proline-rich transmembrane protein 3
P14131	Rps16	40S ribosomal protein S16
P03930	Mtatp8	ATP synthase protein 8
P08228	Sod1	Superoxide dismutase [Cu-Zn]
Q63810	Ppp3r1	Calcineurin subunit B type 1

CHAPTER VI

General conclusion

Conclusion and future perspectives

In the past, the effects of Meth in the brain have been widely studied and characterized. As such, it is well established that Meth causes dopaminergic impairment, oxidative stress, mitochondrial dysfunction, glutamate excitotoxicity, blood brain barrier dysfunction and neuroinflammation. The existent literature reports microgliosis either in Meth users [1], or in animal models [2-4]. However, the mechanisms that underlie the Meth-related neuroinflammatory process are still poorly understood. An important finding was that glial cell modulators attenuate Meth self-administration, meaning that neuroinflammation could be related with addictive and relapse processes [5, 6]. Therefore, we hypothesized that limiting the neuroinflammatory process could be relevant to control addictive behavior.

Recently, we have reported that Meth cannot stimulate microglia in a cell-autonomous manner [7]. Our results showed that Meth leads to microgliosis and microglia activation in a process mediated by astrocytes *via* glutamate release in a TNF/IP_3R2-Ca^{2+}-dependent manner [7]. Previous observations in other neurological disorders showed that neurons may attenuate microglia reactivity using neuroprotective mechanisms [8]. Indeed, under physiological conditions, the maintenance of microglia in a homeostatic state is highly dependent on the dynamic crosstalk between neurons and microglia [9]. Considering this, the first aim of this project was to dissect the signaling mechanisms involved in the neuron-microglia crosstalk under Meth exposure. As the crosstalk between microglia and neurons can occur by contact-dependent and/or independent mechanisms, we first investigated if contact independent mechanisms were sufficient to mediate microglia homeostasis dysregulation by Meth-exposed neurons. Using an *in vitro* strategy similar the one we have used to explore the contribution of astrocytes in Meth-induced microglia activation [7], we verified that the neuronal conditioned media obtained from neurons exposed to Meth failed to induce an alteration in the microglia profile. Since contact-dependent mechanisms between neurons and microglia under Meth exposure seemed necessary to cause microglia activation, we then devised an *in vitro* strategy, using microfluidic devices, to explore this possibility. We observed that Meth-exposed neurons in direct contact with microglia also did not induce alterations in microglia profile. These results clarified that neither indirect nor direct neuron-microglia contact was sufficient to promote an inflammatory response throughout neuronal cells under Meth exposure. As our previous results indicate that astrocyte mediation was necessary to induce microglia activation under Meth exposure [7], next we evaluate the role of neuronal cells in this process. Our results showed that contact-dependent mechanisms between neurons and microglia counteract microglia activation and

enhance synaptic plasticity by increasing the expression of the neuroimmune regulatory molecule CD200. In this scenario, understanding the inflammatory process and the crosstalk between glial cells and neurons under drug addiction will provide a more comprehensive understanding of the mechanisms involved in modulation of psychostimulant-induced neuroinflammation and hopefully devise new therapeutic strategies.

Therefore, we next moved forward to *in vivo* studies, using a chronic model of Meth administration in which we anticipated that addressing also the withdrawal period would be critical to obtain an integrated perspective of the whole inflammatory process. Our first goal was the determination of the proteome profile of mice after chronic Meth administration and after a short- and long-term Meth withdrawal period. After the identification of proteins that could be promising candidates in the Meth addiction process, our next aim was the validation of its importance in the addictive behavior. Interestingly, we found that CD47 protein levels, also an important neuroimmune regulatory protein, were decreased after chronic Meth administration. Taking into consideration that the interaction between neurons and microglia, through CD47 and its receptor SIRPα regulate microglial phagocytosis and synaptic pruning [10-12], next, we evaluated the microglia profile and synapse numbers, in order to understand if microglial phagocytic activity was increased. Our results showed an alteration in microglia profile after chronic Meth administration, which might reflect a more phagocytic profile.

Regarding the short- and long-term withdrawal period, we found that CD47 protein levels were reestablished to the control levels. However, we observed a significant decrease of microglial SIRPα during Meth withdrawal and the evaluation of microglia showed that these cells were not in a homeostatic state. In fact, our results seem to suggest that microglia could be in a “prime” state. Similarly to CD47, the SIRPα decrease could also result in an increase in microglial phagocytosis [11]. In this scenario, it will be of utmost interest to further evaluate the microglia phagocytic profile after Meth reinstatement.

Next we sought to deeper understand the regulatory mechanisms of CD47 expression during chronic Meth exposure. In the literature, we found that IFN-γ is strongly correlated with the expression of CD47 in cancer cells [13, 14]. Considering this, we evaluated whether IFN-γ could be regulating CD47 after chronic Meth administration. We found a decrease of meningeal T cells and a decrease in the production of IFN-γ by these cells after chronic Meth exposure and this decrease lasts at least until two days of Meth withdrawal. Although, it is not yet well established how cytokines reach the CNS parenchyma, the existent literature shows that cytokines produced in meningeal cells, such as IFN-γ, are important modulators of neuronal activity and behavior [15]. To understand the possible correlation between CD47 and IFN-γ under Meth exposure we

will perform a stereotaxic injection of IFN-γ in the cisterna magma and the CD47 levels, the microglia profile and its phagocytic activity in the hippocampus will be evaluated. Additionally, contrary to what was expected, we found that IFN-γ knockout (KO) mice have higher CD47 levels in comparison with wild-type animals (data not shown). This unexpected upregulation of CD47 in the IFNγ KO mice could be a compensatory mechanism or could suggest that IFN-γ modulates CD47 differently in different models. Curiously, other authors reported that IFN-γ KO mice exhibit social deficits and hyper-connectivity of fronto-cortical brain regions [15] and it was also described that these KO mice present increased dendritic length in the dorsal hippocampus and enhanced performance in learning and memory tasks [16]. These data may suggest that IFN-γ KO mice display increased “don´t eat me” signaling pathways, resulting in an impairment of microglia phagocytosis. Considering this, we will also take advantage of this model to get a better understanding of the relationship between IFN-γ and CD47 in the brain after chronic Meth exposure.

These results are consistent with the notion that cytokines are important players in the communication between the periphery and the CNS. Not only cytokines derived from immune cells residing in the immunological niches in CNS reach the brain parenchyma and influence resident cells and behavior [17-19], but also communication between the periphery and the CNS seems to intensify when the BBB is disrupted [17, 18]. Several studies demonstrated that psychostimulants impact on cytokines production and release both in the CNS and at the peripheral level [20-23] and it is also well established that psychostimulants lead to BBB dysfunction [24]. In this scenario, and taking into consideration our hypothesis that IFN-γ could be an important modulator of CD47 levels under chronic Meth exposure, we aimed also at understanding the cytokine profile and the peripheral-to-central immune crosstalk in different stages of the drug addiction disease. With this in mind, we performed a systematic review of the literature, in which we included studies that evaluated cytokines at both central and peripheral levels, in animal models and in studies in patients suffering from problematic drug use. These studies also covered different stages of the addictive process, extending from acute exposure, to short- or long-term administrations, withdrawal and reinstatement. By doing so, we found that the cytokines most frequently evaluated were TNF-α, IL-6 and IL-1β. Additionally, most of the studies evaluated cytokine profiles only at central level and just very few assessed simultaneously cytokines at central and peripheral level. Regarding IFN-γ, the available data is still very limited, impeding the comprehension of the role of this cytokine in the addictive process. Further studies, using arrays of several cytokines will need to be performed to better determine which cytokines, upon the classical ones, may be involved in the progression from sporadic use to the development of addiction.

In a close future, we are planning to conduct such evaluation both at peripheral and central levels, to identify possible biomarkers and therapeutic targets.

In summary, this work provided evidence that Meth critically impacts on neuroimmune regulation. On the one hand, we showed that increased expression of CD200, one of the neuroimmune regulatory molecules, counteracted Meth-induced microglia activation. On the other hand, we found that CD47-SIRPα signaling, another neuroimmune regulatory ligand-receptor pathway, was disrupted after chronic Meth administration and during Meth withdrawal, impacting on synapse numbers. Collectively, these data showed that neuroimmune regulatory molecules may be important therapeutic targets in drug addiction. However, for therapeutic interventions further studies will be necessary to find modulators of this molecules and the better modulatory strategy needs to be tested in the addictive behavior.

References

1. Sekine, Y., et al., *Methamphetamine causes microglial activation in the brains of human abusers.* J Neurosci, 2008. **28**(22): p. 5756-61.
2. Goncalves, J., et al., *Methamphetamine-induced early increase of IL-6 and TNF-alpha mRNA expression in the mouse brain.* Ann N Y Acad Sci, 2008. **1139**: p. 103-11.
3. McConnell, S.E., et al., *Characterization of binge-dosed methamphetamine-induced neurotoxicity and neuroinflammation.* Neurotoxicology, 2015. **50**: p. 131-41.
4. Thomas, D.M., et al., *Methamphetamine neurotoxicity in dopamine nerve endings of the striatum is associated with microglial activation.* J Pharmacol Exp Ther, 2004. **311**(1): p. 1-7.
5. Snider, S.E., E.S. Hendrick, and P.M. Beardsley, *Glial cell modulators attenuate methamphetamine self-administration in the rat.* Eur J Pharmacol, 2013. **701**(1-3): p. 124-30.
6. Clark, K.H., C.A. Wiley, and C.W. Bradberry, *Psychostimulant abuse and neuroinflammation: emerging evidence of their interconnection.* Neurotox Res, 2013. **23**(2): p. 174-88.
7. Canedo, T., et al., *Astrocyte-derived TNF and glutamate critically modulate microglia activation by methamphetamine.* Neuropsychopharmacology, 2021.
8. Feng, D., et al., *CD200 dysfunction in neuron contributes to synaptic deficits and cognitive impairment.* Biochem Biophys Res Commun, 2019. **516**(4): p. 1053-1059.
9. Kabba, J.A., et al., *Microglia: Housekeeper of the Central Nervous System.* Cell Mol Neurobiol, 2017.
10. Lehrman, E.K., et al., *CD47 Protects Synapses from Excess Microglia-Mediated Pruning during Development.* Neuron, 2018. **100**(1): p. 120-134 e6.
11. Ding, X., et al., *Loss of microglial SIRPalpha promotes synaptic pruning in preclinical models of neurodegeneration.* Nat Commun, 2021. **12**(1): p. 2030.
12. Biber, K., et al., *Neuronal 'On' and 'Off' signals control microglia.* Trends in Neurosciences, 2007. **30**(11): p. 596-602.
13. Sockolosky, J.T., et al., *Durable antitumor responses to CD47 blockade require adaptive immune stimulation.* Proc Natl Acad Sci U S A, 2016. **113**(19): p. E2646-54.

14. Basile, M.S., et al., *Differential modulation and prognostic values of immune-escape genes in uveal melanoma.* PLoS One, 2019. **14**(1): p. e0210276.
15. Filiano, A.J., et al., *Unexpected role of interferon-gamma in regulating neuronal connectivity and social behaviour.* Nature, 2016. **535**(7612): p. 425-9.
16. Monteiro, S., et al., *Absence of IFNgamma promotes hippocampal plasticity and enhances cognitive performance.* Transl Psychiatry, 2016. **6**(1): p. e707.
17. Croese, T., G. Castellani, and M. Schwartz, *Immune cell compartmentalization for brain surveillance and protection.* Nat Immunol, 2021. **22**(9): p. 1083-1092.
18. Salvador, A.F., K.A. de Lima, and J. Kipnis, *Neuromodulation by the immune system: a focus on cytokines.* Nat Rev Immunol, 2021. **21**(8): p. 526-541.
19. Alves de Lima, K., J. Rustenhoven, and J. Kipnis, *Meningeal Immunity and Its Function in Maintenance of the Central Nervous System in Health and Disease.* Annu Rev Immunol, 2020. **38**: p. 597-620.
20. Canedo, T., et al., *Astrocyte-derived TNF and glutamate critically modulate microglia activation by methamphetamine.* Neuropsychopharmacology, 2021. **46**(13): p. 2358-2370.
21. Coelho-Santos, V., et al., *The TNF-alpha/NF-kappaB signaling pathway has a key role in methamphetamine-induced blood-brain barrier dysfunction.* J Cereb Blood Flow Metab, 2015. **35**(8): p. 1260-71.
22. Mata, M.M., et al., *Methamphetamine decreases CD4 T cell frequency and alters pro-inflammatory cytokine production in a model of drug abuse.* Eur J Pharmacol, 2015. **752**: p. 26-33.
23. Pianca, T.G., et al., *Differences in biomarkers of crack-cocaine adolescent users before/after abstinence.* Drug Alcohol Depend, 2017. **177**: p. 207-213.
24. Sajja, R.K., S. Rahman, and L. Cucullo, *Drugs of abuse and blood-brain barrier endothelial dysfunction: A focus on the role of oxidative stress.* J Cereb Blood Flow Metab, 2016. **36**(3): p. 539-54.

APPENDIX

cells

MDPI

Article

Neuron–Microglia Contact-Dependent Mechanisms Attenuate Methamphetamine-Induced Microglia Reactivity and Enhance Neuronal Plasticity

Joana Bravo [1,2,3,4], Inês Ribeiro [5,6], Ana Filipa Terceiro [1,2,3], Elva B. Andrade [2,3,4,7], Camila Cabral Portugal [2,8], Igor M. Lopes [2,9], Maria M. Azevedo [2,10], Mafalda Sousa [2,10], Cátia D. F. Lopes [11], Andrea C. Lobo [1,2], Teresa Canedo [1,2,12], João Bettencourt Relvas [2,8,12] and Teresa Summavielle [1,2,4,*]

1 Addiction Biology, i3S-Instituto de Investigação e Inovação em Saúde, Universidade do Porto (UP), 4200-135 Porto, Portugal; joana.bravo@ibmc.up.pt (J.B.); afterceiro@ibmc.up.pt (A.F.T.); andrea.lobo@ibmc.up.pt (A.C.L.); teresa.canedo@ibmc.up.pt (T.C.)
2 IBMC—Instituto de Biologia Molecular e Celular, Universidade do Porto (UP), 4200-135 Porto, Portugal; elva.andrade@ibmc.up.pt (E.B.A.); camila.portugal@ibmc.up.pt (C.C.P.); igor.lopes@ibmc.up.pt (I.M.L.); maria.azevedo@ibmc.up.pt (M.M.A.); mafsousa@ibmc.up.pt (M.S.); jrelvas@ibmc.up.pt (J.B.R.)
3 ICBAS—Instituto de Ciências Biomédicas de Abel Salazar, Universidade do Porto (UP), 4050-313 Porto, Portugal
4 Escola Superior de Saúde, Politécnico do Porto, 4200-072 Porto, Portugal
5 Life and Health Sciences Research Institute (ICVS), School of Medicine, University of Minho, 4710-057 Braga, Portugal; id9531@alunos.uminho.pt
6 ICVS/3B's—PT Government Associate Laboratory, 4806-909 Braga/Guimarães, Portugal
7 Immunobiology, i3S-Instituto de Investigação e Inovação em Saúde, Universidade do Porto (UP), 4200-135 Porto, Portugal
8 Glial Cell Biology, i3S-Instituto de Investigação e Inovação em Saúde, Universidade do Porto (UP), 4200-135 Porto, Portugal
9 Laboratory Animal Science, i3S-Instituto de Investigação e Inovação em Saúde, Universidade do Porto (UP), 4200-135 Porto, Portugal
10 Advanced Light Microscopy Scientific Platform, i3S-Instituto de Investigação e Inovação em Saúde, Universidade do Porto (UP), 4200-135 Porto, Portugal
11 Molecular Bionics Group—Institute for Bioengineering of Catalonia (IBEC), 08028 Barcelona, Spain; clopes@ibecbarcelona.eu
12 FMUP—Faculdade de Medicina da Universidade do Porto, 4200-319 Porto, Portugal
* Correspondence: tsummavi@ibmc.up.pt

check for updates

Citation: Bravo, J.; Ribeiro, I.; Terceiro, A.F.; Andrade, E.B.; Portugal, C.C.; Lopes, I.M.; Azevedo, M.M.; Sousa, M.; Lopes, C.D.F.; Lobo, A.C.; et al. Neuron–Microglia Contact-Dependent Mechanisms Attenuate Methamphetamine-Induced Microglia Reactivity and Enhance Neuronal Plasticity. *Cells* **2022**, *11*, 355. https://doi.org/10.3390/cells11030355

Academic Editor: Lars Tönges

Received: 13 December 2021
Accepted: 17 January 2022
Published: 21 January 2022

Publisher's Note: MDPI stays neutral with regard to jurisdictional claims in published maps and institutional affiliations.

Copyright: © 2022 by the authors. Licensee MDPI, Basel, Switzerland. This article is an open access article distributed under the terms and conditions of the Creative Commons Attribution (CC BY) license (https://creativecommons.org/licenses/by/4.0/).

Abstract: Exposure to methamphetamine (Meth) has been classically associated with damage to neuronal terminals. However, it is now becoming clear that addiction may also result from the interplay between glial cells and neurons. Recently, we demonstrated that binge Meth administration promotes microgliosis and microglia pro-inflammation via astrocytic glutamate release in a TNF/IP_3R2-Ca^{2+}-dependent manner. Here, we investigated the contribution of neuronal cells to this process. As the crosstalk between microglia and neurons may occur by contact-dependent and/or contact-independent mechanisms, we developed co-cultures of primary neurons and microglia in microfluidic devices to investigate how their interaction affects Meth-induced microglia activation. Our results show that neurons exposed to Meth do not activate microglia in a cell-autonomous way but require astrocyte mediation. Importantly, we found that neurons can partially prevent Meth-induced microglia activation via astrocytes, which seems to be achieved by increasing arginase 1 expression and strengthening the CD200/CD200r pathway. We also observed an increase in synaptic individual area, as determined by co-localization of pre- and post-synaptic markers. The present study provides evidence that contact-dependent mechanisms between neurons and microglia can attenuate pro-inflammatory events such as Meth-induced microglia activation.

Keywords: methamphetamine; neuron-to-microglia; neuroprotection; contact-dependent; CD200; PSD95

1. Introduction

Methamphetamine (Meth) is a potent and widely abused synthetic stimulant, classically recognized by its addictive potential [1]. Clinically, Meth use is associated with important neurological changes that result in impaired judgment, psychomotor agitation, aggression, psychosis, altered cognitive function, anxiety, and depression as well as other negative outcomes, such as cardiac dysfunction, dysregulation of body temperature, renal and liver failure, and higher risk of stroke (reviewed in [2]). At the cellular and molecular level, numerous publications have reported that Meth exposure targets the dopaminergic system, binding to the dopamine transporter (DAT) and leading to marked depletion of dopamine (DA), mainly in the striatum, but also in other regions that receive dopaminergic innervation, such as the hippocampus, amygdala, and frontal cortex [2,3]. Through its interaction with the vesicular monoamine transporter 2 (VMAT-2), Meth is also recognized to cause high oxidative stress and mitochondrial dysfunction [3]. In addition, Meth administration increases extracellular glutamate levels in the striatum and hippocampus, which seems to synergize with DA to cause methamphetamine-induced neurotoxicity [4]. The hippocampus is particularly affected by high glutamate release and by Meth administration, which results in impaired memory function [5,6]. Of note, antagonists of glutamate receptors were shown to block Meth-associated toxicity and limit its negative behavioral impact [7].

Importantly, it has become increasingly accepted that the interplay between neuronal and glial cells is also a relevant mechanism for Meth action [8,9]. Using human cerebral organoids, it was recently demonstrated at single-cell resolution that, upon exposure to Meth, most upregulated pathways were associated with immune response and oxidative stress [10]. In accordance, a single dose of Meth given to rats was sufficient to increase the levels of pro-inflammatory cytokines in several brain regions [11].

Recently, we have shown that a binge administration of Meth leads to microgliosis and microglia activation in a process mediated by astrocytes via glutamate release in a TNF/IP_3R2-Ca^{2+}-dependent manner [12]. In addition, we have also shown increased levels of pro-inflammatory cytokines IL-1ß and TNF in the striatum and hippocampus [12]. However, how Meth-induced glial reactivity may affect neurons is yet unknown.

The neuronal ability to sense the surrounding environment is crucial for maintaining homeostasis in the brain parenchyma [13]. There is now considerable evidence showing that immune and neuronal systems communicate through contact-dependent regulatory molecules or other soluble factors, such as neurotransmitters, neuromodulators, cytokines, neuropeptides, and miRNAs [13–15]. In this context, the communication between neurons and microglia seems to critically regulate neuroinflammatory responses [14,16,17]. In fact, it has been previously shown, in different neurological disorders, that neurons might attenuate microglia reactivity resorting to various neuroprotective mechanisms [17,18].

Several neuroimmune regulatory proteins, highly expressed in neurons, were already shown to modulate microglial activation, including CD200, CD22, CX3CL1, and CD95, among others [13]. Notably, receptors to these ligands are mostly restricted to myeloid cells. In particular, the interaction of CD200 and its receptor (CD200r) seems to act as a potent immune suppressor, promoting microglia quiescence [13]. In accordance, CD200-deficient mice display severe progression of neuroinflammation [19]. Opposing this, triggering the CD200/CD200r signaling pathway can limit microglia activation and inflammatory responses by inhibiting NF-κB and mitogen-activated protein kinase (MAPK) pathways, thus limiting the production of the inflammatory cytokines IL-1ß and IL-6 [18]. Also, CD200/CD200r signaling was shown to be involved in the spontaneous recovery of synaptic plasticity after stroke via the inhibition of microglia activation and reduction of inflammatory factors release [18]. Corroborating this, in animal models of Alzheimer's disease, restoration of neuronal CD200 improved cognitive function and prevented further synaptic impairment [20].

In this scenario, understanding how glial activation by Meth affects the crosstalk between glial cells and neurons will provide a more comprehensive understanding of

the mechanisms involved in modulation of psychostimulant-induced neuroinflammation. Here, we used primary neuronal cultures to investigate how neurons affect microglia activation under Meth exposure. Our results reveal that contact-dependent mechanisms between neurons and microglia, namely through CD200/CD200r signaling, attenuate Meth-induced microglia reactivity and enhance synaptic plasticity.

2. Materials and Methods

2.1. Animals

Timely pregnant Wistar dams were necessary to obtain both 18-day embryos (E18) and postnatal day-one or -two pups (P1–P2). All procedures were conducted following the Directive 2010/63/EU and approved by the competent authorities, Direcção Geral de Alimentação e Veterinária (DGAV) and i3S Animal Ethical Committee (ref.2018-13-TS and DGAV 003891/2019-02-15). Researchers involved in animal experimentation were FELASA certified. All efforts were made to minimize animal suffering and the number of dams/pups used. Dams were housed under specific pathogen-free conditions and controlled environment (20 °C, 45–55% humidity) with free access to food and water.

2.2. Neuronal Cell Culture

Hippocampal, striatal, and mesencephalic neurons were obtained from Wistar rat embryos (E18) as described before [21]. Briefly, rat embryo brains were dissected in Hank's buffer solution (HBSS) (Gibco, ThermoFisher Scientific, Waltham, MA, USA) and enzymatically treated with trypsin (1.5 mg/mL) (Gibco, ThermoFisher Scientific, Waltham, MA, USA) for 15 min [21]. The tissue was dissociated in serum-free Neurobasal medium (Gibco, ThermoFisher Scientific, Waltham, MA, USA) supplemented with B27 (Gibco, ThermoFisher Scientific, Waltham, MA, USA), glutamine (0.5 mM, Sigma-Aldrich, St. Louis, MO, USA), and gentamycin (0.12 mg/mL) (Gibco, ThermoFisher Scientific, Waltham, MA, USA) [21]. The cells were seeded on cell culture plates coated with 0.1 mg/mL of poly-d-lysine (PDL) (Sigma-Aldrich, St. Louis, MO, USA). Hippocampal cell cultures were supplemented with glutamate (25 µM, Sigma-Aldrich, St. Louis, MO, USA). Hippocampal cells were cultured at a density of $0.75 \times 10^5/cm^2$ and co-cultured striatal and mesencephalic neurons were plated at a density of $1.25 \times 10^5/cm^2$ (in a proportion of 2:1 striatal to mesencephalic cells). Cell cultures were kept at 37 °C in a humidified incubator with 5% CO_2/95% air for 12 days in vitro (DIV). At DIV8, the medium was partially replaced.

2.3. Microglia and Astrocyte Purified Cultures Obtained from Mixed Glial Cell Cultures

The mixed glial cell cultures (MGC) were obtained from newborn Wistar pups (P1–P2) [12,22]. The pups' brains were dissected in HBSS with 1% Penicillin-Streptomycin (P/S) (Gibco, ThermoFisher Scientific, Waltham, MA, USA). The meninges were removed, and the cortex and hippocampi were collected. After complete tissue dissociation, DNAse I (0.1 U/mL) (Irvine, CA, USA) and 0.25% trypsin (Gibco, ThermoFisher Scientific, Waltham, MA, USA) were added and incubated for 15 min at 37 °C. The cells were suspended in Dulbecco's Modified Eagle Medium (DMEM) (1x)/Glutamax (Gibco, ThermoFisher Scientific, Waltham, MA, USA) supplemented with 10% of FBS and 1% of P/S. The cell suspension was distributed by T-75 flasks coated with 0.01 mg/mL of PDL at a density of two brains/flask. The cell cultures were maintained for 10 days at 37 °C in a humidified incubator with 5% CO_2/95% air; the medium was partially replaced at DIV4 and then totally replaced every 2 days.

To prepare the purified microglial cultures, MGCs were shaken at 200 rpm for 2 h in an iNFORS HT Minitron incubator with a radius of 2.5 cm at 37 °C. The cell suspension obtained was centrifuged at 1200 rpm for 10 min and suspended in Dulbecco's Modified Eagle Medium: Nutrient Mixture F-12 (DMEM/F-12) (Gibco, ThermoFisher Scientific, Waltham, MA, USA) supplemented with 10% of FBS and 1% of P/S. Purified microglia were plated at a density of $0.5 \times 10^5/cm^2$. Purity of microglia cell cultures was 99% as previously reported [23].

To obtain purified astrocytic cultures, the MGCs were shaken at 220 rpm overnight to remove non-astrocytic cells, and adherent cells were detached with 0.25% trypsin. The cell suspension was centrifuged at 1200 rpm for 10 min and partially split in DMEM/Glutamax supplemented with 10% of FBS and 1% of P/S in a non-coated flask.

Purified astrocytes were obtained after two consecutive splits. Cells were plated for the experiment at a density of $0.5 \times 10^5/cm^2$.

2.4. Microglia Incubation with Neuron-Conditioned Medium

At DIV12, the neuronal cell cultures were treated with Meth 100 µM (Sigma-Aldrich, St. Louis, MO, USA) for 24 h [12,24]. Untreated neuron-conditioned medium (NCM Ctrl) and conditioned medium from Meth-treated neurons (NCM Meth) were then collected, centrifuged (1200 rpm, 1 min), and added to microglial cultures.

2.5. Co-Cultures of Neurons and Microglia in Microfluidic Devices

Co-cultures of neurons and microglia were performed in an Axon Investigation System, adapted from [25] (AXIS150, Merck Millipore, Burlington, MA, USA). The microfluidic devices were placed on the top of a glass coverslip (22 mm × 22 mm) coated with 0.1 mg/mL PDL, channel side down, creating a microfluidic chamber composed of two compartments separated by 150 µm length × 5 µm height × 10 µm width microgrooves. Neuronal cells were plated in one of the compartments at a density of 1×10^5/device. At DIV12 for neurons, microglial cells were plated in the opposite chamber at a density of 1×10^5/device.

2.6. Astrocytic-Conditioned Medium

At DIV2, purified astrocytes were incubated with Meth 100 µM for 24 h. The medium from untreated astrocytes (ACM Ctrl) or from Meth-treated astrocytes (ACM Meth) was collected and centrifuged at 1200 rpm for 1 min.

2.7. Treatment of Neuron–Microglia Co-Cultures

To carry out this study, three different conditions were used: (1) Meth 100 µM was added to the neuronal side in the microfluidic device for 24 h; (2) the conditioned media obtained from astrocytes treated with Meth 100 µM for 24 h (ACM Meth) or from control astrocyte cultures (ACM Ctrl) were added to the microglial/axonal compartment for 24 h; (3) ACM Ctrl or ACM Meth were added to the microglia/axonal compartment, and Meth 100 µM was added to the neuronal compartment for 24 h.

2.8. Immunocytochemistry and Image Acquisition

Cells were fixed with 4% PFA, permeabilized with 0.25% Triton X-100, and blocked with 3% BSA. Next, cells were incubated overnight at 4 °C with the primary antibody, as per the manufacturer's recommendations, washed, and incubated with the secondary antibody for 1 h at RT. Then, cells were incubated with DAPI for 5 min or Hoechst 33,342 (1 µg/mL) for 10 min for the neuronal cell viability assay. Coverslips were mounted with fluorescent mounting media (Dako, Agilent, Santa Clara, CA, USA). Imaging was performed using a Zeiss AxioImager Z1 fluorescence microscope equipped with an Axiocam MR v3.0 camera, an HXP 120 light source, and a 40x/1.30 objective. The following filter sets were used to image DAPI, Alexa 488, Alexa 568, and DyLight 650, respectively: 49—Excitation: G 365 Beam Splitter: FT 395 Emission: BP 445/50; 38HE—Excitation: BP 470/40 (HE) Beam Splitter: FT 495 (HE) Emission: BP 525/50 (HE); 43HE—Excitation: BP 550/25 (HE) Beam Splitter: FT 570 (HE) Emission: BP 605/70 (HE); 50—Excitation: BP 640/30 Beam Splitter: FT 660 Emission: BP 690/50. Antibodies are detailed in Supplementary Table S1.

2.9. Phagocytic Assay

The phagocytic assay was performed as previously described [12,23]. Microglial cultures were incubated with fluorescent latex beads 0.5 µm in diameter (Sigma-Aldrich, St. Louis, MO, USA) for 30 min at 37 °C. Briefly, the beads were diluted in cell culture

medium (1:1000); then, cells were washed then fixed with 4% PFA, and the staining for iba1 (Wako) was performed. The number of beads per cell was counted.

2.10. Fluorescence Intensity Quantification

The fluorescence intensity of microglial cells was quantified using the ImageJ software [26], as previously reported [12]. Fluorescence channels were separated, the image converted to 32-bit, and the background subtracted using 50%-off pixels radius by the rollerball algorithm. Then, cells were segmented using the Triangle algorithm with automatic complementation for both the bottom and upper threshold ramps, with background values set to black and foreground values set to red. Individual segmented cells were transposed to ImageJ's ROI manager using the "analyze particles" tool. A range between 1000 and infinity of non-calibrated pixels defined each segmented cell. Mean gray values for the intensities were returned for each cell individually using the multi-measure function on ImageJ's ROI manager.

2.11. RNA Extraction, cDNA Synthesis, and qRT-PCR

RNA from cell cultures was isolated using the PureLink®RNA Mini-Kit (ThermoFisher Scientific, Waltham, MA, USA) according to the manufacturer's specifications, and its quality was checked by the Experion automated electrophoresis system (Bio-Rad, CA, USA) [12]. Of note, in the microglial and neuronal cell cultures, the microfluidic device was removed, and the RNA was extracted from total cell culture.

The synthesis of cDNA was performed using 500 ng of RNA through SuperScript® III First-Strand Synthesis SuperMix (Invitrogen, Waltham, CA, USA). The qRT-PCR reactions, using equal amounts of total RNA from each sample, were performed on the CFX96 Touch™ Real-Time PCR Detection System (Bio-Rad), using the iTaq™ universal SYBR® Green supermix (Bio-Rad). All primers (Sigma-Aldrich, St. Louis, MO, USA) are described in Supplementary Table S2. Raw data were analyzed using the $2^{-\Delta CT}$ method, with S18 serving as the internal control.

2.12. Flow Cytometry of Microglia

Cells were collected from microfluidic devices using Accutase (Gibco, ThermoFisher Scientific, Waltham, MA, USA) for 5 min, centrifuged at 1200 rpm for 5 min, washed with PBS 1x, and incubated with Zombie Aqua (BioLegend, CA, USA) for dead cell exclusion. After washing, cells were fixed with 2% PFA, resuspended in FACS buffer (2% BSA in PBS), and incubated with the antibodies described in Supplementary Table S3 for 20 min at 4 °C (adapted from [12,27]. Data were acquired in a FACSCanto II flow cytometer (BD Biosciences, Franklin Lakes, NJ, USA). Post-acquisition analysis was performed using FlowJo software v10 (Tree Star, Ashland, OR, USA).

2.13. Quantification of Synaptic Proteins

The acquired images were analyzed using ImageJ, as described elsewhere [28–30]. The puncta were analyzed for number, area, and intensity in the selected region, per dendritic length. Briefly, neurite isolated segments containing both PSD95 and VGlut1 stainings were thresholded using Li and Moments algorithms, respectively. The obtained mask was applied on the original images to determine the fluorescence intensity and area. The background value was then subtracted from the obtained intensity value, and this result was multiplied by the puncta area, obtaining the intensity per area. The thresholded signals were then used to determine the co-localization. For this, VGlut1 channel was set as binary, and PSD95 channel was used to define the total puncta. The puncta positive for VGlut1 and PSD95 were defined as co-localized.

2.14. Statistical Analysis

Data presentation is described in figure legends. Identification and removal of outliers were performed with the automatic GraphPad Prism® software (version 9.1.2. for macOS) using the ROUT (robust non-linear regression) method with $Q = 5\%$.

Statistical analyses for qRT-PCR and flow cytometry data were performed in the GraphPad Prism® software using paired Student's *t*-test. For immunocytochemistry data, a linear mixed model analysis was performed using SAS® Visual Statistics with REML function, followed by Tukey–Kramer multiple comparison test, using the culture as a random variable. The data of PSD95 positive for VGlut1 intensity do not follow the normal distribution, so a transformation of the data was carried out using the square root function before the linear mixed model application. Adjusted *p*-value was considered for these data. Differences were considered at the significance level of $p < 0.05$.

3. Results

3.1. Neurons Exposed to Meth Do Not Promote Microglial Activation through Contact-Dependent or -Independent Mechanisms

We have previously shown that the conditioned media of astrocytes (ACM) exposed to Meth can activate microglial cells [12]. Thus, we started by evaluating the role of neurons in the activation of microglia under the same conditions of Meth exposure. To this end, we incubated primary microglia with conditioned media obtained from primary hippocampal cultures treated with Meth (NCM Meth) or with conditioned media obtained from control hippocampal cultures (NCM Ctrl) (Figure 1A) for 24 h. We found that NCM Meth did not promote increased expression of classical microglial activation markers, such as iNOS (Figure 1B) and iba 1 (Figure 1C). The phagocytic capacity of microglia exposed to NCM Meth was found to be decreased (F (1540) = 4.35, $p < 0.05$) (Figure 1D). Furthermore, we observed no differences in the mRNA levels of pro-inflammatory cytokines TNF, IL-1β, and IL-6 (Figure 1E) or in the mRNA levels of anti-inflammatory cytokines IL-10 and TGF-β (Figure 1F). We also verified that the dose of Meth used in the neuronal cultures was not affecting cell viability (Supplementary Figure S1A).

To verify whether these results were specific for hippocampal neurons, which do not express some of the classical targets of Meth, such as the dopamine transporter (DAT) and the vesicular monoamine transporter (VMTA2), we repeated this evaluation using a co-culture of striatal GABAergic neurons and dopaminergic neurons from the mesencephalic region (Supplementary Figure S1B). Remarkably, we observed that NCM Meth from these co-cultures also did not activate microglial cells, as it did not result in increased iNOS expression (Supplementary Figure S1C), iba 1 intensity, or changes in phagocytic activity (Supplementary Figure S1D). These results suggest that, upon Meth exposure, neurons do not induce microglial activation through contact-independent mechanisms.

Since the conditioned media of neurons exposed to Meth did not induce microglia activation, and taking into consideration that microglia and neurons also communicate through cell-to-cell contact via several regulatory molecules [13,14], we tested the hypothesis that the crosstalk between neurons and microglia under Meth exposure could be contact-dependent. We used co-cultures of microglia and hippocampal neurons in microfluidic devices, which allow direct contact between microglia and axons, and exposed neurons to Meth for 24 h (Figure 2A). Of note, hippocampal neurons can extend long axons throughout the grooves that separate the two microfluidic compartments, while striatal neurons cannot. Our findings revealed that neurons exposed to Meth did not significantly increase iNOS expression (Figure 2B) or microglia phagocytic capacity (Figure 2D) and only modestly increased iba1 expression (Figure 2C). Since arginase 1 can outcompete iNOS to downregulate production of nitric oxide and is, therefore, considered a good anti-inflammatory marker for microglia [31], we also evaluated the expression of arginase 1 in these co-cultures. However, we found that in the presence of Meth, arginase 1 was decreased (F (1892) = 24.71, $p < 0.0001$) (Figure 2E). This set of results suggests that exposing neurons to Meth was not sufficient to promote a robust pro-inflammatory state in

microglia. To further confirm this, the mRNA expression levels of the pro-inflammatory cytokines TNF-α, IL-1β, and IL-6 and the anti-inflammatory cytokines Il-10 and TGF-β were evaluated. No differences were found between groups (Figure 2F,G). Together, these data indicate that neurons exposed to Meth do not trigger pro-inflammation in microglia in a cell-autonomous way, either through contact-dependent or -independent mechanisms.

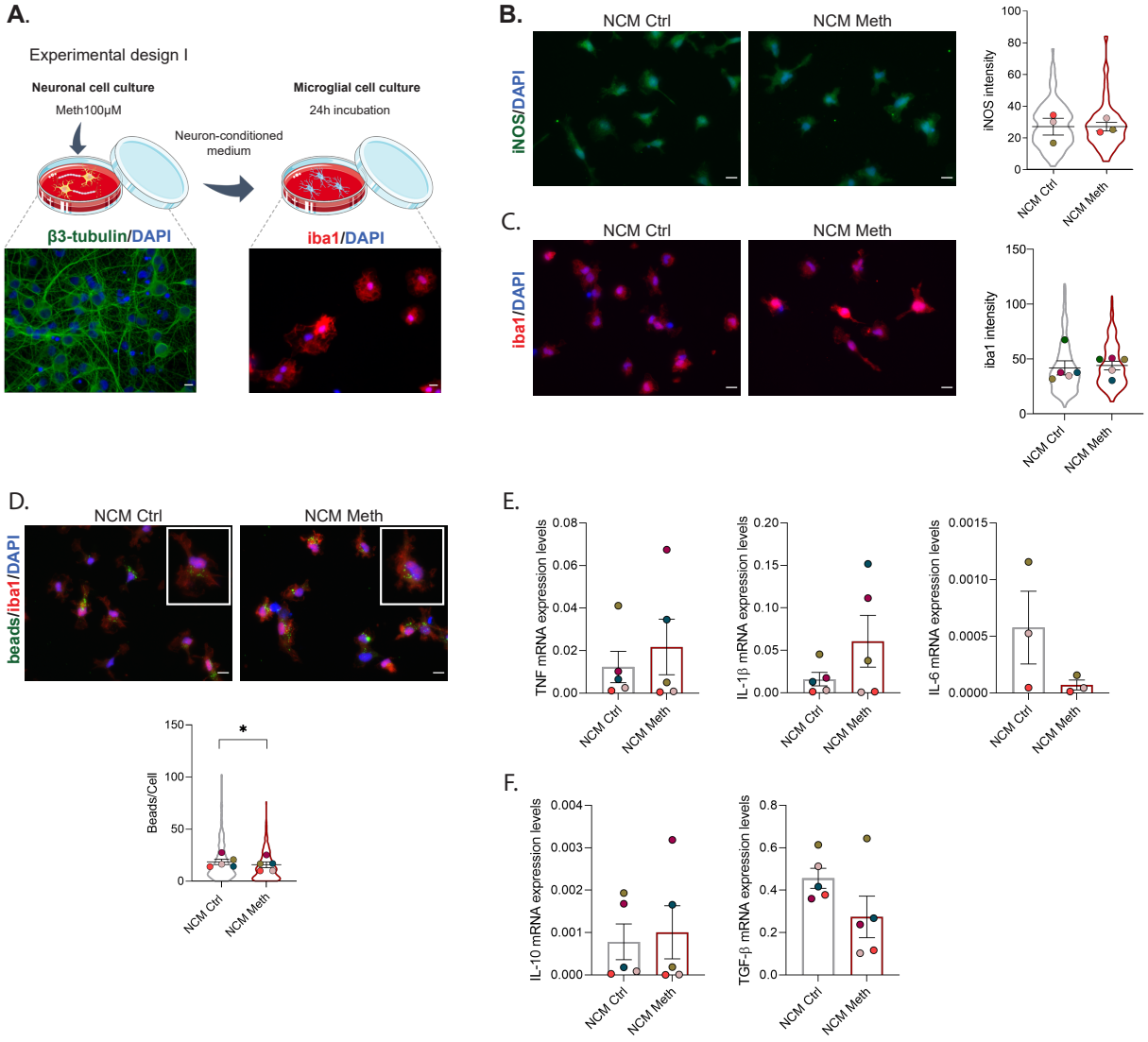

Figure 1. Neurons exposed to Meth do not promote microglial activation through contact-independent mechanisms. (**A**) Experimental design I—Neuronal cell cultures from the hippocampus were incubated with 100 μM Meth for 24 h. Following that, primary microglial cell cultures were incubated for 24 h with the conditioned media obtained from neurons treated with Meth (NCM Meth) or from control neuronal cell cultures (NCM Ctrl). (**B**) Fluorescence imaging of microglial cells immunolabeled for iNOS (green) incubated with NCM Ctrl or NCM Meth for 24 h. Results express the iNOS intensity (mean ± SEM) of three independent cultures (NCM Ctrl—132 cells; NCM Meth—143 cells). (**C**) Fluorescence imaging of microglial cells immunolabeled for iba1 (red) incubated with NCM Ctrl or NCM Meth for 24 h. Results express iba1 intensity (mean ± SEM) of five independent cultures (NCM Ctrl—252 cells; NCM Meth—265 cells). (**D**) Fluorescence imaging of microglial cells immunolabeled for iba1 (red) incubated with microbeads (green) and treated with NCM Ctrl or NCM Meth for 24 h. Results represent the number of beads per cell (mean ± SEM) of five independent cultures (NCM Ctrl—267 cells; NCM Meth—264 cells). Statistical analysis for (**B**–**D**)

was performed using a linear mixed model followed by Tukey–Kramer comparison test (* $p < 0.05$). Symbol colors represent the mean of each independent cell culture and the violin plots the variability of all cells quantified. Scale bar: 10 µm. (**E**) RT-qPCR for TNF, Il-1β, and Il-6 from microglia exposed to NCM Ctrl and NCM Meth for 24 h. (**F**) RT-qPCR for Il-10 and TGFβ from microglia exposed to NCM Ctrl and NCM Meth for 24 h. In both cases, results were normalized to the S18 gene and are expressed as the mean ± SEM of five independent cultures. Statistical analysis was performed using paired Student's *t*-test.

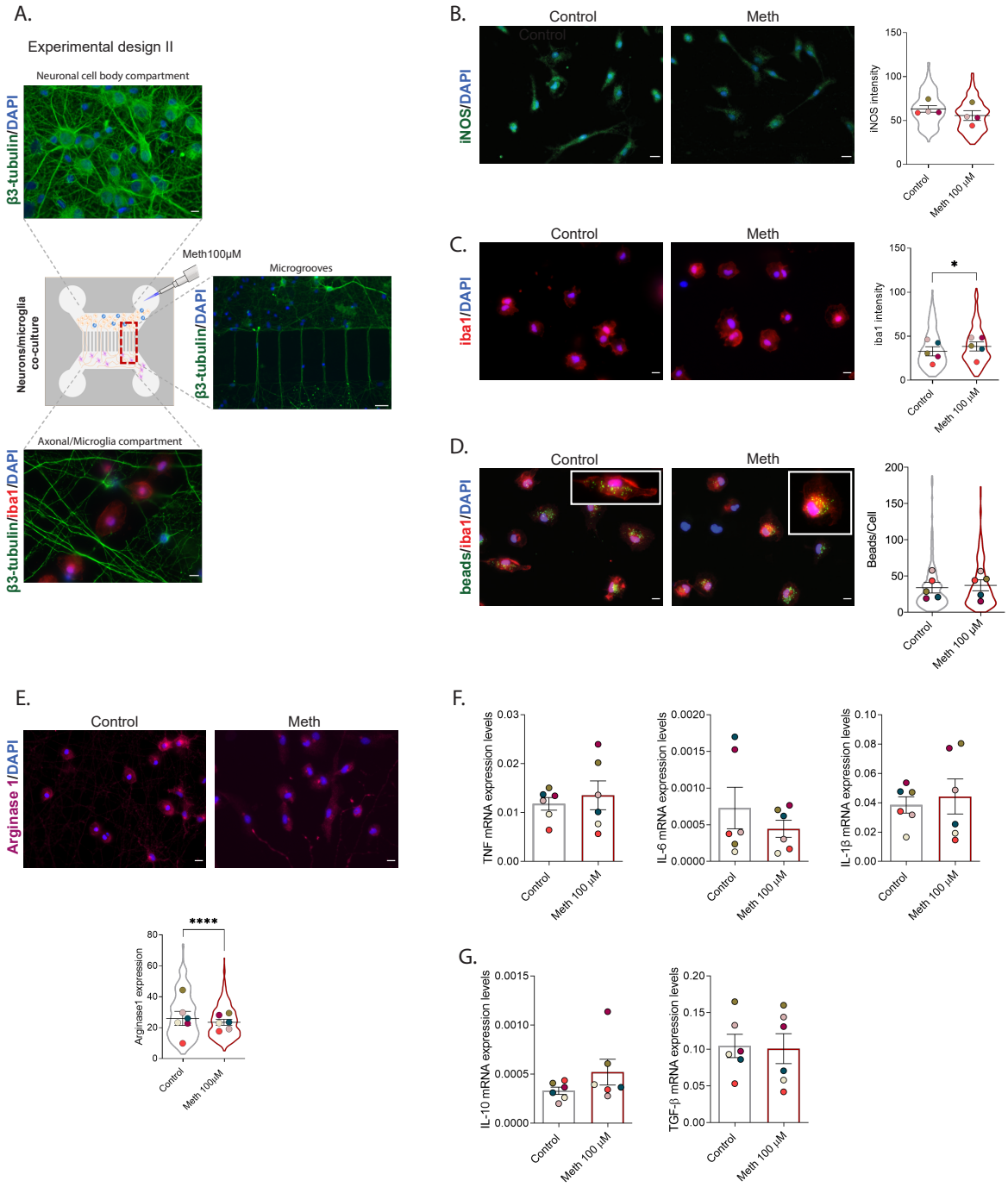

Figure 2. Neurons exposed to Meth and in direct contact with microglia do not promote its activation. (**A**) Experimental design II—neuronal cell culture from the hippocampus was seeded in one side of a microfluidic device, and the axons were allowed to extend to the other compartment for 12 days. On

DIV12, microglial cells were seeded in the axonal compartment. On DIV13, Meth 100 μM was added to the neuronal compartment for 24 h. (**B**) Fluorescence imaging of microglial cells cultured in a microfluidic device with neurons exposed to Meth 100 μM for 24 h. Microglial cells were immunolabeled for iNOS (green), and the results express the iNOS intensity (mean ± SEM) of four independent cultures (Ctrl—297 cells; Meth—325 cells). (**C**) Fluorescence imaging of microglial cells immunolabeled for iba1 (red) incubated with NCM Ctrl or NCM Meth for 24 h. Results express iba1 intensity (average ± SEM) of five independent cultures (Ctrl—199 cells; Meth—206 cells)**.** (**D**) Fluorescence imaging of microglial cells cultured in a microfluidic device with neurons exposed to Meth 100 μM for 24 h. Microglia were incubated with microbeads (green) and immunolabeled for iba1 (red). Results represent the number of beads per cell (mean ± SEM) of five independent cultures (Ctrl—268 cells; Meth—211 cells). (**E**) Fluorescence imaging of microglial cells cultured in a microfluidic device with neurons exposed to Meth 100 μM for 24 h. Microglial cells were immunolabeled for arginase 1 (magenta), and results express the arginase 1 intensity (mean ± SEM) of six independent cultures (Ctrl—489 cells; Meth—410 cells). Statistical analysis for B, C, D, and E was performed using a linear mixed model followed by Tukey–Kramer comparison test (* $p < 0.05$ and **** $p < 0.0001$). Symbol colors represent the mean of each independent cell culture and the violin plots the variability of all cells quantified. Scale bar: 10 μm. (**F**) RT-qPCR for TNF, Il-1β, and Il-6 from microglia and neuron co-culture cells, cultured in a microfluidic device where neurons were exposed to Meth 100 μM for 24 h. (**G**) RT-qPCR for Il-10 and TGFβ from microglia and neuron co-cultured cells, in a microfluidic device where neurons were exposed to Meth 100 μM for 24 h. In both cases, results were normalized to the S18 gene and are expressed as the mean ± SEM of six independent cultures. Statistical analysis was performed using paired Student's *t*-test.

3.2. Microglia Activation Induced by Meth-Exposed Astrocytes Is Partially Prevented by Neurons

Since we have recently shown that Meth-induced microglial reactivity requires both astrocyte-released TNF and glutamate [12], we next sought to verify whether this was also the case in co-cultures of neurons and microglia. To do so, co-cultures of neurons and microglia were performed in microfluidic devices, and conditioned media of primary astrocytes, treated with Meth (ACM Meth) or untreated (ACM Ctrl), were added to the microglial/axonal compartment (Figure 3A). Confirming our previous results [12], ACM Meth increased iNOS levels in microglia (F (1729) = 120.67, $p < 0.0001$), independently of the presence of primary neurons (Figure 3B). However, no significant effects were observed in iba 1 expression (Figure 3C) or microglia phagocytic capacity (Figure 3D). Of note, arginase 1 was concomitantly increased in ACM Meth-treated microglia (F (1591) = 59.30, $p < 0.0001$) (Figure 3E). Because we previously reported that ACM Meth increased the transcript expression of pro-inflammatory cytokines in microglia cultures [12], we also evaluated the mRNA levels of the pro-inflammatory cytokines TNF, IL-1β, and IL-6. Interestingly, no significant changes were observed (Figure 3F). The mRNA expression levels of the anti-inflammatory cytokines IL-10 and TGF-β were also unaltered (Figure 3G). Next, we repeated these experiments, adding Meth to the neuronal compartment while still exposing microglia to ACM Meth (Supplementary Figure S2A). In these conditions, we also observed an increase in both iNOS (F (1942) = 53.45, $p < 0.0001$) and arginase 1 expression (F (1942) = 53.45, $p < 0.0001$) (Supplementary Figure S2B,D), while the phagocytic capacity (Supplementary Figure S2C) and the cytokines' mRNA expression levels were not affected (Supplementary Figure S2E,F). Importantly, if we compare the present results with those that we have previously reported when exposing microglia to ACM [12], we no longer observe increased IL-1β and IL-6, and, although iNOS expression is still augmented, its competitor arginase 1 is also higher. Collectively, these results suggest that Meth-induced microglia activation via astrocytes is attenuated in the presence of neuronal cells.

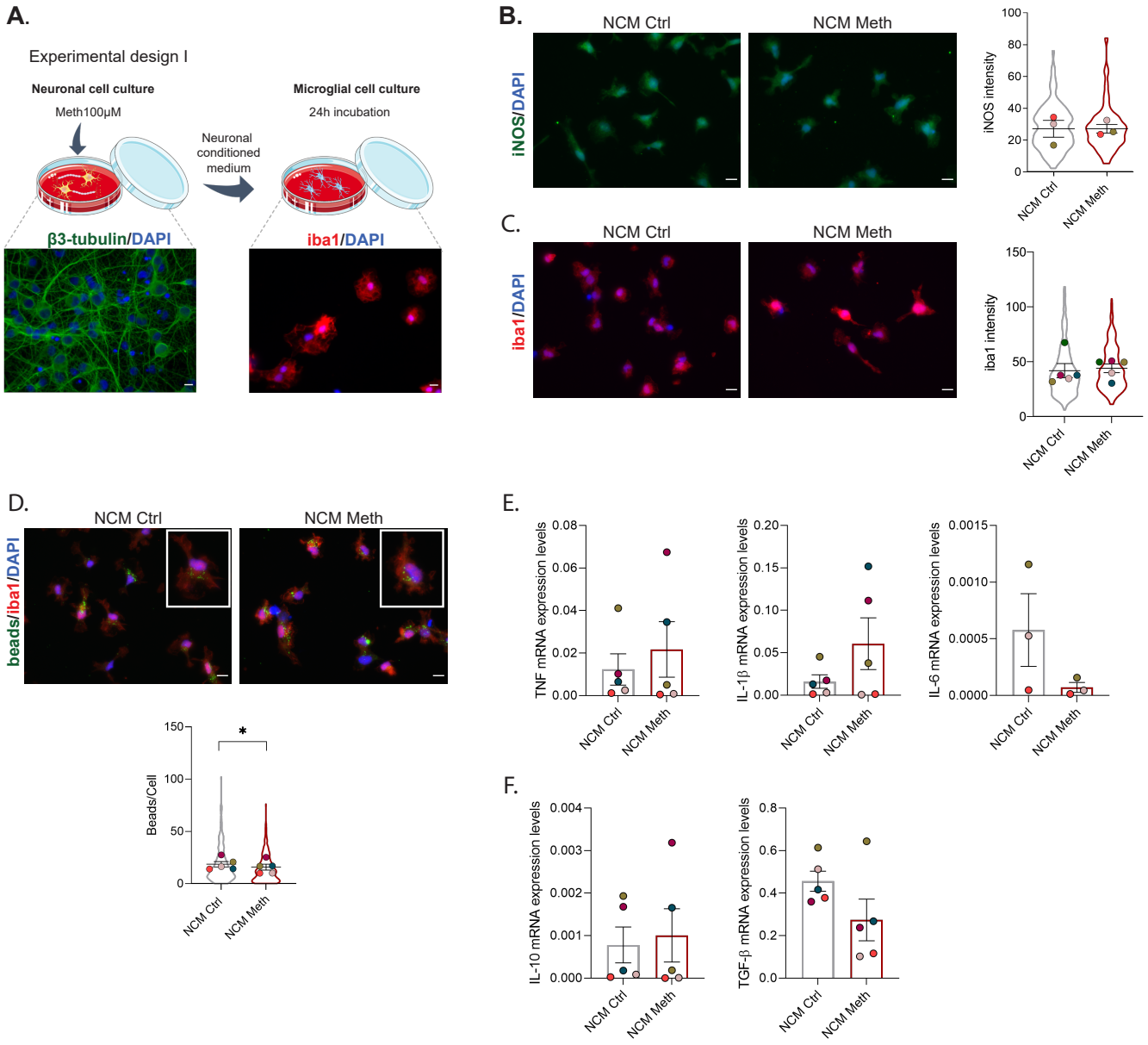

Figure 3. Neurons partially prevented microglia activation via Meth-exposed astrocytes. (**A**) Experimental design III—primary cell cultures of astrocytes were incubated with Meth 100 μM for 24 h. Neuronal cells from the hippocampus were seeded in one side of a microfluidic device, and the axons were allowed to extend to the other compartment for 12 days. On DIV12, microglial cells were seeded in the axonal compartment. The conditioned media obtained from astrocytes treated with Meth (ACM Meth) or from control astrocyte cultures (ACM Ctrl) were added to the microglia/axonal compartment for 24 h. (**B**) Fluorescence imaging of microglial cells co-cultured with neurons and exposed to the ACM Ctrl or ACM Meth for 24 h. Microglial cells were immunolabeled for iNOS (green), and results express the iNOS intensity (mean ± SEM) of five independent cultures (ACM Ctrl—405 cells; ACM Meth—329 cells). (**C**) Fluorescence imaging of microglial cells immunolabeled for iba1 (red) incubated with NCM Ctrl or NCM Meth for 24 h. Results express iba1 intensity (mean ± SEM) of four independent cultures (Ctrl—151 cells; Meth—184 cells). (**D**) Fluorescence imaging of microglial cells co-cultured with neurons and incubated with ACM Ctrl or ACM Meth for 24 h. Microglia were incubated with microbeads (green) and immunolabeled for iba1 (red). The results represent the number of beads per cell (mean ± SEM) of five independent cultures (ACM Ctrl—183 cells; ACM Meth—248 cells). (**E**) Fluorescence imaging of microglial cells co-cultured with neurons and exposed

to ACM Ctrl or ACM Meth for 24 h. Microglial cells were immunolabeled for arginase 1 (magenta), and results express the arginase 1 intensity (mean ± SEM) of six independent cultures quantified (ACM Ctrl—310 cells; ACM Meth—287 cells). Statistical analysis for B, C, D, and E was performed using a linear mixed model followed by Tukey–Kramer comparison test (**** $p < 0.0001$). Symbol colors represent the mean of each independent cell culture and the violin plots the variability of all cells quantified. Scale bar: 10 µm. (**F**) RT-qPCR for TNF, Il-1β, and Il-6 from microglia and neuron co-culture cells, cultured in a microfluidic device where neurons were exposed to Meth 100 µM for 24 h. (**G**) RT-qPCR for Il-10 and TGFβ from microglia and neurons co-culture cells, cultured in a microfluidic device with microglia exposed to ACM Ctrl or ACM Meth for 24 h. In both cases, results were normalized to the S18 gene and are expressed as mean ± SEM of five independent cultures. Statistical analysis was performed using paired Student's *t*-test.

3.3. Neurons Increased Self-Protection from Meth-Induced Activation of Microglia through Contact-Dependent Mechanisms

Because neurons can use several contact-dependent mechanisms to protect themselves from reactive microglia [14,16], we next evaluated the expression of neuroimmune regulatory molecules known to downregulate the microglial pro-inflammatory response. To do so, neurons and microglia were co-cultured in microfluidic devices, and ACM Meth or ACM Ctrl was added to the axonal/microglial side. After 24 h, the mRNA levels of ligand–receptor pairs relevant to the crosstalk between neurons and microglia were determined in the axonal/microglial compartment. We found a significant increase in CD200 mRNA levels ($p < 0.05$) without significant changes in its receptor CD200r (Figure 4A). The expression of CD22 and its receptor CD45 was not altered (Figure 4B). We also observed an increase in the mRNA levels of CX3CL1 that was close to reaching significance ($p = 0.0565$) but no differences for its receptor CX3CR1 (Figure 4C). Concerning the pair CD95–CD95L, the mRNA expression levels of CD95 were not altered (Figure 4D), and CD95L mRNA levels were not detectable. To further confirm these results, we also evaluated the protein expression of CD95 and CD200r specifically in microglia by flow cytometry, and no differences were observed either in CD95 (Figure 4E) or in CD200r levels (Figure 4F). These results indicate that neurons in contact with microglia activated via Meth-exposed astrocytes increased the expression of CD200, which is a well described self-protection mechanism.

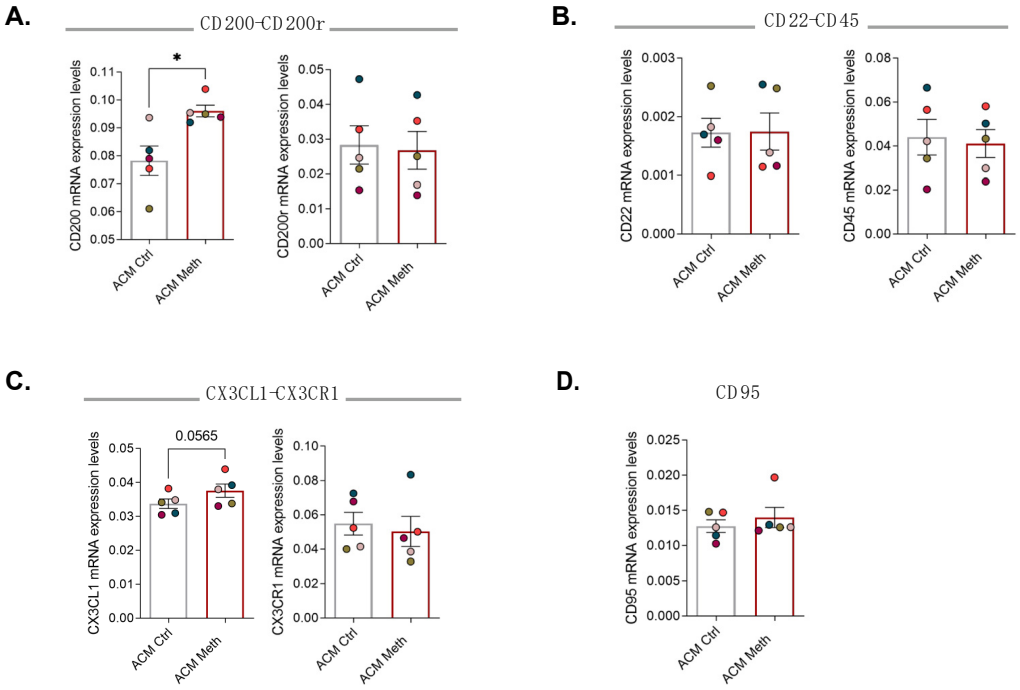

Figure 4. *Cont.*

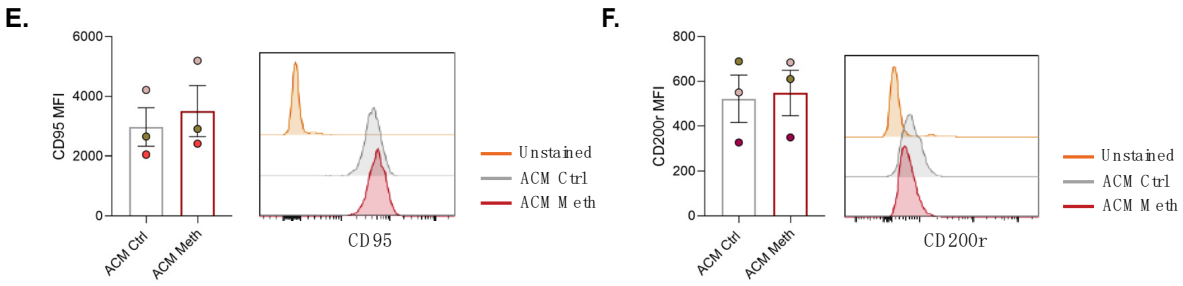

Figure 4. Neurons increased self-protection through contact-dependent mechanisms. RT-qPCR for ligand–receptor immunoregulatory pairs from microglia and neurons co-cultured in microfluidic devices, where microglial cells were exposed to ACM Ctrl or ACM Meth for 24 h. (**A**) Results for CD200 and CD200r, (**B**) CD22 and CD45, (**C**) CX3CL1 and CX3CR1, and (**D**) CD95. The results were normalized to the S18 gene and are expressed as the mean ± SEM of five independent cultures. Symbol colors represent the mean of each independent cell culture. Statistical analysis was performed using paired Student's *t*-test (* $p < 0.05$). Quantification of (**E**) CD95 and (**F**) CD200r on microglia by flow cytometry, presented as median fluorescence intensity (MFI). Results are expressed as mean ± SEM of three independent cultures. Symbol colors represent the mean of each independent cell culture. Statistical analysis was performed using paired Student's t-test. Representative histograms are shown; orange histogram represents unstained cells, gray the ACM Ctrl group, and red the ACM Meth group.

3.4. Synaptic Proteins Expression Increases in Co-Cultures of Neurons and ACM Meth-Microglia

Since we found increased CD200 levels and the signaling of CD200/CD200r has been associated with the modulation of microglia activation and synaptic plasticity in other neurological diseases [18,20], we evaluated how exposure to ACM Meth was affecting synaptic proteins. For that, we used the same co-cultures of neurons and microglia in microfluidic devices with ACM Meth or ACM Ctrl added to the axonal/microglial side and evaluated the expression and co-localization of PSD95 and VGlut1. PSD95 is a post-synaptic marker and the most abundant scaffold protein of excitatory synapses, while VGlut1 is a presynaptic maker, highly expressed in the mouse hippocampus, specifically in excitatory synapses. Both proteins display a punctate distribution, and their co-localization is defined as a synapse [29,30]. Compared with the ACM Ctrl condition, when ACM Meth was added to the axonal/microglial compartment, we observed an increase in PSD95 puncta number (F (1254) = 11.92, $p < 0.001$), area (F (1252) = 29.38, $p < 0.0001$), and intensity (F (1251) = 51.97, $p < 0.0001$) (Figure 5A–D) and a decrease in VGlut1 puncta numbers (F (1258) = 5.71, $p < 0.05$) (Figure 5E,F). However, no significant differences were observed in VGlut1 puncta area or intensity (Figure 5E–H). As the co-localization between both markers is accepted as an indicator of active synapses (since both pre- and postsynaptic terminals are present) [30], we also evaluated their co-localization and found a significant increase in the PSD95/VGlut1-positive puncta area (F (1247) = 17.53, $p < 0.0001$) and intensity (F (1244) = 49, adj $p < 0.0001$) (Figure 5I–L), reflecting an increase in synaptic area in the presence of ACM Meth, but no significant differences in PSD95/VGlut1-positive puncta numbers (Figure 5I,J). Collectively, these data show that neuronal/microglial co-cultures present higher levels of synaptic proteins and that synapses display an increased area of PSD95 when exposed to the ACM of Meth-treated astrocytes.

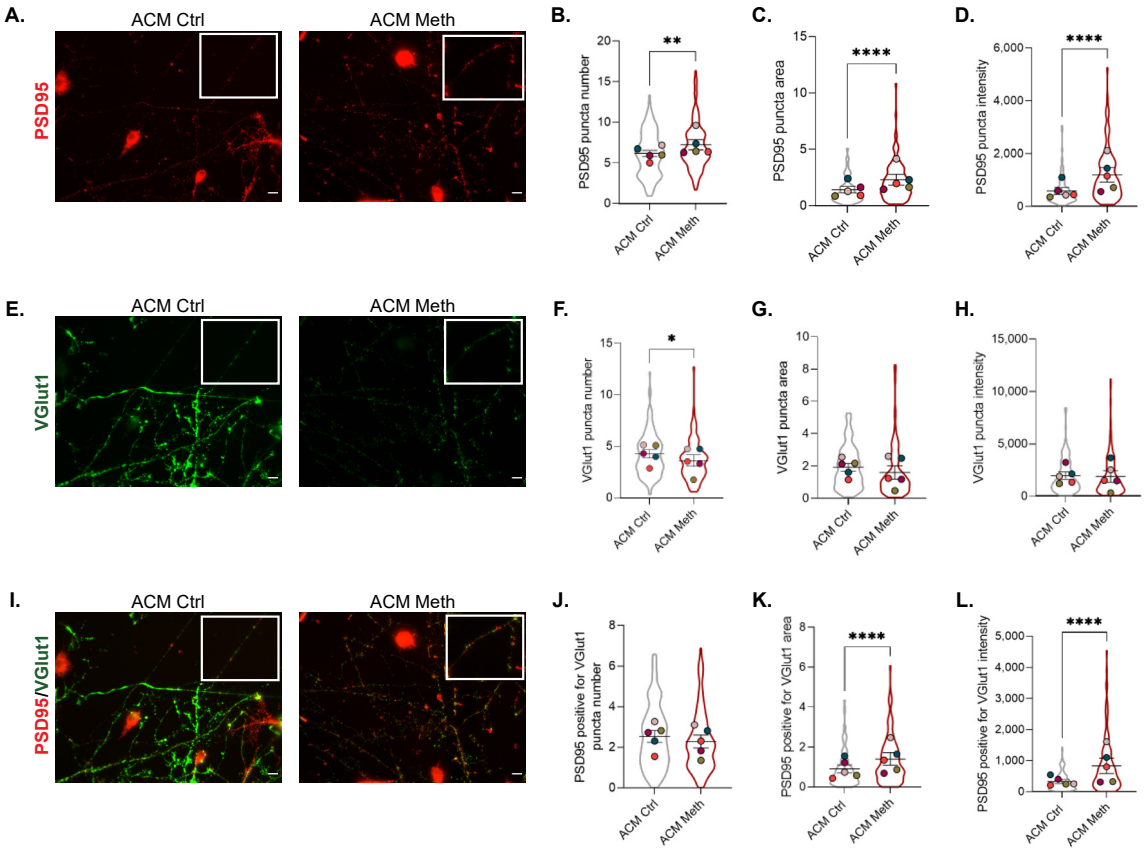

Figure 5. Synaptic plasticity was concomitantly increased. (**A**) Fluorescence imaging of microglial cells co-cultured with neurons and exposed to ACM Ctrl or ACM Meth for 24 h. Cells were immunolabeled for PSD95 (red), and results represent the PSD95 puncta (**B**) number, (**C**) area, and (**D**) intensity. (**E**) Fluorescence imaging of microglial cells co-cultured with neurons and exposed to ACM Ctrl or ACM Meth for 24 h. Microglial cells were immunolabeled for vGlut1 (green), and results represent the Vglut1 puncta (**F**) number, (**G**) area, and (**H**) intensity. (**I**) Fluorescence imaging of microglial cells co-cultured with neurons and exposed to ACM Ctrl or ACM Meth for 24 h. Cells were immunolabeled for PSD95 (red) and VGlut1 (green), and results represent the (**J**) PSD95 plus vGlut1-positive puncta number, (**K**) puncta area, and (**L**) puncta intensity. Symbol colors of each graph represent the mean of each independent cell culture (n = 5) and the violin plots the variability of all neuronal segments quantified (ACM Ctrl—149; ACM Meth—111 segments). Statistical analysis was performed using a linear mixed model followed by Tukey–Kramer comparison test. Scale bar: 10 µm. * $p < 0.05$, ** $p < 0.01$, and **** $p < 0.0001$.

4. Discussion

We have recently demonstrated that an acute binge Meth exposure (4 × 5 mg/kg with 2 h intervals) requires astrocytes to induce microglia activation through glutamate release in a TNF/IP_3R2-Ca^{2+}-dependent manner [12]. Herein, we explored in vitro how neurons may contribute to modulate microglia under Meth, demonstrating that contact-dependent mechanisms between neurons and microglia seem to attenuate Meth-induced microglia activation.

Multiple mechanisms mediating Meth-induced neurotoxicity have been widely described, such as impairment of the dopaminergic system, increase of oxidative stress, mitochondrial dysfunction, and glutamate excitotoxicity [2,32,33]. The primary goal of this study was to further identify other mechanisms involved in Meth-mediated inflammation that could possibly rely on neuron–glia communication. As the crosstalk between microglia and neurons can occur by contact-dependent and/or -independent mechanisms, we first investigated whether contact-independent mechanisms were sufficient to mediate

microglia activation by Meth-exposed neurons. Using a strategy similar to the one we have previously used to explore the contribution of astrocytes in Meth-induced microglia activation [12], we verified that neuron-conditioned media obtained from neurons exposed to Meth failed to induce a pro-inflammatory profile in primary microglia. Since these results could be explained by the fact that hippocampal neurons lack the Meth-binding proteins DAT and VMAT-2, we used co-cultures of striatal and dopaminergic neurons to confirm that this was not the case. A second possibility was that direct contact between neurons and microglia could be necessary to promote microglia activation, which we explored by resorting to neuron–microglia co-cultures in microfluidic chambers. Interestingly, although arginase outcompetes iNOS and limits NO production [34], it did not lead to upregulation of iNOS, and we only found a modest increase in iba 1 and decreased arginase 1 expression in microglial cells. These results clarified that neither direct nor indirect neuron–microglia contact was sufficient to promote a robust inflammatory response under Meth exposure, indicating that astrocyte mediation was, in fact, necessary, as we previously reported [12]. Confirming this, when we added ACM Meth to the axonal/microglial compartment, microglia exhibited increased iNOS expression. Nevertheless, if we compare these results with those obtained in the absence of neurons, we verify that this response is clearly attenuated, indicating that neurons may be promoting this attenuation.

Previous studies demonstrated that neurons may induce an anti-inflammatory profile in microglial cells to protect themselves from excessive microglia activation [14,16]. Several neuronal membrane proteins, including CD200, CD22, CD95, CD47, and other proteins such as NCAM or ICAM-5, were shown to modulate microglial activation through specific counter-receptors [14]. As an example, neurons can contribute to inhibit the lipopolysaccharide (LPS)-induced release of NO and pro-inflammatory cytokines by glial cells [35]. As such, understanding the role of these ligand–receptor pairs has gained increased relevance over the last few years. Among the most explored, CD200 is highly expressed in neurons and other cells, but its receptor, CD200r, is found predominantly in myeloid cells. Interestingly, knocking out CD200 in mice leads to robust activation of microglia [36], while overexpressing it seems to protect from different pro-inflammatory events [14]. Likewise, the interaction of CD22 and its microglial receptor CD45 was shown to prevent LPS-induced neuroinflammation [37]. It was also reported that neurons may induce microglial apoptosis through increased expression of CD95L (or Fas ligand) [38], while CD95L expression in hippocampal neurons protects them against reactive T cells [39]. In the present work, we found increased expression of CD200 when ACM Meth was added to the axonal/microglial compartment, which likely reflects a neuronal defense strategy against astrocyte-driven activation of microglia. Supporting this view, in the presence of neuronal cells, ACM Meth no longer promotes increased levels of IL-1ß and IL-6, which is compatible with the activation of the CD200/CD200r signaling pathway and NF-κB pathway inhibition [18]. Of note, there is still an important gap in the literature concerning which receptors may be mediating Meth action over inflammation-related pathways [40].

Interestingly, the CD200/CD200r signaling pathway was reported to increase dendritic spine density and PSD95 [18], an essential indicator of synaptic plasticity [41,42]. ACM Meth resulted in an increased number of PSD95 puncta, indicating higher density of PSD95 along the neurite [43], and increased area and intensity of PSD95 puncta co-localized with VGLUT1, which is a mechanism that can allow more anchoring of receptors, such as NMDA-R and AMPA-R, thus promoting increased synapse strength [30]. Of note, the dynamics of PSD95 seem to respond also to glutamate variations, which we have reported to be increased in ACM Meth [12]. On the other hand, we found decreased VGlut1 puncta numbers, a major player in vesicular glutamate uptake, in which dysregulation in response to Meth was previously reported [44]. Acute exposure to psychoactive substances, such as Meth, has long been associated with high levels of synaptic plasticity, contributing to the drug-driven effects in neuronal function [45,46]. Although the exact mechanisms regulating Meth-associated changes in synaptic plasticity and their direct link to CD200 require further exploration, there is already enough evidence supporting the involvement

of CD200/CD200r signaling in suppressing inflammatory responses. Interestingly, this seems to be exerted through reduced activation of MAPK [18], which is also involved in the regulation of classic RhoGTPases, such as RhoA, Rac1, and Cdc42, that are well known for their roles in spine formation and maintenance [47,48].

5. Conclusions

In summary, using microfluidic chambers as an effective tool to explore contact-dependent mechanisms between neurons and microglia, we report that hippocampal neurons in direct contact with primary microglia counteract microglia activation by increasing the expression of the neuroimmune regulatory molecule CD200. Furthermore, our data also suggest that the activation of the CD200/CD200r signaling pathway is likely contributing to increased synaptic plasticity. These results highlight CD200 and its receptor as molecules with promising therapeutic potential in the field of addiction.

Supplementary Materials: The following are available online at https://www.mdpi.com/article/10.3390/cells11030355/s1, Table S1: Antibodies for immunocytochemistry; Table S2: Primer sequences used in qRT-PCR; Table S3: Antibodies for flow cytometry; Figure S1; and Figure S2.

Author Contributions: Conceptualization, J.B., J.B.R. and T.S.; Formal analysis, J.B., I.R., A.F.T., E.B.A., C.C.P., I.M.L., T.C. and T.S.; Funding acquisition, T.S.; Investigation, J.B., I.R., A.F.T., C.C.P., and T.S.; Methodology, J.B., I.R., A.F.T., E.B.A., C.C.P., M.M.A., M.S., C.D.F.L., A.C.L. and T.C.; Project administration, T.S.; Supervision, J.B.R. and T.S.; Writing—original draft, J.B., C.D.F.L. and T.S.; Writing—review and editing, J.B., I.R., A.F.T., E.B.A., C.C.P., M.M.A., M.S., A.C.L., T.C., J.B.R. and T.S. All authors have read and agreed to the published version of the manuscript.

Funding: This work was funded by national funds through FCT—Fundação para a Ciência e a Tecnologia, I.P., under the project UIDB/04293/2020, by FEDER—Fundo Europeu de Desenvolvimento Regional—funds through the COMPETE 2020—Operational Program for Competitiveness and Internationalisation (POCI), Portugal 2020, and by Portuguese funds through FCT—Fundação para a Ciência e a Tecnologia/Ministério da Ciência (FCT), Tecnologia e Ensino Superior in the framework of the project POCI-01-0145-FEDER-030647 (PTDC/SAU-TOX/30647/2017) in T.S. lab. FEDER Portugal (Norte-01-0145-FEDER-000008000008—Porto Neurosciences and Neurologic Disease Research Initiative at I3S, supported by Norte Portugal Regional Operational Program (NORTE 2020), under the PORTUGAL 2020 Partnership Agreement, through the European Regional Development Fund (ERDF); FCOMP-01-0124-FEDER-021333). E.B.A. and C.C.P. employment contracts are financed by national funds through FCT in the context of CEEC (CEECIND/03675/2018 to EBA) and the program contract described in paragraphs 4, 5, and 6 of art. 23 of Law no. 57/2016, of August 29, as amended by Law no. 57/2017 of July 2019. J.B., I.R., A.F.T., and T.C. were supported by FCT (PD/BD/135450/2017, 2020.08365.BD, 2020.07188.BD, SFRH/BD/117148/2016). C.D.F.L. was financed in the framework of the project PTDC/EMD-EMD/31540/2017 (POCI-01-0145-FEDER-031540).

Institutional Review Board Statement: The study was conducted following the Directive 2010/63/EU and approved by the competent authorities, Direcção Geral de Alimentação e Veterinária (DGAV) and i3S Animal Ethical Committee (ref.2018-13-TS and DGAV ref.003891/2019-02-15).

Informed Consent Statement: Not applicable.

Data Availability Statement: Not applicable.

Acknowledgments: We acknowledge the support of the following i3S Scientific Platforms: Animal Facility, Cell Culture, and Genotyping (CCGen), Translational Cytometry Unit (TraCy), Advanced Light Microscopy (ALM), a member of the national infrastructure PPBI-Portuguese Platform of BioImaging (POCI-01–0145-FEDER-022122). We also acknowledge Eva Carvalho and Miguel Morais, from Nanomaterials for Targeted Therapies group (i3S), for kindly sharing astrocytes and microglial cells whenever necessary.

Conflicts of Interest: The authors declare no conflict of interest.

References

1. Nestler, E.J.; Luscher, C. The Molecular Basis of Drug Addiction: Linking Epigenetic to Synaptic and Circuit Mechanisms. *Neuron* **2019**, *102*, 48–59. [CrossRef]
2. Krasnova, I.N.; Cadet, J.L. Methamphetamine toxicity and messengers of death. *Brain Res. Rev.* **2009**, *60*, 379–407. [CrossRef]
3. Jayanthi, S.; Daiwile, A.P.; Cadet, J.L. Neurotoxicity of methamphetamine: Main effects and mechanisms. *Exp. Neurol.* **2021**, *344*, 113795. [CrossRef] [PubMed]
4. Tata, D.A.; Yamamoto, B.K. Interactions between methamphetamine and environmental stress: Role of oxidative stress, glutamate and mitochondrial dysfunction. *Addiction* **2007**, *102* (Suppl. 1), 49–60. [CrossRef]
5. Simões, P.F.; Silva, A.P.; Pereira, F.C.; Marques, E.; Grade, S.; Milhazes, N.; Borges, F.; Ribeiro, C.F.; Macedo, T.R. Methamphetamine induces alterations on hippocampal NMDA and AMPA receptor subunit levels and impairs spatial working memory. *Neuroscience* **2007**, *150*, 433–441. [CrossRef]
6. Avila, J.A.; Memos, N.; Aslan, A.; Andrejewski, T.; Luine, V.N.; Serrano, P.A. Voluntary oral methamphetamine increases memory deficits and contextual sensitization during abstinence associated with decreased PKMζ and increased κOR in the hippocampus of female mice. *J. Psychopharmacol.* **2021**, *35*, 1240–1252. [CrossRef] [PubMed]
7. Miller, D.R.; Bu, M.; Gopinath, A.; Martinez, L.R.; Khoshbouei, H. Methamphetamine Dysregulation of the Central Nervous System and Peripheral Immunity. *J. Pharmacol. Exp. Ther.* **2021**, *379*, 372. [CrossRef]
8. Cadet, J.L.; Bisagno, V. Glial-neuronal ensembles: Partners in drug addiction-associated synaptic plasticity. *Front. Pharmacol.* **2014**, *5*, 204. [CrossRef] [PubMed]
9. Miguel-Hidalgo, J.J. The role of glial cells in drug abuse. *Curr. Drug Abuse Rev.* **2009**, *2*, 76–82. [CrossRef]
10. Dang, J.; Tiwari, S.K.; Agrawal, K.; Hui, H.; Qin, Y.; Rana, T.M. Glial cell diversity and methamphetamine-induced neuroinflammation in human cerebral organoids. *Mol. Psychiatry* **2021**, *26*, 1194–1207. [CrossRef]
11. Frank, M.G.; Adhikary, S.; Sobesky, J.L.; Weber, M.D.; Watkins, L.R.; Maier, S.F. The danger-associated molecular pattern HMGB1 mediates the neuroinflammatory effects of methamphetamine. *Brain Behav. Immun.* **2016**, *51*, 99–108. [CrossRef]
12. Canedo, T.; Portugal, C.C.; Socodato, R.; Almeida, T.O.; Terceiro, A.F.; Bravo, J.; Silva, A.I.; Magalhaes, J.D.; Guerra-Gomes, S.; Oliveira, J.F.; et al. Astrocyte-derived TNF and glutamate critically modulate microglia activation by methamphetamine. *Neuropsychopharmacology* **2021**, *46*, 2358–2370. [CrossRef] [PubMed]
13. Chavarria, A.; Cardenas, G. Neuronal influence behind the central nervous system regulation of the immune cells. *Front. Integr. Neurosci.* **2013**, *7*, 64. [CrossRef]
14. Tian, L.; Rauvala, H.; Gahmberg, C.G. Neuronal regulation of immune responses in the central nervous system. *Trends Immunol.* **2009**, *30*, 91–99. [CrossRef] [PubMed]
15. Brás, J.P.; Bravo, J.; Freitas, J.; Barbosa, M.A.; Santos, S.G.; Summavielle, T.; Almeida, M.I. TNF-alpha-induced microglia activation requires miR-342: Impact on NF-kB signaling and neurotoxicity. *Cell Death Dis.* **2020**, *11*, 415. [CrossRef]
16. Biber, K.; Neumann, H.; Inoue, K.; Boddeke, H.W. Neuronal 'On' and 'Off' signals control microglia. *Trends Neurosci.* **2007**, *30*, 596–602. [CrossRef] [PubMed]
17. Hernangomez, M.; Klusakova, I.; Joukal, M.; Hradilova-Svizenska, I.; Guaza, C.; Dubovy, P. CD200R1 agonist attenuates glial activation, inflammatory reactions, and hypersensitivity immediately after its intrathecal application in a rat neuropathic pain model. *J. Neuroinflammation* **2016**, *13*, 43. [CrossRef] [PubMed]
18. Sun, H.; He, X.; Tao, X.; Hou, T.; Chen, M.; He, M.; Liao, H. The CD200/CD200R signaling pathway contributes to spontaneous functional recovery by enhancing synaptic plasticity after stroke. *J. Neuroinflammation* **2020**, *17*, 171. [CrossRef]
19. Denieffe, S.; Kelly, R.J.; McDonald, C.; Lyons, A.; Lynch, M.A. Classical activation of microglia in CD200-deficient mice is a consequence of blood brain barrier permeability and infiltration of peripheral cells. *Brain Behav. Immun.* **2013**, *34*, 86–97. [CrossRef]
20. Feng, D.; Huang, A.; Yan, W.; Chen, D. CD200 dysfunction in neuron contributes to synaptic deficits and cognitive impairment. *Biochem. Biophys. Res. Commun.* **2019**, *516*, 1053–1059. [CrossRef]
21. Braz, S.O.; Cruz, A.; Lobo, A.; Bravo, J.; Moreira-Ribeiro, J.; Pereira-Castro, I.; Freitas, J.; Relvas, J.B.; Summavielle, T.; Moreira, A. Expression of Rac1 alternative 3′ UTRs is a cell specific mechanism with a function in dendrite outgrowth in cortical neurons. *Biochim. Biophys. Acta Gene Regul Mech.* **2017**, *1860*, 685–694. [CrossRef] [PubMed]
22. Chen, Y.; Balasubramaniyan, V.; Peng, J.; Hurlock, E.C.; Tallquist, M.; Li, J.; Lu, Q.R. Isolation and culture of rat and mouse oligodendrocyte precursor cells. *Nat. Protoc.* **2007**, *2*, 1044–1051. [CrossRef] [PubMed]
23. Socodato, R.; Portugal, C.C.; Domith, I.; Oliveira, N.A.; Coreixas, V.S.; Loiola, E.C.; Martins, T.; Santiago, A.R.; Paes-de-Carvalho, R.; Ambrosio, A.F.; et al. c-Src function is necessary and sufficient for triggering microglial cell activation. *Glia* **2015**, *63*, 497–511. [CrossRef] [PubMed]
24. Bortell, N.; Basova, L.; Semenova, S.; Fox, H.S.; Ravasi, T.; Marcondes, M.C. Astrocyte-specific overexpressed gene signatures in response to methamphetamine exposure in vitro. *J. Neuroinflammation* **2017**, *14*, 49. [CrossRef] [PubMed]
25. Lopes, C.D.; Gomes, C.P.; Neto, E.; Sampaio, P.; Aguiar, P.; Pego, A.P. Microfluidic-based platform to mimic the in vivo peripheral administration of neurotropic nanoparticles. *Nanomedicine (Lond)* **2016**, *11*, 3205–3221. [CrossRef]
26. Schindelin, J.; Arganda-Carreras, I.; Frise, E.; Kaynig, V.; Longair, M.; Pietzsch, T.; Preibisch, S.; Rueden, C.; Saalfeld, S.; Schmid, B.; et al. Fiji: An open-source platform for biological-image analysis. *Nat. Methods* **2012**, *9*, 676–682. [CrossRef]

27. Andrade, E.B.; Magalhaes, A.; Puga, A.; Costa, M.; Bravo, J.; Portugal, C.C.; Ribeiro, A.; Correia-Neves, M.; Faustino, A.; Firon, A.; et al. A mouse model reproducing the pathophysiology of neonatal group B streptococcal infection. *Nat. Commun.* **2018**, *9*, 3138. [CrossRef] [PubMed]
28. Santos, S.D.; Iuliano, O.; Ribeiro, L.; Veran, J.; Ferreira, J.S.; Rio, P.; Mulle, C.; Duarte, C.B.; Carvalho, A.L. Contactin-associated protein 1 (Caspr1) regulates the traffic and synaptic content of alpha-amino-3-hydroxy-5-methyl-4-isoxazolepropionic acid (AMPA)-type glutamate receptors. *J. Biol. Chem.* **2012**, *287*, 6868–6877. [CrossRef]
29. Verstraelen, P.; Garcia-Diaz Barriga, G.; Verschuuren, M.; Asselbergh, B.; Nuydens, R.; Larsen, P.H.; Timmermans, J.P.; De Vos, W.H. Systematic Quantification of Synapses in Primary Neuronal Culture. *iScience* **2020**, *23*, 101542. [CrossRef]
30. McLeod, F.; Marzo, A.; Podpolny, M.; Galli, S.; Salinas, P. Evaluation of Synapse Density in Hippocampal Rodent Brain Slices. *J. Vis. Exp.* **2017**, *128*, 56153. [CrossRef]
31. Cherry, J.D.; Olschowka, J.A.; O'Banion, M.K. Neuroinflammation and M2 microglia: The good, the bad, and the inflamed. *J. Neuroinflammation* **2014**, *11*, 98. [CrossRef]
32. Yu, S.; Zhu, L.; Shen, Q.; Bai, X.; Di, X. Recent advances in methamphetamine neurotoxicity mechanisms and its molecular pathophysiology. *Behav. Neurol.* **2015**, *2015*, 103969. [CrossRef]
33. Shin, E.J.; Dang, D.K.; Tran, T.V.; Tran, H.Q.; Jeong, J.H.; Nah, S.Y.; Jang, C.G.; Yamada, K.; Nabeshima, T.; Kim, H.C. Current understanding of methamphetamine-associated dopaminergic neurodegeneration and psychotoxic behaviors. *Arch. Pharm. Res.* **2017**, *40*, 403–428. [CrossRef]
34. Krystofova, J.; Pathipati, P.; Russ, J.; Sheldon, A.; Ferriero, D. The Arginase Pathway in Neonatal Brain Hypoxia-Ischemia. *Dev. Neurosci.* **2018**, *40*, 437–450. [CrossRef] [PubMed]
35. Chang, R.C.; Hudson, P.; Wilson, B.; Liu, B.; Abel, H.; Hemperly, J.; Hong, J.S. Immune modulatory effects of neural cell adhesion molecules on lipopolysaccharide-induced nitric oxide production by cultured glia. *Brain Res. Mol. Brain Res.* **2000**, *81*, 197–201. [CrossRef]
36. Hoek, R.M.; Ruuls, S.R.; Murphy, C.A.; Wright, G.J.; Goddard, R.; Zurawski, S.M.; Blom, B.; Homola, M.E.; Streit, W.J.; Brown, M.H.; et al. Down-regulation of the macrophage lineage through interaction with OX2 (CD200). *Science* **2000**, *290*, 1768–1771. [CrossRef]
37. Mott, R.T.; Ait-Ghezala, G.; Town, T.; Mori, T.; Vendrame, M.; Zeng, J.; Ehrhart, J.; Mullan, M.; Tan, J. Neuronal expression of CD22: Novel mechanism for inhibiting microglial proinflammatory cytokine production. *Glia* **2004**, *46*, 369–379. [CrossRef]
38. Beier, C.P.; Wischhusen, J.; Gleichmann, M.; Gerhardt, E.; Pekanovic, A.; Krueger, A.; Taylor, V.; Suter, U.; Krammer, P.H.; Endres, M.; et al. FasL (CD95L/APO-1L) resistance of neurons mediated by phosphatidylinositol 3-kinase-Akt/protein kinase B-dependent expression of lifeguard/neuronal membrane protein 35. *J. Neurosci.* **2005**, *25*, 6765–6774. [CrossRef]
39. Medana, I.; Li, Z.; Flugel, A.; Tschopp, J.; Wekerle, H.; Neumann, H. Fas ligand (CD95L) protects neurons against perforin-mediated T lymphocyte cytotoxicity. *J. Immunol.* **2001**, *167*, 674–681. [CrossRef]
40. Shi, S.; Chen, T.; Zhao, M. The Crosstalk Between Neurons and Glia in Methamphetamine-Induced Neuroinflammation. *Neurochem. Res.* **2022**. [CrossRef]
41. Taft, C.E.; Turrigiano, G.G. PSD-95 promotes the stabilization of young synaptic contacts. *Philos Trans. R Soc. Lond B Biol Sci* **2014**, *369*, 20130134. [CrossRef]
42. El-Husseini, A.E.; Schnell, E.; Chetkovich, D.M.; Nicoll, R.A.; Bredt, D.S. PSD-95 involvement in maturation of excitatory synapses. *Science* **2000**, *290*, 1364–1368. [CrossRef] [PubMed]
43. Berry, K.P.; Nedivi, E. Spine Dynamics: Are They All the Same? *Neuron* **2017**, *96*, 43–55. [CrossRef] [PubMed]
44. Mark, K.A.; Quinton, M.S.; Russek, S.J.; Yamamoto, B.K. Dynamic changes in vesicular glutamate transporter 1 function and expression related to methamphetamine-induced glutamate release. *J. Neurosci.* **2007**, *27*, 6823–6831. [CrossRef] [PubMed]
45. Dietz, D.M.; Dietz, K.C.; Nestler, E.J.; Russo, S.J. Molecular mechanisms of psychostimulant-induced structural plasticity. *Pharmacopsychiatry* **2009**, *42* (Suppl. 1), S69–S78. [CrossRef] [PubMed]
46. Kutlu, M.G.; Gould, T.J. Effects of drugs of abuse on hippocampal plasticity and hippocampus-dependent learning and memory: Contributions to development and maintenance of addiction. *Learn. Mem.* **2016**, *23*, 515–533. [CrossRef]
47. Nakahata, Y.; Yasuda, R. Plasticity of Spine Structure: Local Signaling, Translation and Cytoskeletal Reorganization. *Front. Synaptic Neurosci.* **2018**, *10*, 29. [CrossRef]
48. Murakoshi, H.; Wang, H.; Yasuda, R. Local, persistent activation of Rho GTPases during plasticity of single dendritic spines. *Nature* **2011**, *472*, 100–104. [CrossRef]